MicroRNA Profile and Function in Kidney Ischaemia and Reperfusion Injury

Gerhard R. Situmorang

Thesis submitted in partial fulfilment of the requirements of the regulations for the degree of Doctor of Philosophy

Institute of Cellular Medicine
Newcastle University, UK

May 2018

For God, For Country, For Alma Mater

Table of Contents

Abstract

Ischaemia and reperfusion injury (IRI) in renal allografts is an important contributing factor to chronic allograft dysfunction. MicroRNAs (miRNA) have been shown to play important roles in cellular adaptation to pathological conditions, including IRI. This study aimed to evaluate changes in miRNA profile following IRI, and how the changes in particular miRNAs may influence renal proximal tubular epithelial cell (PTEC) morphology and function, potentially contributing to the development of chronic allograft dysfunction. To achieve this, several objectives were set. These included: (1) isolation and culture of primary human PTECs, (2) miRNA expression profiling following IRI and selection of candidate miRNA, and (3) in vitro and human pathology validation to explore the molecular mechanism of the candidate miRNA.

Primary PTECs were isolated from normal renal tissue. These cells showed features of epithelial cells under light microscope and electron microscope. The cells were also characterised using immunofluorescent staining, which showed positive expression of epithelial cell markers, and negative expression for mesenchymal cell markers. MiRNA profiling using NanoString platform was performed on cell lines (HKC-8 and HK-2) and primary PTECs, which were exposed to either hypoxia or free radicals. Results revealed distinct miRNA signature changes following IRI in cells. However, only a small proportion of microRNAs were found to be significantly up/down-regulated in either cell lines or primary cells, which included miR-21, miR-376, miR-190b, miR-34a, miR-210, miR-363, miR-142 and miR-130b. MiR-21 was shown to be up-regulated in all cells following both type of injuries. Online target prediction analysis also showed miR-21 to be involved in pathways relevant to cellular response to IRI and the development of fibrosis.

The role of miR-21 was studied in detail. Up-regulation of miR-21 following ischaemia was shown to suppress SMAD7 and facilitate intra-nuclear localisation of SMAD3. In the presence of exogenous TGF-b1 or hypoxia, over-expression of miR-21 in cells led to an increase in SMAD3 activity. Over-expression of miR-21 also led to phenotypic shift in HKC-8 cells, characterised as a decrease in E-cadherin and an increase in α-SMA and Collagen-1 expression. Human pathology evaluation confirmed high expression of miR-21 in the tubular cells of severely ischaemic kidneys compared to non-ischaemic kidneys.

In conclusion, changes in miRNA profile were observed in acute IRI in the kidney. One of the significantly affected miRNAs was miR-21. MiR-21 up-regulation resulted in sensitisation of tubular cells to TGF-b1, which may be essential in cellular repair processes, but may also contribute to deterioration of long-term organ function.

Acknowledgements

"The fear of the Lord is the beginning of knowledge,… "

Proverbs 1:7a

Glory be to God, for only because of His power and blessings that I had the courage and strength to start, and complete this PhD project.

I am most grateful to my supervisor, Prof. Neil Sheerin for his wisdom, knowledge and guidance throughout my PhD years. The faith he put in all his students, the time he sacrificed, and the genuine care he showed, is an outstanding example of the character of a leader and a teacher. I am also thankful for the support and guidance given by my co-supervisors; Prof. Simi Ali, Prof. John Kirby and Prof. Akmal Taher. Your wisdom, thoughts and care is something that I will never be able to return.

I am especially thankful to Victoria Shuttleworth, Shameem Ladak, Rishab Kapoor and Dr. Ian Logan. I knew nothing about laboratory work when I picked up this project. It is your kindness, patience and willingness to keep me supervised, which have helped me progress and learn slowly throughout these last 3 years. I would also like to thank other members of Neil Sheerin's lab group: Lucy Bates, Pande Wisnu, and Lotfia Nawafa, members of Kirby and Ali's lab group: Avinash Sewpaul, Nina Jordan, Laura Ferreras, Rachel Etherington, Barbara Innes and Ben Miller, as well as members of various labs within Newcastle University: Dr. Trevor Booth, Dr. Niall Kenneth, Dr. Anna Moles, Dr. Git Chung, Dr. Kile Green, Dr. Olivier Govaere, Dr. Steven Ball, Xin Xu, and Marco Youssef. I have learned a lot of things from all of you, and I truly appreciate your time, effort and help.

I would like to offer my upmost gratitude to my teachers, Prof. Djoko Rahardjo, Dr. Rochani and Prof. Rainy Umbas who have been genuinely supportive and caring. A line of email or message from them, were amongst the things that kept me going. Also to my teachers and seniors at the Department of Urology FKUI/RSCM; Dr. Arry Rodjani, Dr. Chaidir Mochtar, Dr. Nur Rasyid, Dr. Irfan Wahyudi, Dr. Ponco Birowo, Dr. Harrina Rahardjo and Dr. Rizal Hamid, as well as to my fellow co-workers in the department; Dr. Gampo Alam, Dr. Fina Widia and Dr. Widi Atmoko. The opportunity, support and attention you have given me would not be forgotten. To the administrative team, nurses, general staff and interns at the Department of Urology FKUI/RSCM, your prayer and support is truly appreciated.

I am thankful for the support and permission granted by the Dean of the Faculty of Medicine, Universitas Indonesia (FKUI) and the Director of Cipto Mangunkusumo National

Referral Hospital (RSCM), and the Head of the Department, who have allowed me to temporarily leave my academic and clinical work to pursue this PhD degree. I would like to thank the Indonesian government, which have sponsored me through the Indonesian Endowment Fund for Education. May this knowledge and skills be useful in achieving a better Indonesia.

I am also grateful for the support and understanding from my beloved parents (Dr. Tunggul Situmorang and Mrs. Rotua Siahaan), and my parents in law (Drs. Wilmar Pandjaitan and Mrs. Tien Silaen). Without their support, understanding and sacrifices, this PhD years would not have been possible. Also to my brothers (Tony and Daniel) and my sister (Tika), and their young families, I am thankful for your prayer and support.

Last, but not least, I am most grateful to my wife, Astrid, and my two little princesses, Anabel and Isabel. You have sacrificed so much for this dream to come true, and for that I could only thank you. You are my life, my inspiration, my strength, I am so blessed to have you.

Per scientiam, pro Deo et humanitate

List of Tables

List of Figures

List of Abbreviations

AAVs	Adeno-associated viruses
ADP	Adenosine di-phosphate
AGO	Argonoute
AKI	Acute kidney injury
AMP	Adenosine mono-phosphate
AP	Alkaline phosphatase
ATP	Adenosine tri-phophate
BCA	Bicinchoninic acid
BD	Binding density
CaMKs	Calmodulin-dependent protein kinases
CKD	Chronic kidney disease
CM-H_2DCFDA	Chloromethyl-2,7-dichlorodihydrofluorescein
$CoCl_2$	Cobalt chloride
Cr	Creatinine
C_T	Cycle threshold
DA	Digital analyser
DAMPs	Damage-associated molecular proteins
DAPI	4',6-diamidino-2-phenylindole
DBD	Donor after brain death
DCD	Donor after circulatory death
DCF	2',7'-di-chlorofluorescein
DCs	Dendritic cells
DGF	Delayed graft function
DGRC8	DiGeorge syndrome critical region 8
DIG	Double-digoxigenin
DMEM	Dulbecco's modified Eagle's medium
DMSO	Dimethyl sulfoxide
DNA	Deoxyribonucleic acid
DNA	Complementary DNA
e.t.c	Electron transport chain
ECL	Enhanced chemiluminescent
EMT	Epithelial-to-mesenchymal transition

EndoMT	Endothelial-to-mesenchymal transition
ER	Endoplasmic reticulum
ESRD	End-stage renal disease
FBS	Foetal bovine serum
FFPE	Formalin-fixed paraffin embedded
FITC	Fluorescein isothiocyanate
FOV	Field of view
GFR	Glomerular filtration rate
GLUT	Glucose transporter
H_2O_2	Hydrogen peroxide
HIF	Hypoxia inducible factor
HRE	Hypoxia response element
IF	Immunofluorescent
IFN-γ	Interferon gamma
IRI	Ischaemia and reperfusion injury
ISH	*In situ* hybridisation
JNK	c-Jun N-terminal kinase
LNA	Locked-nucleic acid
M-CSF	Macrophage colony stimulating factor
miRNA	Micro RNA
mPT	Mitochondrial permeability transition pore
mRNA	Messenger RNA
N-TAD	N-terminal transactivation domain
NAD	Nicotinamide adenine dinucleotide
NK	Natural killer
NOS	Nitric oxide synthetase
PBS	Phosphate buffer saline
PDGF	Platelet-derived growth factor
PHD	Prolyl hydroxylase domains
PRRs	Pattern recognition receptors
PTC	Peri-tubular capillary
PTECs	Proximal tubular epithelial cells
PTEN	Phosphate and tension homologue
qPCR	Quantitative polymerase chain reaction

RNA	Ribonucleic acid
ROS	Reactive oxygen species
RRT	Renal replacement therapy
RT	Reverse transcription
SD	Standard deviation
SEM	Scanning electron microscope
siRNA	Short interfering RNA
TECs	Tubular epithelial cells
TGF-β	Tumour growth factor beta
TLRs	Toll-like receptors
TRECK	Toxin receptor-mediated cell knock-out
UFP	Unfolded proteins
UTR	Un-translated region
UUO	Unilateral ureteral obstruction
VEGF	Vascular endothelial growth factor
VHL	Von Hippel-Lindau
WB	Western blotting
XO	Xanthine oxidase
$\Delta\Delta C_T$	Comparative C_T method
α-SMA	Alpha smooth muscle actin

Chapter 1. Introduction

1.1. Chronic Kidney Disease & Kidney Transplantation

1.1.1. CKD: Overview & Epidemiology

The universal definition of chronic kidney disease developed by the National Kidney Foundation, 2002, encompasses any structural or functional abnormalities of the kidney remittent for more than 3 months. CKD may be present with or without reduction in glomerular filtration rate (GFR) and manifest by either pathological abnormalities or detection of markers of kidney damage in blood or urine, or using available imaging tests (National Kidney Foundation, 2002). Based on the classification developed by the National Kidney Foundation-Kidney Disease Improving Global Outcomes team (NKF-KDIGO), CKD is classified into clinical stages, based on the severity of GFR loss and degree of albuminuria, which is associated with disease progression and prognosis.

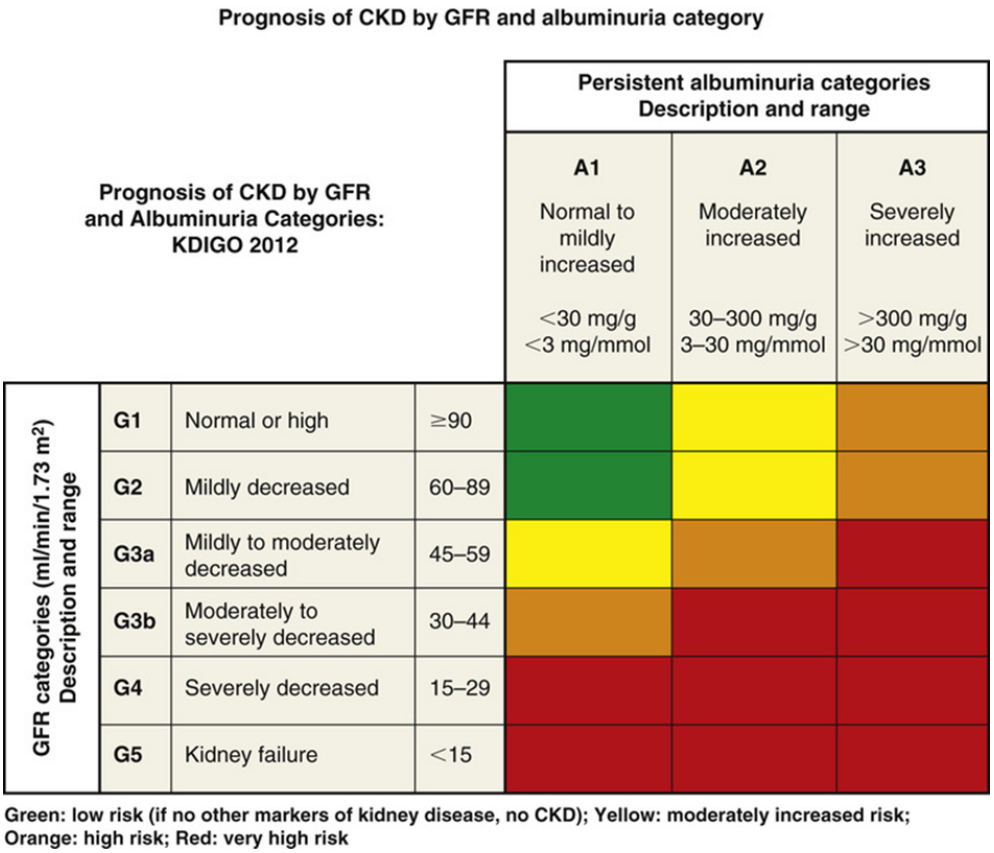

Figure 1-1 Classification and prognosis of CKD

Clinical stages and prognosis of CKD based on GFR and albuminuria according to the National Kidney Foundation (National Kidney Foundation-Kidney Disease Improving Global Outcomes, 2012)

As seen from Figure 1-1, CKD is a disease entity with a wide spectrum of severity. Although the classification and definition may appear to be robust and clear, it has been proven difficult to estimate the magnitude of problems related to CKD. CKD is not associated with the presence of pathognomonic signs and symptoms; thus, successful early detection of CKD relies largely on the availability of supplementary tests as well as on the identification of population at risk.

Moreover, CKD is not a solitary disease entity, but is associated with many underlying diseases (e.g. glomerulonephritis, urinary tract stone disease, hypertension, and diabetes). In addition, it is associated with many complications (e.g. cardiovascular diseases, anaemia, mineral and bone disorders). The kidneys, through their involvement in regulation of blood pressure, acid-base and electrolyte balance, and other homeostatic functions, also play pivotal role in initiating or exacerbating systemic complications of a disease. The relationship between CKD with poor patient outcomes, especially with the incidence of end-stage renal disease, cardiovascular complications and early mortality highlights the importance of adequate and prompt management of CKD. Furthermore, recent reports have identified CKD as a growing global health problem. Analysis from 188 countries for the global burden of disease documented an increase in mortality related to CKD in 2013 compared to year 1990, regardless of the underlying cause. (GBD 2013 Mortality and Causes of Death Collaborators, 2015). Regardless, it is likely that this rate is an underestimation, since it does not take into account the number of CKD-related cardiovascular events leading to mortality.

1.1.2. The Role of Kidney Transplantation in Alleviating the Global Burden of CKD

Since the first successful transplant performed by Dr. Joseph Murray in 1954, kidney transplantation has evolved from a therapeutic modality for a selected few to a routine procedure offered to wide spectrum of patients, aimed to not only enhance quality of life, but also to save life. Previously only considered as an adjunct to dialysis, kidney transplantation has currently emerged as a therapy of choice for end-stage renal diseases (ESRD). A series of studies describe the importance of kidney transplantation as an integral component of renal replacement therapy, both from medical perspective as well as from health economic standpoint.

One of the earliest evidence highlighting the pivotal role of kidney transplantation was published by Wolfe et al., which reported a survival advantage in patients receiving a kidney transplant from a deceased donor compared to patients who remained on the waiting list (Wolfe *et al.*, 1999). The benefit of transplantation is observed even in high-risk groups, such as elderly patients and patients with diabetes. Relative risk death is better in transplanted

patients, even after considering the risk of surgery, early complications, infections and cardiovascular events. The significance of transplantation is further emphasised by the negative effect of longer time in dialysis before transplantation on the post-transplant mortality rate, suggesting that dialysis is associated with more complication, such as infection and impaired cardiovascular dynamics (Cosio *et al.*, 1998; Pesavento, 2009).

Numerous studies on cost-analysis of kidney transplantation have also been published. Although results may vary between different countries and regions, it is generally accepted that kidney transplantation has a significantly higher first-year cost compared to maintenance dialysis. This initial higher cost, however, decreases significantly during subsequent years post-transplant and falls considerably below the cost of chronic maintenance dialysis. Overall, transplantation generally reduces overall cost associated with the management of ESRD.

Despite global disparities in its uptake, kidney transplantation clearly plays a pivotal role in alleviating global burden of CKD, even more, considering its much-improved outcome and cost-effectiveness. With a steady increase in CKD prevalence worldwide, and limited health budgets, kidney transplantation should appeal as a therapeutic option for CKD, hence, the number is expected to continue to rise.

1.1.3. Chronic Graft Loss in Kidney Transplantation; Magnitude of the Problem

The literature uses interchangeable terminologies to describe chronic graft loss. Chronic allograft dysfunction is a terminology used to describe deterioration of function, primarily related to the development of fibrosis and glomerulosclerosis. The term chronic reflects the persistent and ongoing loss of function, and the late occurrence of a clinically detectable injury. The use of term chronic graft loss, however, is not always the same across different publications. Some literatures reserve the use of this term specifically for long-term functional loss, in which no clear aetiology could be identified, as in the cases related to initial IRI. Others adopt the term more generally to include other causes, such as due to the use of nephrotoxic agents or chronic rejection.

Successful efforts have been made to improve short-term allograft survival and patient survival through advancement in immunosuppressive therapy, better organ allocation and careful recipient selection. Despite the short-term improvement achieved, transplanted organs are still lost in the longer-term. This can be attributed to immunologic and non-immunologic events that occur from the time of the transplant procedure as well as de novo events arising at later time points post-transplant. Chronic graft loss affects all solid organ transplantation, with varying degrees of severity, regardless of the source of donor. Data from National Health Service Blood and Transplant (NHSBT) in the United Kingdom, documented a steady decline

in long-term graft survival in both adult and paediatric kidney transplant cohorts. There is 5-15% reported graft loss at 10-year post-transplant in recipients receiving organs from living donors (NHSBT, 2017). The rate of graft loss increases to approximately 20-30% in transplantation from donors after brain death and circulatory death (NHSBT, 2017). Indeed, available data suggests that chronic graft loss remains one of the biggest hurdles in kidney transplantation.

The rate of long-term graft loss is not expected to decrease unless the contributing factors are identified and prevention strategies developed. One of these contributing factors is ischaemia reperfusion injury (IRI) that leads to acute allograft injury. As the global burden of CKD steadily increases, the demand for kidney transplantation is also expected to rise. To meet this increasing demand and to overcome potential shortage of available donors, several strategies have been introduced, including the use of extended criteria donor. Inadvertently, however, this also means increasing the use of organs with more severe IRI, and therefore escalates the likelihood of earlier deterioration of function, increasing the prospect of developing chronic allograft dysfunction.

1.1.4. Chronic Graft Loss as a Consequence of Acute Kidney Injury

An increasing number of clinical epidemiology studies have reported an association between acute kidney injury (AKI) and the development of CKD. One of the clearest finding is described by Mammen et al. in a large paediatric intensive care unit cohort, in which only 1 of 126 patients had CKD at immediately post discharge. However, the percentage of patients developing CKD increased to 10.3% during 1-3 years follow-up period. In addition, 46.8% of patients in this study developed hypertension, microalbuminuria or mildly decreased GFR, which are considered risk factors for CKD (Mammen *et al.*, 2012; Heung and Chawla, 2014).

In the context of IRI, a transplant cohort serves as an ideal model to investigate the link between acute ischaemic injury and development of late organ dysfunction. Acute ischaemic injury in kidney transplantation manifests clinically as delayed graft function (DGF). DGF is associated with prolonged hospitalisation and the need for renal replacement therapy post-transplant. Nevertheless, recovery of organ function is usually achieved in patients with DGF, indicating a degree of resolution of acute ischaemic injury. Interestingly, regardless of this short-term resolution of function, DGF is still associated with increased risk of long-term graft loss, earlier functional deterioration and higher probability of rejection. This indicates an apparent association between acute events caused by ischaemia and persistent cellular damage, which impacts long-term function. Despite the well-established epidemiological link between AKI and CKD, available evidence to explain the causative relationship between the

two clinical entities is still lacking (Rifkin *et al.*, 2012). This is one of the reasons that highlights the significance of my work.

1.2. Delayed Graft Function; the Clinical Hallmark of IRI in Transplantation

1.2.1. Definition of Delayed Graft Function; Consensus and Controversies

Delayed graft function (DGF) in kidney transplantation is best defined as the inability of a transplanted kidney to function immediately after transplantation. DGF has been closely associated with IRI and the homeostatic dysregulation and immunological injury associated with IRI. It is considered as a form of AKI unique to the transplant setting.

Although the term DGF has been adopted globally, the specific clinical criteria used to define DGF may vary between centres. A systematic review by Yarlagadda et al. has addressed this issue, concluding that current utilisation of heterogeneous clinical criteria used to define DGF may have certain limitations and lead to unreliable, delayed and inaccurate identification of DGF cases (Yarlagadda *et al.*, 2008). The review highlighted the three most common diagnostic criteria used to define DGF; (1) the need for renal replacement therapy (RRT) after transplantation, (2) failure of serum creatinine to decrease or (3) the combination of criteria (1) and (2). Yaralagadda et al. reviewed the available literature and listed over 10 definitions of DGF, as shown in Table 1-1.

The most commonly found definition of DGF in the literature; the need for RRT after transplantation is associated with several problems, which are mainly due to the subjectivity (clinician-dependent) of the decisions made in initiating RRT. In addition, there is a marked variation in the time frame used, ranging from the first 4 days to 10 days after the transplant procedure. Defining DGF based on the requirement of RRT alone may also potentially include patients undergoing post-transplant RRT for a specific indication, such as volume overload or hyperkalaemia, despite a functioning graft. On the other hand, this definition may exclude patients with poor allograft function and low GFR who still have significant residual renal function (such as pre-emptively transplanted patients).

Although serum creatinine is clinically still valued as the gold standard measurement of renal function, there have been several publications highlighting its inadequacy in reflecting the actual severity of tubular injury (Bosch, 1995; Herrera and Rodriguez-Iturbe, 1998; Malyszko *et al.*, 2015), especially considering that creatinine level may be influenced by many factors, including muscle mass, diet, drugs and hydration status. Moreover, transplant patients may undergo dialysis to optimise their condition prior to transplantation, which may also mask a high creatinine level caused by DGF (Yarlagadda *et al.*, 2008).

Table 1-1. Various clinical criteria used to define DGF

Dialysis-based definitions
▪ Need for dialysis in the first week after transplantation ▪ Need for dialysis in the first week after transplantation once hyperacute rejection, vascular and urinary tract complications were ruled out ▪ Need for dialysis after transplant ▪ Need for dialysis in the first 10 days after transplant ▪ Absence of life-sustaining renal function that requires dialysis performed for hyperkalaemia ▪ Need for dialysis in the first 7 days after transplant with specific exclusion of single early post-operative dialysis performed for hyperkalaemia ▪ Return to maintenance haemodialysis within the first 4 days after transplantation
Creatinine-based definitions
▪ Serum creatinine increased or remained unchanged or decreased <10%/day during 3 consecutive days after transplant ▪ Creatinine (Cr) reduction ratio <30% and /or urine creatinine on day 2 <1000 mg ▪ Serum Cr >2.5 mg/dL on Day 7 or the need for post-transplant hemodialysis ▪ Time required for the kidney to reach Cr clearance >10 mL/min greater than 1 week. ▪ Failure of creatinine to decline in the first 48 h in the absence of rejection
Combination of dialysis and creatinine based definitions
▪ Failure of serum creatinine to fall below pre-transplant levels, within 1 week regardless of the urine output ▪ Rise in serum Cr at 6–8 h post-operatively or <300cc of urine despite adequate volume and diuretics ▪ Dialysis requirement after transplant or a serum Cr >150μmol/L at day 8 ▪ Urine output <1L in 24h and <25% fall in serum Cr from baseline in first 24 h post-transplant ▪ Urine output <75 mL/h in first 48 h or failure of serum Cr to decrease by 10% in the first 48 h ▪ Need for dialysis in the first week after transplant or failure of serum Cr to decrease within 24 h after transplant

Modified from (Yarlagadda *et al.*, 2008)

Despite the existing heterogeneity in the clinical criteria used to define DGF, no current development has been reported to homogenise or improve our diagnosis of DGF. Several novel biomarkers, such as kidney injury molecule (KIM)-1 or neutrophil gelatin-associated lipocalin (NGAL) have been proposed, on the basis that they show better correlation with the degree of actual tubular injury occurring after IRI. However, the validation and uptake of their use clinically use is still limited, especially compared to the already widely accepted serum creatinine.

In addition, DGF is used to describe lack of immediate function due to IRI. In reality, this functional delay may be the result of several conditions distinct from IRI (such as antibody-mediated rejection, thrombotic microangiopathy, acute calcineurin inhibitor toxicity and primary non-function), which may present independently of, or coexist with, IRI (Yarlagadda *et al.*, 2008). Hence, a true diagnosis of DGF can only be made after excluding the presence of these other conditions, which is not always be straightforward. Considering

the aforementioned problems, it is still a challenge to reach a universal consensus on the definition of DGF.

1.2.2. Delayed Graft Function: Incidence and Risk Factors

Reports on DGF incidence vary greatly between different centres. Disparity in clinical criteria used to identify DGF is the main reason for such variation. In general, DGF has been reported to affect 3-16% of recipients receiving a living donor kidney (Senel *et al.*, 1998; Yarlagadda *et al.*, 2008; Sharma *et al.*, 2010; Healthcare Systems Bureau Division of Transplantation and United Network for Organ Sharing, 2012; Salamzadeh *et al.*, 2012; Redfield *et al.*, 2016). Predictably, the incidence is higher and varies more in deceased donor cohorts, ranging from 5-50% in all cases (Yarlagadda *et al.*, 2008) to 18-35% in donation after brain death (DBD) cohorts and 35-43% in donation after circulatory death (DCD) cohorts (Healthcare Systems Bureau Division of Transplantation and United Network for Organ Sharing, 2012). The wide range of incidence reported suggests a difference in DGF definition used. Interestingly, none of the definitions used is superior in predicting graft failure at 1 year in the DBD cohort.

Inconsistency in defining DGF also affects the way the literature reports causes and risk factors for DGF. Generally, when DGF is viewed as a clinical entity, per se, and not considered as a specific pathological consequence of IRI, risk factors of DGF can be classified into two groups; (1) risk factors related to procurement and pre-existing donor characteristics and (2) risk factors associated with the recipients as listed in Table 1-2 below.

Table 1-2 Risk factors of the development of DGF

Procurement / Donor Associated	Recipient Associated
▪ Non-heart-beating (DCD) donor ▪ Inotropic use ▪ Extensive ischaemia time ▪ Older age donor (>55 years) ▪ Increased BMI ▪ Marginal donor (diabetic or hypertensive disorders)	▪ Hypovolaemia ▪ Increased BMI ▪ Intra-operative albumin administration ▪ Allosensitisation (number of previous transplants) ▪ Inherited thrombophilia ▪ Pre-formed antidonor antibodies ▪ Cyclosporine nephrotoxicity ▪ Ureteral leakage ▪ Ureteral obstruction

Modified from (Perico *et al.*, 2004).

When a more stringent definition of DGF is used, which designates DGF uniquely as a consequence of IRI, then the risks are limited to only the factors which contribute to a significant increase in IRI severity, such as prolonged ischaemia time and non-heart beating

donor. Clinical data analysis obtained from various cohorts strongly supports ischaemia time as a strong risk factor of DGF (Ojo *et al.*, 1997; Senel *et al.*, 1998; Lebranchu *et al.*, 2005; Jeldres *et al.*, 2009; Jung *et al.*, 2010; Sharma *et al.*, 2010; Salamzadeh *et al.*, 2012; Ounissi *et al.*, 2013; Redfield *et al.*, 2016).

1.2.3. Delayed Graft Function; Early Consequences and Its Implication to Long-term Graft Survival

The most apparent early consequences of DGF are related to a more complex post-operative clinical course for the recipient, such as utilisation of RRT, requirement for additional intensive/high level care and medications, all of which result in prolonged hospitalisation and increased cost. Currently available data suggests an increase hospital length of stay of up to 8 days for patients with DGF (Miglinas *et al.*, 2013; Redfield *et al.*, 2016). An interesting approach to address the question of cost analysis related to DGF was made in the study by Snyder et al. Using a developed hypothetical analysis model, the study acknowledged a higher cost associated with an increased DGF incidence as a potential short-term complication of adding DCD kidneys to the donor pool. However, it also concluded that the cost is acceptable when compared to keeping the patients on dialysis (Snyder *et al.*, 2013).

DGF has also been shown to influence graft survival, patient survival and rejection rates. During shorter-term follow-up (within 1-year post-transplantation), DGF patients are reported to have poorer graft survival and significantly higher acute rejection rates (Dominguez *et al.*, 2004; Yarlagadda *et al.*, 2009; Miglinas *et al.*, 2013). During longer-term follow-up, however, the deleterious effect of DGF on graft and patient survival is less consistent. This may partly be attributable to the differences in the degree of the initial insult suffered by the allograft, hence producing either reversible or irreversible degrees of injury. It is plausible that the graft lost by the 1-year time point had suffered significantly more severe IRI, and thus underwent irreversible changes compared to the grafts that survived. Grafts that survived past the 1-year point may not have been as severely injured, thus regaining more normal function, resulting in a less clear cut link between DGF and graft survival.

Nevertheless, a systematic analysis of currently available evidence compiled by Yarlagadda et al. clearly suggests detrimental effect of DGF on acute rejection and long-term renal function. The result of this meta-analysis of 33 studies showed that the DGF cohort had a 41% increased risk of graft loss at 3.2 years follow-up, significantly higher serum creatinine level at 1 year and 3.5 years follow-up, and DGF was associated with 38% relative increase in the risk of acute rejection (Bronzatto *et al.*, 2009; Yarlagadda *et al.*, 2009). However, the study did not find any significant difference in 5-year patient survival between the DGF and

non-DGF group. Taken together, this analysis has provided a clear link between acute ischaemic kidney injury and long-term deterioration in function, despite a period of relatively "normal" function during earlier stages. Identification and validation of a mechanistic link between acute IRI and progression to chronic organ dysfunction has been gaining a lot of research interest. Several mechanisms have been proposed for the development of chronic dysfunction, which involves the role of cellular changes during ischaemia (oxygen and energy deprivation, pH alteration and ion re-distribution), the role of inflammatory mediators, the role of oxidative stress, the role of cellular components within the kidney (endothelial, epithelial and immune cells), and the role of epigenetics. It is important to consider these mechanisms not as separate pathophysiologic entities, rather as components of an intricate mechanistic network, which much overlap and cross-talk. The detailed mechanisms of which IRI leads to tissue injury and delayed function will be discussed in the following section on the biology of IRI.

1.3. Biological Basis of Ischaemia Reperfusion Injury

1.3.1. Organ Specific response to IRI

The cascade of responses subsequent to cessation and restoration of blood in different organs will generally follow a common and fundamental pattern, which will be discussed in detail in following subsections. The universal use of cold preservation in organ transplant procedures is based upon the knowledge that cellular damage can be delayed at low temperature in all organs. Nevertheless, the capacity of different organs to tolerate ischaemia, the threshold of injury reversibility, and the capability to limit the injury may vary significantly. Reports have shown that the time required to induce irreversible damage is different for different organs. This may partly be attributed to organ specific basal energy requirements, but also determined by tissue variation in the structure and function of microvascular beds and other cellular components within the organ (Kalogeris *et al.*, 2012). In the kidney, normothermic ischaemia of 30 minutes or less has been found to be well tolerated and caused no irreversible organ damage (Kalogeris *et al.*, 2012).

1.3.2. The Kidney; Anatomical & Physiological Considerations

The anatomy of the nephron and renal microcirculation plays a crucial role in understanding the effect of ischaemia on the kidney. In physiological conditions, kidneys receive approximately 20% of cardiac output. This blood flow is primarily channelled to the cortex, whereas a small proportion supplies the medullary region. This creates a gradient of

oxygen tension within the kidney, with the cortex being the most oxygenated region, the medulla being relatively hypoxic, and the papillae being the least oxygenated. Blood flow to the medulla is supplied by an intricate microvasculature network, which arises from the vasa recta, the continuation of efferent arterioles of the juxtamedullary glomeruli. Studies in rats have shown that pre- and post-glomerular arterio-venous shunting creates a relatively hypoxic environment within the kidney (Ngo et al., 2014). In comparison to other parts of the body, the kidney operates at lower oxygen tensions, both during normoxia and hypoxia (Safran et al., 2006). Moreover, in response to hypoxia, kidney blood flow may alter dramatically, especially to the outer medullary region. Altogether, these factors predispose the kidney to hypoxic damage. To date there is substantial evidence describing how hypoxia induces acute kidney injury (Granger and Korthuis, 1995; Kosieradzki and Rowinski, 2008; Basile et al., 2012). However, demonstrating the role of hypoxia in the progression of kidney injury in the longer-term, is more challenging. Several studies have shown an association of chronic hypoxia in the renal tubulointerstitium with oxidative stress and chronic inflammation, and that these factors are involved in the progression of CKD (Eckardt et al., 2005; Nangaku, 2006; Fine and Norman, 2008; Heyman et al., 2008). A recent rodent study has shown the significance of hypoxia alone in the progression of CKD. The authors reported increased urinary protein excretion and tubular vimentin expression as well as infiltration of inflammatory cells, in rats treated with dinitrophenol, a mitochondrial uncoupler, which increased renal oxygen consumption without altering oxidative stress (Friederich-Persson et al., 2013)

1.3.3. Cellular Response to Acute IRI and Pathways of Progression to Long-Term Functional Impairment

1.3.3.1. ATP Depletion and Intracellular pH Alteration

Cessation of an oxygen supply adequate to maintain normal cellular function is the main driver of ischaemic injury. This is immediately followed by a switch to an anaerobic pathway of energy production, which will only generate small amounts of high-energy phosphates and lead to decrease in intra-cellular pH due to the build-up of lactate, protons and nicotinamide adenine dinucleotide (NAD^+). Conversion of pyruvate to lactic acid is necessary to regenerate the lost NAD^+ in the anaerobic glycolysis pathway. This process acidifies the cytoplasm up to a point where the low pH starts to inhibit phosphofructokinase, a key enzyme of the glycolysis pathway. Insufficient blood flow to remove accumulating lactate will eventually stop energy production and further worsen the level of acidosis.

Ischaemic condition in cells results in metabolic substrate depletion. Ischaemic tissues contain much fewer glycogen granules than normal tissue (Kosieradzki and Rowinski, 2008). Exhaustion of cellular glycogen arrests anaerobic glycolysis. Unavailability of adequate adenosine tri-phosphate (ATP) to initiate glycolysis will also result in metabolic arrest, even if there is still glycogen available. Degradation of ATP to adenosine di-phosphate (ADP) and adenosine mono-phosphate (AMP) occurs very rapidly during ischaemia, aggravating energy source deprivation. AMP will be metabolised further to adenine nucleotides and hypoxanthine, which will contribute significantly to generation of reactive oxygen species during subsequent reperfusion (Devarajan, 2006).

1.3.3.2. Altered Ion Exchange and its Consequences

Intracellular accumulation of hydrogen ions will be compensated by increased Na^+/H^+ exchange resulting in the influx of sodium ions. In turn, the sodium ions will be exchanged for Ca^{2+} by the Na^+/Ca^+ exchanger. ATP depletion causes the cell to inactivate ATPases, including Na^+/K^+ ATPase and Ca^{2+} ATPase, resulting in even more intracellular Ca^{2+}. Some reports have suggested that this influx of extracellular Ca^{2+} only takes place during prolonged ischaemia and reperfusion, whilst during the initial phase of ischaemia, the increase in intracellular Ca^{2+} is primarily due to active redistribution of endoplasmic reticulum (ER) calcium (Schumacher et al., 1998; Kosieradzki and Rowinski, 2008). Reperfusion further increases intracellular Ca^{2+}. As extracellular H^+ is removed after the re-establishment of blood flow, the proton gradient will increase across cell membrane, leading to an increase in Na^+/H^+ exchanger function, which increases intracellular Ca^{2+} (Kalogeris et al., 2012).

The overload of Ca^{2+} is an important underlying mechanism for subsequent cellular pathology following IRI, which may lead to cell death. Ca^{2+} overload is detrimental to cell survival by triggering mitochondrial permeability transition pore (mPTP/mPT) activity, activating pathological Ca^{2+}/calmodulin-dependent protein kinases (CaMKs), stimulating calpains and generating danger signals (Kalogeris et al., 2012). Opening of mTP allows H^+ to move back into the mitochondrial matrix disrupting ATP synthesis. The opening of this non-selective pore will also lead to sudden influx of water, which in turn may cause mitochondrial swelling and rupture. Danger signals, such as calcium pyrophosphate and uric acid exert their effects by binding to inflammasomes. Binding to inflammasomes initiates cytokine release, which in turn activates transcription factors (NFkB), stimulating even more cytokine and chemokine release eventually leading to exacerbation of IRI.

The disruption in trans-membrane ion channels and the phospholipid bilayer due to ischaemic damage, eventually leads to accumulation of water in the intracellular

compartment. In addition, glycolysis pathway arrest and dephosphorylated ATP lead to continuous accumulation of metabolic intermediates and products (e.g. glucose-6-phosphate, a-glycerol phosphate, lactate, NADH, inorganic phosphatases, etc.), all of which cause an increase in intra-cellular osmolarity (Kosieradzki and Rowinski, 2008). Hyperosmolarity attracts water to the intracellular compartment, which leads to ischaemic oedema. In the transplantation setting, the use of hypertonic preservation solution was introduced to prevent ischaemic oedema, as introduction of isotonic fluid may generate a greater osmotic gradient.

Furthermore, oedema can develop in the cytosol affecting the outer cellular membrane, as well as within the cell organelles, further compromising cellular function. Different organelles will be impaired by the state of altered ion exchange and ischaemic oedema in different ways. For instance, ER requires a carefully regulated milieu to perform its function. Ischaemia impairs this fine-tuned environment by altering ion concentration/gradient and pH, preventing ER from performing many important biochemical reactions important to the cell, such as the folding of proteins (Kalogeris et al., 2012). The state of accumulation of misfolded and unfolded proteins in ER is known as ER stress., which will activate the unfolded protein response (UPR), in an attempt to degrade the unfolded protein. Failure to eradicate the unfolded protein causes cells to undergo apoptosis (Minamino et al., 2010).

1.3.3.3. The Role Hypoxia-Inducible Factor (HIF)

Cellular adaptation to hypoxia is largely regulated by a heterodimeric transcription factor, hypoxia-inducible factor (HIF), which consists of two sub-units; α and β. Whereas the β sub-unit is relatively insensitive to alteration in oxygen levels, the cellular concentration of the sub-unit alpha (HIF-α) is highly dependent on cellular oxygen levels, a process that involves hydroxylation of conserved residues (Tanaka *et al.*, 2014; Burslem *et al.*, 2017). HIF-α has two major isoforms; HIF-1α, HIF-2α and one additional minor isoform HIF-3α (Tanaka *et al.*, 2014; Tanaka, 2017). The main difference between HIF-1α and HIF-2α lies mostly in the variation of their N-terminal transactivation domain (N-TAD), which determine their binding to specific target genes (Loboda *et al.*, 2012). The difference in their regulation and action is still not fully understood. HIF-1α is detectable after a short-term hypoxic period, whilst HIF-2α is known to be only activated in chronic hypoxia, thus is associated with the regulation and survival of cancer cells and cellular adaptation to hypoxia (Hu *et al.*, 2003; Ratcliffe, 2007). Understanding of the role of HIF-3α is even less complete. Available literatures hypothesise that HIF-3α acts as negative regulator of HIF-mediated transcription (Loboda *et al.*, 2012).

1.3.3.3.1. The Regulation of HIF

HIF-1α is continuously expressed at low levels in the cell. In normoxia, HIF-1α levels are kept low by the action of HIF-prolyl hydroxylase domains (PHDs). In order to perform their catalytic function, the enzyme PHDs require O_2, Fe, and 2-oxoglutarate (an intermediate in the Tri-carboxylic acid cycle) (Rabinowitz, 2013). PHDs hydroxylate two proline residues in HIF-1α, which enables recognition of HIF-1α by von Hippel-Lindau tumour suppressor (pVHL), leading to proteosomal degradation of HIF-1α . This degradation process occurs very rapidly, resulting in a very short half-life of HIF-1α, thus making it undetectable in normoxic conditions. During hypoxia, catalytic function of PHDs is reduced or diminished, leading to accumulation of HIF-1α in the cytoplasm. Existing HIF-1α will form complexes with the constitutively expressed HIF-1β, leading to subsequent binding of the complex to hypoxia-response element (HRE) region, initiating gene transcription. A co-activator protein p300/CBP (CREB-binding protein) has been identified in a stable complex with HIF-1α, which was closely linked with HIF activity in inducing several hypoxia responsive genes (e.g. erythropoietin enhancer and vascular endothelial growth factor) (Arany *et al.*, 1996).

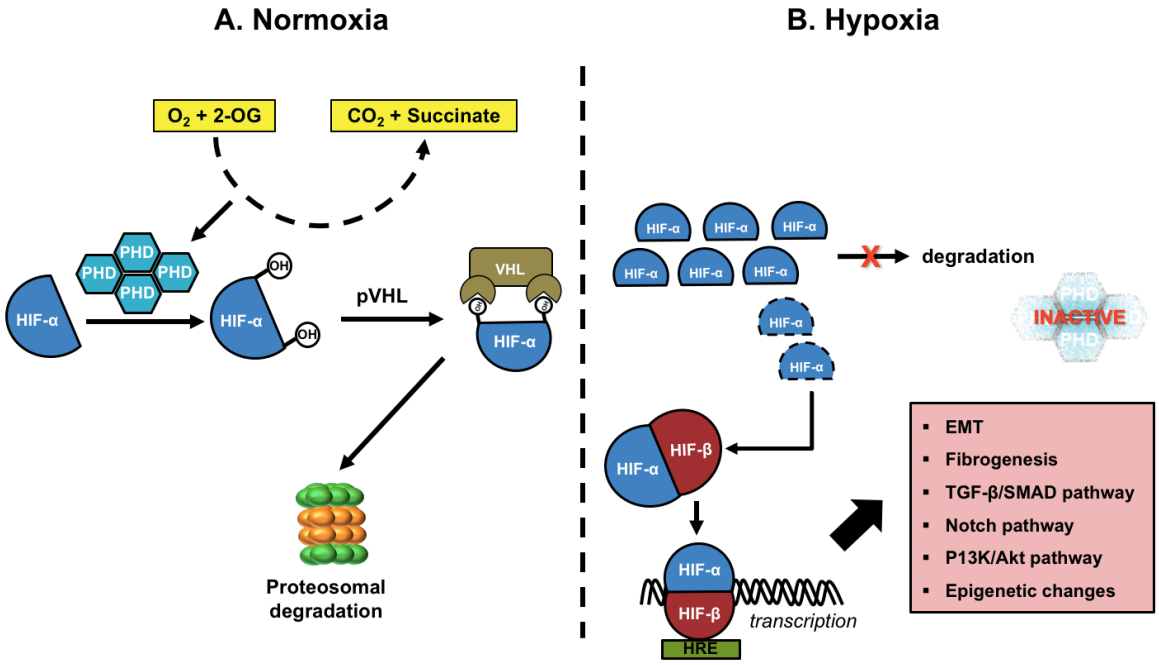

Figure 1-2 Regulation of Hypoxia-Inducible Factor

Schematic illustration of HIF-α regulation during normoxia and hypoxia. (HIF = hypoxia-inducible factor; PHD = prolyl hydroxylase domains; VHL = von Hippel Lindau; HRE = hypoxia-response element)

Study of ischaemic rat kidneys identified that HIF-1α was expressed predominantly in tubular epithelial cells, while HIF-2α was expressed mainly in vascular endothelial cells and interstitial fibroblasts (Rosenberger *et al.*, 2002; Tanaka, 2017). HIF regulates the transcription of numerous genes to control haematopoiesis, angiogenesis and anaerobic metabolism in response to hypoxia (Mole *et al.*, 2009). Conde et al. found that HIF-1α is expressed during ischaemia, but disappears 24 hour after hypoxia is reversed, then reappears in late reperfusion (Conde *et al.*, 2012), suggesting recurrence of tissue hypoxia during the cell regenerative phase (Nangaku *et al.*, 2013). In human kidney allograft biopsies, up-regulation of HIF is detected immediately after engraftment, at 10-14 days post procedure, but not after 3 months (Rosenberger *et al.*, 2007). From these findings, we can conclude that kidney hypoxia occurs not only during the acute phase of ischaemic injury but also during the recovery phase (Tanaka *et al.*, 2014), presumably due to the activity of oxygen-consuming regenerative processes.

1.3.3.3.2. HIF and the Development of Fibrosis

The activation of HIF plays a pivotal role in both immediate cell responses to injury as well as long-term regulation of fibrosis. Current evidence is contradictory regarding the actual role of HIF in progression of CKD. Experiments using cobalt chloride ($CoCl_2$) and dimethyloxalyglycine (DMGO) to stabilise HIF and increase expression of HIF target genes in a mouse model of renal fibrosis showed up-regulation of vascular endothelial growth factor (VEGF), glucose transporter 1 (GLUT1) and cell proliferation, indicating a reno-protective effect of HIF (Deng *et al.*, 2010). Another study in mice assessed the relationship between HIF-1, ischaemic acute kidney injury (AKI) and the development of fibrosis by increasing HIF levels using pre-ischaemic pharmacological inhibition of PHD. Kobayashi et al. documented repression of fibrogenesis in mice subjected to unilateral ureteral obstruction (UUO) by global activation of HIF (Kobayashi *et al.*, 2012). Using a murine model of IRI, Kapitsinou et al. showed a protective effect of pre-ischaemic PHD inhibition in mice subjected to acute ischaemic kidney injury. Pre-ischaemic increase in HIF level caused by PHD inhibition was associated with reduced fibrotic area and less alpha-smooth muscle actin (α-SMA) expression at 21-day post IRI (Kapitsinou *et al.*, 2012). Interestingly, this anti-fibrotic effect was not observed when PHD inhibition was given after IRI, or in PHD-inhibitor treated animals lacking endothelial HIF-2α (Kapitsinou *et al.*, 2012; Kapitsinou *et al.*, 2014).

Conversely, extensive evidence is available to support a pro-fibrotic role of HIF. Wang et al. showed decreased collagen and α-SMA induction by silencing HIF-1α gene in rats with

chronic renal ischaemia (Wang *et al.*, 2014c). Moreover, HIF-1α knockout was shown to prevent transforming growth factor-β1 (TGF-β1) induced epithelial-to-mesenchymal transition (EMT) in mouse proximal tubular epithelial cells subjected to unilateral ureteral obstruction (UUO) (Higgins *et al.*, 2007). Endothelial HIF-2α was also reported to play an important role in protection against ischaemic kidney injury. Despite some discrepancies, current findings clearly indicate an association between ischaemia, post-ischaemic increases in HIF levels and long-term pro-fibrotic changes. Post-ischaemic renal fibrogenesis occurs through several mechanisms, such as direct transcriptional regulation of pro-fibrotic genes, epithelial-to-mesenchymal transition (EMT) and induction of epigenetic changes, all of which may be driven by HIF activation, either through direct regulation or indirectly, involving crosstalk with multiple signalling pathways (Higgins *et al.*, 2008; Liu *et al.*, 2017).

1.3.3.4. Mitochondrial Dysfunction and Oxidative Stress

The role of mitochondria is central and very complex in the cellular response to IRI. Initially, to neutralise the continuous increase of intracellular Ca^{2+}, cells will initiate the uptake of Ca^{2+} into the mitochondria using a mitochondrial Ca^{2+} uniporter. However, this mechanism alone will not be sufficient, especially if the initial ischaemic insult is severe or prolonged.

There are several ways how mitochondria contribute to cell death after IRI. Firstly, ischaemia alone inhibits mitochondrial metabolism, resulting in rapid depletion of ATP. Secondly, during the initial phase of ischaemia, the relatively acidic intracellular milleu keeps the mitochondrial permeability transition pore (mTP) in the mithocondrial membrane inactive. However, upon reperfusion, mTP pores open, which in turn alters mitochondrial transmembrane potential significantly, allowing non-selective in/efflux of molecules leading to mitochondrial depolarisation (Kalogeris et al., 2012; Elshenawy et al., 2017). Prolonged opening of mPTP leads to apoptosis, and has been used to differentiate between irreversible and reversible reperfusion injury. Moreover, the mitochondrial electrochemical gradient is also disrupted, interfering with mitochondrial capacity to generate ATP. Thirdly, mitochondria act as a source of reactive oxygen species (ROS) after an ischaemic insult, mainly attributed to the disturbance in the electron transport chain (e.t.c). Lastly, mitochondrial morphology may also be impaired following IRI. Conditions such as low ATP level and increased ROS generation can cause excessive mitochondrial fission, which also contributes to post-ischaemic cell death (Kalogeris et al., 2012).

Tissue injury due to oxidative stress plays a role in the reperfusion component of IRI. However, it is important to understand that the severity of reperfusion injury is a result of the

severity of ischaemia. Various sources of ROS have been identified in different tissues; these include xanthine oxidase (XO), NADPH oxidase, nitric oxide synthase (NOS), lipoxygenase/cyclooxygenase, monoamine oxidase and the mitochondria. Similar sources of ROS have also been identified in kidney IRI (Granger and Kvietys, 2015).

Degradation of ATP to ADP and AMP during ischaemia leads to accumulation of hypoxanthine, which acts as the main fuel for ROS formation. Availability of O_2 and restoration of ATP in tissue upon reperfusion enables the conversion of hypoxanthine to xanthine, generating superoxide and hydrogen peroxide, which subsequently leads to production of more reactive secondary species. Moreover, altered redox status caused by the initial ischaemic injury means that there is higher level of NADH available relative to NAD^+, which has been shown to be capable of enhancing production of O_2^- independent of XO. (Granger and Kvietys, 2015).

There are two forms of superoxide-producing nitrous oxide (NOXs) known to be involved in tissue reperfusion injury. The main isoform is from macrophages and neutrophils (phagocyte NOXs), and the other isoform is produced by non-phagocytic cells of the vascular wall (vascular NOXs) (Kalogeris et al., 2012). Phagocyte NOXs remain inactive until stimulated, and are responsible for 'respiratory burst' of oxidant production, characterised by sudden and marked increase of oxidant synthesis, immediately following phagocyte activation by inflammatory mediators (Kvietys and Granger, 2012; Raedschelders et al., 2012). Physiologically, this serves as a host defence mechanism, whereby the reactant species are released extracellularly or into phagolysosomes (Kalogeris et al., 2012). On the other hand, vascular NOX is present in a fully-active state, but at low-levels of constitutive activity and has subtle oxidant effects. A minor proportion of vascular NOX is maintained in a separate compartment in the cytosol, and behaves similar to phagocyte NOX (Kalogeris *et al.*, 2012; Kvietys and Granger, 2012). Although the generation of ROS from phagocyte NOX and vascular NOX are distinct, the activation of both cell types has been shown to be involved in the pathogenesis of IRI in most organs, including the kidney (Kvietys and Granger, 2012; Raedschelders et al., 2012).

In conclusion, a high mitochondrial ROS level is a major feature of cellular reperfusion injury, which reflects increased ROS production and inadequate ROS disposal. This leads to further deleterious effect to the cells, such as alteration in mitochondrial oxidative phosphorylation, depletion of ATP, increase in intra-cellular calcium levels, activation of proteases and lipid peroxidation (Paller *et al.*, 1984; Weinberg, 1991; Ratliff *et al.*, 2016). Furthermore, oxidative stress may also damage cellular proteins and DNA, which may lead to apoptosis and cell death (Kehrer and Klotz, 2015).

1.3.3.5. Endothelial Injury and Vascular Rarefaction

Depending on its severity, ischaemia alone may cause endothelial injury/dysfunction. As a consequence, dysfunctional endothelium will no longer able to serve as an adequate barrier between the interstitium and the vascular compartment, lose its ability to control adhesion and infiltration of immune/inflammatory cells and fail to regulate key haemostatic mechanisms (Kalogeris *et al.*, 2012). Endothelial cells contribute to progression of IRI by two main mechanisms; (1) increased permeability and (2) vasomotor dysregulation.

Increased endothelial permeability can be attributed to direct injury to the endothelial cells, actin cytoskeleton alterations, cell-to-cell junctional dissociation and enhanced leukocyte-endothelial interactions (Sutton, 2009; Verma and Molitoris, 2015). In normal conditions, the endothelium is maintained as a monolayer, which requires the formation of junctional complexes. These junctional complexes are highly sensitive to physiological or pathophysiological stimuli, such as ROS, cytokines, lipid mediators and proteases (Kalogeris et al., 2012). The release of pro-inflammatory mediators and ROS during IRI will induce phosphorylation, internalisation and degradation of junctional complex proteins resulting in endothelium structural damage (Kumar et al., 2009). Disruption of glycocalyx and up-regulation of cellular adhesion molecules, such as ICAM, VCAM and selectins that will promote accumulation of leukocytes (Bonventre and Yang, 2011).

Increased level of prostaglandin H_2, leukotrienes C4 and D4 and increased sympathetic nerve stimulation have all been documented to follow endothelial injury, leading to excessive vasoconstriction. As the result of increased sympathetic activity, there is a reduction in circulating NO, which will further amplify the degree of vasoconstriction (Bonventre and Yang, 2011). The injured endothelium will also release chemotactic cytokines, increasing leukocyte-endothelial adhesion during reperfusion. Increased leukocyte activation and leukocyte-endothelial adhesion stimulates the release of vasoactive cytokines, including TNF-a, IL-1b, IL-6, IL-12, IL-15, IL-18 and IL-32, which in turn amplify the vasoconstriction that occurs (Bonventre and Yang, 2011). As a consequence, a greater degree of ischaemia will ensue, adding more injury to the initial insult as well as affecting subsequent repair processes.

A significant reduction in peritubular capillary (PTC) density has been suggested as a possible factor that makes the post-ischaemic kidney susceptible to further deterioration of function. Using the bilateral ischaemia reperfusion rat model, Basile et al. showed a 30-50% permanent reduction in PTC in the outer medullary region despite normal tubular morphology. The ischaemic group was also reported to develop subsequent tubulointerstitial fibrosis after longer follow-up (Basile *et al.*, 2001). Similar findings were also reported in a

kidney transplant cohort. Loss of PTC after during the first 3 months post-transplant was associated with increased interstitial fibrosis, tubular atrophy and reduced renal function (Steegh *et al.*, 2011).

Basile et al. (Basile and Yoder, 2014) summarised three possible mechanisms in which post-ischaemic PTC loss could contribute to the development of long-term fibrosis; (1) exacerbation of pre-existing hypoxia, (2) changes in outer medullary haemodynamics and (3) endothelial-to-mesenchymal transition (EndoMT), which promotes proliferation of new fibroblasts. Exacerbation of hypoxia is mainly the result of increased intra-renal microvascular resistance due to vasoactive cytokine activity, as discussed previously. This is also closely tied to alteration in medullary haemodynamics. It is hypothesised that hypoxia and medullary haemodynamic alterations lead to apoptosis, which perpetuates PTC loss. EndoMT was proposed as an alternative explanation of PTC loss. A study on bilateral ischaemic kidney mouse model showed co-existing staining of endothelium (CD31 or cablin) and mesenchymal marker (S100A4) (Basile *et al.*, 2011). The role of EndoMT is still not clearly understood, but recently has been gaining increasing interest.

Moreover, IRI induced inflammatory conditions reduces naturally occurring anti-coagulant activity (Verma and Molitoris, 2015). The combination of excessive vasoconstriction, leukocyte activation and subsequent coagulation system activation may lead to mechanical obstruction of the renal micro-capillary network and reduction in blood vessel patency, which further compromises regional microcirculation, especially in the outer renal medulla.

1.3.3.6. Role of Damaged Tubular Epithelial Cells, Failed Tubular Recovery & Tubular Maladaptive Repair

The proximal tubular epithelial cells (PTECs) are the main site of injury in the acutely ischaemic kidney. Consequently, the severity and recurrence of injury at this site acts as an important factor in determining reversibility of the damage and progression to long-term organ failure. Tubular injury induced by diphtheria toxin showed that tubular injury alone can initiate interstitial fibrosis, which primarily developed around proximal tubules (Takaori *et al.*, 2016). Further experiments utilising toxin receptor-mediated cell knock-out (TRECK) enabled selective injury only to proximal tubules, which again induced transition of fibroblasts to myofibroblats, leading to fibrosis. Repeated and more severe selective injury was reported to induce interstitial fibrosis, distal tubular injury and glomerulosclerosis and atubular glomeruli (Takaori *et al.*, 2016; Takaori and Yanagita, 2016).

Ischaemic tubular injury is most evidently found in the S3 segment of the proximal tubule (Heyman et al., 2010), and recent studies have highlighted the significant role of PTECs in renal IRI (Han et al., 2002; Chevalier, 2016). Ischaemic injury to TEC initially results in loss of cytoskeletal integrity. The degree of cytoskeletal alteration depends on the severity and duration of ischaemia. This loss of cytoskeletal integrity further modifies cellular polarity, cell-to-cell interactions as well as cell-to-matrix interactions, and loss of function (Sutton and Molitoris, 1998).

Kidney tubular epithelial cells (TECs) have been shown to play active roles in progression of post-ischaemic tissue damage. There is substantial evidence that TECs release pro-inflammatory and chemotactic cytokines in response to IRI (Sutton and Molitoris, 1998; Kapper et al., 2002; Moll et al., 2013), which includes TNF-α, IL-6, IL-1β and TGF-β in addition to chemokines, such as MCP-1, IL-8, RANTES and ENA-78 (Kapper et al., 2002). This leads to recruitment of immune cells, important for repair following IRI, but also involved in the damage that occurs. In addition, damaged epithelial cells produce damage-associated molecular patterns (DAMPs), which act as warning signals by activating a series of pattern recognition receptors (PRRs), known as Toll-like receptors (TLR2, TLR3 and TLR4), express complement receptors and other co-stimulatory molecules which regulate T lymphocyte activity (Leemans et al., 2005; Wu et al., 2007; Bonventre and Yang, 2011). Down-regulating the expression of TLR-2 on kidney parenchymal cells were also shown to reduce the level of pro-inflammatory cytokines (IL-1β, IL-6, MCP-1) produced by the kidney, thus providing functional and structural protection against IRI progression (Leemans et al., 2005). Wu et al. demonstrated up-regulation of TLR4 post IRI in TECs and inhibiting TLR4 effectively prevented progression of IRI (Wu et al., 2007). Futhermore, TLR4 knockout mice also showed reduced tubular injury with better preservation of renal function after induction of IRI compared with wild type mice (Pulskens et al., 2008).

Dedifferentiation of proximal tubule cells caused by IRI may not always be followed by complete re-differentiation and resolution of injury. Rodent kidneys subjected to IRI still had a proportion of abnormal tubules with flat epithelium without brush borders after 14 days. These cells were morphologically abnormal, atrophic and growth arrested. As well as showing strong TGF-β signalling, these abnormal cells also showed persistent loss of phosphate and tension homologue (PTEN) associated with increased expression of vimentin, pro-fibrotic c-Jun N-terminal kinase (JNK) activation and platelet-derived growth factor (PDGF)-B production (Lan *et al.*, 2012a).

Tubular cell secretion of cytokines and growth factors is important for cell survival and repair, however, this should halt once complete regeneration is achieved (Bonventre, 2010;

Venkatachalam *et al.*, 2015). Study of five different murine models of acute kidney injury revealed large numbers of proximal tubule were arrested in the G2/M phase of the cell cycle, which is associated with persistent activation of JNK signalling and higher production of *COL4A1* and *ACTA2* mRNA levels (Yang *et al.*, 2010). A number of studies by Venkatachalam et al. also showed that tubular cell arrest and atrophy is linked with increased secretion of fibrogenic peptides, which accelerates proliferation of interstitial pericytes/fibroblasts through multiple pathways, including PI3K-Akt-mTOR, ERK-MAPK, JNK-MAPK and previously mentioned TGF-β pathways (Suzuki *et al.*, 2001; Canaud and Bonventre, 2015; Venkatachalam *et al.*, 2015), eventually resulting in nephron loss. These findings are the basis of validating several cell cycle arrest biomarkers in the detection of acute kidney injury (Kashani *et al.*, 2013).

Tubular cells maladaptive repair is also associated with activation of several other pro-fibrotic pathways, such as Notch and Wnt signalling. Recent work using a mouse model with inducible proximal tubule Wnt1 secretion displayed interstitial myofibroblast activation and proliferation and increased matrix protein production (Maarouf *et al.*, 2016). Interestingly, no evidence of inflammatory cytokine expression, leukocyte infiltration, or epithelial injury were detected in these fibrotic kidneys, demonstrating direct paracrine Wnt1 activity in initiating interstitial fibrosis through tubulointerstitial crosstalk (Maarouf *et al.*, 2016).

1.3.4. IRI and Immune System Activation

IRI is a result of various mechanisms, including the host inflammatory/immune response. The immune system activation exerts its effect largely upon reperfusion of an ischaemic kidney. However, it is important to recognise that the initiation of inflammation occurs during ischaemia, whilst post-ischaemic events contribute to its amplification. These reperfusion events include oxygen re-fuelling, ROS generation, endothelial dysfunction, leukocyte recruitment, chemokine and cytokine synthesis and complement activation (Jang *et al.*, 2009; Kvietys and Granger, 2012). The ischaemic kidney is not merely the target of immune activation. Instead, it plays an active role in promoting immune activation.

An acute inflammatory component of IRI involves the expression of cell surface adhesion molecules. To evaluate the effect of IRI on the expression of these adhesion molecules, rat renal grafts were cold preserved for 2, 4, 6, 12, 24 and 48 hours, before being transplanted into syngeneic recipients (Dragun *et al.*, 2001). This study revealed that longer duration of cold-ischaemia led to loss of endothelial integrity and increased expression of VCAM-1. Ischaemic grafts also displayed enhanced intra-graft pro-coagulant capacity and a worse tubular necrosis score (Dragun *et al.*, 2001). Unexpectedly, renal functions measured

by creatinine and urea was not different between grafts with shorter ischaemia and grafts with longer ischaemia time. This implies that there are potentially injurious processes occurring after moderate IRI that are clinically undetectable. Whether the same can be extrapolated to the effects of IRI on long-term allograft function in patients receiving ischaemic allografts but who do not develop DGF remains an important research question.

1.3.4.1. The Role of Neutrophils and Macrophages

Neutrophil adhesion to dysfunctional endothelial cells is a rapid and important component in the initiation of damage to the ischaemic kidney. Recruitment of neutrophils by endothelial cells requires the expression of ICAM1, E and P selectin, which cross-talk with integrins and L-selectin on polymorphonuclear (PMN) cells (Thornton *et al.*, 1989; Kosieradzki and Rowinski, 2008; Yago *et al.*, 2015), however the exact mechanism and trafficking of neutrophils in renal IRI is not yet clear. Neutrophils have been shown to migrate into the transplanted organ within 6 hours of reperfusion and are attracted by chemokines, such as CXCL8, CXCL10, IL-17 and MCP-I (Neto *et al.*, 2004; Kosieradzki and Rowinski, 2008; Chaturvedi *et al.*, 2013; Kolaczkowska and Kubes, 2013). Damaged cells will be killed by neutrophils by direct phagocytosis or degranulation, releasing proteases, myeloperoxidase, nitrogen species, antimicrobial peptides and cytokines (Kinsey *et al.*, 2008). The presence of neutrophils in the glomeruli after reperfusion was reported to have a deleterious consequence to long-term kidney outcomes, with higher serum creatinine levels at 3 and 6 months after transplantation (Koo *et al.*, 1998; Friedewald and Rabb, 2004). Inhibiting the accumulation of neutrophils in the kidney or blocking neutrophils-endothelial interactions may prevent acute kidney injury (Haug *et al.*, 1993; Kelly *et al.*, 1994; Kelly *et al.*, 1996; Jang and Rabb, 2009; Chaturvedi *et al.*, 2013; Yago *et al.*, 2015). In contrast, others have failed to reproduce the beneficial effects of neutrophil depletion and reported neutrophil independent mechanisms in the pathophysiology of acute tubular injury (Thornton *et al.*, 1989; Salmela *et al.*, 1999; Melnikov *et al.*, 2002). Nevertheless, the majority of evidence supports a role of neutrophils in the development of post-ischaemic injury, by mechanisms including obstruction of renal microvasculature and the releasing free radicals and proteases (Friedewald and Rabb, 2004).

The role of macrophages in renal response to IRI is complex. Macrophages has been shown to promote tubular injury during the initial phase of IRI. On the other hand, suppressing macrophage function during the repair process (at later time points post reperfusion) has been shown to suppress tubular proliferation, thus impairing the normal recovery process. Studies have described the involvement of macrophages in the early inflammatory response, during cellular regeneration and tissue repair as well as the

development of fibrosis. These diverse roles are played by different sub-types of macrophages based on their activation and functional states. Classical activation of macrophages is driven by interferon gamma (IFNγ). Ischaemia induced cellular injury also produces DAMPs, which will contribute to macrophage activation. These classically activated M1 macrophages are pro-inflammatory in nature, thus associated with tissue damage. However, they also play an important role in clearing apoptotic cells and debris, thereby initiating the repair process (Huen and Cantley, 2015). Alternatively activated macrophages include M2a macrophages, which are responsible for wound healing and M2b macrophages, also known as immunoregulatory macrophages. Generally, M2 macrophages activate regulatory T-cells (T_{Reg}) and restore renal tissue homeostasis (Huen and Cantley, 2017), by promoting tubular proliferation and limiting renal injury. M2a macrophages are activated through IL-4/IL-13 binding to IL-4 receptor, which leads to production of growth factors, collagen precursor synthesis and generation of extracellular matrix. M2b macrophages regulate inflammatory response by producing immunosuppressive cytokines, IL-10 and TGF-β. Production of TGF-β is to limit inflammatory cytokine production, but at the same time may contribute to activation of pro-fibrotic pathways. When injury persists, chemokines, macrophage colony stimulating factors (M-CSF) and IL-34, are secreted to sustain monocyte recruitment and retention of macrophages (Huen and Cantley, 2017). Blockade of M-CSF receptor has protective effects following transplantation (Jose *et al.*, 2003). Retention of M2b macrophages in the injured tissue will produce macrophages-derived factors, which subsequently activate and support myofibroblasts, inducing extracellular matrix deposition and fibrosis. The signals responsible for retaining pro-fibrotic macrophages in the kidney remain unclear, but studies using unilateral ureteral obstructive (UUO) rodent model suggest a role for the chemokine receptors CCR1, CCR2, CX3CR1 (Huen and Cantley, 2017).

1.3.4.2. The Role of Complement System

The complement system plays an important role in the post-ischaemic inflammatory process. The importance of complement in the kidney transplantation setting was highlighted in several studies, primarily linking complement allotype and complement gene expression to transplant outcome (Brown *et al.*, 2006; Naesens *et al.*, 2009). In IRI, complement has been identified as an important mediator (Zhou *et al.*, 2000; Sheerin *et al.*, 2008; Danobeitia *et al.*, 2014).

Complement activation in the kidney occurs predominantly through the alternative pathway. A murine study of renal IRI identified the re-distribution of the complement inhibitor, complement receptor 1-related protein (Crry) from the tubular basolateral surface

prior to complement activation and C3 deposition (Thurman et al., 2006). Interestingly, in a non-ischaemic milieu, the deposition of C3 on the basolateral surface was not correlated with any apparent abnormality. Mice deficient in Crry showed worse renal injury, which was correlated with increased mononuclear phagocyte infiltration and TEC apoptosis (Miao et al., 2014). In addition, injured peritubular endothelium may allow plasma C3 into the tubulointerstitial space, providing sufficient C3 to exceed local complement regulation (Brar and Quigg, 2014).

A number of studies have also investigated the role of C5 in the response to renal IRI and kidney transplantation. Ischaemic insult to the kidney has been shown to involve both C3a and C5a with up-regulation of their respective receptors (C3aR and C5aR). C3a and C5a generated during IRI were shown to increase pro-inflammatory cytokine/chemokine production by macrophages, and was associated with increased kidney injury molecule (KIM)-1 expression by proximal TECs (Peng *et al.*, 2012). A comparison between the two complement components, however, showed a predominant role of C5 (Peng *et al.*, 2012). Moreover, the membrane attack complex C5b-9 has been linked to up-regulation of collagen gene expression in renal TECs, and suggested as a potential target for IRI prevention (Zhou *et al.*, 2000; Abe *et al.*, 2004).

1.3.4.3. The Role of Lymphocytes

Several lymphocyte sub-populations have been identified as important components of the renal response to IRI. This includes; natural killer (NK) and NKT cells, renal dendritic cells (DCs), T cells and B cells. Substantial evidence is available to link all of these sub-types to the renal response to IRI, mainly linking their actions to direct targeting of injured tubular and endothelial cells, activation of neutrophils and macrophages, and secretion of pro-inflammatory cytokines, such as IFN-γ, TNF-α, IL-4 and IL-10.

Although initially regarded as by-standers, current evidence suggests that T cells are involved in the pathogenesis of IRI. Depletion of CD4 and CD8 T cells in mice with renal IRI has been shown to improve renal function and reduce neutrophil infiltration and tubular atrophy (Rabb *et al.*, 2000). Furthermore, reconstitution of T cells in these T cell-deficient mice restored the level of injury (Burne *et al.*, 2001). Pre- and post-ischaemic adoptive transfer of regulatory T cells (Tregs) has been shown to protect the kidney from ischaemic injury, reduce TNF-α and IFN-γ production and accelerate repair (Kinsey *et al.*, 2009; Monteiro *et al.*, 2009; Kinsey *et al.*, 2013; Kinsey and Okusa, 2014).

B cells are involved in the adaptive immune response to IRI by releasing antibody. To date, available studies showed a predominantly harmful effect of post-ischaemic B cell

activation (Linfert *et al.*, 2009). Depleting B cells in mice improves renal function and reduces tubular injury after ischaemia (Burne-Taney *et al.*, 2003). A study by Jang et al. reported that B cell-deficient mice subjected to ischaemia showed more tubular proliferation, less tubular atrophy and higher expression of IL-10 and VEGF (Jang *et al.*, 2010). Further adoptive transfer of B cells into these mice exerted the opposite effect, suggesting that B cells may interfere with the post-ischaemic repair processes in the kidney. In contrast, another study found worse post-ischaemic renal injury in mice lacking all mature B cells (Renner *et al.*, 2010), suggesting a more complex and divergent role for B cells in the progression of IRI.

1.4. MicroRNA; an Overview of Structure, Biology and Function

1.4.1. Introduction to MicroRNA

A microRNA (miRNA) is a small non-coding RNA consisting of only ~20-30 nucleotides in length. miRNA was first discovered in the nematode *Caenorhabdtis elegans* by the joint work of Victor Ambros, Rosalind Lee and Rhonda Feinbaum in 1993 (Lee *et al.*, 1993). Their initial work identified Lin-4 as a small non-coding RNAs, which acts as an endogenous regulator of various genes that control developmental timing in *C. elegans* (Carthew and Sontheimer, 2009). This finding led to a series of important discoveries, which have shaped our current understanding of the complexity and regulation of the transcriptome. MiRNAs are highly conserved across different mammalian species and play a pivotal role in cellular functions in normal conditions, such as cellular proliferation, cell cycle and developmental processes, cellular differentiation and apoptosis, as well as in a range of pathological processes, including cancer, degenerative diseases, auto-immune diseases, fibrogenic processes and IRI (Friedman *et al.*, 2009; Bernardo *et al.*, 2012). A miRNA can play its regulatory function by targeting several messenger RNAs (mRNAs), and may influence one or more pathways involved in cellular function. This ability to regulate multiple genes in a pathophysiological network is an attractive feature for the use of miRNA as biomarkers and therapeutic targets. The effect of a stimulus, such as ischaemia and reperfusion injury is exerted not only by one distinct mechanism, but through several synergistic pathways. Identification and targeting key miRNAs involved in this process would allow more comprehensive monitoring of a pathologic process and potentially enable a greater therapeutic effect.

MiRNA is not the only post-transcriptional regulatory mechanism identified in cells. Evidence is available on the role of other non-coding RNAs, such as long non-coding RNA (lncRNA) and short interfering RNA (siRNA), in the regulation of various cellular functions.

As the name implies, the nucleotide length is the main difference between lncRNA (more than 200nt) and short non-coding RNAs (i.e. siRNA and miRNA). LncRNA affects both RNA processing and protein function by complementary binding to its target RNA or directly interacting with target protein and facilitating riboprotein complex formation (Wilusz *et al.*, 2009). In principle, siRNA and miRNA function through similar mechanisms, thus cannot be distinguished based on their function alone. However, differences exist in their nature, structure, precursor and function as described in Table 1-3.

Table 1-3 Distinction between the main features of siRNA and miRNA

Characteristics	miRNA	siRNA
Occurrence	Naturally occurs across all species (plants, animals, human)	Occurs in plants and lower animal species. Presence in mammals is questioned
Structure	Single stranded, 19-25nt	Double stranded, 21-22nt
Interaction to target and Mode of action	No exact complementarity to target mRNA required. Result: mRNA decay, translational repression of many target mRNAs	Exact match to target mRNA needed Result: mRNA endonucleolytic cleavage, specific genes knock-down, minor off-target effects
Biogenesis	Expressed by miRNA encoding genes (different from genes that they regulate)	Expressed by the same genes that they regulate
Precursors	Precursor miRNA (pre-miRNA); hairpin structure containing 70-100nt with interspersed mismatches	Double stranded RNA containing 30 to >100nt
Clinical applications	Diagnostic tool / biomarker Therapeutic target	Therapeutic target

Increasing evidence links miRNAs to various physiological and pathological processes positioning miRNA as an attractive candidate for a diagnostic tool or therapeutic target (Schena *et al.*, 2014; Wilflingseder *et al.*, 2014). Moreover, unlike mRNA, the short nature of miRNA and its resistance to cleavage make miRNA very stable (Bhatt *et al.*, 2011; Scian *et al.*, 2013a; Wilflingseder *et al.*, 2014). MiRNAs are reliably detected in body fluids or tissues. To compensate their diminutive size and lack of exact homology to target mRNA sequence miRNAs are present in high copy number, which facilitates in situ detection of miRNAs in blood, urine and fresh frozen and formalin fixed paraffin embedded tissues (Nuovo, 2010).

1.4.2. MicroRNA Biology and Function

MicroRNAs are found intracellularly in protein complexes and extracellularly in microvesicles in body fluids, such as urine or plasma (Bhatt *et al.*, 2011; Maluf *et al.*, 2014; Wilflingseder *et al.*, 2014). MicroRNA biosynthesis involves a relatively complex pathway (Figure 1-3). Pri-miRNA, which is several kilobases in length, is derived from transcription of miRNA genes. Pri-miRNA has a distinct hairpin structure, which is recognised by a nuclear

protein, DiGeorge syndrome critical region 8 (DGRC8). The DGRC8 pri-miRNA complex recruits the RNAse Drosha to form the Microprocessor complex. This process leads to the cleavage pri-miRNA at the base of stem-loop, producing pre-miRNAs containing approximately 70 nucleotides. Pre-miRNA is transferred to the cytoplasm by exportin 5. In the cytoplasm, pre-miRNA is further cleaved to mature miRNA, which consists of 21-25 nuclotides by the enzyme Dicer. The mature miRNA will interact with members of the argonaute protein (AGO) family to form the RNA-induce silencing complex (RISC), which is the effector complex of miRNA. MiRNA then plays its role by either blocking protein translation or degradation of target messenger RNA (mRNA) (Bhatt *et al.*, 2011). The RISC is directed to target mRNA based on the complementary sequences in the miRNA and mRNA (Bhatt *et al.*, 2011). The biology of miRNA can be modified by the introduction of miRNA mimic to over-express a certain miRNA, or by miRNA inhibitor or anti-miR (Figure 1-3). The modification of miRNA expression has the potential to be exploited in miRNA research and future therapies.

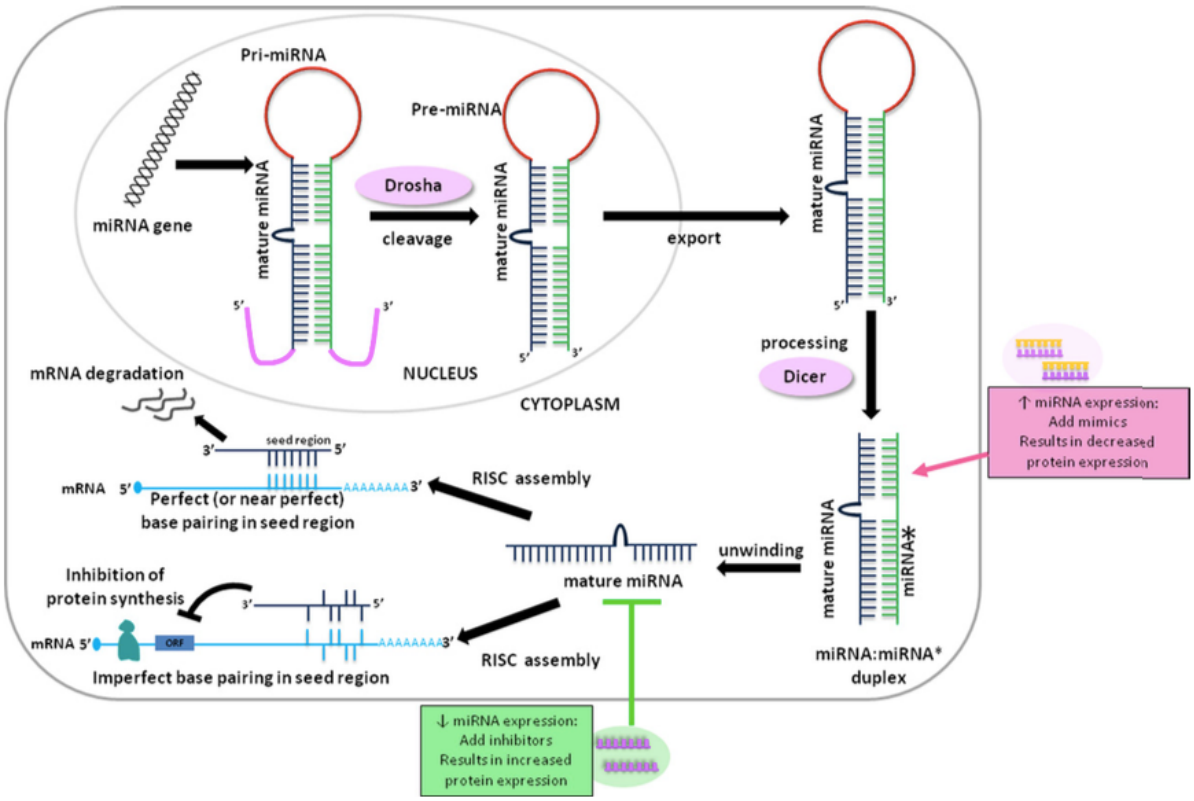

Figure 1-3 Illustration of miRNA biology and mechanism of action

Primary miRNAs (Pri-miRNA) are transcribed from a miRNA gene. This is followed by Drosha processing, which cleaved Pri-miRNAs into precursor miRNA (Pre-miRNA). Following export of Pre-miRNA into the cytoplasm, Dicer processes Pre-miRNAs into mature miRNA, which will be assembled into RNA-induce silencing complex (RISC) to perform its function (Bernardo *et al.*, 2012)

1.4.3. MiRNA Nomenclature

MiRNA nomenclature begins with the species of its origin; 'hsa' for homo sapiens, 'mmu' for mouse, 'rno' for rat, 'd' for drosophilia, and many others. Description of whether it is a mature sequence or a precursor follows the description of the species. Precursor hairpins are written as 'mir', the gene that encodes a particular miRNA is written as 'MIR', whilst mature sequence is written as 'miR'. This is then followed by number(s) as the actual name of the miRNA, which usually, but not always indicate the order of naming or timing of discovery relative to other miRNAs. Closely related miRNA with nearly identical sequences are annotated with an additional lower case after the number set (for example, miR-34a). In addition, identical miRNA sequences may be excised from opposite arms of the same precursor. These miRNAs will be labelled by adding '5p' or '3p' at the end of their annotations, indicating excision from either the 5'- or 3'- arm respectively (for example, miR-21-5p or miR-21-3p). Addition of asterisk is given to indicate the "passenger" strand of the mature miRNA, which is usually thought to be degraded, except in a small number of miRNAs where it may also be functional.

1.5. MicroRNAs; Their Relevance to Normal Cellular Function and Disease Processes

Studies have identified specific miRNAs involved in regulating distinct cellular functions, such as cellular division, apoptosis, cellular metabolism, intra-cellular signalling, immunity and cellular movement. Abnormalities in the level of miRNAs, therefore, will also affect specific cellular functions leading to pathological outcomes. A role for miRNAs in the pathogenesis of human diseases have been identified in developmental disorders, cancer, autoimmune, infectious and inflammatory diseases involving almost all human organs.

1.5.1. MicroRNAs in Human Developments and Diseases

MiRNAs are involved in regulating at least 60% of transcripts of the human genome, and therefore play a part in diverse cellular functions and disease processes. The roles of miRNAs in human diseases are complex and diverse. The apparent connection between miRNAs and the development of disease is supported by substantial miRNA profiling data showing altered expression of certain miRNAs in various disease processes. In some diseases, the degree of miRNA up-/down-regulation has also been associated with disease sub-types, severity and progression, highlighting the potential of miRNA as a meaningful diagnostic and prognostic marker.

MiRNAs play a role in the pathogenesis of cancer through two possible mechanisms; (1) by suppressing translation of tumour suppressor genes, or (2) by inhibiting important cellular regulatory processes such as apoptosis and cell differentiation (Waldman and Terzic, 2009). The link between miRNAs and various form of cancer is well established, largely based on the abundant profiling studies available. This includes cancer of the lung, head and neck, gastrointestinal tract (oesophageal, gastric, colon), reproductive organs (breast, ovary, endometrium, and cervix), kidney and various haematological malignancies (Waldman and Terzic, 2009; Li and Kowdley, 2012). Because miRNA is tissue specific, the up-/down-regulation of a miRNA is often unique for different type of cancer and organs involved, which is crucial for their use as screening tool, prognostic indicator or potential therapeutic target.

Cardiovascular research is one of the earliest fields where the role of miRNA was recognised. MiRNAs play important role in the regulation of the cardiovascular system through several components, including endothelial cells, myocardium and the regulation of angiogenesis and vascular regression. So far, changes in miRNA expression level has been linked with cardiac hypertrophy, cardiac failure and cardiac development, primarily through miR-1, miR-133 and miR-208, which are expressed at a high level in the heart (Ardekani and Naeini, 2010; Li and Kowdley, 2012).

MiRNA has also been demonstrated to play a very important role in the development of the brain and pathogenesis of various diseases involving the nervous system. Interestingly, the level of expression of several miRNAs was shown to be specific not only to different cell types of the nervous system, but also to certain neurodevelopmental phases (Ardekani and Naeini, 2010). Changes in the level of a distinct miRNA, therefore, may indicate an abnormality in a specific developmental stage. More importantly, this provides a strong support that miRNAs play a pivotal role in determining the fate of cellular lineage, as well as in cellular division, cellular programming and apoptosis (Ardekani and Naeini, 2010).

Recent studies have demonstrated regulatory function of several miRNAs in inflammatory and immunological pathways. A recent study on cultured human endothelial cells identified the role of miR-126 in preventing leukocyte adherence to endothelial cells by inhibiting the expression of an adhesion molecule VCAM-1 (Harris *et al.*, 2008). Another study using murine macrophages showed that secretion of cytokines, such as TNF-α and IFN-β induces miR-155 expression, which has been linked to activation of immunological pathways through several actions, including granulocyte/monocyte expansion and B- and T-cell activation (O'Connell *et al.*, 2007). The role of miRNAs in cellular differentiation was also found in the development of inflammatory cells. Several studies have identified key miRNAs, such as miR-17 and miR-150, involved in B-cell maturation (Zhou *et al.*, 2007;

Ventura *et al.*, 2008), miR-424 in monocyte differentiation (Rosa *et al.*, 2007) and miR-223 in granulocyte differentiation and activation (Johnnidis *et al.*, 2008). The link between miRNAs and the immune system is further highlighted by significant changes in the expression profile of several miRNAs in inflammatory and autoimmune diseases, such as rheumatoid arthritis (Stanczyk *et al.*, 2008; Tili *et al.*, 2008) and systemic lupus erythematosus (Dai *et al.*, 2007).

The evidence mentioned above is only a small part of the abundant literature on the role of miRNAs in various human disease processes, which clearly reflects the biological importance and potential clinical utilisation of miRNAs.

1.5.2. MicroRNAs in Kidney Physiology and Disease

Early studies involving Dicer-knock-out mice highlighted the importance of miRNAs in maintaining structural and functional integrity of various components of the kidney, including renal endothelium, the glomerular barrier and tubular epithelial cells. The abnormalities observed suggest that miRNAs play a vital role in kidney development and kidney physiology. Conditional knock-out of Dicer in the ureteric bud epithelium of mice resulted in hydronephrosis and parenchymal cyst formation (Pastorelli *et al.*, 2009). Selective deletion of Dicer in mouse podocytes induce cytoskeletal changes, which in turn causes proteinuria and glomerulosclerosis, leading to rapidly progressing chronic kidney disease (Harvey *et al.*, 2008; Shi *et al.*, 2008). Removal of Dicer from renin secreting cells of mice was also shown to deplete the number of juxtaglomerular cells, decrease renin gene expression and renin concentration in the plasma, and most importantly lowered systemic blood pressure (Sequeira-Lopez *et al.*, 2010). The resulting pathologies included marked vascular deformity and fibrosis. In mouse proximal tubular epithelial cells, inhibition of Dicer resulted in global down-regulation of miRNAs, especially in the renal cortex (Wei *et al.*, 2010). However, this abnormal miRNAs expression level was not followed by histological changes or abnormal renal function. Interestingly, this change made the tubular cells more resistant to IRI, with improved renal function, less tissue damage, reduced apoptosis and better survival (Wei *et al.*, 2010).

The link between miRNA with various renal pathologies, such as acute kidney injury, fibrosis, polycystic kidney and neoplasm has been extensively studied (Spiegel *et al.*, 2011; Chung *et al.*, 2013; Hou and Zhao, 2013; Amrouche *et al.*, 2014; Schena *et al.*, 2014; Wilflingseder *et al.*, 2014). As the leading cause of CKD, the association between diabetic nephropathy and miRNAs has been a major focus of research. Several miRNAs have been identified as important in the pathogenesis and progression of diabetic nephropathy, mainly based on studies using animal models.

The expression of a miR-192 was shown to be significantly higher in the mesangial cells of diabetic mice. MiR-192 targets SMAD-interacting protein 1 (SIP1), which regulates the expression of TGF-β induced Collagen type 1 and type 2. This is crucial in the progression of diabetic nephropathy (Kato *et al.*, 2007). Based on this study, it is plausible that miR-192 acts as an effector of the TGF-β pathway. In contrast, another study demonstrated that treatment of tubular epithelial cells with TGF-β down-regulates the expression of miR-192, which correlated with increased fibrosis and decreased estimated GFR in diabetic nephropathy patients (Krupa *et al.*, 2010). The results of both studies imply that the same miRNA may respond differently to the same stimulus (i.e. TGF-β stimulation) in different cell types, which makes interpreting and obtaining a comprehensive picture of a miRNA's role more complex and challenging.

The expression of a miRNA may fluctuate throughout the course of a disease. An animal study highlighting the role of miR-21 in diabetic nephropathy showed initial down-regulation of miR-21 in early phase of the disease (Zhang *et al.*, 2009). MiR-21 provides a degree of protection by preventing renal mesangial cell hypertrophy through inhibition of PI3K/Akt pathway (Zhang *et al.*, 2009). However, other studies have shown that higher levels of miR-21 in renal biopsy specimens of diabetic nephropathy patients, and this is associated with more advanced renal pathology, including higher degrees of fibrosis (McClelland *et al.*, 2015). In addition, miR-216a and miR-217 have also been linked to the progression of diabetic nephropathy, primarily through PTEN inhibition, which in turn activates the Akt kinase pathway (Kato *et al.*, 2009).

The association between miRNAs and other kidney diseases were largely made by comparing miRNAs expression in affected patients to a normal cohort. Some of the kidney diseases associated with abnormal miRNA expression include; IgA nephropathy (miR-148b, miR-200c, miR-141, miR-205 and miR-192) (Wang *et al.*, 2010; Szeto and Li, 2014), autosomal dominant polycystic kidney disease (down-regulation of miR-15a) (Lee *et al.*, 2008), lupus nephritis, hypertension (loss of down-regulation of angiotensin receptor-1 (AGTR1) by miR-155) (Sethupathy *et al.*, 2007), and renal-cell carcinoma, which is associated with dysregulation of a hypoxia-regulated miRNA, miR-210 (Jung *et al.*, 2009).

The role of miRNAs in the progression of acute kidney injury to chronic kidney disease is especially interesting. Epithelial-to-mesenchymal transition (EMT) has been proposed as an important contributor to the long-term development of fibrosis following acute injury in the kidney, and substantial evidence is available to link changes in miRNA profile to the development of EMT. The miR-200 family is among the most extensively studied miRNAs,

and they are involved in the regulation of EMT. Down-regulation of the miR-200 family induces EMT in a TGF-β dependent manner, which is implicated in progression of fibrosis and also in tumour metastasis (Gregory *et al.*, 2008). In addition, induction of EMT was associated with a decrease in the expression level of miR-205. Inhibition of mature miR-205 in Madin-Darby canine kidney epithelial cells lead to changes in cell phenotype including elongated cell morphology, loss of plasma membrane E-cadherin and ZO-1 expression and increased cytoskeletal stress-fibre formation (Gregory *et al.*, 2008). Other miRNAs have also been examined in the context of fibrogenesis, among many are; miR-363, miR-192, miR-200, miR-21-, miR-34a, miR-155 and miR-127 (Goodwin *et al.*, 2010; Shapiro *et al.*, 2011; Aguado-Fraile *et al.*, 2012; Chau *et al.*, 2012; Saikumar *et al.*, 2012; Li *et al.*, 2013; van den Akker *et al.*, 2015).

1.5.3. MicroRNA in Kidney Transplantation and Ischaemia/Reperfusion Injury; Current Knowledge

In the kidney transplantation setting, miRNA expression has been profiled in association with rejection, interstitial fibrosis, tubular atrophy as well as ischaemia and reperfusion injury. Correlation between intrarenal miRNAs, clinical and histological profile of a kidney transplant cohort revealed a set of differentially expressed miRNAs in acute rejection cases compared to normal allograft tissues (Anglicheau *et al.*, 2009). The study identified overexpression of miR-142-5p, miR-155 and miR-223 during acute rejection, and highlights the potential for these miRNAs to predict acute rejection episodes (Anglicheau *et al.*, 2009). Another profiling study detected down-regulation of 12 miRNAs (including miR-324-3p, miR-611, miR-654) and up-regulation of 8 miRNAs (including miR-658, miR-320, miR-381) in acute rejection cases (Sui *et al.*, 2008). Interestingly, despite a very similar approach used, the changes in miRNAs listed were distinct and there was a lack of overlap between the two studies. This may be attributed to differences in patient characteristics or disparity in the technology of the profiling platform used. Moreover, it is important to acknowledge the contribution of potential confounding factors in these studies. These factors may be related to the renal function, presence of viral infection, effect of immunosuppressive drugs in the kidney and time since transplantation, all of which may affect the level of expression of miRNAs.

Several authors have published the expression profiles of miRNA following IRI in the kidney. Numerous studies have been published, with most of the work performed in rodents. There is very little data to validate the observations made in rodent models to human cells or

diseases. Currently available studies on miRNA profile in kidney performed using ischaemia or reperfusion model are listed in Table 1-4.

Table 1-4. Existing evidence in the involvement of various miRNAs in the renal response to IRI

miRNA	Model	Treatment	Expression / Results	Effect / Target	Ref.
miR-10a	Rat	45 min. bilateral renal pedicle clamping followed by reperfusion. Microarray profiling	Up-regulated within 1hr	Not stated	(Wang *et al.*, 2014a)
miR-18a	Wistar rats	30 min. renal bilateral IRI	Up-regulated in kidney tissue Blood: Down-regulated Urine: Undetectable	Not stated	(Saikumar *et al.*, 2012)
miR-20a	C57BL/6 mice	30min. unilateral warm ischaemia	Rapidly up-regulated	Not stated	(Goodwin *et al.*, 2010) (Shapiro *et al.*, 2011)
miR-21	C57BL/6 mice	30min. unilateral warm ischaemia	Rapidly up-regulated	Not stated	(Goodwin *et al.*, 2010) (Shapiro *et al.*, 2011)
	Mice	30 min. unilateral warm ischaemia	Rapidly up-regulated		(Chau *et al.*, 2012)
	Mice	miR-21+/+ vs mir-21-/-	More Mpv17l in mir-21-/-	amplifies ROS generation by targeting Mpv17l	(Chau *et al.*, 2012)
	Mice	miR-21-/-	Higher serum creatinine after IRI	Not stated	(Jia *et al.*, 2013)
	Mice	Xenon pre-conditioning (protection for IRI)	Up-regulated	Not stated	(Jia *et al.*, 2013)
	Wistar rats	30 min. renal bilateral IRI	Up-regulated in kidney tissue Down-regulated in blood Down-regulated initially, modestly elevated within 72h in urine	Not stated	(Saikumar *et al.*, 2012)
	Mice	IPC (ischaemic pre-conditioning) vs Sham	Up-regulated in IPC	Not stated	(Xu *et al.*, 2014)
	Mice	miR-21-/- and IPC	Exacerbate IRI	Up-regulate PDCD4 (increase apoptosis)	(Xu *et al.*, 2014)
	Mice	miR-21-/-, no IPC	No effect on IRI	N/A	(Xu *et al.*, 2014)

	BALB/c mice	Bilateral renal ischaemia (45min.) followed by reperfusion. Sham vs IRI assigned to: pre-miR-21, antagomiR-21, PBS	Pre-miR-21 + IRI: lower plasma BUN, creatinine, histological scores. Decreased PDCD4 mRNA and active caspase-3, caspase-8 protein expressions.	Anti-apoptotic properties by supressing expression of PDCD4 gene and active caspase-3, caspase-8.	(Hu *et al.*, 2014)
miR-24	Human	Observation on kidney transplant biopsy specimens with prolonged cold ischemic time	Up-regulated	Regulating H2A histone family, member X, heme oxygenase1	(Lorenzen *et al.*, 2014)
	Mice	Unilateral I/R injury	Up-regulated		(Lorenzen *et al.*, 2014)
	HK2 cells	ATP depletion (chemical anoxia) for 1hr + ATP repletion for 30min. Transfection with miR-24 precursors miR-24 silencing	Increased apoptosis Increased ROS production Altered functional parameters Ameliorate apoptosis, rescued functional parameters		(Lorenzen *et al.*, 2014)
miR-34	HK-2 cells	1% O2	Down-regulated	Promote EMT	(Du *et al.*, 2012)
miR-126	Mice	Bilateral renal pedicle clamping in control vs miR-126 overexpressed mice	N/A	Increase circulating Lin-/Sca-1+/cKit+ haematopoietic stem and progenitor cells, thus promotes vascular integrity and supports recovery	(Bijkerk *et al.*, 2014)
miR-127	Rat (NRK-52E) HK2 cells	Ischaemia / reperfusion	Up-regulated	Mediated by HIF-1α Target KIF3B, involved in cell trafficking. Involved in cell-matrix and cell-to-cell adhesion maintenance	(Aguado-Fraile *et al.*, 2012)
miR-146a	C57BL/6 mice	30min. unilateral warm ischaemia	Up-regulated after day 3	Not stated	(Goodwin *et al.*, 2010) (Shapiro *et al.*, 2011)
miR-155	Wistar rats	30 min. renal bilateral IRI	Up-regulated in kidney tissue Down-regulated in blood Unchanged (slight non-significant decrease) in urine	Not stated	(Saikumar *et al.*, 2012)

miR-187	C57BL/6 mice	30min. unilateral warm ischaemia	Rapidly down-regulated, continue to decrease	Not stated	(Goodwin *et al.*, 2010) (Shapiro *et al.*, 2011)
miR-192	C57BL/6 mice	30min. unilateral warm ischaemia	Rapidly down-regulated, continue to decrease	Not stated	(Goodwin *et al.*, 2010) (Shapiro *et al.*, 2011)
	Rat	45 min. bilateral renal pedicle clamping followed by reperfusion. Microarray profiling	Up-regulated after 6hr	Not stated	(Wang *et al.*, 2014a)
miR-194	C57BL/6 mice	30min. unilateral warm ischaemia	Down-regulated, remain at level ≈ control	Not stated	(Goodwin *et al.*, 2010) (Shapiro *et al.*, 2011)
	Rat	45 min. bilateral renal pedicle clamping followed by reperfusion. Microarray profiling	Up-regulated after 6hr	Not stated	(Wang *et al.*, 2014a)
miR-199a-3p	C57BL/6 mice	30min. unilateral warm ischaemia	Up-regulated after day 3	Not stated	(Goodwin *et al.*, 2010) (Shapiro *et al.*, 2011)
miR-210	Human	Urinary miRNA profile of stable transplant patients vs acute rejection	Low miR-210 associated with higher decline in GFR 1 year post-transplant	Not stated	(Lorenzen *et al.*, 2011b)
	Human	Plasma miRNA of AKI patients vs healthy control	Up-regulated	Not stated	(Lorenzen *et al.*, 2011a)
	BALB/c mice	30min. bilateral clamping of renal pedicle, followed by de-clamping	Up-regulated, most prominent at 4hr and 24hr after reperfusion	Targeting VEGF signalling pathway to regulate angiogenesis post IRI.	(Liu *et al.*, 2012)
miR-214	C57BL/6 mice	30min. unilateral warm ischaemia	Up-regulated after day 3, wane by day 21	Not stated	(Goodwin *et al.*, 2010) (Shapiro *et al.*, 2011)
miR-494	Mice	Not stated	Up-regulated rapidly (within 1 hr)	Reduce overexpression of ATF3	(Lan *et al.*, 2012b)
miR-714	C57BL/6 mice	27min. bilateral renal pedicle clamping	Up-regulated at 3, 6 and 24hr.	Not stated	(Bellinger *et al.*, 2014)
miR-805	C57BL/6 mice	30min. unilateral warm ischaemia	Down-regulated, remain at level ≈ control	Not stated	(Goodwin *et al.*, 2010)

					(Shapiro *et al.*, 2011)
miR-877*	C57BL/6 mice	27min. bilateral renal pedicle clamping	Up-regulated at 3, 6 and 24hr.	Not stated	(Bellinger *et al.*, 2014)
miR-1188	C57BL/6 mice	27min. bilateral renal pedicle clamping	Up-regulated at 3, 6 and 24hr.	Not stated	(Bellinger *et al.*, 2014)
miR-1224	C57BL/6 mice	27min. bilateral renal pedicle clamping	Up-regulated at 3, 6 and 24hr.	Not stated	(Bellinger *et al.*, 2014)
miR-1897-3p	C57BL/6 mice	27min. bilateral renal pedicle clamping	Up-regulated at 3, 6 and 24hr.	Closely associated with Nucks1 gene expression, which putative downstream targets include genes linked to renal injury, inflammation and apoptosis	(Bellinger *et al.*, 2014)

Although there have been a lot of studies performed to identify which miRNAs are involved in the renal response to IRI, little has been done to elucidate their actual mechanism of action to. Furthermore, as described in Table 1-4, most published reports conducted their experiments on immortalised cell lines or animal models, and only a small number of studies have attempted to correlate these observations with results from clinically available tissues or perform experimental validation on primary human cells.

Published data have suggested the potential of microRNAs to be utilised as biomarkers, therapeutic targets or to provide additional insights to the mechanisms of ischaemia and reperfusion injury in the kidney, especially in the transplantation setting. However, at present, this potential has not yet being fulfilled as results have been inconclusive and in some cases contradictory due to differences in study design and the technology platform used (van den Akker *et al.*, 2015).

1.6. Introduction to Methodology in MicroRNA Research

A growing interest in understanding the physiological role of miRNAs has led to the development and modification of novel molecular genetic techniques. Principally, methodologies in miRNA include five major components; (1) small RNA isolation, (2) miRNA detection or profiling, (3) target determination and validation, (4) miRNA regulation and (5) clinical correlation.

1.6.1. Isolation of Small RNAs

Developments in RNA isolation techniques have enabled researchers to capture small RNAs with <200nt either using specifically optimised kits for small RNA isolation or by isolating total RNA using a phenol-based reagent such as TRIzol® or TRI Reagent®, without the need for a small RNA enrichment step. Recovery of small RNA, including miRNAs has been performed successfully using Phenol based isolation techniques, and is the recommended procedure for isolating total RNA for miRNA profiling using microarray platforms.

1.6.2. MicroRNA Detection and Profiling

There are various methods available commercially to profile and detect expression of miRNAs. However, their technical development has not come without challenges. Bernardo et al. attributed these challenges to several miRNA features; (1) the short nature and lack of common sequence (e.g. poly(A) tail) in mature miRNAs, (2) the presence of target sequence in not only mature miRNA, but also in pri- and pre-miRNAs and (3) the sequence similarities between miRNAs of the same family, which may differ by only one nucleotide (Bernardo *et al.*, 2012). Principally, microarray or deep sequencing platforms and real-time quantitative polymerase chain reaction (qPCR) are the most common instruments utilised in miRNA profiling.

Microarray and deep sequencing enable researchers to simultaneously determine the relative change in expression level, rather than the absolute abundance, of a large set of miRNAs. The use of pre-designed microarray probes, which rely on available databases and prior knowledge of known miRNAs, limit the ability of this method to find new miRNA sequences. The introduction of deep sequencing platforms (or next generation sequencing/RNA-seq) overcomes this problem by its ability to provide absolute quantification of all RNA species in a sample. The technology provides opportunity for novel miRNA discovery. Predictably, this leads to the generation of a very large and complex dataset, which require new methods of data interpretation, bioinformatic analysis, validation and functional experiments (Koshiol *et al.*, 2010; Bernardo *et al.*, 2012).

qPCR is a method commonly used to validate the results obtained from microarray or deep sequencing. The quantification step is preceded by reverse transcription of the miRNA of interest, which can be performed either by adding a stem-loop primer specific to a particular miRNA or by adding a universal sequence (poly(A) tail) to all miRNAs. The first method is quantified using TaqMan® assays, while the latter utilises SYBR based qPCR. The

use of miRNA specific primers provides more efficient and specific amplification, as well as allowing discrimination between mature miRNA and pre-miRNA. However, the technique is more expensive and requires separate reverse transcription reaction for each miRNA of interest. On the other hand, despite being more cost effective and less laborious, the use of a universal primer would not be able to differentiate mature from pre-miRNA sequence.

In situ hybridisation (ISH) is the only technique available to visualise and localise miRNA in cells or tissue. Knowing the distribution of a particular miRNA is important in understanding its biological role. However, the steps involved in this technique require thorough and lengthy optimisation. Short probes used in ISH are less specific and may yield inconsistent and false negative results, especially when detecting low copy number miRNAs. Northern blotting is the least commonly used method, due to the time required, and the technical challenges involved in working with small and low copy number miRNAs. This technique requires high concentration of RNA in a sample to start with. Nonetheless, it is the only technique capable to detect both miRNA and its precursor. Both ISH and northern blotting have benefited from recent development of locked-nucleic acid (LNA) probes. LNA is formed by addition of a methylene bridge to nucleic acid analogues to "lock" the RNA conformation, resulting in higher binding affinity to complementary RNA, enhanced single nucleotide discrimination and better resistance to exo- and endonucleases, thus improving overall assay sensitivity and specificity (Vester and Wengel, 2004).

1.6.3. Target Prediction and Validation

The miRNA – mRNA interaction is determined by the seed region of miRNA, which contains a short nucleotide sequence. This property enables miRNA to bind with multiple mRNA targets, at the same time allowing a single mRNA to be regulated by multiple miRNAs. Using prediction databases that match miRNA seed region sequences to that of mRNAs, it is possible to predict potential target genes of a particular miRNA, which justifies further experimental validation. Currently, there are a number of miRNA prediction programmes freely accessible online, each relying on its own unique algorithm based on knowledge on miRNA behaviour. Target prediction of a miRNA is not recommended based on only a single database, due to differences in the criteria used by each algorithm. Available comparative studies failed to identify a single database that is consistently superior to the others. To combine the strengths of each programme, it is recommended to use three to four computational approaches in predicting miRNA targets or a single algorithm that combines several prediction databases (Li *et al.*, 2010; Witkos *et al.*, 2011; Bernardo *et al.*, 2012).

To further verify miRNA targets, several experimental validation methods have been proposed. Reporter assays are amongst the most commonly used method. In principle, cell lines need to be transfected with plasmid containing luciferase reporter vector incorporated with the 3' UTR of the predicted miRNA target. MiRNA-mRNA binding is confirmed by co-transfecting the cells with either miRNA mimic or inhibitor. A change in luciferase expression is expected if miRNA-mRNA binding occurs. Alternatively, qPCR and Western blotting can be used to quantify the predicted targets of a miRNA, thus indirectly identifying potential miRNA-mRNA interactions. The same methodologies may also be applied to evaluate regulation and functionality of a miRNA of interest. Transfection of miRNA mimic or inhibitor to cultured cells may lead to a change in protein expression and consequently phenotypic alteration. Introduction of double-stranded miRNA mimic will complement endogenous mature miRNA leading to further protein inhibition. On the other hand, a miRNA inhibitor, which is single-stranded oligonucleotide, will block endogenous miRNA binding, increasing protein synthesis. These changes can then be assessed by several methods including immunofluorescence studies and Western blotting.

In vitro validation of miRNA target is often followed by determination of its regulation and function *in vivo*. This is most commonly achieved by administering miRNA inhibitor *in vivo* to reduce the level of mature miRNA, thus increasing target mRNA and protein levels. In contrast, *in vivo* application of miRNA mimics in miRNA research is very limited, largely due to their significant off-target effects. Both miRNA inhibitors and miRNA mimics used *in vivo* must be chemically modified in a way to facilitate permeability into cells, delay excretion and enhance *in vivo* stability. However, these requirements can be problematic especially for miRNA mimics, as they will result in miRNA uptake by tissues that do not normally express the miRNA of interest, resulting in unwanted side effects (Rooij, 2011). A number of developments have been made to address this issue, including the use of viral vectors for miRNA mimic delivery. The use of adeno-associated viruses (AAVs) also enables continuous expression of miRNA, thus ensuring more effective replacement of down-regulated miRNAs. Different AAVs serotypes have different tissue specificity which can also be exploited to facilitate more directed delivery (Rooij, 2011).

1.7. Aims and Hypothesis

The aims of this study are to:

1. Profile microRNA in kidney proximal tubular epithelial cell lines and human primary proximal tubular epithelial cells following ischaemia and reperfusion injury.

2. Identify key potential microRNAs which are involved in the renal response to ischaemia and reperfusion injury.
3. Analyse functional aspects of those key microRNAs *in vitro* to try to explain their potential role in cellular response to injury.
4. Validation of key microRNAs profile *in vivo*.

This study hypothesises that ischaemia – reperfusion injury will result in changes in microRNA expression in renal proximal tubular epithelial cells, which will affect their morphology and function.

Chapter 2. General Methods and Reagents

2.1. Risk Assessment

All experiments conducted are in compliance with Biological Control of Substances Hazardous to Health (BIOCOSH) and Control of Substances Hazardous to Health (COSHH) regulations. Risk assessment form was submitted and approved by the University Biological Committee. All laboratory work was conducted in accordance with Institutional rules and regulations.

2.2. Project Overview

This project is divided into three main experimental steps as illustrated in Figure 2-1. The first part of the project was focused on the generation of primary PTECs, which involved optimisation of the isolation protocol and characterisation of the cells isolated. The second part of the project was directed at generating protocols for inducing ischaemia and reperfusion injury in the cells and evaluating the changes induced by these injuries. More importantly, the second part of the project concentrated in profiling the changes of miRNAs, selection of candidate miRNAs, and prediction and validation of their target genes. The last part of the project was aimed at interrogating the biomolecular role of specific miRNAs *in vitro* and validating their expression and distribution in human tissues.

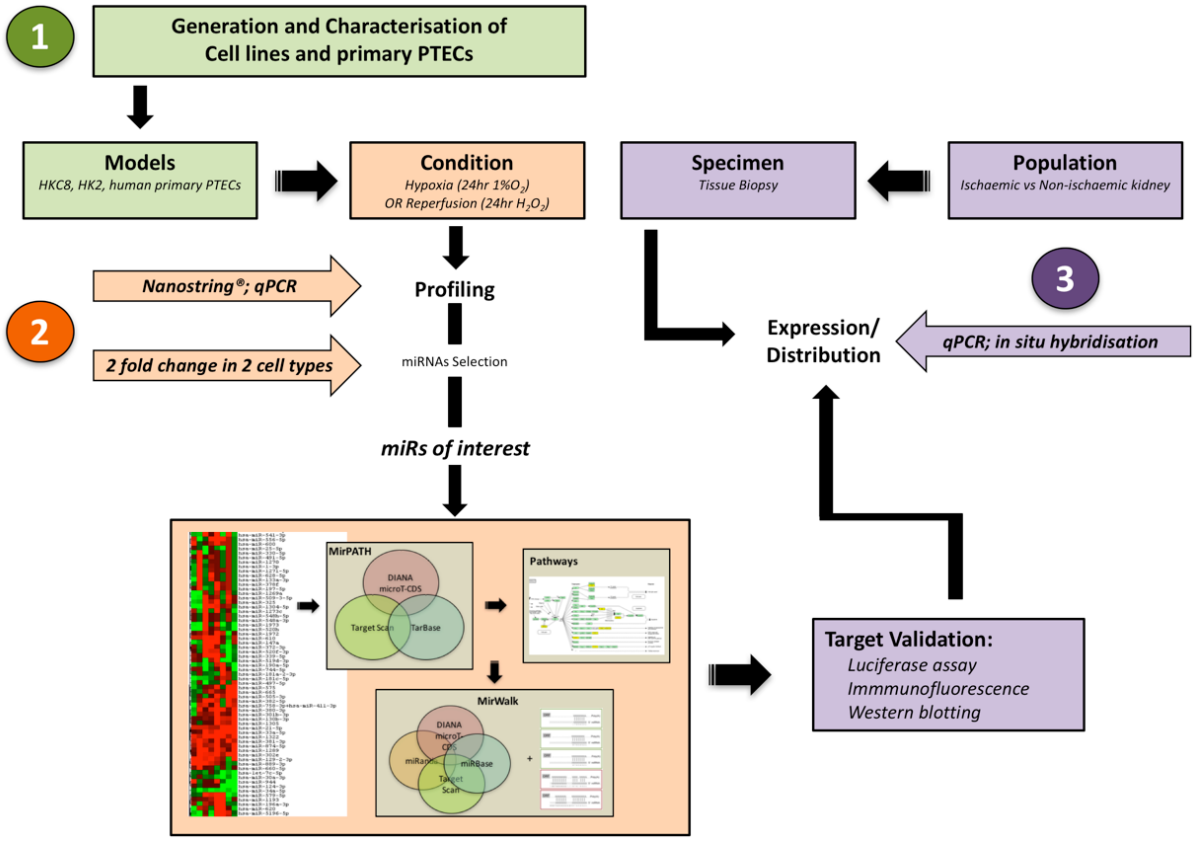

Figure 2-1. Project flowchart

Summary of the overall experimental steps involved in the study. Numbers indicate the sequence in which these experimental steps were conducted.

2.3. Tissue Culture; HKC-8 & HK-2 Cells

2.3.1. Cells Lines Used

HKC-8 is an immortalised human cortical kidney tubular epithelial cell developed in the National Cancer Institute, Bethesda, US. The cell line was immortalised by transfection with an Adenovirus-12 SV40 vector. HKC-8 has been well characterised and demonstrated to have a profile of cell integrins typical of the proximal tubule (Thraves *et al.*, 1990). Its biochemical properties were also found comparable to other established cell lines, including LLC-RK1, OK and HK-2 cells (Racusen *et al.*, 1996). HKC-8 has been used in several studies, including those focusing on the role of epithelial cells in renal fibrosis (Moll *et al.*, 2013).

HK-2 is an immortalised proximal tubular epithelial cell line from normal adult human kidney developed in the Fred Hutchinson Cancer Research Centre, USA. It is derived from a primary proximal tubular epithelial cell culture of normal adult human renal cortex. The cells were immortalised by recombinant retrovirus containing HPV 16 E6/E7 genes (Ryan *et al.*,

1994). It has been shown to retain functional characteristics of primary tubular epithelium and demonstrated reproducible experimental results compared with freshly isolated proximal tubular epithelial cells (Ryan *et al.*, 1994).

2.3.2. Culture & Maintenance of HKC-8 and HK-2 Cells

HKC-8 and HK-2 cells were cultured in specified growth medium as described in Table 2-1. The cells were grown in a humidified incubator at 37°C with 5% CO_2 until they reached approximately 80% confluence. To passage, the culture medium was removed and replaced with 4 mL of sterile Dulbecco's Phosphate Buffer Saline (DPBS; Sigma-Aldrich, USA). DBPS was removed prior to incubation with 0.5 gram/L Trypsin – 0.2 gram/L EDTA (Lonza, Switzerland) for 5 minutes. Trypsin-EDTA will break cell adhesion to the culture dish and cell-to-cell adhesion. Detached cells were recovered by adding culture medium before centrifugation for 5 minutes at room temperature. The supernatant was discarded. Cells were seeded onto a plastic flask. For experimental purposes, the cells were seeded in 6-well plates at 100,000 cells/mL/well, with 2mL cells suspension in each well.

Table 2-1 Specification of culture media, media supplementation, centrifugation and seeding protocol for cell line

Cells	Base Culture Medium	Medium supplementation	Rotor speed (G)	Seeding vessel	Seeding density
HKC-8	DMEM / HAM F-12 (Lonza)	5% FBS (Sigma) 100 U/mL Penicillin 100 µg/ml Streptomycin (Sigma)	1,000 g	$75cm^2$ flask 6-wells plate	2×10^5 cells/mL 0.5×10^5 cells/mL/well
HK-2	DMEM – high glucose (4.5 gram/L) (Lonza)	5% FBS (Sigma) 100U/mL Penicillin 100µg/ml Streptomycin (Sigma)	300 g	$25cm^2$ flask 6-wells plate	1.5 x 105 cells/mL 0.5×10^5 cells/mL/well

2.3.3. Cell Counting

Cells were counted manually using a haemocytometer. The pellet was re-suspended in 1 mL culture media. 10 µL of cell suspension was mixed with 10 µL of 0.4% Trypan blue (Sigma-Aldrich, USA) to estimate cell count per millilitre. The mixture placed in a haemocytometer and a bright field inverted microscope was used to count the number of cells. Viable cells should exclude the blue dye, thus will appear clear against the blue background.

2.3.4. Cryopreservation, Recovery & Passage Selection

Alternatively, cells were cryopreserved by re-suspending the cell pellet in foetal bovine serum (FBS) containing 10% Dimethylsulfoxide (DMSO; Sigma-Aldrich). The suspension was stored in a 1.5 mL cryovial which was frozen gradually at -80°C before transferring to liquid nitrogen for long-term storage. If required, cryopreserved cells were thawed slowly to 37°C. Once thawed, complete culture media was added to the suspension. The mixture was centrifuged for 5 minutes (centrifuge speed is described in Table 2-1) at room temperature and cells re-suspended in media. Subsequent culture and propagation were performed as described previously. To ensure reproducibility, I only used cells with passage number 38-40 for HKC-8 cells, and passage number 10-15 for HK-2 cells.

2.4. Isolation of Primary Proximal Tubular Epithelial Cells

2.4.1. Tissue Origin and Ethical Approval

Ethical approval was obtained from National Research Ethics Committee, East Midland, UK for works on gene and protein expression in the kidney (REC reference number 13/EM/0311). Kidney tissue was derived from macroscopically normal parts of nephrectomy specimens removed for oncological indications. The tissue was collected in sterile RPMI 1640 media (isolation media; Sigma-Aldrich, USA) supplemented with 5% FBS and Penicillin (100 U/mL) / Streptomycin (100 µg/ml), and was immediately transported at 4°C for cell isolation.

2.4.2. Isolation Protocol

All isolation steps were conducted in a sterile environment dedicated to human primary cell work. The renal fibrous capsule and medulla (if present) were removed, leaving only the renal cortex. Tissue was inspected for any macroscopic pathology, which if evident would exclude the sample from further isolation steps. Gross weight of the specimen should be at least 1.5 gram wet weight. Renal cortex was minced into approximately 1 mm^3 pieces. Collagenase-4 (Sigma-Aldrich, USA) was added to isolation medium to make the final concentration of 0.67 mg/ml and tissue was incubated at 37°C for 2 hours on an automated rocker. The suspension then passed through a 40 µm cell strainer. Discontinuous Percoll (Sigma-Aldrich, USA) gradients were made up in two densities; 1.04 gram/mL in isolation medium and 1.07 gram/mL in PBS. The sieved suspension was loaded onto the gradient and spun down at 900 g for 25 minutes at 4°C. A band containing tubular epithelial cells should

be visible after the centrifugation. This population was recovered by careful aspiration and was seeded into a 25 cm^2 flask for further culture. The seeding density in a 25 cm^2 flask should not exceed approximately 1.5 x 10^5 cell/mL. This seeding density should reach 80-90% confluency in 5-7 days. Culture media was replaced every 2-3 days by mixing the new media with 1mL of conditioned media. The detail of media used and their respective supplementation can be found in Table 2-2.

Table 2-2 Type and composition of media used in isolation and culture of human primary PTECs

Cells	Base Culture Medium	Medium supplementation
Isolation medium	RPMI 1640 (Sigma)	5% FBS (Sigma) 100 U/mL Penicillin 100 µg/ml Streptomycin (Sigma)
Culture medium	DMEM / HAM F-12 (Lonza)	REGM SingleQuot Kit + growth factors (Lonza), containing: 0.5 mL Insulin 0.5 mL Hydrocortisone 0.5 mL GA-1000 0.5 mL Adrenaline 0.5 mL T3 0.5 mL Transferrin 2.5 mL FBS Human epithelial growth factor

2.4.3. Passaging Cells

Cells were passaged once they reached 80% confluency. Confluent cells were washed and detached using trypsin EDTA as previously described in section 2.3.2. Trypsin was neutralised by adding growth media before pelleting the cells by centrifugation at 500 g for 5 minute. To maintain subsequent passages, 25 cm^2 flask was used with 1.5 x 10^5 cell/mL seeding density. For use in specific experiments, cells were seeded in accordance to the experimental protocol, using multi-well plates.

2.4.4. Cryopreservation, Recovery & Passage Selection

Cryopreservation was performed by re-suspending the cell pellet in freezing medium containing FBS and 10% DMSO (Sigma-Aldrich, USA). The suspension was transferred to 1.5 mL cryovials. Cell cooling was performed gradually at a rate of approximately 1°C per minute using a cryo-freezing container until reaching -80°C. Cryovials were placed in liquid nitrogen for long-term storage. Recovery was performed as described for HKC-8 and HK-2 cells.

2.5. RNA Isolation and Quality Control

2.5.1. Protocol

Cells were harvested from flasks or plates by trypsinisation and centrifugation. Remaining growth medium was replaced with DPBS (Sigma-Aldrich, USA), and samples were kept on ice (4°C). RNA was isolated using miRvana microRNA isolation kit (Ambion, Life Technologies, USA). Briefly, DPBS was removed followed by disruption of cells using lysis buffer and denaturing solution in 1:1 ratio, using 300 μL of lysis buffer for every 1 million cells. Purification and DNA removal were performed by adding Acid-Phenol: Chloroform extraction mixture, followed by 5 minute centrifugation at 12,000 g at room temperature. The mixture should separate into aqueous and organic phases after centrifugation. Using 100 μL pipette, the upper aqueous phase was carefully transferred into a fresh micro-centrifuge tube. The volume of aqueous phase collected should be recorded at this step, in order to accurately determine the volume of 100% ethanol to be added subsequently. Pure ethanol was added to the sample, and the mixture was passed through the filter cartridge. Samples were washed and centrifuged three times using two types of Washing Solutions provided in the kit (once with Was Solution 1, and twice with Wash Solution 2/3). The flow-through was discarded after each washing step. To ensure complete removal of organic compunds, the filter cartridge, was centrifuged at 11,000 g for 2 minutes at room temperature. The filter cartridge was transferred into a new collection tube. 100 μL of nuclease-free water was heated at 60°C, and then added to the centre of the filter cartridge. The tube was centrifuged at 12,000 g to elute the final RNA product. The product was immediately placed on ice for analysis or quality control, or stored in -80°C.

2.5.2. RNA Quality Control

RNA quality was evaluated by spectrophotometry (NanoDrop ND-1000: Thermo Scientific, USA) and agarose gel electrophoresis. Purity of RNA was assessed from the ratio of absorbance of a sample at 260 nm and 280 nm, as well as 260 nm and 230 nm. A ratio equivalent to 1.8 – 2.0 was considered acceptable for RNA. Lower than acceptable ratio indicates possibility of protein or other contaminants with absorption close to 280 nm. An acceptable ratio value of 260/230 nm absorbance was 2.0-2.2. Lower absorbance value may be a sign of carbohydrate, phenol or other contaminants, which absorb at 230 nm. Each RNA

sample was validated individually before being used in downstream gene expression analysis assay.

Based on absorbance measurements the RNA was free of significant contamination. Figure 2-2 shows the spectrophotometry results of RNA isolated from human primary PTEC, HKC-8 and HK-2 cells. Absorbance ratios at 230 nm, 260 nm and 280 nm were all within acceptable range (Figure 2-2). The isolation method was also proven to yield a good RNA concentration. In summary, the spectrophotometry results indicated that relatively pure RNA was isolated from cells. Consistent RNA concentration obtained from each cell line indicated consistent cell seeding density and reproducibility of the RNA isolation methods used.

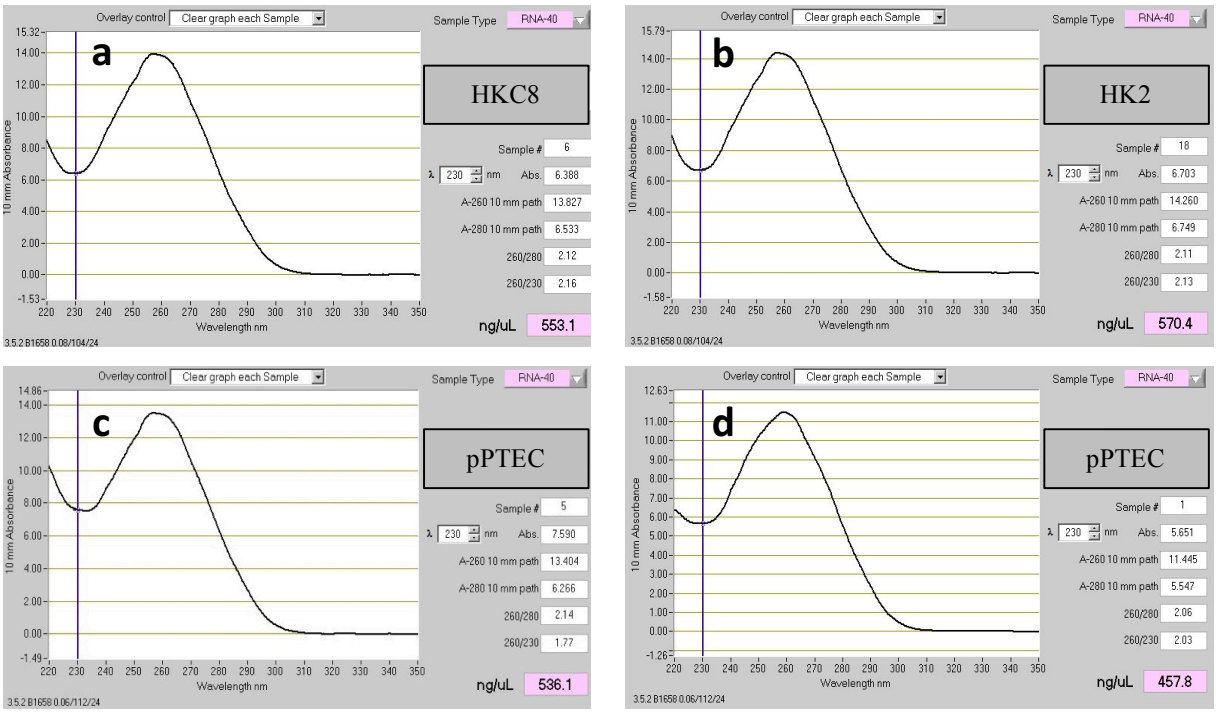

Figure 2-2 Spectrophotometry results of RNA isolated from different cell types
The figures demonstrate absorbance at 280 nm, 260 nm and 230 nm. Results were randomly selected representative of RNA isolation result from (a) HKC-8 cell, (b) HK-2 cell and (c,d) human primary PTECs obtained from two different patients

In addition, RNA integrity was evaluated using agarose gel electrophoresis. A 1.2% agarose gel was prepared in 1x TBE buffer (Table 2-3) containing 0.5 µg/mL Ethidium Bromide. The mixture of RNA and loading dye was heated at 65°C for 5 minutes before loading. Electrophoresis was performed in 1x TBE buffer at 10 V/cm.

Table 2-3 1x TBE buffer composition

Reagents	Weight	Concentration
Tris Base	10.8 gram	89mM
Boric Acid	5.5 gram	89mM
Na_2EDTA	0.93 gram	2mM

Subsequently, the gel was imaged under UV light (Syngene G:Box gel dock and software) to detect the presence RNA bands. 1 kb DNA ladder (Promega, USA) was used as reference and positive control. Visible and intact 28s rRNA and 18s rRNA bands indicates good RNA integrity. Figure 2-3 illustrated the integrity of RNA isolated from HKC8 cells, with two distinct bands (18s and 28s rRNA) visible on RNA gel electrophoresis.

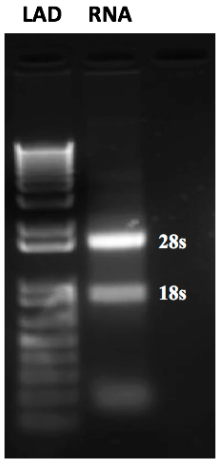

Figure 2-3. RNA gel electrophoresis

Gel electrophoresis of RNA isolated from HKC-8 cells. 1 μg of total RNA was loaded into a lane (denoted as RNA). 1 kb DNA ladder (denoted as LAD) was used as a reference and positive control.

2.6. Gene Expression Analysis

2.6.1. Reverse Transcription

First strand cDNA was synthesised using TaqMan® Small RNA Assays - Reverse Transcription Kit (Life Technologies, USA). This is a commercially available kit, with pre-formulated primer and probe sets designed to detect and quantify mature microRNAs (miRNAs). Principally, the assay consists of two main steps; (1) hybridisation of a miRNA specific stem-loop reverse transcription (RT) primer to a single-stranded miRNA, and (2) addition of reverse-transcriptase enzyme, which extends the cDNA (Figure 2-4).

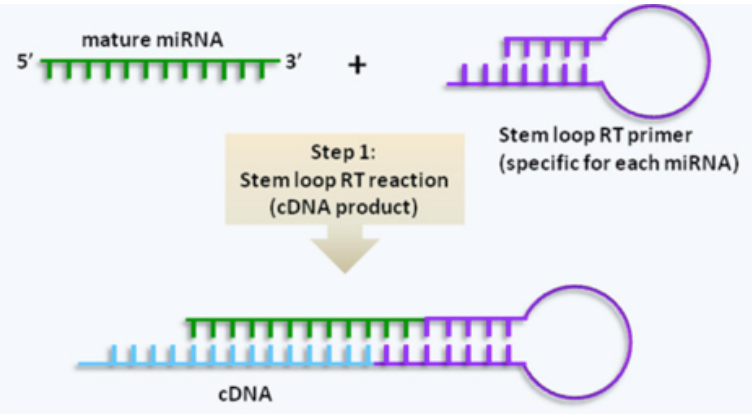

Figure 2-4 Reverse transcription of a miRNA

Illustration of the first step in quantifying miRNA expression using real-time PCR, which involved addition of a specific stem-loop RT primer followed by reverse-transcriptase enzyme. Source: (Bernardo *et al.*, 2012)

Briefly, a master-mix containing the components listed in Table 2-4 was made in accordance to the assay protocol. The master mix was then added to the mixture of 5x miRNA specific reverse-transcription primer and the RNA sample. The composition of each RT reaction is summarised in Table 2-4.

Table 2-4 Components of RT Reaction

RT master mix Component	**Vol. (µL) / reaction**
100mM dNTPs (with dTTP)	0.15
MultiSCribe™ RTase, 50U/uL	1.00
10x RT Buffer	1.50
RNase Inhibitor, 20U/uL	0.19
Nuclease-free water	4.16
Master mix volume	**7.00**
+ 5x RT primer	3.00
+ RNA sample	5.00
Total volume	**15.00**

Each reaction was performed in a 0.2 mL nuclease-free microtube which was centrifuged for 2 minute at 2,000 g at room temperature. After a 5-minute incubation period on ice, the samples were placed in a thermal-cycler (TC-512, Techne Bibby Scientific). The thermal cycler settings shown in Table 2-5 were used.

Table 2-5 Reverse transcription thermal cycler setting

Step	**Time**	**Temperature**
Hold	30 minutes	16°C
Hold	30 minutes	42°C
Hold	5 minutes	85°C
Hold	∞	4°C

2.6.2. Real-time PCR

2.6.2.1. Materials & Protocol

TaqMan qPCR Assay kits (Life Technologies, USA) were used to quantify miRNA expression. Each PCR reaction contained the components shown in Table 2-6. The initial phase of the assay denatured the double-stranded cDNA by increasing temperature. TaqMan oligonucleotide probes contain a reporter fluorescent dye on the 5' end and quencher dye on 3' end. When target sequence is detected, the probe anneals, allowing it to be cleaved by the 5' nuclease activity of Taq DNA polymerase. This cleavage separates the reporter dye from the quencher, increasing emission (Figure 2-5). The increase in fluorescence intensity will be proportional to the number of amplicons produced, as more reporter dye molecules are cleaved with each PCR cycle. This method permits specific hybridization between probe and target, and measurement of multiple targets in one reaction. Primers used in this study are listed in Table 2-7

Table 2-6 Components of PCR Reaction

Component	**Vol. (µL) / reaction**
TaqMan Small RNA Assay (20x)	1.00
Product from RT Reaction	1.33
SensiFAST™ Probe-HiROX mix	10.00
Nuclease-free water	7.67
Total volume	**20.00**

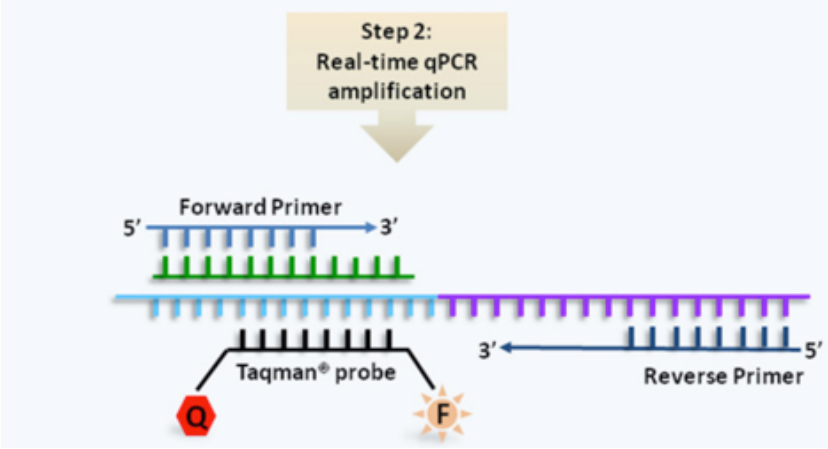

Figure 2-5 Amplification and miRNA detection by TaqMan probe

MiRNA sequence was amplified using forward and reverse primer, and TaqMan probe specific for the miRNA. TaqMan probe is dual labelled with a fluorophore (F) and a quencher (Q). Source: (Bernardo *et al.*, 2012)

Table 2-7 PCR Primers

Primer Name	Nucleotide sequence	Source
hsa-miR-21-5p	UAGCUUAUCAGACUGAUGUUGA	Life Technologies, USA
hsa-miR-34a-5p	UGGCAGUGUCUUAGCUGGUUGUU	Life Technologies, USA
hsa-miR-363-3p	AAUUGCACGGUAUCCAUCUGUA	Life Technologies, USA
hsa-miR-210-5p	AGCCCCUGCCCACCGCACACUG	Life Technologies, USA
hsa-miR-142-3p	UGUAGUGUUUCCUACUUUAUGGA	Life Technologies, USA
hsa-miR-130b	CAGUGCAAUGAUGAAAGGGCAU	Life Technologies, USA

Each reaction was loaded into a 96-well plate. The real-time PCR system (7500 Fast real Time PCR System, Applied Biosystem, USA) was set in accordance to the manufacturer's protocol (Table 2-8)

Table 2-8 PCR Setup for MicroRNA

Step	Enzyme Activation	PCR	
	Hold	Cycle (40 cycles)	
		Denature	Anneal/extend
Temperature	95°C	95°C	60°C
Time	10 minutes	15 seconds	60 seconds

Run mode: standard
Sample volume = 20µL

2.6.2.2. Data Analysis

During the initial phases of a PCR, little change in fluorescent signal should be detected. This is regarded as baseline. A fixed fluorescence threshold was set above the baseline for each PCR amplification plot. The cycle number at which the fluorescence detection passes the fixed threshold was recorded (C_T or threshold cycle) for each reaction.

Comparative quantification ($\Delta\Delta C_T$) was used to determine the fold difference in gene expression. This method of qPCR analysis allows comparison between a given sample with a control sample (control / calibrator) and a reference gene (normaliser / endogenous control). The calculation for this analysis is summarized below (tar ^{C} = target gene in control; ref ^{C} = reference gene in control; tar ^{S} = target gene in sample; ref ^{S} = reference gene in sample).

$$C_T tar^C - C_T ref^C = \Delta C_T calibrator$$

$$C_T tar^S - C_T ref^S = \Delta C_T sample$$

$$\Delta C_T sample - \Delta C_T calibrator = \Delta\Delta C_T$$

$$Fold\ difference = 2^{-\Delta\Delta CT}$$

2.6.2.3. Reference Gene Selection

An ideal reference gene should be expressed constantly and with high abundance across the cell lines of interest and under different conditions. Several human endogenous controls have been identified, with RNU48, among others, reported as the most highly abundant across a selection of 38 human tissues (C_T = 22.2 ± 0.8) (Biosystems, 2007). RNU48 also showed relatively stable expression in National Cancer Institute-60 human cell-lines (C_T = 22.2 ± 1.4) (Biosystems, 2007). I confirmed this abundance and stability of expression by analysing C_T values of RNU48 across the cell lines used in this study as well as across different treatment conditions (Figure 2-6). Threshold cycle of RNU48 was similar in HKC-8 and HK-2 cells. This is the basis of selecting RNU48 as reference gene in our study.

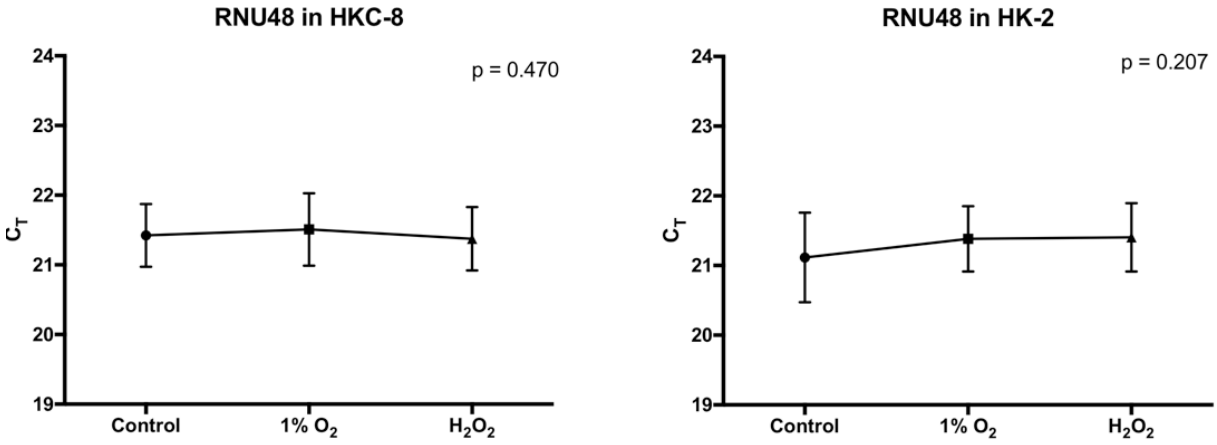

Figure 2-6 RNU48 threshold cycle in HKC-8 and HK-2 cells in various treatment conditions
C_T values of RNU48 in HKC-8 and HK-2 cells. Comparison was made between the cells incubated in 1% O_2 for 24-hour, the cells treated in H_2O_2 and untreated cells. Each point represents the mean of C_T values + SD of three samples. Detection of the difference between the mean was performed using one-way ANOVA test.

2.6.2.4. Primer Efficiency

The efficiency of both the reference and target primers were measured by performing PCR for reference and target gene on serial dilutions of cDNA (1:10, 1:100, 1:1,000 and 1:10,000). The C_T values of each dilution were used to generate a standard curve. The slope (y) was obtained from the standard curve and was used to calculate percentage amplification efficiency (E) using the formula below:

$$E = [(10^{-1/slope})-1] \times 100\%$$

The acceptable percentage amplification efficiency result should be between 85% - 110% (Biosystems, 2014). Experiments to validate primer efficiency were performed for three genes of interests (miR-21, miR-34a and RNU48), which were used in the initial phase of this study. Through serial dilutions of cDNA, each primer set showed an increase in C_T values (Figure 2-7). The efficiency for all primers was close or within the accepted range.

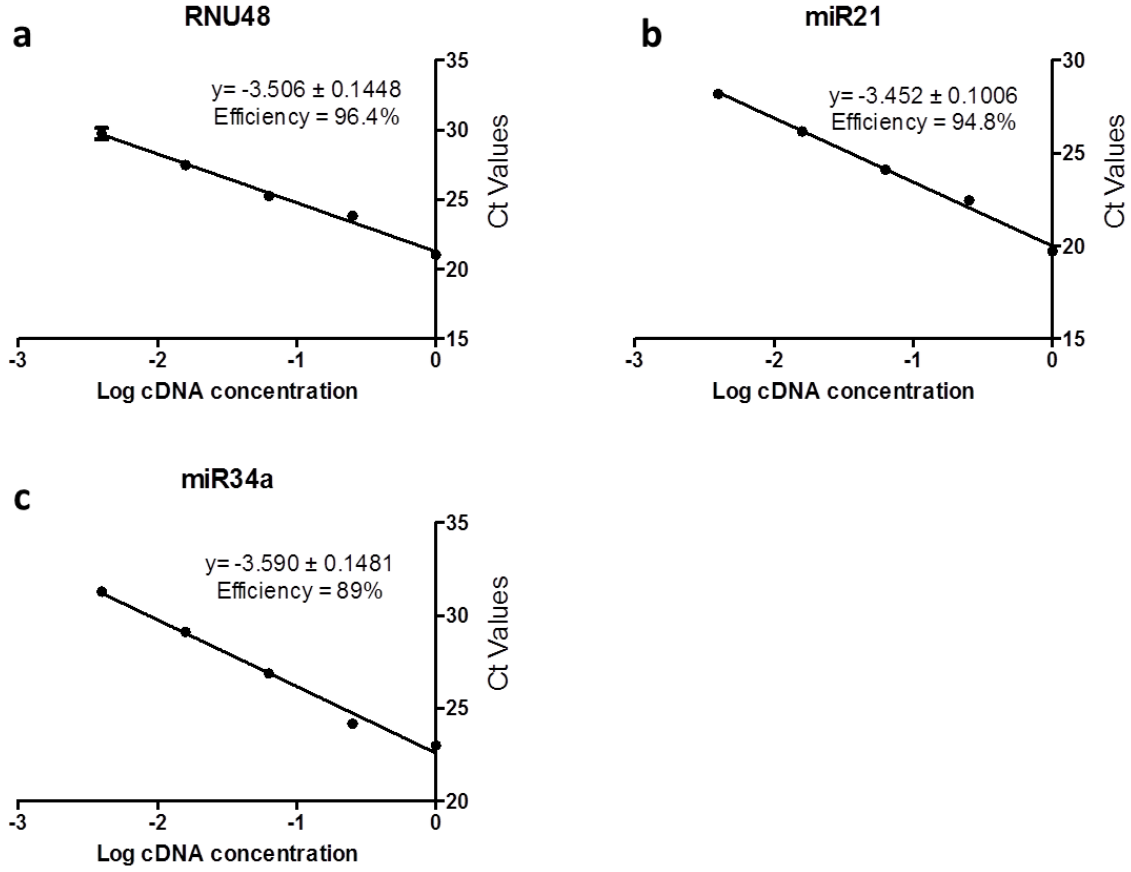

Figure 2-7 Primer efficiency validation of RNU48, miR-21 and miR-34a

Primer efficiency validation of (a) RNU48 as reference gene, (b) miR-21 and (c) miR-34a. Three replicates were for each cDNA dilution of a primer. The experiments were performed using RNA isolated from untreated HKC-8 cells. Percentage efficiency (E) was calculated from the slope (y) generated from each standard curve, using the formula $E = [(10^{-1/slope})-1] \times 100\%$. The acceptable range is between 85%-110%

2.7. Luciferase Assays

2.7.1. Materials and Protocol

Reagents and buffers used in all luciferase assays were performed using a Luciferase Assay System kit (Promega, USA). The system required lysis of the cells containing the luciferase, which was followed by addition of luciferase assay reagent that generates nearly

constant light for at least 1 minute. The amount of light generated reflects the activity of firefly luciferase present.

Briefly, cells containing the luciferase reporter under the control of a promoter of interest were used for this assay. After removal of growth medium, cells were washed gently with sterile PBS. Cells were lysed by dispensing 100 μL of 1x Lysis Reagent provided in the kit, into each well used in a 24-well plate. Samples underwent a freeze-thaw cycle at 37°C for 10 minutes followed by -80°C for 10 minutes before mechanically detached from plate using a cell scraper. The cell suspension was mixed well and centrifuged at 2,000 g for 15-30 seconds. 30 μL of each cell suspension was transferred into a designated well in a 96-well white opaque plate. 70 μL of luciferin reagent was added to each 30 μL sample immediately prior to luciferase activity measurement. Luciferase activity was measured using a multimode microplate reader (Molecular Devices, USA). The remaining 50 μL of cell suspension was used for protein quantification. Luciferase activity was normalised to the total protein concentration of the sample. Normalised values were analysed to detect differences in luciferase activity between samples.

The cells containing the luciferase reporter used in this study include SMAD3-luciferase HKC-8 cells, HRE-luciferase HKC-8 cells, and pGL3-luciferase HKC-8 cells. The details of these cells will be discussed under sub-sections describing their use in specific experiments.

2.8. Western Blotting

2.8.1. Materials

Buffers and reagents used for Western blotting (WB) are listed in Table 2-9. Western blot technique was used in various experimental steps of this project. Primary and secondary antibodies used are listed in Table 2-10 and Table 2-11 respectively.

Table 2-9 General buffers, washing solutions and other reagents used in Western blotting

Buffers / Reagents	Contents	Source
RIPA buffer	150 mM NaCl 50 mM Tris (pH 7.5) 0.1% sodium dodecyl sulfate (SDS) 1% Triton x-100 0.5% deoxycholic acid 10 µL/mL phosphatase inhibitor protease inhibitor made up to 50 mL with nanopure water	Sigma Sigma Sigma Sigma Sigma Abcam Thermo Scientific
4X Laemmli sample buffer	355 mM 2-mercaptoethanol (50 µL) + 950 µL of 4X Laemmli buffer	Sigma Bio-Rad, USA
10X MOPS running buffer	MOPS 52.3 gram Tris (base) 30.3 gram SDS 5 gram EDTA 1.5 gram Make up to 1 L with distilled water	Sigma Sigma Sigma Sigma
10X Transfer buffer	Tris (base) 30.2 gram Glycine 144 gram Make up to 1 L with distilled water	Sigma Sigma
10X Tris-buffered saline (TBS)	NaCl 87.6 gram Tris (base) 12.1 gram pH 8.0 Make up to 1 L with distilled water	Sigma Sigma
TBS Tween (TBST)	9 volumes of distilled water 1 volume of 10X TBS 0.05% w/v Tween-20	 Sigma
Blocking solution	5% w/v non-fat dry milk in 1X TBST	Not applicable
General diluent for antibodies (see Table 2-10 and Table 2-11 for exception)	1% w/v non-fat dry milkin 1X TBST	Not applicable
Developing substrates	Pierce ECL Western blotting substrates	Thermo Scientific
Film developer	RG X-ray developer solution	Champion Photochemistry
Film fixer	RG X-ray fixer solution	Champion Photochemistry

2.8.2. General Protocol

Protein lysates for Western blotting were prepared by mixing cells with a pre-made cell disruption (RIPA) buffer. From here on, cells were kept at 4°C. 100 µL of RIPA buffer was added to every well in a 6-well plate. Cells were scraped and transferred into a microcentrifuge tube and sonified twice for 10 second with approximately a 5-10 second interval. Lysates were centrifuged at 4°C, at maximum speed (12,000 g) for 15 minutes. Supernatant was aspirated without disturbing the debris at the bottom of the tube, and transferred into a clean tube. Protein concentration was measured using the BCA protein assay. Lysates were diluted to 1 µg/µL in 4X Laemmli sample buffer containing 2-mercaptoethanol. Samples were heated to 95°C for 5 minutes.

Protein electrophoresis was performed using pre-cast 4-12% Acrylamide protein gel, 1.0 mm (Invitrogen, USA), immersed in 1X MOPS running buffer. Protein gels were run at 120 constant voltage for approximately 2 hours. Proteins were transferred to a 0.2 μm-pore PVDF membrane (Amersham, USA) using a semi-dry transfer method for 30 minutes at 1 A; 25 V. The membrane was washed and blocked using blocking solution at room temperature for 1 hour. Subsequently, the membrane was incubated in the diluted primary antibody at 4°C overnight. The antibody was diluted in the diluent listed in Table 2-10. Diluted secondary antibody was applied after the membrane was adequately washed (four times 10 minutes washing time) using 1X TBS. Diluent for secondary antibody is listed in Table 2-11. The membrane was incubated in secondary antibody for 2 hours at room temperature. Prior to film exposure, Pierce enhanced chemiluminescent (ECL) substrates were applied onto the membrane for 1 minute. Protein bands were visualised by exposing the membrane to a film for a designated exposure time, followed by film development and fixing.

2.8.3. Protein Band Intensity Analysis

Protein band intensity was quantified using image analysis software, ImageJ (Schindelin *et al.*, 2015). The band intensity of a particular protein was normalised to the intensity of a loading reference protein (GAPDH) band of the respective sample. The normalised intensity measurements were compared to identify the effect of a particular treatment given.

Table 2-10 Primary Antibodies

Protein	Antibody	Source	Host	Target	Application	Clonality	Dilution	Diluent	Secondary Antibody
ZO-1	Anti-ZO-: sc-10804	Santa Cruz Bio, Inc.	Rabbit	Human	IF	Polyclonal	1 : 100	PBS	1
E-Cadherin	Anti-E-Cadherin	BD Transduction Lab.	Mouse	Human	IF WB	Monoclonal	1 : 100 1 : 2000	PBS General	2 5
K-Cadherin	Anti-K-Cadherin: sc-1503	Santa Cruz Bio, Inc.	Goat	Human	IF	Polyclonal	1 : 100	PBS	4
Cytokeratin	Anti-Cytokeratin 19	Abcam	Rabbit	Human	IF	Polyclonal	1 : 100	PBS	1
α-SMA	Anti- α-Actin: sc-32251	Santa Cruz Bio, Inc.	Mouse	Human	IF WB	Monoclonal	1 : 100 1 : 1000	PBS General	2 5
Vimentin	Anti-Vimentin	Abcam	Rabbit	Human	IF	Polyclonal	1 : 100	PBS	1
Collagen I	Anti-Collagen I	Abcam	Rabbit	Human	IF	Polyclonal	1 : 100	PBS	3
Collagen I	Anti-Collagen I alpha 1	Novus Bio	Rabbit	Human	WB	Polyclonal	1 : 1000	Blocking sol.	6
SMAD3	Anti-SMAD3	Abcam	Rabbit	Human	IF	Polyclonal	1 : 100	PBS	3
SMAD7	Anti-SMAD7	Invitroge	Rabbit	Human	WB	Polyclonal	1 : 1000	Blocking sol.	6
HIF-1α	Anti-HIF-1α	Santa Cruz Bio, Inc	Mouse	Human	IF	Monoclonal	1 : 100	PBS	2
GAPDH	Anti-GAPDH	Sigma	Mouse	Human	WB	Monoclonal	1 : 2000	General	5
GAPDH	Anti-GAPDH	Sigma	Rabbit	Human	WB	Polyclonal	1 : 2000	General	6

Table 2-11 Secondary Antibodies

Number	Antibody	Source	Host	Target	Application	Dilution	Diluent
1	Alexa Fluor 488	AbCam	Goat	Rabbit	IF	1 : 200	Pure water
2	Alexa Fluor 488	Invitrogen	Goat	Mouse	IF	1 : 200	Pure water
3	Alexa Fluor 546	Invitrogen	Goat	Rabbit	IF	1 : 200	Pure water
4	FITC	Abcam	Rabbit	Goat	IF	1 : 200	Pure water
5	HRP-conjugate	Dako	Goat	Mouse	WB	1 : 2000	General
6	HRP-conjugate	Dako	Goat	Rabbit	WB	1 : 2000	General

2.9. Immunofluorescence

2.9.1. Materials

For immunofluorescent (IF) staining, the buffers/reagents are used (Table 2-12). Immunofluorescent staining technique was used in various experimental steps of this project. Primary and secondary antibodies used are listed in Table 2-10 and Table 2-11 respectively.

Table 2-12 General buffers and reagents used in immunofluorescence technique

Buffers / Reagents	Contents	Source
Phosphate buffered saline (PBS)	1.15 gram Na_2HPO_4 8.0 gram NaCl 0.2 gram KCl 0.2 gram KH_2PO_4 in 1000 mL distilled water, pH adjusted to 7.4	Sigma
Blocking solution	5% goat serum in PBS	Sigma
Mounting medium	Anti-fading agent 0.015 mol/L sodium azide	Dako

2.9.2. General Protocol

Briefly, cultured cells were grown on 13 mm diameter sterile coverslips in 6-well plates until a visible monolayer of cells was formed. Cells were fixed with ice-cold methanol for 10 minutes, followed by three washes with PBS, each for approximately 3 minutes. Coverslips were incubated in 5% serum from the secondary antibody host to block non-specific binding. The blocking solution was removed and coverslips were incubated overnight at 4°C with primary antibody. Residual unbound primary antibody was removed by washing the coverslips with PBS three-times, each for approximately 3 minutes. This was followed by incubating the coverslips in secondary antibody for 2 hours at room temperature. Nuclei were counter-stained with 100 µL DAPI (4',6-diamidino-2-phenylindole; Sigma-Aldrich) 1 : 3,000 dilution in PBS for 10 minutes at room temperature. Coverslips were washed with PBS before mounting onto microscopy slides using fluorescence mounting medium. Visualisation was performed using Zeiss AxioImager fluorescent microscope available in BioImaging Core Facility, Newcastle University and Leica Fluorescent microscope at the Biobank Imaging Service Unit, Newcastle University, UK. For each immunofluorescent experiment performed, the expression of a protein of interest in the treatment group was compared to its expression in a non-treated group (control). Negative control using cells fixed onto a slide, which were given primary antibody or secondary antibody only were used to detect possible non-specific signal.

2.9.3. Quantitation of Fluorescence Staining

Area of fluorescence (μm^2) indicates the level of expression of a protein of interest in one field of view. Area of fluorescence was quantified using image analysis software, ImageJ (Schindelin *et al.*, 2015). Mean area of fluorescence were calculated from three different slides. Data analysis was performed as mentioned in subsequent statistical analyses section.

2.10. Protein Quantification – Bicinchoninic Acid (BCA) Protein Assay

Total protein concentration was quantified using the colorimetric based BCA protein assay (Pierce™ BCA Protein Assay, Thermo Scientific™, USA). Briefly, 25 µL of each sample was added to 200 µL of a mixture of reagents containing BCA and 4% cupric sulphate. Reduction of Cu^{2+} to Cu^{1+} by protein will chelate BCA molecules, producing a purple-coloured product, which exhibits a strong absorbance at 562 nm. A multimode micro-plate reader was used to detect absorbance of standards and samples arranged in a clear-bottom 96-well plate. Using a set of protein standards with known concentration (20-2000 µg/mL), a standard curve was generated (Figure 2-8), which was used to calculate protein concentration in test samples.

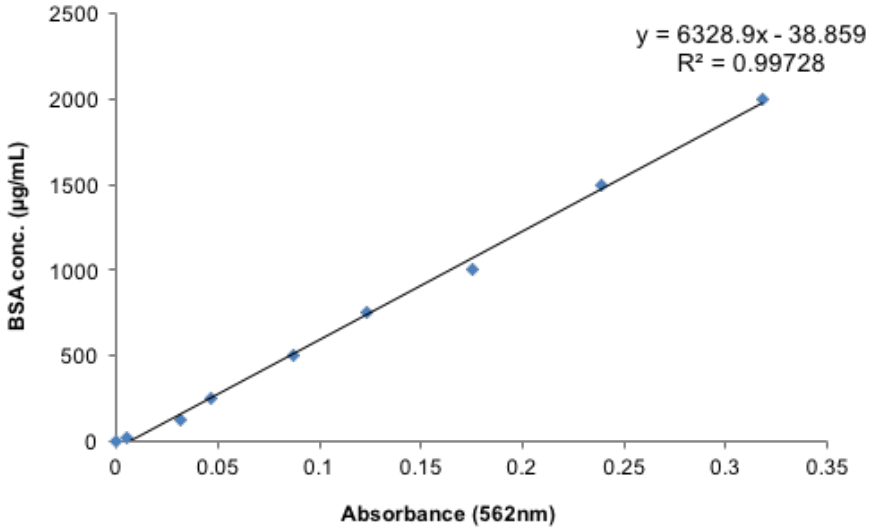

Figure 2-8. Standard curve of BCA method

An example of a BSA curve generated by linear regression used in protein quantification. The graph was produced from serial protein standards provided in the assay kit.

2.11. Characterisation of Human Primary Proximal Tubular Epithelial Cells

2.11.1. Light Microscopy

Inverted bright-field microscopy was used to visualise cellular morphology. Isolated cells from different patients were imaged at each passage from passage 1 to passage 5. The main objective was to evaluate morphological resemblance of the isolated cells to the known features of human PTECs. In addition, light microscopy would also identify reproducibility of the isolation technique, to find potential variation in cellular morphology that may exist between different samples and to determine potential morphological changes occurring after passaging cells. Qualitative comparisons were made between different passages of the same cell lineage and between different cell lineages at the same passage number.

2.11.2. Immunofluorescent staining

Immunofluorescence allows qualitative evaluation of the presence of membrane and cytosolic proteins specific for epithelial and mesenchymal cells. Preparation of slides is described in section 2.9.2. To characterise primary PTEC, I used several epithelial cell protein markers; ZO-1, E-Cadherin, K-Cadherin and Cytokeratin. To detect potential cellular contamination, the isolated cells were also stained for the presence of mesenchymal cell markers; α-SMA, Vimentin and Collagen I. The details of primary antibodies used are listed in Table 2-10. Characterisation of primary PTECs was performed using cells at passage 2.

2.11.3. Scanning Electron Microscopy

Scanning electron microscopy was used to assess the presence of microvilli as a typical feature of renal tubular epithelial cells. Two different cell isolates were randomly selected for electron microscopy. Cells were grown on 13mm diameter coverslips until a monolayer of cells was formed. To remove contaminants cells were washed with PBS. Fixation of cells was performed using 2% glutaraldehyde in Sorenson's phosphate buffer at 4°C for at least overnight. This was followed by removal of excess fixative by PBS washes 2 times 15 minutes. Cells underwent step-wise dehydration by immersion in a graded series of ethanol concentrations. Subsequent mounting, plating and imaging were performed in the Electron Microscopy Research Facilities, Newcastle University. Briefly, the specimens were dried using a Critical Point Drying (CPD) procedure, whereby carbon dioxide was removed after transition from the liquid to the gas phase. This step is critical to ensure the integrity of specimen surface in the SEM chamber. The dried specimen was mounted on a metallic stub to

be later inserted into the SEM. Before visualisation, the specimen was coated with 20-30 nm of gold-palladium to increase its conductivity as well as to prevent the build-up of high voltage charges (Bozzola, 2007). The preparation of SEM slides and image acquisition were performed with the assistance of the Electron Microscopy Research Services Unit, Newcastle University, United Kingdom.

2.12. Methods to Induce Hypoxia or Simulating the Effect of Hypoxia

To induce hypoxia or mimicking the effect of hypoxia, several methods were used. These include the use of 1% O_2 chamber, increasing HIF-1α expression by transient transfection of HIF-1α plasmid, or stabilisation of HIF-1α by cobalt chloride ($CoCl_2$) treatment.

2.12.1. Hypoxic Chamber

Hypoxia was induced by incubating cells in a 1% O_2 incubator available in the Institute of Cellular and Molecular Biology, Newcastle University, United Kingdom. The incubator is equipped with airtight ports to maintain relatively constant internal O_2 concentration, even during sample placement into the chamber or removal from the chamber.

2.12.2. HIF-1α Plasmid Transfection

A HIF-1α plasmid with pcDNA3 backbone vector (William Kaelin; Addgene, USA, see Figure 2-9) was used (Kondo *et al.*, 2002). Bacteria (Dh5-alpha strain *Escherichia coli*) containing the plasmid was transferred onto a culture petri dish containing solidified LB agar supplemented with ampicillin, and incubated overnight at 37°C. 100 mL LB broth solution containing 50 μg/mL ampicillin was prepared. One colony of plasmid-containing bacteria from the agar plate was added to the broth and incubated at 37°C overnight with continuous mixing. The bacteria were harvested by centrifugation at 2,000 g for 5 minutes at room temperature. Chargeswitch-Pro® filter plasmid Maxiprep Kit (Invitrogen, UK) was used to isolate the plasmid. Briefly, the bacterial cell pellet was re-suspended in 7 mL resuspension buffer. The suspension was mixed gently with 7 mL lysis buffer, before incubating it at room temperature for 5 minutes. An equal volume of precipitation buffer was added to the cells until a white precipitate was visible. Plasmid DNA was filtered by running the lysate through a filter column, which was centrifuged at 4,000 g for 2 minutes at room temperature. After centrifugation, the flow-through collected was discarded. Wash Buffer was added to the column, followed by centrifugation at 4,000 g for 2 minutes. To elute the purified plasmid

DNA, Elution Buffer was added to the column before centrifugation at 4,000 g for 1 minute. The DNA quality was assessed using a Nanodrop® spectrophotometer. Isolated DNA could be used directly or stored at -20°C.

HIF-1α plasmid DNA was transfected into HKC-8 cells using a reverse transfection method. Transfection mixture containing 50 µL basal media for HKC-8, without antibiotic or serum supplementation, 1.5 µL transfection reagent (Lipofectamine LTX reagent, Invitrogen, USA) and 500 ng of plasmid DNA was prepared inside each well prior to seeding the well with approximately 30,000 HKC-8. For experiments using the HIF-1α plasmid, the backbone vector pcDNA3 (AddGene, USA, see Figure 2-10) was transfected to HKC-8 cells as the control plasmid.

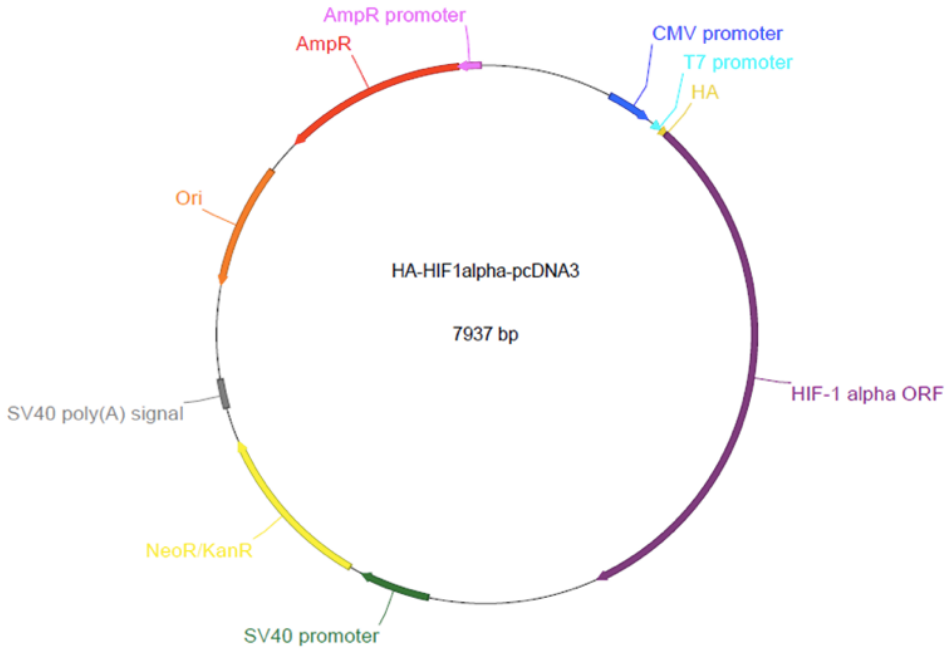

Figure 2-9 Map of the HIF-1α plasmid

Genetic sequence mapping of the HIF-1α plasmid Source: AddGene, USA

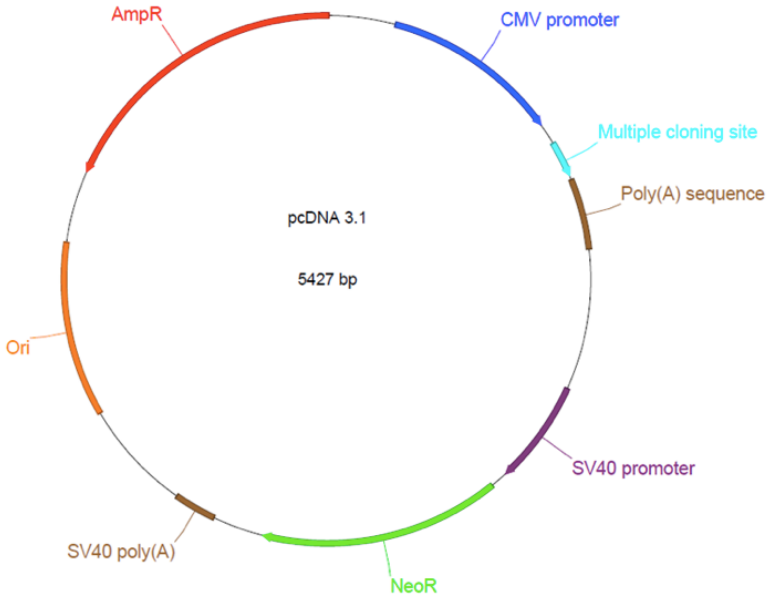

Figure 2-10 Plasmid map of pcDNA
Genetic sequence mapping of the pcDNA backbone vector Source: AddGene, USA

2.12.3. Cobalt Chloride Treatment

Treating cells with $CoCl_2$ will replace Fe in the enzyme HIF-prolyl hydroxylase domains (PHDs), responsible for degrading HIF-1α. This will inhibit their ability to recognise HIF-1α. Thus, $CoCl_2$ has been widely used as a method to simulate hypoxic effect in cells. A 10mM stock solution of $CoCl_2$ was prepared by dissolving 0.024 gram of $CoCl_2$ powder (237.93 gram/mL; molecular weight = 237.93, Sigma, USA) in 10mL of complete media. The stock solution was sterile filtered and diluted to a working solution of 100 µM using complete media.

2.13. Assessment of the Effect of Hypoxia

The effect of Hypoxia on the cells was validated using immunofluorescent staining for hypoxia-induced factor 1 – alpha (HIF-1α) and using HKC-8 cells transfected with hypoxia responsive element (HRE) luciferase. HKC-8 cells were used to assess hypoxia and findings with HKC-8 extrapolated to other cells, on the basis that all these cells possess common renal tubular epithelial features and therefore should behave in a similar pattern under a given condition.

2.13.1. Immunofluorescence for HIF-1α

HKC-8 cells were grown on 13 mm diameter coverslips in 6-well plate until reaching 90% confluency. Cells were serum starved 24 hours prior to hypoxia at in 1%O_2 for 24 hours. HKC-8 cells treated with 100 μM cobalt chloride ($CoCl_2$; Sigma-Aldrich) for 72 hours were used as positive control. Slides were prepared as described in section 2.9.2. To assess the effect of hypoxia, HKC-8 cells were stained for HIF-1α protein. In hypoxic conditions, HIF-1α stabilisation is expected, indicated by intra-nuclear localisation of HIF-1α staining.

2.13.2. Hypoxia Response Element – Luciferase Reporter Assay

A luciferase reporter containing three hypoxia response elements (HRE) from the Pgk-1 gene (Navdeep Chandel; AddGene, USA, see Figure 2-11) was used (Emerling *et al.*, 2008). The HRE-luciferase is contained in a pGL3 vector plasmid. DNA isolation from the bacteria containing the plasmid were performed as for the HIF-1α plasmid described in 2.12.2.

HRE-luciferase plasmid DNA was transfected into HKC-8 cells using a reverse transfection method. Briefly, approximately 30,000 HKC-8 cells were seeded in each well of a 24-well plate. Each well contained 50 μL basal media for HKC-8, without antibiotic or serum supplementation, 1.5 μL transfection reagent (Lipofectamine LTX reagent, Invitrogen, USA) and 500 ng of plasmid DNA. Transfected HKC-8 cells were incubated in standard incubator to serve as control, and in a 1% O_2 incubator for 12 and 24 hours as treated groups. HRE-luciferase transfected HKC-8 cells were also treated with 100 μM of $CoCl_2$ for 48 hours as positive control.

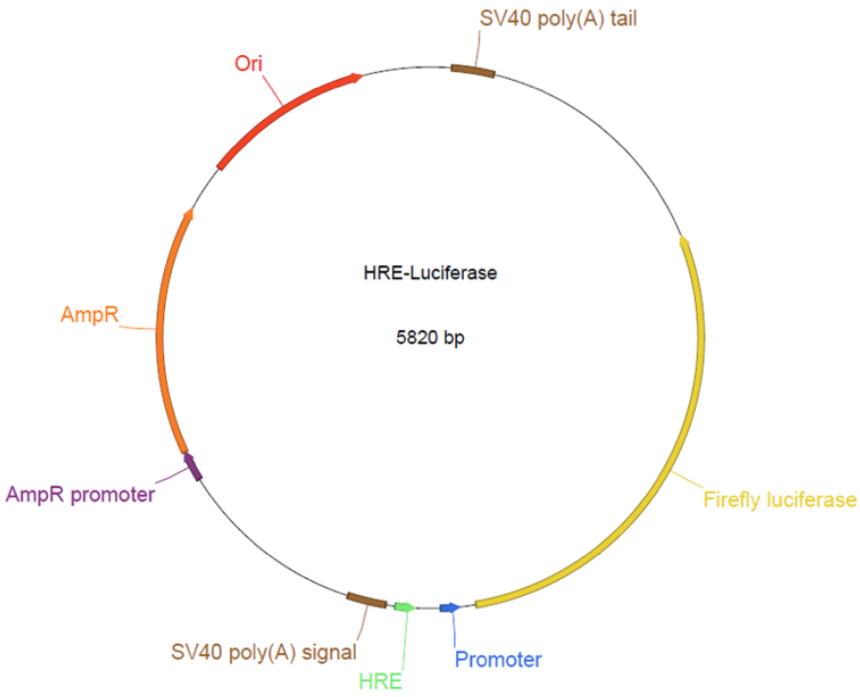

Figure 2-11 Plasmid map of HRE-luciferase

Genetic sequence mapping of HRE-luciferase plasmid developed by Navdeep Chandel. Source: AddGene, USA

The pGL3 plasmid (see Figure 2-12) was also transfected to HKC-8 cells as a vector control. At each designated time points, cells were harvested for the measurement of luciferase activity, according to luciferase assay preparation protocol described in section 2.7.1.

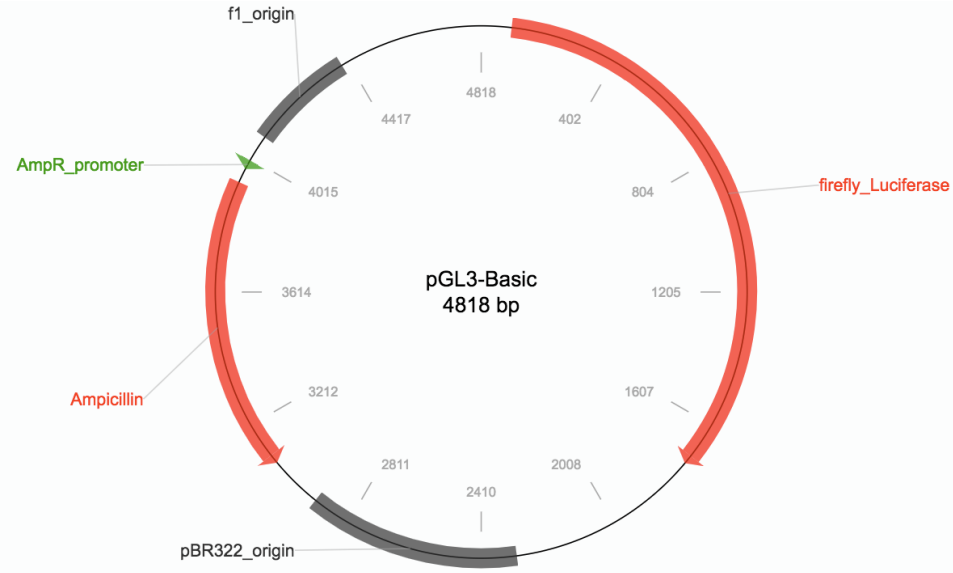

Figure 2-12 Plasmid map of pGL3 vector

Genetic sequence of pGL3 basic plasmid, as a vector control for HRE-luciferase plasmid. Source: Addgene, USA

2.14. Inducing Oxidative Stress

Treatment with hydrogen peroxide (H_2O_2) has been widely used as a method to induce oxidative stress in cells. H_2O_2 stock solution of 1,000 μM was prepared by adding 11.33 μL of H_2O_2 (30% w/w; 8.82 M, Sigma) into 10mL complete media. Working concentration of 100-800 μM was diluted in sterile working environment from the stock solution. Preliminary viability study was performed on each cell line to determine the optimal concentration of H_2O_2. HKC-8, HK-2 or primary cells were grown to 80% confluency in 6-well plates. Cells were serum starved for 24 hours before treatment.

2.14.1. Viability Assay

Varying concentrations of hydrogen peroxide (from 100 μM to 1,000 μM in 100 μM intervals) in complete culture media was used to recreate reperfusion injury. Cells were kept in H_2O_2 treated media for 4 hours before the media was replaced with normal complete media. The cells remained in the fresh media for the following 20 hours. Cell viability was calculated by dividing the number of live cells (non-stained cells in Trypan blue exclusion assay) by the total number of cells recovered. The H_2O_2 concentration which showed evidence of cell injury with a sufficient number of surviving cells to permit analysis was regarded as optimal. This concentration would then be used to induce oxidative stress in that particular cell line.

2.14.2. Reactive Oxygen Species Detection

To qualitatively analyse oxidative stress in a cell population, a molecular probe detection reagent was used. Measurement of dichlorofluorescein (DCF) oxidation is a commonly used method to detect reactive oxygen species (ROS). In its reduced and acetylated form, 2',7'-di-chlorofluorescein (DCF) is non-fluorescent. Intracellular esterase will cleave the lipophilic blocking groups, which yield a charged form of the dye (Jakubowski and Bartosz, 2000). Carboxy-H_2DCFDA is the carboxy derivative of fluorescein, which carries additional negative charge, allowing greater stability. Oxidation of these molecular probes can be quantified by measuring the increase in fluorescence using flow cytometry. For this experiment, a H_2DCFDA derivative with a thiol-reactive chloromethyl group, 5-(and-6)-chloromethyl-2,7-dichlorodihydrofluorescein diacetate, acetyl ester (CM-H_2DCFDA) was used. H_2O_2 treated HKC-8 cells were re-suspended in PBS containing 1 μM H_2DCFDA dye and incubated for 30 minutes at 37°C. The suspension was centrifuged at 1,000 g for 5 minutes at room temperature. The pellet formed was re-suspended in PBS. Cell fluorescence

was assessed using a FACS Canto II flow cytometer (BD Biosciences, UK). HKC-8 cells without exposure to dye was also analysed to measure cell auto-fluorescence. Results were analysed using FACS Diva Clinical Software (BD Biosciences).

2.15. MicroRNA Profiling using NanoString® nCounter Platform

2.15.1. Assay Principle

NanoString® nCounter is a direct digital detection platform for individual target molecules (i.e. microRNA) by utilising fluorescent spots that are spatially ordered (also known as molecular probes). Each colour arrangement represents a different type of target molecules, creating a huge diversity of colour barcodes. The assay colour barcodes bind to target miRNAs in one-to-one ratio, allowing the targets to be added directly without the need of amplification or enzymatic reaction. Each code will be sorted, individually counted, and cross-referenced to a target identity. This will give digital count of target molecules present in a sample. The assay involves three main steps; ligation and hybridisation, purification / immobilisation and counting.

In ligation and hybridisation step, unique miRNA tag (miRtag) was added to the sample. This enables extension of a miRNA for downstream detection. This ligation process is assisted by a temporary binding to a bridge sequence with partial complementarity to both the miRNA and the miRtag (see Figure 2-13). The ligated target miRNA is then hybridised to reporter and capture probes, forming a target-probe complex (see Figure 2-14).

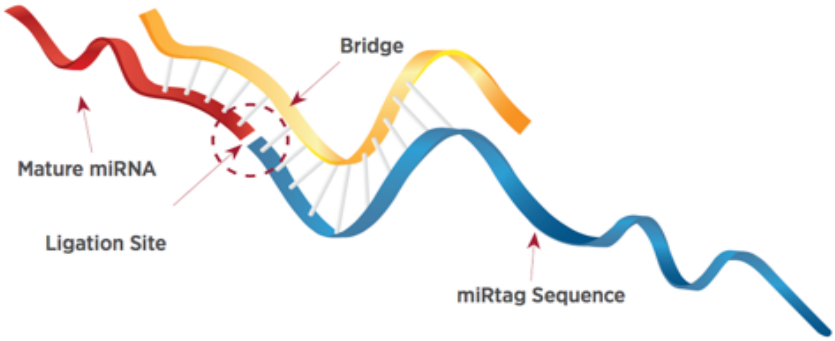

Figure 2-13 Target miRNA ligation by NanoString system
Illustration of ligation of a target mature miRNA sequence by miRTag sequence with temporary binding to a bridge sequence unique to both the target miRNA and miRtag. Source: NanoString Technologies, Inc. (NanoString Technologies Inc, 2014)

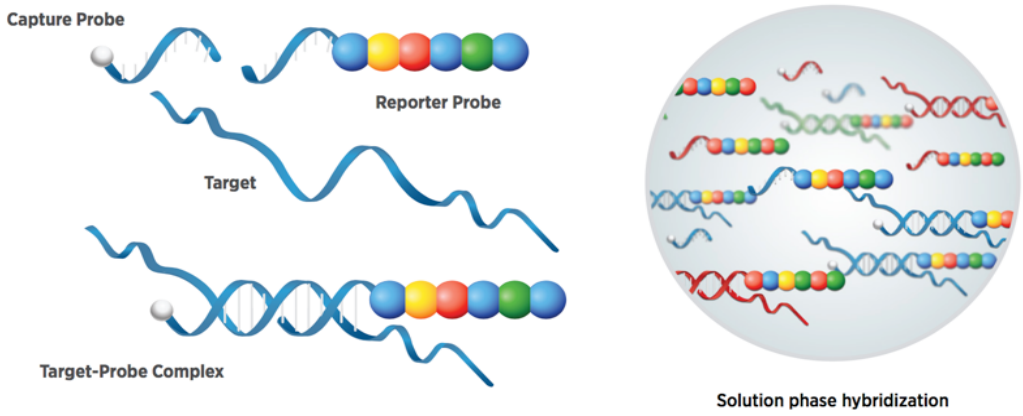

Figure 2-14 Hybridisation of miRNA in NanoString system

Illustration of miRNA hybridisation to capture and target probes to form target-probe complex. Source: NanoString Technologies, Inc. (NanoString Technologies Inc, 2014)

Excess probes are then washed, before the purified complexes are inserted to a sample cartridge (see Figure 2-15). Electrical current will immobilise, arrange and fix these complexes onto the cartridge surface. Using the Digital Analyser (DA) unit of the NanoString system, the target-probe complexes were captured using a microscopic CCD camera, and then counted. The count of each barcode is the count of a target miRNA it refers to (see Figure 2-16). The binding of the colour barcodes to the target miRNA is performed occurred in one-to-one ratio. In addition, no amplification step is performed in this system, limiting the possibility of amplification bias.

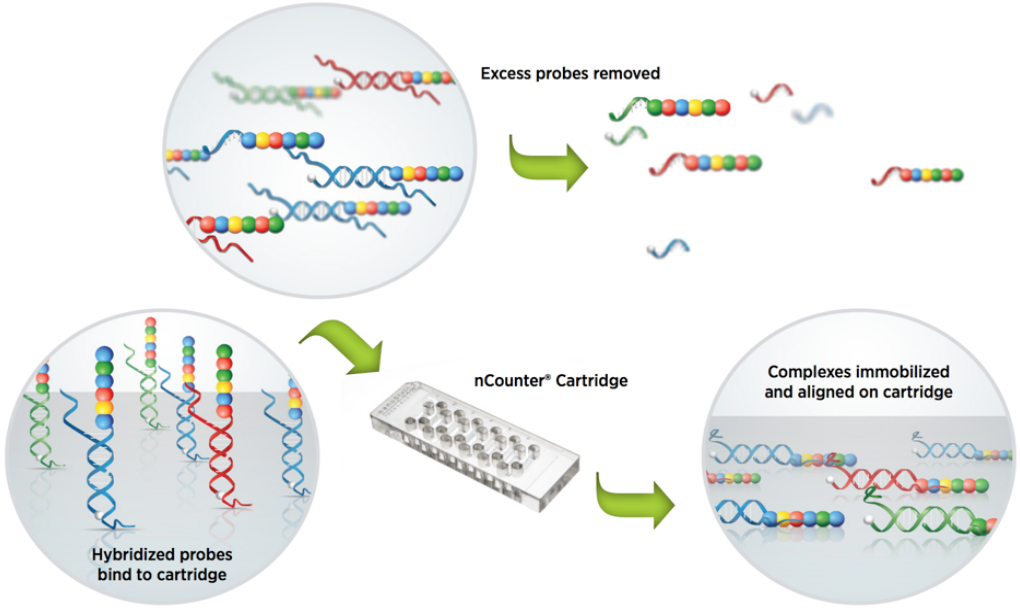

Figure 2-15 Purification and immobilisation step in NanoString system

Illustration of the removal of the excess of probes and immobilisation of target-probe complexes to the assay cartridge. Source: NanoString Technologies, Inc. (NanoString Technologies Inc, 2014)

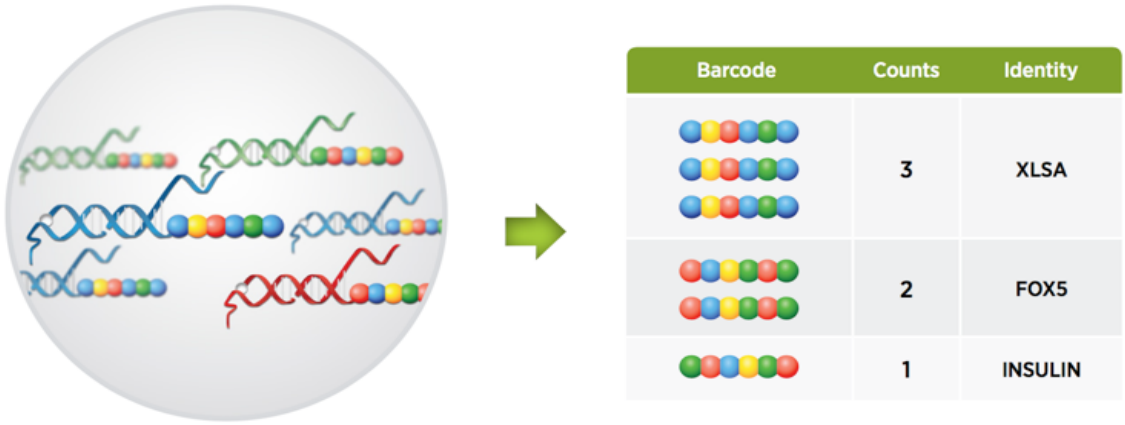

Figure 2-16 Image capture and counting of molecular barcode in NanoString System
Illustration of target-probe complexes being captured and counted in the Digital Analyser (DA) unit of a NanosString system. Counted molecules may be in the form of mRNA (as illustrated) or miRNA. Source: NanoString Technologies, Inc. (NanoString Technologies Inc, 2014)

2.15.2. Assay Preparation and Setup

The preparation for NanoString assay was performed in NanoString core facility, the Department of Academic Haematology, Newcastle University, United Kingdom by a specialised technician. The nCounter Human v3 microRNAs Expression Assay CodeSet was used to profile miRNAs in the samples. All experiments performed in NanoString system should be designed in sets of a maximum of twelve assays. In this experiment, four cell types were used: HKC-8, HK-2, and two primary PTECs isolated from two different patients. Each cell type was treated with either hypoxia or H_2O_2 for 2 and 12 hours. Each cell type has a corresponding non-treated control, which were kept in standard normoxic incubator for 12 hours. In total, 24 samples were arranged for this profiling assay as illustrated in Figure 2-17.

The nCounter assay platform consists of two instruments; the Prep Station and the Digital Analyser (DA). Assay protocol provided by the manufacturer has been previously tested using the same miRNA CodeSet as was used in this experiment, and therefore, was directly applied without further modification. The following description is only a summary of the procedures performed prior to NanoString data analysis. The complete protocol was described in detail in the Appendix, as also described in the manufacturer's protocol (NanoString Technologies Inc., 2010).

Prior to preparation, total RNA samples were normalised to 33 ng/mL using RNAse-free water. Firstly, samples were annealed by mixing each normalised sample with previously prepared mixture of diluted miRNA Assay Controls, Annealing Buffer and miRNA Tag Reagent provided in the assay kit. Annealing step was performed using a thermocycler

programmed according to the assay recommendation. Ligation of miRNA targets was initiated after annealing by the addition of Ligation Master mix provided in the assay kit. After ligation, samples were hybridised to form target-probe complex. Each hybridisation reaction contains the following components; reporter CodeSet, hybridisation buffer, Capture ProbeSet, and an aliquot of the ligated miRNA. Once the hybridisation reaction is completed, the samples were placed in the Prep Station. Purification and immobilisation of the hybridised complexes onto the surface of a specialised cartridge was performed automatically in the Prep Station. The Prep Station allows a maximum of 12 samples per run, which are loaded into a 12-lane cartridge. The cartridge was then analysed in the Digital Analyser to identify and count the barcodes captured for each sample.

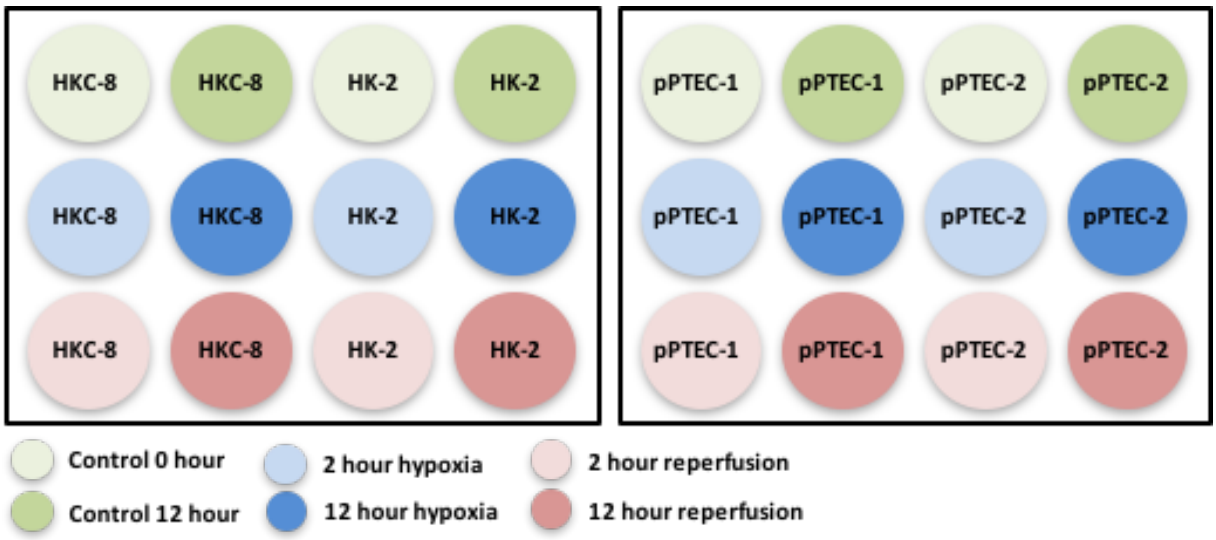

Figure 2-17 Samples setup for miRNAs profiling using Nanostring® nCounter platform

2.15.3. Quality Control Metrics, Normalisation and Background Elimination

The output of Nanostring® nCounter assay is presented in form of a number of counts for each molecular probe. Several quality control measures were applied to screen possible errors related to technical issues of the assay (problems related to cartridge, capture camera, etc.). These measures include field of view count (FOV), binding density (BD) and internal controls (positive ligation controls and negative controls).

Each lane in the cartridge was imaged by the DA in discrete units, known as fields of view (FOV). Imaging problems can be detected by comparing the ratio of successfully imaged FOVs (FOV Counted) to the total number of imaging attempts (FOV Count). A large disparity between the FOV Count and FOV Counted reflects potential technical issues related to inability of the camera to focus, presence of bubbles or insufficient oiling of the cartridge.

The DA maintains its accuracy in capturing colour barcodes (miRNA probes) by excluding any code overlap that may exist in an image. This ensures accuracy of the assay, and provides assurance that the molecular counts provided were in fact a set of truly recognisable codes. However, the data could be compromised if the image captured is saturated, causing a large proportion of the data to be excluded due to codes overlap. To prevent this, the nCounter platform provides a measurement of the number of optical features per square micron, known as the binding density. Binding density includes many system controls that are not affected by samples, and therefore act as an imaging quality control rather than sample performance quality control. In a specific range of binding density (0.05-2.25), the DA can detect and count each reporter barcode accurately. Binding density greater than 2.25 means larger number of reporter overlaps and code exclusions, which may potentially affect data interpretation.

The platform utilises several probes for positive and negative control. These probes were designed against a set of target transcript sequences derived from the External RNA Control Consortium (ERCC), which are of similar size to a miRNA. The positive control transcript sequences were ligated and hybridised in the same manner as endogenous miRNAs. This enables them to act as controls for the entire miRNA analysis process, from sample preparation through hybridisation. In addition, these positive controls were also used in data normalisation step. Positive control counts are used to normalise all platform associated sources of variation (e.g. purification, hybridisation, conditions, etc.), which may indicate under-performance of a lane/lanes. The nCounter platform calculates geometric mean of positive control counts of each lane. The average of these calculated values across all lanes is used as the reference against which each lane is normalised. A scaling factor is then calculated for each of the lanes based on the calculated value for the positive control in each lane relative to the average of this value for the positive controls across all lanes. This scaling factor may then be used to adjust the counts for each gene target and negative controls in the associated lane. The typical range of this positive control normalisation scale is between 0.3 to 3. This normalisation using positive control, however, will not account for differences in sample input between technical/biological replicates. To account for differences between sample inputs, normalisation using either a set of reference genes or large numbers of reporters (known as global normalisation i.e. 100 microRNAs that are highly expressed across all samples) was used. The assay also uses several negative control probes, for which no transcript is supplied. These can be used to estimate systematic background counts within any single hybridisation reaction.

2.16. Profiling Analysis and Target Prediction

2.16.1. Selection Criteria

Several microRNAs were chosen from the NanoString® output based on their degree of expression after ischaemia or reperfusion injury. Up/down-regulation of the level of expression of 2-fold or greater was considered significant. As mentioned previously, only those microRNAs which were consistently up/down-regulated in either HKC-8 and HK-2 cells or both primary PTECs were included in the subsequent functional analysis works.

2.16.2. MiRNA Functionalitiy and Target Gene Prediction

A selection of miRNAs which fulfil the selection criteria were analysed to identify their potential role in specific biological pathways. Analysis of miRNA functionality and prediction of target genes were performed in two steps as illustrated in Figure 2-18. MiRNAs, that fulfilled the selection criteria were firstly analysed for their association with specific genes and biological pathways using DIANA-MirPath v.3.0 (Vlachos *et al.*, 2015). This database enables combinatorial prediction of multiple miRNA targets in a specific biological pathway derived from the Kyoto Encyclopedia of Genes and Genomes (Kanehisa and Goto, 2000). I opted to use the a priori method provided by DIANA-MirPath v3.0 to identify all genes targeted by at least one of the selected miRNAs (known as the gene union approach). DIANA-MirPath identified potential target genes of these miRNAs in three different indexes; DIANA-microT-CDS (Vlachos *et al.*, 2015), Tarbase v7.0 (Sethupathy *et al.*, 2006) and TargetScan (Agarwal *et al.*, 2015). KEGG biological pathways associated with these genes were listed. Only biological pathways which were identified by all three indexes were selected.

Secondly, I selected a specific miRNA from the MiRPath analysis result, which is associated with a pathway relevant to cellular response to IRI. Using MiRWalk 2.0 database (Dweep and al., 2015), I identified potential target genes of individual miRNA of interest with respect to the certainty of its miRNA-mRNA interactions. The results only include target sites for miRNAs at the 3'UTR with three types of canonical sites; the 7mer1A (adenine in position 1 at the 5' end of miRNA), the 8mer (matched adenine in position 1 and an additional match in position 8) and the 7mer-m8 (match in position 8). MiRWalk allows simultaneous prediction using several established target prediction algorithms. For the purpose of this study, four target predictor algorithms were chosen, which includes MiRWalk's own database, DIANA-MirPath, TargetScan, and MiRanda (John *et al.*, 2004; Betel *et al.*, 2008).

Only those targets that were predicted by all four programs were regarded as candidates for further in vitro validation experiments.

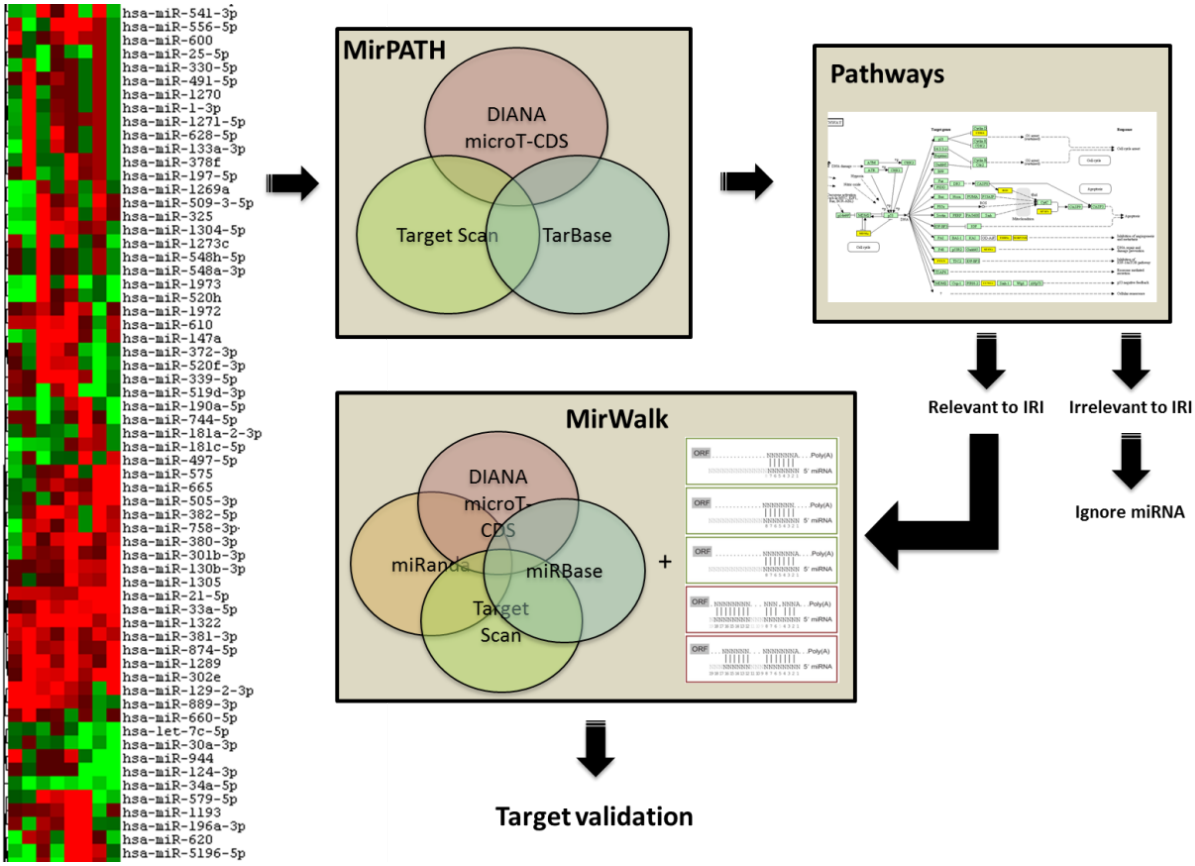

Figure 2-18 MiRNAs functionalities and miRNA target prediction steps

Flow-chart of steps performed in the analyses of miRNA functionality and miRNA target prediction. The steps include identification of relevant pathways involved using MiRPath. Subsequently, the miRNAs identified in the relevant pathways were imported into MirWalk to predict potential target genes

2.17. Transfection of MicroRNA Mimic and Inhibitors

2.17.1. Materials and Protocol

Transfection of miRNA mimic and inhibitor was performed using the transfection reagent Lipofectamine® RNAiMAX (Life Technologies™, USA) using the reverse transfection method, in accordance to the manufacturer's protocol. Briefly, transfection complexes containing serum-deprived medium (Opti-MEM® medium, Gibco®, Life Technologies™, USA), RNAiMAX transfection reagent and the desired miRNA mimic or inhibitor were added into each well. The final transfection complex contained 25 pmol of miRNA mimic/inhibitor and 7.5 µL of RNAiMAX in one well of a 6-well plate or 5 pmol of miRNA mimic/inhibitor and 1.5 µL of RNAiMAX in a one well of a 24-well plate. HKC-8

cell suspension was then added to the well and incubated in 5%CO_2 incubator at 37°C for 24 hours to allow the cells to incorporate the mimic and inhibitor molecules.

2.17.2. Assessing Transfection Efficiency

2.17.2.1. Fluorescent-labelled microRNA mimic transfection control

The effectiveness of the transfection protocol was evaluated using a fluorescence-labelled (miRIDIAN® Dy547) miRNA mimic based on the cel-miR-67 (Dharmacon, USA). This non-targetting miRNA transfection control was introduced to HKC-8 cells using the exact same protocol as was used to transfect the miRNA mimic/inhibitor of interest. The cells were transfected for 24 and 48-hour to capture intracellular uptake of miRNA mimic molecules. Visualisation of mimic delivery was performed by fluorescence microscopy at maximal absorbance/emission wavelengths of 557/570 nm.

2.17.2.2. Expression of miR-21 after Transfection

The level of expression of miR-21 after transfection of miR-21 mimic was used as an indicator of success of the transfection method. HKC-8 cells were transfected with miR-21 mimic according to the protocol described in the previous section. After a 24-hour incubation, cells were harvested for RNA isolation. Expression analysis was performed by qPCR for miR-21. The expression level of miR-21 in mimic transfected HKC-8 cells was compared to miR-21 level in non-transfected HKC-8 cells and HKC-8 cells transfected with scrambled mimic control.

2.18. Luciferase Reporter Assay to Assess TGF-β Activity

To assess activation of TGF-β pathway, a clone of HKC-8 cell lines containing the SMAD3 luciferase reporter construct pCAGA12-luc was generated in our facility (see Figure 2-19). The plasmid was a courtesy of Jean-Michel Gauthier (Dennler *et al.*, 1998). This stably transfected cell line was maintained in full media for HKC-8 cells listed in Table 2-1 with the addition of 300 μg/mL Hygromycin B as a selection agent. The cells were used in the experiments to investigate the role of TGF-β1 in the PTEC response to IRI and the effect of miR-21 in modifying this response.

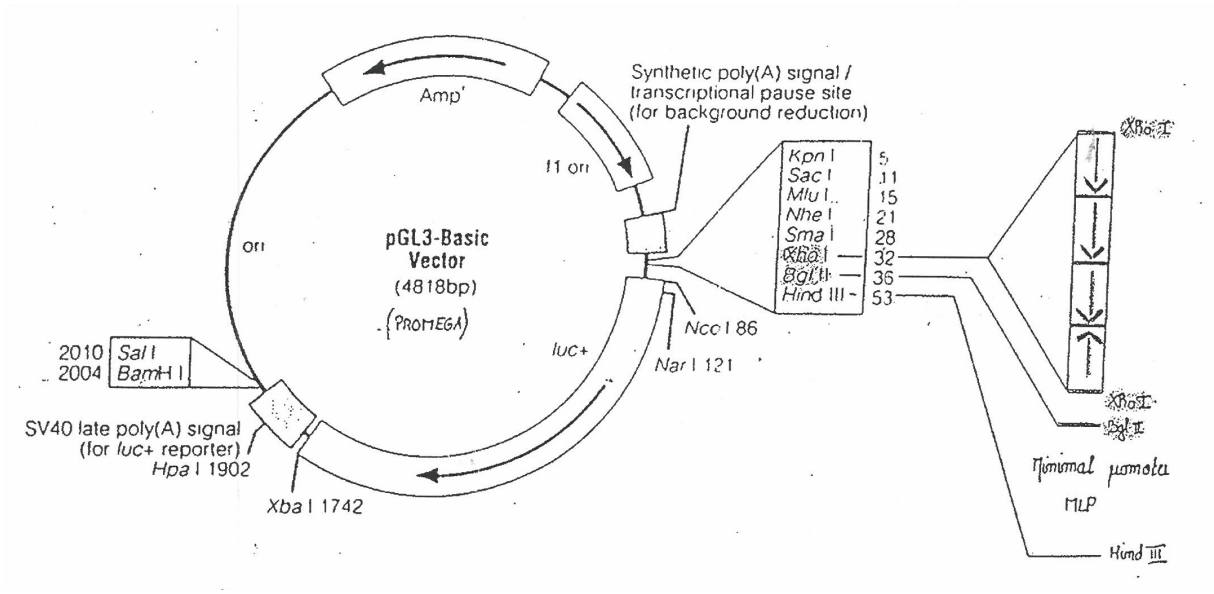

Figure 2-19 Plasmid map of SMAD3 luciferase reporter

Plasmid map of SMAD3 luciferase reporter construct pCAGA12-luc which was stably transfected to HKC-8 cells to generate a clone of SMAD3-luciferase reporter HKC-8 clone.

2.18.1. Determining the Effect miR-21 Over-expression in PTECs on TGF-β Signalling

SMAD3-luciferase HKC-8 cells were seeded onto transfection complex containing miR-21 mimic or scrambled sequence miRNA mimic in 6-well plates. After 24-hour of incubation, transfection media was substituted with media containing 0, 0.1, 0.25, 0.5, 1, 2.5 and 5 ng/mL TGF-β, and were incubated for another 24-hour. Cells were harvested and prepared for measurement of luciferase activity as described in section 2.7.1.

2.18.2. Establishing the Role of IRI in TGF-β Activity in PTECs

SMAD3-luciferase HKC-8 cells were transfected with miR-21 mimic and scrambled miRNA mimic control. Hypoxia was induced in these transfected cells by incubation in 1%O_2 for 12-hours. To induce reperfusion injury, cells were treated with 400 µM H_2O_2 for 4 hours, followed by incubation in normal growth medium for the remaining 24 hours. Cells were harvested and lysed in accordance to the luciferase assay measurement protocol described in section 2.7.1.

2.18.3. Evaluating the effect of miR-21 over-expression in the post ischaemic response to TGF- β1

SMAD3-luciferase HKC-8 cells were transfected with miR-21 mimic and scrambled miRNA mimic control. Hypoxia was induced in these transfected cells by incubation in 1%

O_2 for 12-hours. TGF-β was introduced in several concentrations (0, 1, 5 and 10 ng/mL) after induction of hypoxia. Cells were harvested and lysed in accordance to the luciferase assay measurement protocol described in section 2.7.1.

2.18.4. Evaluating the effect of miR-21 inhibition in ischaemic PTECs

HKC-8 cells containing SMAD3-luciferase reporter gene were co-transfected with miR-21 mimic, miR-21 inhibitor and their respective scrambled control. The cells were subsequently exposed to 1%O_2 to simulate hypoxia. Luciferase activity was measured as an indicator of TGF-β pathway activity.

2.19. Protein Expression Studies to Assess the Link between TGF-β1, miR-21 and Ischaemia in PTECs

Western blot and immunofluorescence were used to assess how TGF-β1 may alter PTEC morphology, and to evaluate the implication of over-expressing or inhibiting miR-21 on the expression and distribution of SMAD3, SMAD7, epithelial marker proteins, such as E-cadherin, and in mesenchymal marker proteins, such as α-SMA and Collagen I. Antibodies used against these proteins were listed in Table 2-10. These protein expression studies were undertaken to achieve the specific objectives summarised in 2.19.1 - 2.19.4.

2.19.1. Assessing the Effect of TGF-β1 on PTEC Morphology

An experiment to assess the effect of TGF-β1 treatment on PTEC phenotype was conducted. For this purpose, only HKC-8 cells were used. Cells were cultured in 6-well plate to 80% confluency. Growth medium was substituted with serum-free medium 24-hour prior to TGF-β treatment. Cells were incubated in 0, 0.1, 0.5, 1, 5 and 10 ng/mL of TGF-β. The effect of TGF-β to cellular expression of α-SMA and E-Cadherin was evaluated by immunofluorescence.

2.19.2. The Effect of Ischaemia on the Expression of SMAD7

HKC-8 cells were incubated in 1%O_2 for 24 hours. Cells were harvested and protein lysates were prepared based on the method described in 2.8.2. SMAD7 expression level was determined by Western blotting.

2.19.3. Evaluating the Effect of miR-21 on the Expression of SMAD7

Total protein was isolated from HKC-8 cells transfected with miR-21 mimic, miR-21 inhibitor and their respective scrambled controls. Transfection of miR-21 mimic and inhibitor was performed on 6-well plates using reverse transfection procedure method described in section 2.17.1. Cells were harvested 24-hour after transfection, and protein lysates were obtained. The level of expression of SMAD7 was visualised by Western blotting.

2.19.4. The Effect of miR-21 on Cellular Morphology

To evaluate whether alteration in miR-21 expression level affects PTEC phenotype changes in response to TGF-β1, we quantified the expression of E-Cadherin, α-SMA and Collagen I in HKC-8 cells transfected with miR-21 mimic. Briefly, HKC-8 cells were seeded onto 6-well plates following the addition of transfection complex containing either miR-21 mimic, srambled miRNA mimic control and transfection reagent only. Cells were incubated in 5% CO_2 incubator for 24-hour to allow transfection of miRNA mimic before being treated with 1 ng/mL TGF-β1.

2.20. Evaluating miR-21 Expression and Distribution in Renal Tissue

2.20.1. Tissue origin and ethical approval

Normal human kidney tissue was obtained from macroscopically normal poles of nephrectomy specimens removed for oncological indications. Ethical approval was obtained from National Research Ethics Committee, East Midland, UK for works on gene and protein expression in the kidney (REC reference number 13/EM/0311). Evaluation of ischaemic kidney tissue was carried out using sections from kidneys that are deemed unsuitable for transplantation, and was rejected by all UK centres due to various reasons. These organs have cold ischaemic time of more than 12-hour. Ischaemic kidney tissue was accessed through the Institute of Transplantation Tissue Biobank, Freeman Hospital, Newcastle upon Tyne, UK (REC reference number 11/NE/0352).

2.20.2. qPCR to quantify miR-21 expression

Tissue RNA was isolated from frozen ischaemic and non-ischaemic kidneys. Tissues were processed immediately after their removal from -80°C, without allowing tissue to thaw. 600 µL of Cell Disruption buffer was added to each tissue sample in a RNAse-free

microcentrifuge tube. Tissue was mechanically homogenised using a Tissue Lyser II (Qiagen, USA). Denaturing solution was added once the sample was homogenised, and RNA isolation process was continued as described in the RNA isolation method in section 2.5.1. Mir-21 expression in ischaemic and non-ischaemic tissue was quantified in accordance to the qPCR protocol mentioned in section 2.6.2.

2.20.3. In situ hybridisation

2.20.3.1. Assay principle

In situ hybridisation (ISH) was used to visualise the expression and distribution of miR-21 in renal tissues. ISH allows detection of a specific nucleic acid sequence (in this case miR-21) in tissue samples using a labelled nucleic acid probe at a specific annealing temperature. In this experiment, ISH was performed using mirCURY LNA™ microRNA ISH kit for formalin-fixed paraffin embedded tissue (FFPE) (Exiqon, Denmark). Initially, the tissues were treated with Proteinase-K to facilitate hybridisation of a specific miRNA sequence by its complementary double-digoxigenin (DIG) labelled probes. The hybridised sequences marked by DIG-labelled probes were then detected using a specific anti-DIG antibody, which was coupled with the enzyme alkaline phosphatase (AP). To visualise, the substrate 4-nitro-blue tetrazolium (NBT) and 5-bromo-4-chloro-3'-indolylphosphate (BCIP) was used. Presence of the enzyme AP will precipitate NBT-BCIP, resulting in the formation of purple fine precipitates on the hybridised complexes. Finally, nuclear fast red staining was added to the slides to provide a better histological orientation.

2.20.3.2. Assay optimisation

ISH optimisation was performed to obtain the optimal conditions for the assay to produce strong and specific signal from the positive control miRNA probe, and minimal signal from the scrambled negative control miRNA probe. Assay parameters which needed optimisation included duration and concentration of Proteinase-K treatment, probe concentration and probe incubation time.

2.20.3.3. Materials and assay protocol

FFPE tissue samples were cut into three 3µm sections, designated for the detection of miR-21, positive control, and scrambled negative control. Residual paraffin was removed by immersing the slides in Xylene, 100% ethanol and 70% ethanol consecutively. This is followed by washing in PBS. The buffers shown in Table 2-13 were used for ISH.

Table 2-13 Buffers and reagents used in in situ hybridisation

Buffers and Reagents	Composition / Description	Source
Proteinase-K buffers	5 mL of 1 M tris-HCl (pH 7.4) 2 mL of 0.5 M EDTA 0.2 mL of 5 M NaCl Add to 900 mL RNAse-free water, adjust volume to 1000 mL	Sigma Sigma Sigma Sigma
SSC Buffer concentrate (20X)	0.3 M sodium citrate in 3M NaCl	Sigma
PBS	1.15 gram Na_2HPO_4 8.0 gram NaCl 0.2 gram KCl 0.2 gram KH_2PO_4 in 1000 mL distilled water, pH adjusted to 7.4	Sigma
PBS-T (0.1%)	1 mL of Tween-20 + 1 L PBS (pH 7.4)	Sigma Sigma
KTBT solution	7.9 gram Tris-HCl (50mM) 8.7 gram NaCl (150mM) 0.75 gram KCl (10mM) Add to 900 mL RNAse-free water, adjust volume to 1000 mL	Sigma Sigma Sigma Sigma
Proteinase-K reagent	To make 15 µg/mL: Add 7.5 µL proteinase-K stock + 10 mL proteinase-K buffer	Exiqon Not applicable
Hybridisation mix	2x miRNA ISH buffer and RNAse-free water (1:1)	Exiqo
Antibody blocking solution	10 mL PBS-T + 200 µL sheep serum + 330 µL 30% BSA	Sigma Sigma Sigma
Antibody dilutant	10 mL PBS-T (0.05%) + 100 µL sheep serum + 330 µL 30% BSA	Sigma Sigma Sigma
Ant-DIG reagent	Sheep-anti-DIG-AP antibody + antibody dilutant (1:800)	Roche Not applicable
AP substrate	1 NBT-BCIP tablet + 10 mL RNAse-free water + 20 µL levamisol	Roche Sigma Vector Laboratorie

Slides were treated with 15 µg/mL of Proteinase-K at 37°C for 10 minutes. Hybridisation was performed using 80 nM of DIG-labelled miR-21 probe, positive control probe (miR-126) or scrambled negative control probe for 2 hours at 50°C. After hybridisation, slides were washed in 5X and 1x saline citrate buffers (SSC buffers) and PBS consequtively. Slides were incubated at room temperature for 15 minutes with blocking solution before the application of anti-DIG antibody for 60 minutes, after which the slides were washed with PBS-T. AP substrate was added to the sections and incubated for 2 hours at 30°C. The final

reaction was terminated using KTBT buffer followed by the addition of nuclear counter staining (nuclear fast red, Sigma, USA). Finally, slides were dehydrated and mounted using Eukitt (Sigma) mounting medium.

Slides were visualised using a Nikon Eclipse microscope (Nikon, Japan). The same imaging parameters were applied to all samples. Images were taken to qualitatively demonstrate the location of miR-21 in renal tissues, as well as to observe differences in miR-21 distribution between ischaemic and non-ischaemic kidneys. Staining was not quantified.

2.21. Statistical Analyses

All statistical analyses were performed using Prism 7.0 (Graph Pad, USA) statistical analysis software. Due to the limited number of samples in each experiment, no normalisation test was performed. Normal distribution was assumed prior to statistical analysis. Comparison of the means of two unmatched groups was performed using unpaired t-test. One-way ANOVA with the appropriate multiple comparison tests (Bonferoni, Dunnet or Tukey) were used to detect statistically significant differences between the means of more than two groups defined by one factor. To determine how a variable is affected by two factors, two-way ANOVA was used. Data was expressed as the mean ± the standard deviation (SD). p Value <0.05 was considered as statistically significant, which was classified into several categories as represented in form of the following symbols: * = $p \leq 0.05$; ** = $p \leq 0.01$; *** = $p \leq 0.001$; **** $p \leq 0.0001$.

Chapter 3. Isolation and Characterisation of Human Primary Tubular Epithelial Cell

3.1. Introduction and Objectives

Although immortalised cell lines are a useful model to validate miRNA targets, their response to IRI may be significantly distinct from human primary cells. Both HKC-8 and HK-2 cells used in this study are among the most common cell lines used in the study of TECs. Nonetheless, several limitations in their use have been observed, including the lack of phenotypic resemblance to human primary PTECs (Sharpe and Dockrell, 2012). I hypothesised that IRI alters the profile of miRNAs in the PTECs, and these changes may be different across different PTEC cell types. Despite these differences, I predicted a set of miRNAs would still be altered in a similar pattern across the different cell types. This set of overlapping miRNAs would be an attractive candidate for further target prediction and validation, and thus would be the focus of my thesis. To achieve this, I generated human primary PTECs derived from normally functioning kidney.

There are several methods described to isolate human PTECs. The initial isolation protocols almost uniformly included the use of mechanical and enzymatic digestion followed by cellular suspension using Percoll centrifugation (Baer *et al.*, 1997; Qi *et al.*, 2007; Brown *et al.*, 2008; A.Vesey *et al.*, 2009; Van der Hauwaert *et al.*, 2013). As an alternative to Percoll centrifugation, the use of cell dissociation followed by cellular separation using anti-Prominin-1 antibody (Legouis *et al.*, 2015), and the consecutive sieving method using 125-µm and 45-µm pores (Sharpe and Dockrell, 2012) have been proposed. Other authors suggested an additional immunogenic separation step following centrifugation of cells, mainly by utilising antibody against CD10 or CD13 (Baer *et al.*, 1997; Van der Hauwaert *et al.*, 2013).

Most authors have documented that isolation of a relatively pure PTEC population is achievable using the Percoll gradient centrifugation method. In addition, this method is easy to learn and adapt, as it does not require additional immunology-based sorting. Based on its reported efficacy, cost-efficiency and practicality I decided to adapt the Percoll gradient method to isolate PTECs from non-ischaemic kidney tissue. The final cellular yield of this method is highly dependent upon the initial tissue dimension and weight. It was therefore crucial to evaluate the success of this technique in the tissue specimens available to our facility which are relatively small. Furthermore, the initial tissue weight may also affect the

final quality and purity of the isolated cells, especially if they were to be used at later passages.

3.2. Results

3.2.1. Light microscopic appearance of primary PTEC

Under light microscope, the isolated cells showed distinct cobblestone-like appearance when a confluent monolayer was formed. This appearance is especially apparent during earlier passage number. Most cells are hexagonal in shape with distinct inter-cellular borders as seen in Figure 3-1.

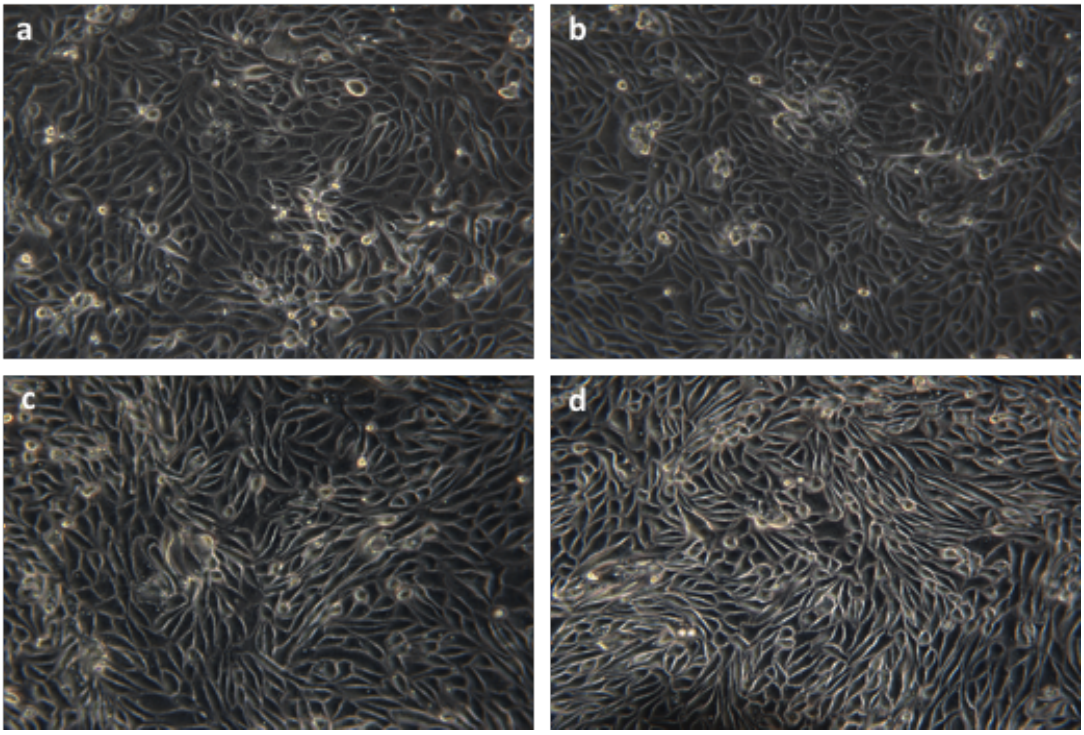

Figure 3-1 Light microscopic images of primary PTECs at passage 1
Each picture (a-d) represents cells isolated from a different patient. Cells were grown in complete media to form a monolayer. Images were acquired at 200x magnification to demonstrate a typical epithelial cobblestone.

Upon seeding, the cells grew in an island-like pattern or clusters, before consolidating to form a confluent monolayer. This characteristic was maintained throughout passage 2 (Figure 3-2) and passage 3 (Figure 3-3), with a reasonably uniform appearance across different patients. On average, the isolated cells reach 80% confluency in 72 to 96 hours after initial seeding.

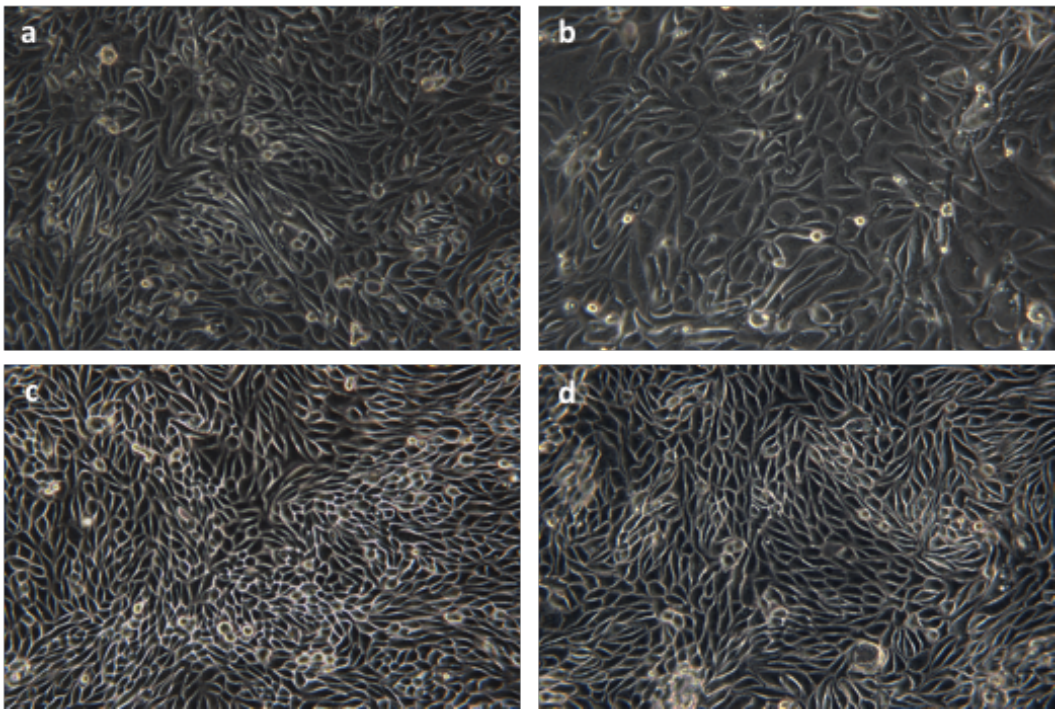

Figure 3-2 Light microscopic appearance of primary PTEC at passage 2

Primary PTEC light microscopy images captured at 200x magnification showing prominent cobblestone appearance. Individual cells have a pentagonal/hexagonal morphology characteristic of epithelial cells. Each picture (a-d) represents cells isolated from a different patient

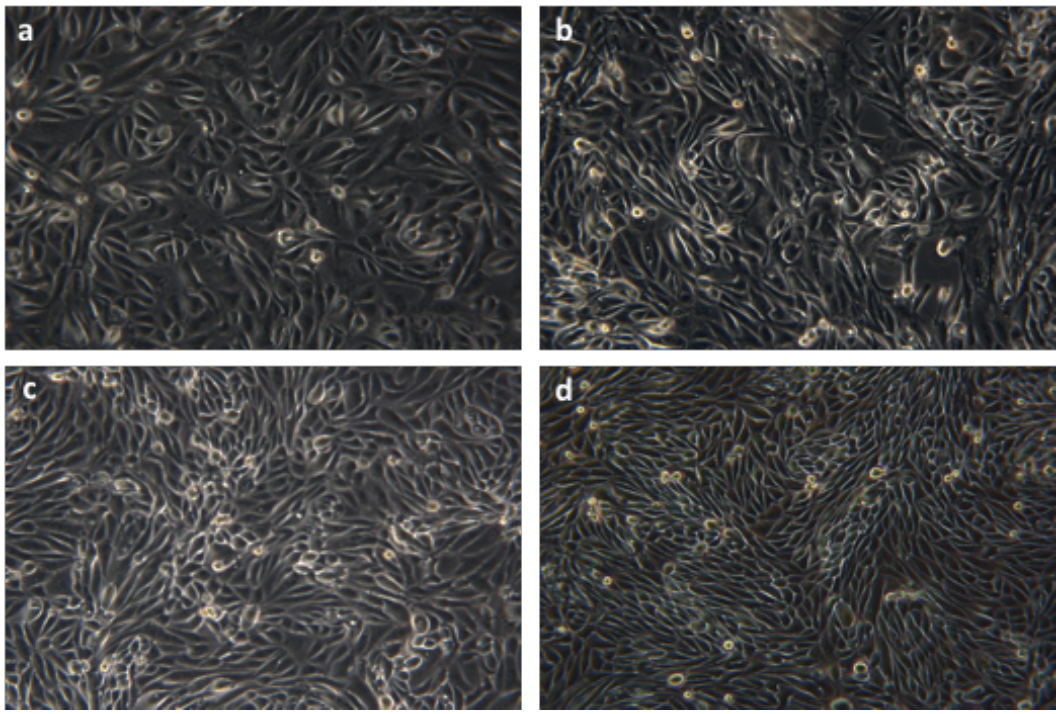

Figure 3-3 Light microscopic appearance of primary PTEC at passage 3

Primary PTEC isolated from four different patients (a-d) forming a monolayer at passage 3. Images were taken under light microscope at 200x magnification. No difference in cell morphology could be seen when compared to earlier passages.

At passage 4, more cells were identified to have a spindle-like shape, which is not a feature of epithelial cells. This characteristic became more prominent as the culture reached later passages. Cellular dedifferentiation started to occur at passage 4 in almost all isolates (Figure 3-4). Although the cells initially grew in clusters, their ability to maintain growth and form a confluent monolayer diminished markedly compared to passage 1 and 2. At passage 4, the cobblestone-like pattern was no longer prominent, and was replaced by an irregular and patchy growth pattern.

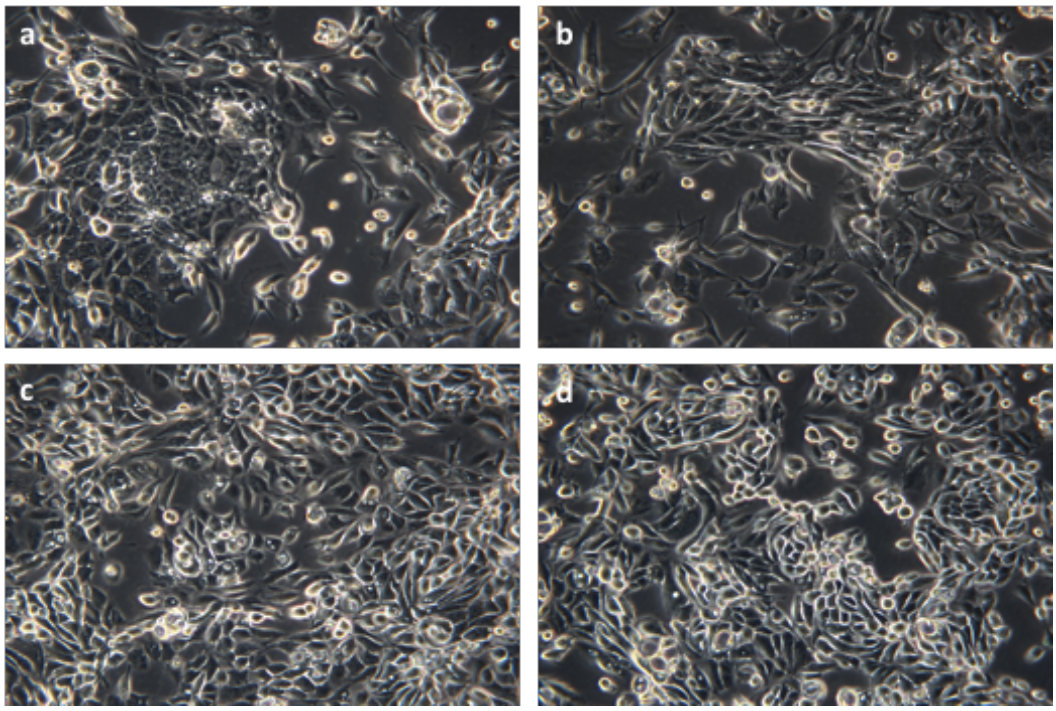

Figure 3-4 Light microscopic appearance of primary PTEC at passage 4
Primary PTEC isolated from four different patients were grown to a monolayer. Images were acquired using a light microscope at 200x magnification, which showed a loss in epithelial morphology. Each image (a-d) represents cells isolated form different patients.

The development of senescence and cellular dedifferentiation were more notable at passage 5 (Figure 3-5). Cells obtained from different patients showed loss of features associated with normal epithelial cells, including change in the shape of cell from hexagonal to a more elongated shape.

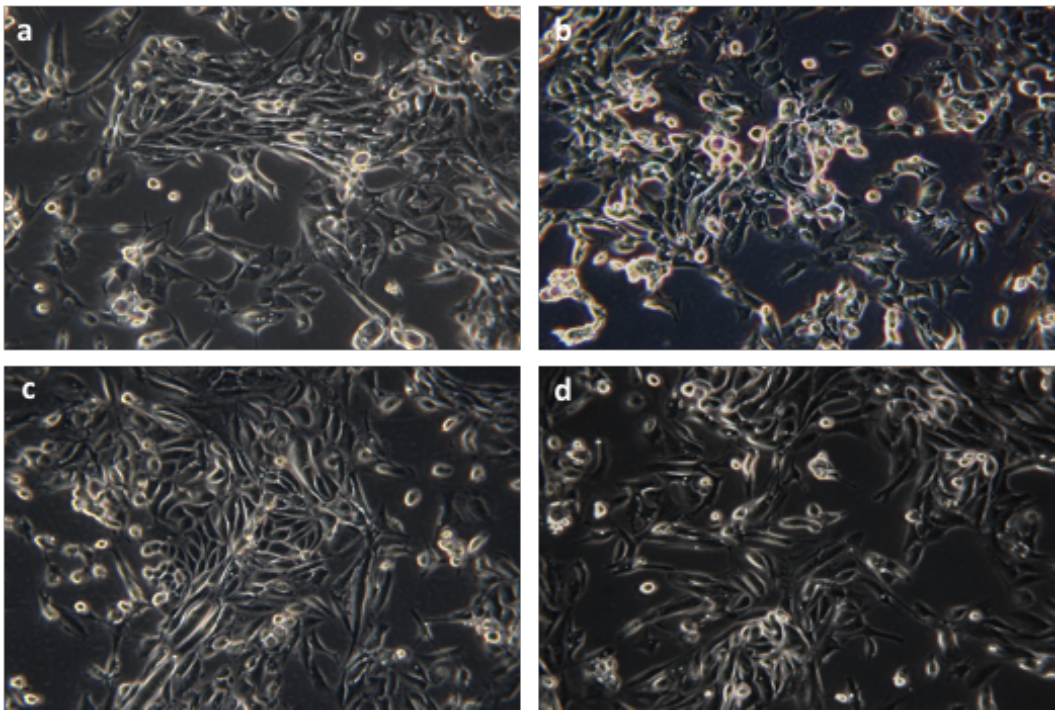

Figure 3-5 Light microscopic appearance of primary PTEC at passage 5

Primary PTEC at passage 5 under light microscopy (imaged at 200x magnification). Cellular arrangement was markedly different from passage 1-3. Each image (a-d) represents cells isolated from different patients.

Furthermore, the formation of hemicysts or "domes" in some of the isolated cells was evident (Figure 3-6), which is indicative of active transcellular transport in these cells. These "domes" were only seen at earlier passage (passage 1-3), and not at later passages.

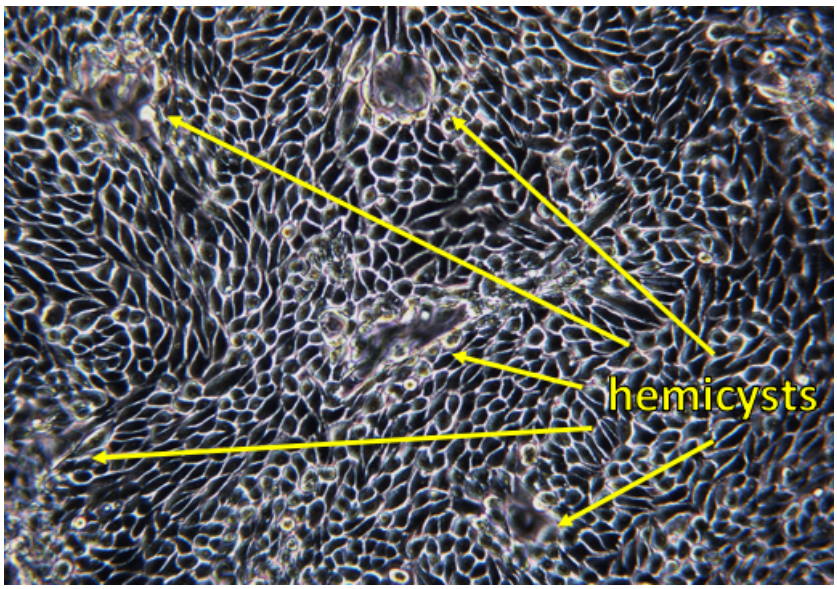

Figure 3-6. Hemicysts formation in primary PTEC

Primary PTEC at passage 2 showing "domes" formation or hemicysts when cells were grown to more than 80% confluency. Image was acquired using a light microscope at 200x magnification.

To evaluate the effect of cryopreservation to the cells, we recovered frozen cells and identified any morphological changes that may be present. These thawed cells from four different isolates showed no morphological abnormality, compared to the freshly isolated cells (Figure 3-7).

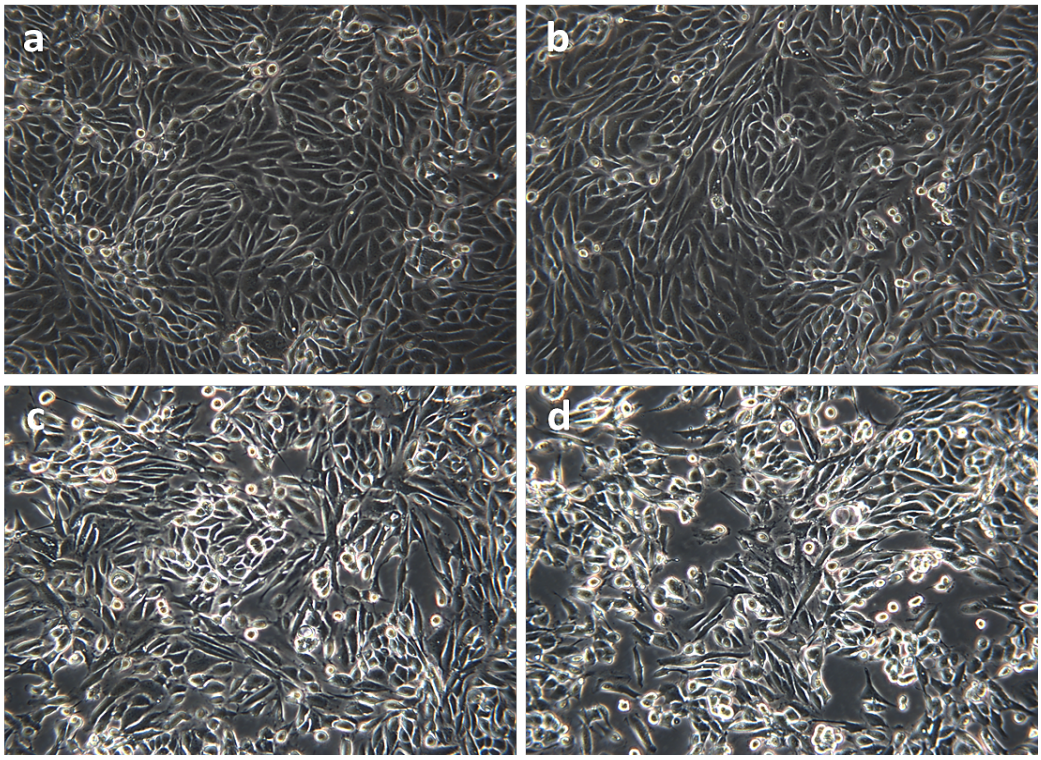

Figure 3-7 Appearance of primary PTEC grown after thawing
Light microscopy images of cells which were frozen at passage 1. Images were taken at 200x magnification. Cobblestone arrangement was prominently shown in (a) passage 2 and (b) passage 3. Morphologic changes started to appear at (c) passage 4 and becoming more apparent at (d) passage 5.

3.2.2. Immunofluorescent characterisation of primary PTEC

Isolated cells were stained to determine the expression of proteins known to be expressed in epithelial cells and non-epithelial cells. Expression of ZO-1, as a tight junction protein, was prominent in almost all cells (Figure 3-8, panel a-c) with a 'honeycomb' appearance indicating the cells are epithelial in nature. E-Cadherin staining was also positive, although was weaker in certain regions of the slides (Figure 3-8, panel d-f). K-Cadherin, a relatively specific marker of proximal tubular epithelial cells, was strongly expressed in almost all cells (Figure 3-8, panel g-i). Unlike E-Cadherin, K-Cadherin (also known as Cadherin-6) was not distinctly expressed on the cell surface, with previous reports describing a cytoplasmic distribution (Paul *et al.*, 1997; Baer *et al.*, 2006; Systems, 2015). Cytokeratin

has been widely used to characterise renal proximal tubular epithelial cells. It was strongly expressed in the cytoplasm of most of the primary PTECs isolated (Figure 3-8, panel j-l). In conclusion, all epithelial markers selected to characterise primary PTEC were consistently expressed across cells originating from different patients.

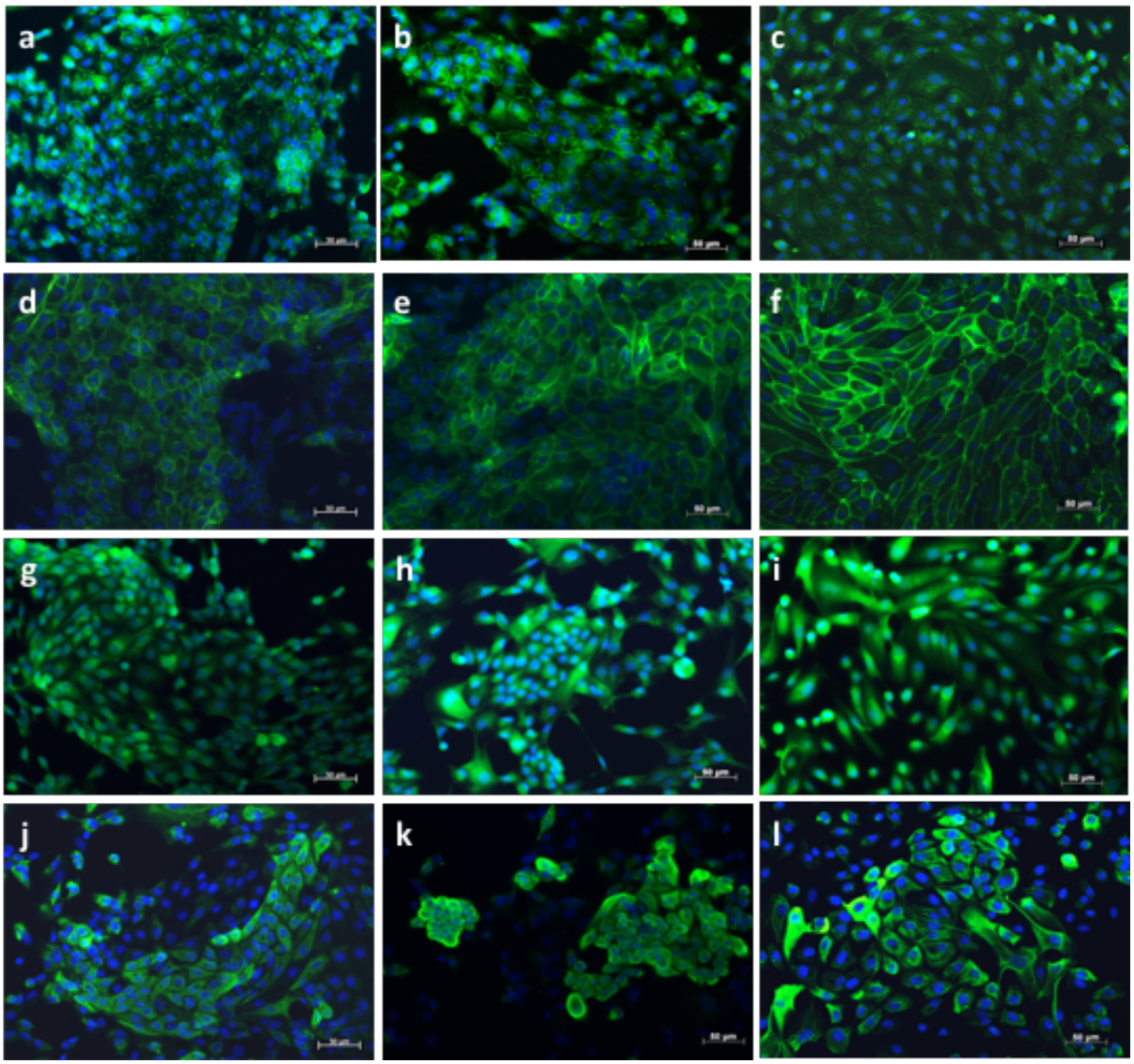

Figure 3-8 Expression of various markers of epithelial cells in the isolated primary PTECs
Immunofluorescent staining of proteins commonly expressed by tubular epithelial cells; (a-c) ZO-1, (d-f) E-cadherin, (g-i) K-cadherin and (j-l) Cytokeratin. Characterisation was made to primary PTEC at passage 2 or 3. Three images were displayed for each antibody (N=3), with each image representing a biological replicate. Images were captured with fluorescence microscope at 200x magnification.

Cells were also stained with non-epithelial markers to rule out possibility of a mixed population. Colagen-1, α-SMA and vimentin were used for this purpose. Our isolated primary PTEC did not show expression of these proteins (Figure 3-9, panel a-c). The results were

compared to primary human kidney fibroblasts isolated from the same tissue origin, which showed positive expression of these proteins (Figure 3-9, panel d-f).

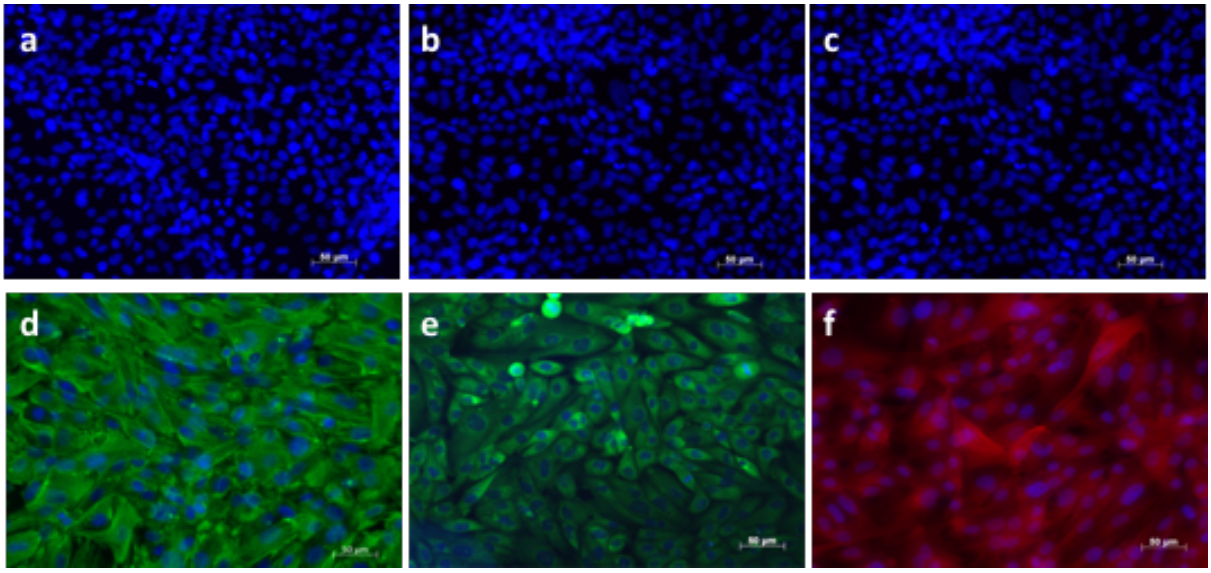

Figure 3-9. Expression of mesenchymal markers in primary PTECs and primary renal fibroblasts

Immunofluorescent staining of mesenchymal markers; (a) Vimentin, (b) α-SMA and (c) Collagen-1 in the isolated primary PTECs. As positive controls, the same mesenchymal markers were applied to human primary fibroblasts isolated from similar tissue (d) Vimentin, (e) α-SMA and (f) Collagen-1. One image is a representation of an experiment conducted on biological duplicates (N=2). Images were acquired at 200x magnification.

3.2.3. Scanning Electron Microscopy

Scanning electron microscopy (SEM) images were taken on cells at passage 2, which highlight the round or hexagonal morphology common for PTEC (Figure 3-10 panel a). Higher SEM magnification showed presence of microvilli as a typical characteristic of epithelial cells (Figure 3-10 panel a-c). However, not all cells have these distinct microvilli on their surface. In a small area (as shown in Figure 3-10 panel b), some of these cells have very short villi. As expected, the isolated population contains some degree of contamination from other cell types (Figure 3-10 panel c), however, lower magnification (Figure 3-10 panel d), demonstrated that most cells were constituted by PTECs. An overview image of the slide also displayed distinct cobblestone-like conformation in a confluent monolayer (Figure 3-10 panel d). As comparison, fibroblasts isolated from similar samples were also imaged with SEM. This revealed a cell population with distinct morphology, mainly having a longer and spindle-like appearance with no microvilli (Figure 3-11).

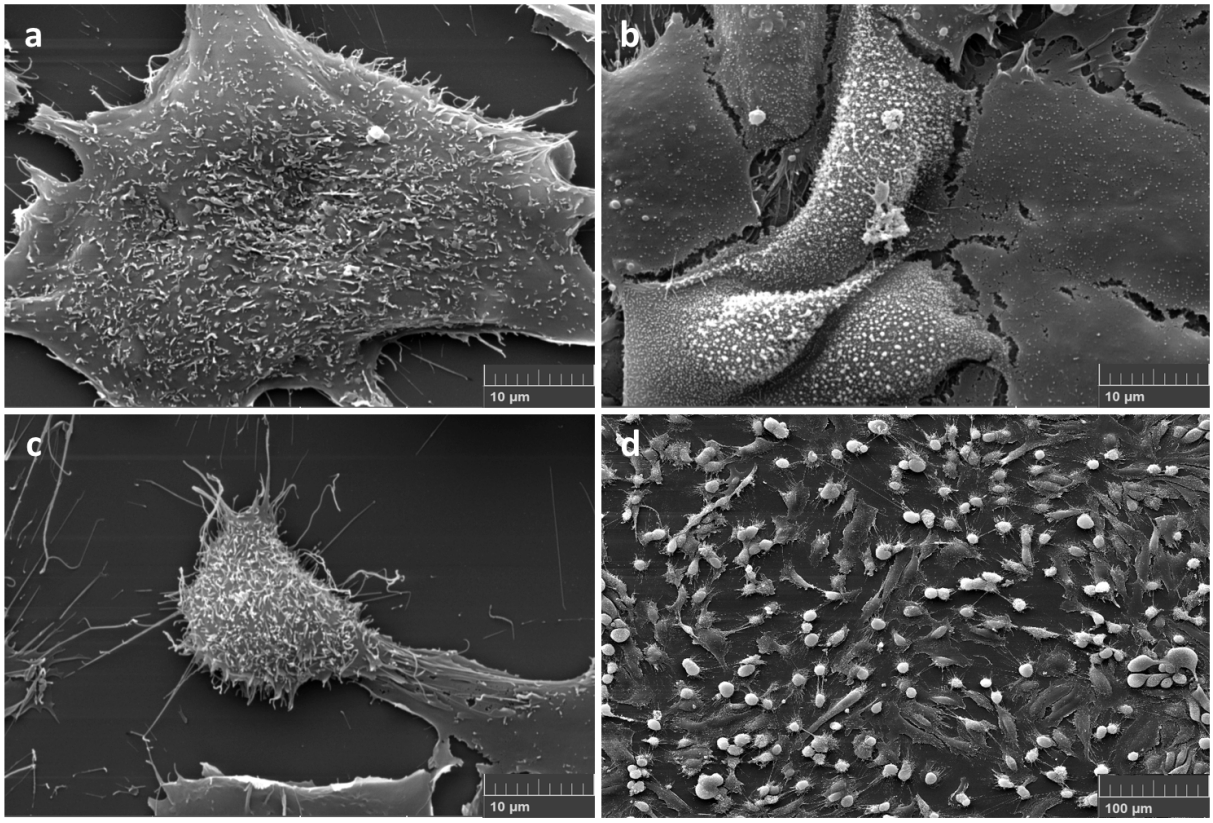

Figure 3-10 SEM images of human primary PTEC

Scanning electron microscopy images of human primary PTECs at passage 3. Images a, b and c were captured at 5,000x magnification to show the presence of microvilli on the cell surface. Image d was taken at 500x magnification to provide an overview on how most area of the visual field was occupied by cells with microvilli.

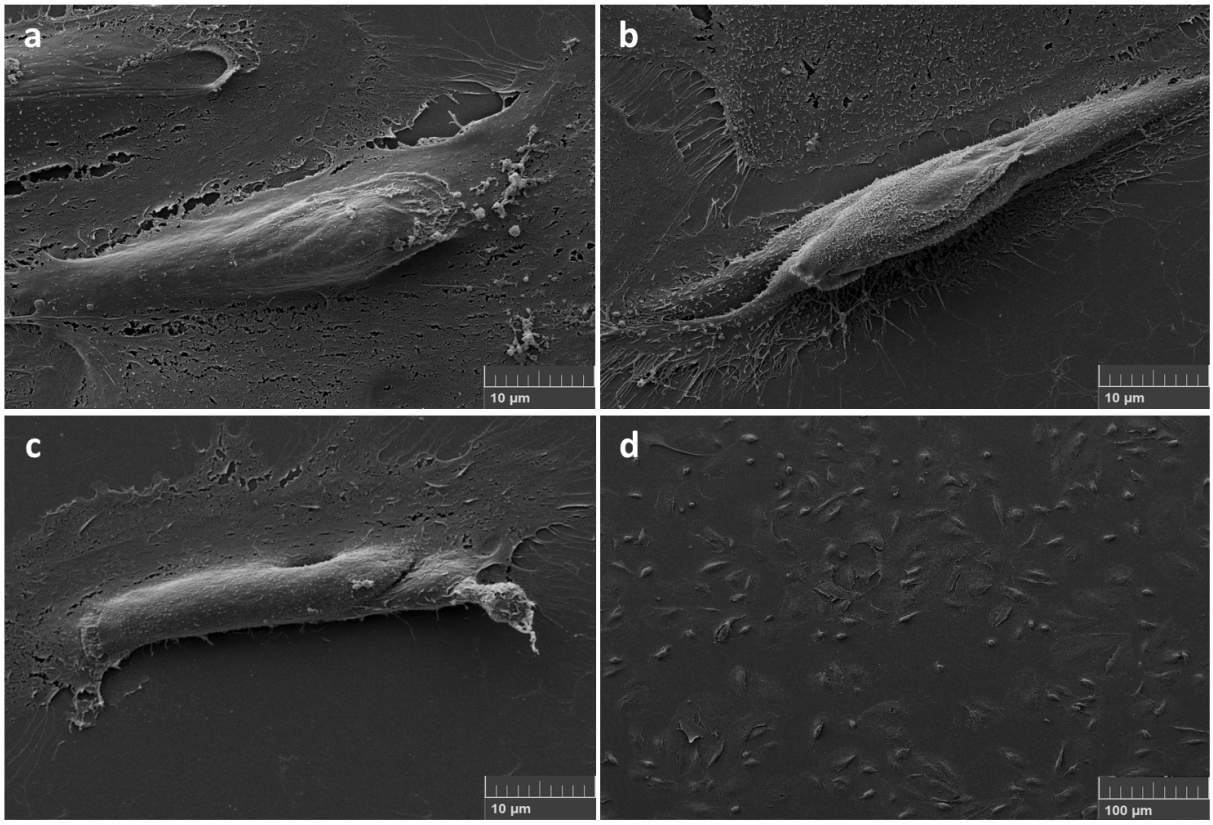

Figure 3-11. SEM images of human primary fibroblasts

Scanning electron microscopy images of human primary renal fibroblast at passage 2. Cells were isolated from tissue source similar to the tissues from which PTECs were isolated. Images a, b and c were acquired at 5,000x magnification to show the absence of microvilli on cell surface. Image d was captured at 500x magnification as an overview of a wider visual field.

3.3. Discussion

Tubulointerstitial pathology has been frequently considered as the hallmark of various abnormalities in the kidney, including acute kidney injury due to IRI. PTEC is a key player in tubulo-interstitial pathology, thus has been the subject of numerous studies. *In vitro* studies using PTECs has been considered an important element of kidney research, as it is able to provide a well-controlled model to study renal response to a particular injury or disease. Despite the availability of animal primary PTECs and some immortalised PTEC cell lines, their genetic and biomolecular profile may not be an adequate representation of human primary PTECs. Establishing an effective and reproducible method to isolate human primary PTECs is therefore an important step in a kidney research.

The most widely utilised method to isolate human primary proximal tubular cells is by Percoll density gradient centrifugation. Several adaptations of this technique have been reported in the literatures. Some authors used an ultracentrifuge to create the gradient density, while others performed collagenase digestion of renal tissue and mechanical sieving prior to the centrifugation step (Qi *et al.*, 2007; Brown *et al.*, 2008; A.Vesey *et al.*, 2009; Sharpe and Dockrell, 2012). Despite being the most common method utilised, there are potential problems associated with this technique. One of the most common criticisms is the heterogeneity of the final product, which may contain not only proximal tubular cells, but also distal tubular cells, kidney fibroblasts and cellular debris. To overcome this problem, some authors reported the use of additional purification technique. This includes immune-magnetic separation technique using microbeads (Baer *et al.*, 1997; Van der Hauwaert *et al.*, 2013). Alternatively, others have proposed cellular sorting technique with the use of antibodies against prominin-1, a surface glycoprotein expressed in the brush border of proximal PTECs (Weigmann *et al.*, 1997; Legouis *et al.*, 2015) or by elimination of the contaminating distal convoluted tubular cells using anti-Tamm-Horsfall glycoprotein (Kamiyama *et al.*, 2012). Despite their highly selective final product, the use of these additional immunogenic separation techniques is expensive, laborious, and are often associated with low cell yield and poor cell viability.

Regardless of the criticism, several authors have evaluated the effectiveness of Percoll density gradient centrifugation protocol, especially when it was preceded with initial collagenase digestion and mechanical sieving steps. Cells characterisation performed by Qi et al. showed that the isolated cells have brush border enzyme activities (high gamma-glutamyl transpeptidase and alkaline phosphatase level) and transport activities indicative of PTEC (Qi *et al.*, 2007). In our Institution, gradient centrifugation protocol with Percoll has been

established and applied to isolate primary PTECs from whole kidney, without the need to perform additional immunogenic separation steps. The isolated cells were mainly used for basic renal physiological experiments and drug transporter related research (Brown *et al.*, 2008).

The use of higher collagenase concentration and longer collagenase exposure will result in less contamination of the final cell population; however, they are also associated with lower cell yield, thus lower cellular density, accelerated cellular dedifferentiation and earlier senescence. Deciding the most appropriate collagenase concentration and digestion time is therefore important to achieve the balance between reasonably pure culture and acceptable cellular yield. Initial optimisation steps to determine the appropriate concentration of collagenase, optimal enzymatic digestion and centrifugation time required, have been performed and reported previously (Brown *et al.*, 2008). With this knowledge, I isolated PTECs from normal sections of human kidney, removed for oncological indications available to our facility using the already established protocol. It is important to mention that the original protocol was optimised for cell isolation from a larger section of renal tissue (approximately a quarter of the total minced cortical region of the whole kidney) compared to the tissues available to us (only sections of macroscopically normal kidney). Smaller tissue specimens were shown to yield cell populations with poorer quality and morphology. Moreover, smaller tissue specimens produced a very feint band of epithelial cells after gradient centrifugation. Manual aspiration of such a fine band is very likely to result in contamination by fibroblasts, erythrocytes or other cellular debris. Indeed, I found a visible contamination and poor growth capacity in cells isolated from tissue specimens that weighed below 1.5 gram. Brown et al. (Brown *et al.*, 2008) documented the yield of around 3.5 million cells/gram wet weight kidney. Using the same collagenase concentration per gram weight of tissue, I have managed to achieve the yield of 1.5 to 2 million cells/gram wet weight of tissue specimen.

Adequate characterisation of the isolated cells is necessary to ensure that the correct phenotype has been obtained in a reasonably pure culture. There are several characterisation methods that can be used. The simplest method is by examining the cell growth pattern and morphology by light microscopy. PTEC has a distinct hexagonal/round shape, initiates their growth in clusters, and when grown in high density, demonstrates the classic cobblestone-like appearance (Qi *et al.*, 2007; A.Vesey *et al.*, 2009). These features were easily identifiable in the cells that I isolated. Viable and functioning tubular cells have an intact cell-to-cell tight junction, and perform active cellular transport. This can be seen as accumulation of fluid between the cell monolayer and the solid growth surface of the culture vessels (Qi *et al.*,

2007), which is often referred to as ‘domes’. Formation of ‘domes’ was also present in the PTECs populations I isolated.

Presence of brush border is a typical feature of PTECs. To visualise this feature, I imaged the isolated cells using SEM. Microcillia were clearly present on the surface of most of the isolated cells. This strongly indicates that the majority of cells isolated have epithelial cell characteristics. However, the appearance of these microvilli appeared to be shorter than what normally seen on PTECs. It is highly likely that this was caused by the static (no continuous flow) environment in which the cells were cultured. Moreover, these primary cells were seeded directly on plastic surface, and not on a collagen matrix, which may affect the appearance of these villi. One other possible explanation is that the isolated cells were a mix population of cells consisting of distal TECs (DTECs) and not PTECs. DTECs are characterised by shorter villi compared to PTECs.

Characterisation by immunofluorescence was performed to confirm that the isolated population are indeed epithelial cells, also to identify the extent of possible contamination by fibroblasts. For this purpose, several proteins, which are expressed in epithelial and mesangial cells, were selected. Zona Occludens-1 (ZO-1) is a tight junction protein presents on cellular membrane. ZO-1 is widely expressed on epithelial cells, but not specific to the renal tubular epithelial cells. This marker was selected to detect the proportion fibroblast contamination in the cultured population. Images from all our tissue samples showed that ZO-1 was strongly expressed in almost all regions of a slide, indicating negligible contamination from fibroblasts. Cytokeratin has been documented to be highly expressed in PTC culture (Qi *et al.*, 2007). In the isolated cells, prominent cytokeratin expression is uniformly identifiable, providing further support that the cells isolated are indeed PTECs.

To further confirm, I decided to stain the cells for cadherins protein. The cadherins protein family are established markers of renal tubular epithelial cells. Their strong expression in the isolated cells clearly highlights the fact that renal tubular epithelial cells constituted majority, if not all, of the cultured cell population. Several papers have reported contradicting evidence of E-Cadherin, K-Cadherin or N-Cadherin expression in renal tubular epithelial cell sub-populations. It was previously accepted that generally E-Cadherin was highly expressed in renal proximal tubular epithelial cells. In contrast, some more recent authors documented that E-Cadherin was highly expressed in distal tubular cells and not as strongly expressed in proximal epithelial cells. K-Cadherin on the other hand was a prominent marker of proximal tubular cells. In a cultured proximal tubular cell population, however, both cadherins have been documented to be expressed equally strongly, as was also shown in the population I isolated. The immunofluorescence suggested stronger expression of K-Cadherin compared to

E-Cadherin, which is a consistent finding in proximal tubular epithelial cell population as documented by several authors (Paul *et al.*, 1997; Baer *et al.*, 2006; Systems, 2015). Mesangial and fibroblast markers, such as collagen-1, α-smooth muscle actin and vimentin were used to exclude cells of mesangial or fibroblast origin. These markers were not expressed in any of the isolated cells.

Although primary culture of PTECs provides a better model to study the human kidney, their use has been restricted by the limited number of passages they could undergo. Some authors reported the end of mitotic lifespan of primary PTECs is reached after approximately 8 to 10 passages, while others have only managed to successfully propagate primary PTECs for 5 passages (Qi *et al.*, 2007; A.Vesey *et al.*, 2009; Sharpe and Dockrell, 2012). Despite these differences, all authors have recommended only to use cells at passage 2 or 3 in experiments, to ensure unaltered characteristics of these cells. This agrees with my findings, which identified significant cellular morphological changes in these cells after four passages. I hypothesised that such an early change may be partly due to direct seeding of these cells to plastic surface with no collagen coating. However, I decided not to modify the seeding method since I was intending to use the cells only at passage 2 or 3 in my experiments.

Taken into consideration the results of all characterisation methods used, I have satisfactorily proved that the isolated cells fulfil the characteristics of PTECs. Furthermore, I have also established a modified gradient centrifugation protocol to isolate PTECs from a relatively small kidney tissue, which has been shown to be relatively easy to perform as well as reproducible. This method also produces a pure final population of cells without the need to perform additional separation techniques. I could confidently conclude that the isolated population is representative of human primary PTECs.

Chapter 4. Effect of Ischaemia and Free Radicals in MicroRNA Profile of Tubular Epithelial Cell

4.1. Introduction and Specific Objectives

Ischaemia and reperfusion injury is one of the contributing factors to the progression of allograft damage after kidney transplantation. As to whether the injury induces reversible or irreversible tissue damage depends upon the duration of injury, frequency and degree of severity. There is substantial evidence available to support that IRI leaves signature miRNA changes, which vary between different organ and tissues. How these miRNA changes affect organ function at shorter or longer time points, however, remains to be comprehensively investigated.

Proximal tubular epithelial cells have been identified as both the target and an active player in the renal response to IRI. Identifying the signature changes in PTEC miRNA after IRI is the first step in selecting key miRNAs involved in the renal response to IRI. The main objective of this part of the study is to create an optimal IRI model *in vitro*, and to further observe how IRI alters miRNA expression level in various types of renal PTECs. Prior to miRNA profiling, an optimal protocol to induce hypoxia and reperfusion in the various cell types used had to be established. An ideal ischaemia or reperfusion treatment should be adequate to induce detectable level of stress resulting in miRNA changes without compromising cellular viability. To determine these optimal treatment conditions, I set up a series of experiment to objectively measure each cell's viability threshold and tolerability to either ischaemia or reperfusion injury.

Profiling miRNA in only one cell type following a specific condition is not ideal, and is considered one of the factors contributing to the lack of overlapping results among existing data. This is an important factor to consider, especially if the profiling is based only on immortalised cell lines, which arguably possesses limited resemblance to primary human cells. By using several cell types in this profiling step, we expect to see an overlapping set of miRNAs, which are consistently up/down-regulated following ischaemia or reperfusion. These miRNAs will be considered strong candidates to be explored and validated further.

4.2. Results: Simulating Ischaemia and Reperfusion Injury

4.2.1. Assessment of the Effect of Hypoxia

4.2.1.1. HIF-1α Nuclear Localisation

After 12 hours of incubation with 1% O_2, HKC-8 cells were stained with anti HIF-1α antibody to assess the response to hypoxia. HKC-8 cells treated with 100 μM $CoCl_2$ for 72 hours were used as a positive control (Figure 4-1 panel d-f). Intra-nuclear staining of HIF-1α was visible in both positive control and HKC8 cells incubated in hypoxia chamber. (Figure 4-1 panel a-f). Chemical stabilisation of HIF-1α by $CoCl_2$ treatment resulted in more HIF-1α nuclear localisation compared to induction of hypoxia using a hypoxia chamber. Nevertheless, it is evident that there was a clear increase in cytoplasmic and intra-nuclear HIF-1α staining in the hypoxic cells compared to the normoxic cells.

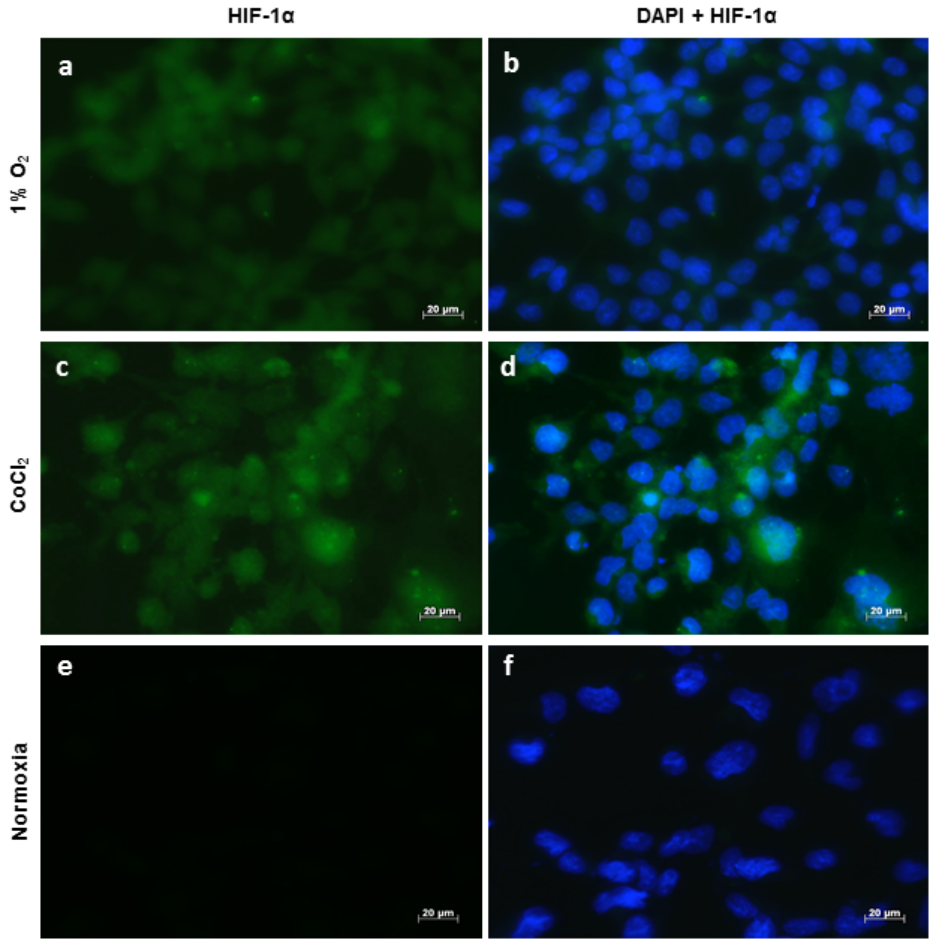

Figure 4-1 HIF-1α expression in HKC-8 cells in ischaemic condition

HIF-1α expression in HKC-8 cells incubated in 1% O_2 for 12 hours (a and b), $CoCl_2$ for 72 hours (c and d), and in normoxia (e and f). Images were taken at 400x magnification using Zeiss Axio imaging unit. Images shown are the representative of images captured from two independent experiments (N=2).

4.2.1.2. HRE-Luciferase Activity

Indirect measurement of hypoxia responsive element activation through luciferase activity enabled demonstration of a functional effect of hypoxia to HKC-8 cells. Incubation in 1% O_2 for 12 hours initiate a HRE activation. Interestingly, further incubation time resulted in less luciferase activity (Figure 4-2). At both time points, HKC-8 cells were clearly shown to be responding to hypoxia, indicated by the significance increase in luciferase activity compared to HKC-8 cells in normoxic environment.

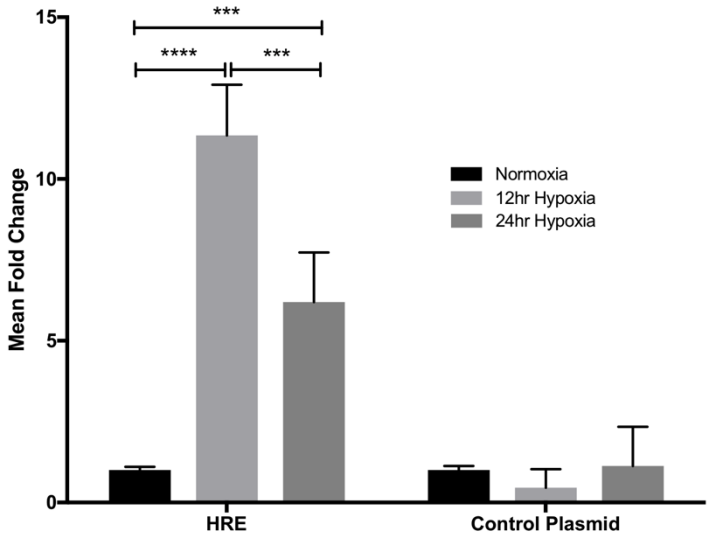

Figure 4-2 HRE luciferase activity following hypoxia

Fold change in luciferase activity of hypoxia response elements (HRE)-transfected HKC-8 cells after 12 and 24-hour incubation in 1% O_2. Luciferase expression was compared to HRE-transfected HKC-8 cells incubated in normoxia. Mean luciferase activity was normalised to the total protein. HKC-8 cells transfected with an empty plasmid (PGL3) were used as plasmid control. Data was presented as fold change of the mean of normalised luciferase activity + SD. One-way ANOVA test was used to detect significant difference between the means. Multiple comparisons between samples were performed using Bonferroni post-hoc analysis. (*** = $p \leq 0.001$; **** $p \leq 0.0001$)

4.2.2. Assessment of Oxidative Stress

4.2.2.1. Viability Assay

To appropriately simulate reperfusion injury, cells should be stressed enough to induce gene expression changes without significant effects on cell viability. 80% viability was chosen as it is an arbitrary cut-off to demonstrate cell loss due to free radical injury, but with sufficient cell survival for analysis. Every cell type responded similarly to H_2O_2 treatment. Increasing concentration of H_2O_2 resulted in gradual cell death in all cells. In HKC-8 cells, the threshold concentration is 400 μM. HK-2 and primary PTECs were more sensitive to H_2O_2

treatment, with a H_2O_2 concentration of 200 μM and 300 μM, respectively sufficient to cause 20% cell death (Figure 4-3).

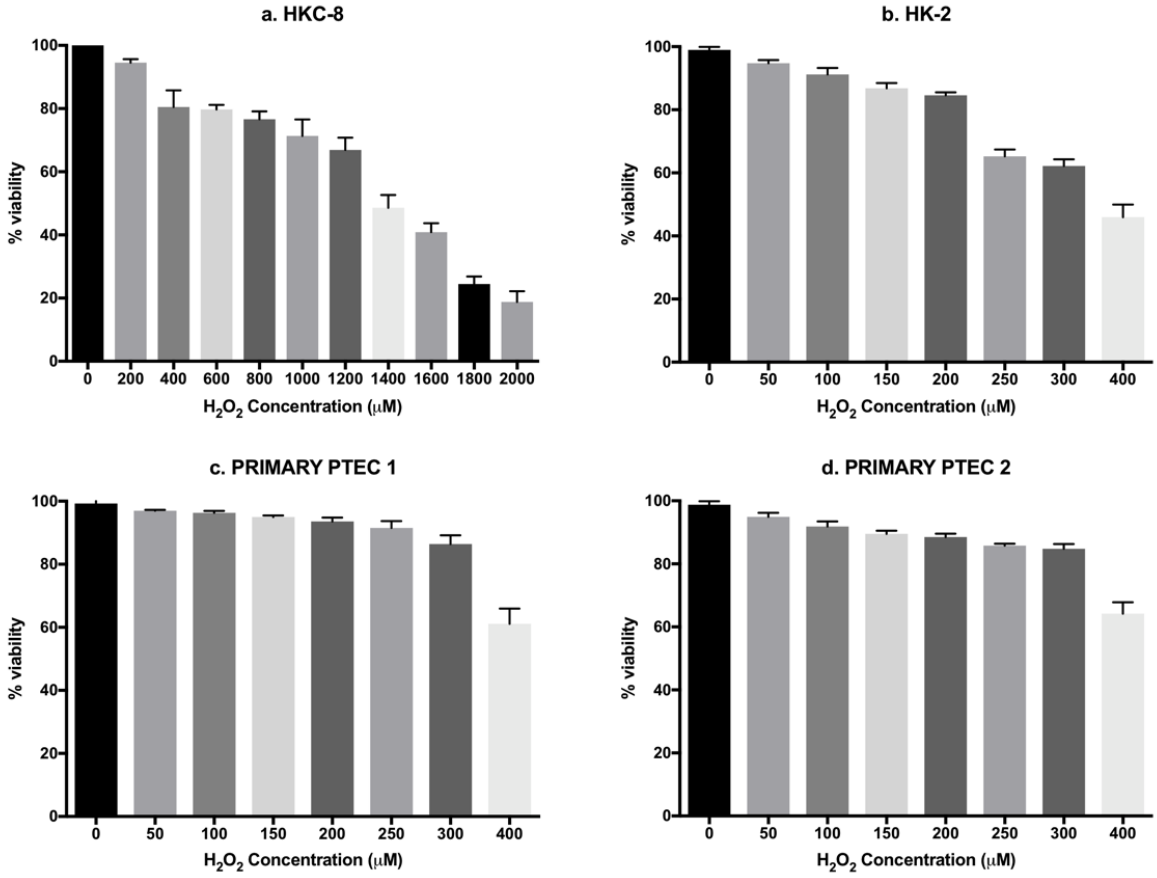

Figure 4-3 PTEC viability after induction of free radical

Percentage viability of various types of cells: (a) HKC-8 cells; (b) HK-2 cells, and (c, d) primary PTEC from two different patients after exposure to short-term H_2O_2 treatment (4 hour in H_2O_2 followed by incubation in fresh complete media for 20-hour). Percentage viability was measured by trypan blue dye exclusion assay. Data was presented as the mean of percentage viability + SD from three replicates (N=3).

The initial phase of this experiment was performed in HKC-8 cells. A wider range of H_2O_2 concentration was used to define the concentrations to use for future experiments. For HKC-8 cells, 400 μM was chosen as the optimal concentration as it resulted in 80% cell viability. HK-2 and primary human cells were more susceptible to free radical injury. The same concentration used for HKC-8 markedly reduced HK-2 and primary human cell viability to 50% and 60% respectively. Therefore, lower concentrations of H_2O_2 were considered as optimal treatment conditions. As the origin of human primary cells varies in terms of patient clinical status, underlying renal disease, and other undefined factors, the response to free radical stress was assessed in cells isolated from each patient. The results suggested the same optimal concentration of H_2O_2.

4.2.2.2. Detection of Oxidative Stress

Fluorescence-activated cell sorting (FACS) was used to detect oxidative activity in cells. Population gating was performed based on FSC (forward scatter) and SSC (side scatter) (Figure 4-4). Unstained cells emitted negligible degree of fluorescence, which was regarded as cell auto-fluorescence (Figure 4-4 panel A). Median intensity emission of CM-H_2DCFDA was plotted against number of events recorded on histograms. Untreated cells stained with dye showed an increase in fluorescence emission compared to unstained cells. This was used as control. As shown in Figure 4-4, there was an increase in fluorescence with increasing hydrogen peroxide concentration up to 400µM. This is represented as shift of the peak to the right (Figure 4-4 panel C-F).

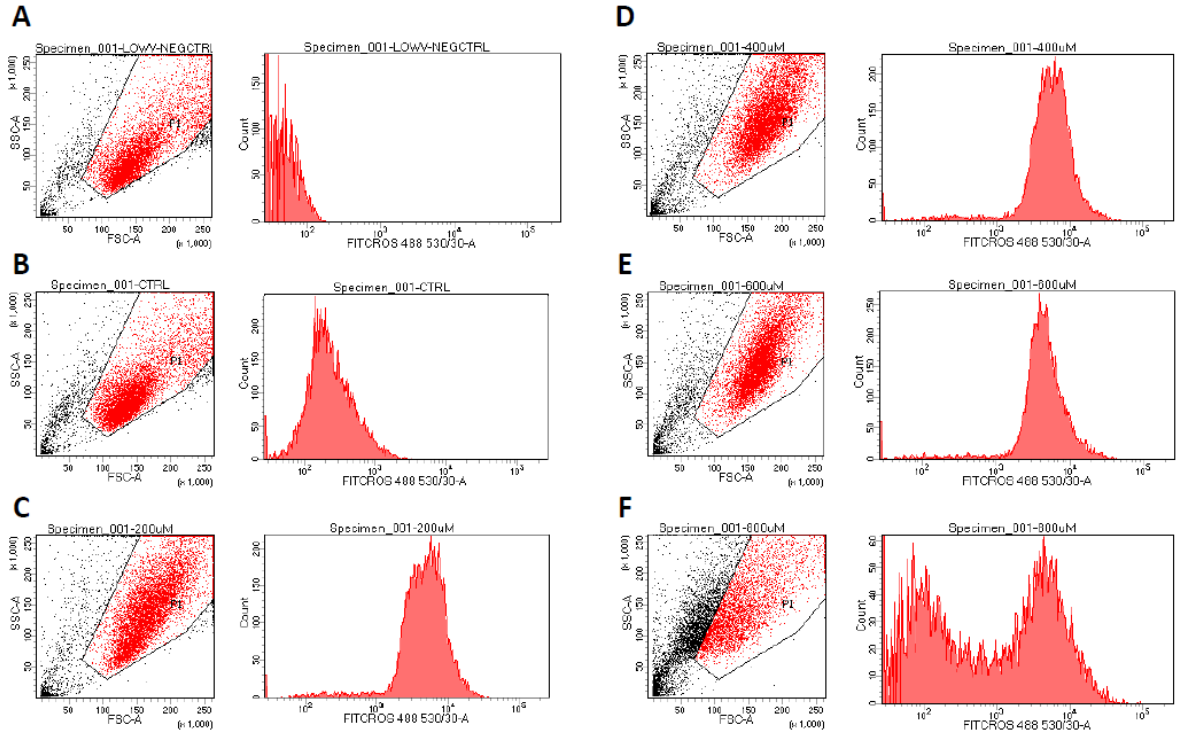

Figure 4-4 ROS molecular probe activity after H_2O_2 treatment

Population gating and fluorescence emission of CM-H_2DCFDA in HKC-8 cells treated with various H_2O_2 concentrations. Cells were exposed to H_2O_2 for 4 hours before incubation in normal media for 20 hours before staining with CM-H_2DCFDA. Results were presented as follows; (A) no probe, no H_2O_2; (B) with probe, no H_2O_2; (C) with probe, 200 µM H_2O_2; (D) with probe, 400 µM H_2O_2; (E) with probe, 600 µM H_2O_2; (F) with probe, 800 µM H_2O_2.

As illustrated in Figure 4-4 (panel D), 400 μM H_2O_2 induced the most ROS in HKC8 cells. Further increases in H_2O_2 concentration resulted in a lower median intensity (Figure 4-4 panel E and F). At 800 μM, generation of ROS fell almost to the level comparable to control. There were two peaks of intensity visible at this concentration (Figure 4-4 panel F). The lower intensity peak may represent unviable cells, as a consequence of higher H_2O_2 concentration.

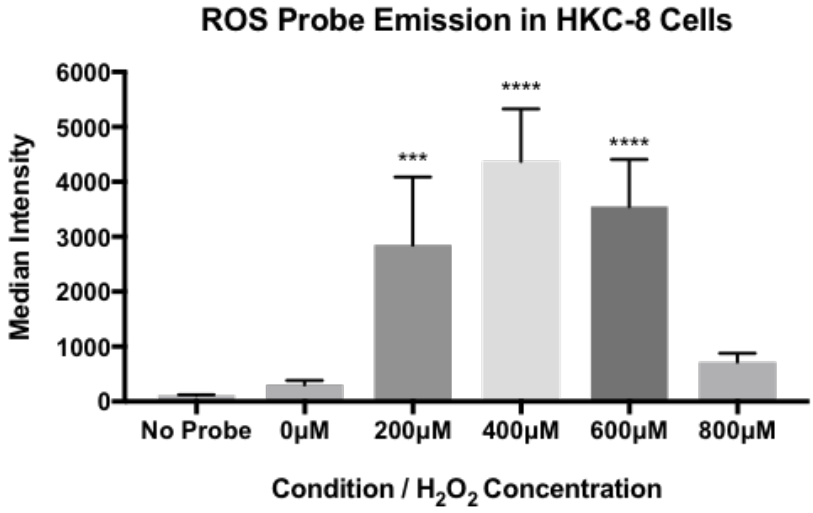

Figure 4-5 Summary of ROS probe activation in H_2O_2 treated PTECs
Graph showing median intensity emission of CM_2-H_2DCFDA in HKC-8 cells treated with different H_2O_2 concentrations. Data is presented as median intensity + SD of three replicates (N=3). One-way ANOVA with Bonferroni post-hoc analysis was used analyse emission at 200 μM, 400 μM, 600 μM and 800 μM compared with emission at 0 μM. (*** = $p \leq 0.001$; **** $p \leq 0.0001$)

4.3. Results; MicroRNA Profiling

4.3.1. MicroRNA Selection Criteria

A change in a miRNA level of expression by 2-fold or greater was considered significant. As different cell types were used, their genetic differences need to be appreciated, especially between cell line (HKC-8 and HK-2 cells) and the two primary PTECs used. Therefore, miRNA selection was not performed only based on the magnitude of change in the level of expression, but also based on the consistency of up or down-regulation. Subsequent analysis will only include miRNAs which were consistently up/down-regulated in either both cell lines (HKC-8 and HK-2 cells) or both primary PTECs. These miRNAs that fulfil the selection criteria were included in the subsequent functional analysis work.

4.3.2. Quality Control and Normalisation Methods

Several quality control metrics were performed to ensure that all samples were correctly processed and captured. This include field of view (FOV) and binding density. The data did not show significant discrepancy between the FOV count and FOV counted; indicating that no technical issues related to imaging performance was encountered in the experiment. The image saturation of all lanes was also within the desired range of binding density, reflecting the integrity of probe counts produced. The quality control metrics verified that there was no quality control issue related to sample quality, sample processing and assay techniques.

To assess the performance of ligation controls, positive and negative controls, a heatmap illustrating their expression level was generated (Figure 4-6). All ligation controls performed as expected, indicated by positive detection of positive ligation controls, and negative expression of negative ligation control. The codeset provides six positive controls, which were ligated and hybridised in the same way as an endogenous miRNA in the codeset. These positive controls should be in six decreasing concentrations after hybridisation process; 128 fM, 32 fM, 8 fM, 2 fM, 0.5 fM and 0.12 fM. The expression of these positive controls were also appropriately visualised in the heatmap. In addition, the expression levels of a set of mRNAs used as reference genes were also displayed, which were shown to be relatively equal across different samples.

To profile miRNAs expression after IRI, I utilised a human miRNA codeset containing 800 miRNAs. Following the manufacturer's recommendation, I chose to normalise the data readings using global normalisation method (using the 100 mostly expressed miRNAs in the dataset). Prior to applying this method, however, it was necessary to ascertain that the expression of these reporter probes did not vary significantly between different samples. Using one of the sample/lane as a reference point, I selected the 100 most highly expressed miRNAs across all samples.

As an alternative to global normalisation method, Nanostring® recommends the use of a set of reference genes in the raw data normalisation process. To evaluate whether the selection of normalisation method has an impact on the detection of miRNA changes, I compared the analysis results of data normalised by global normalisation to the analysis result of data normalised by reference gene normalisation. For the purpose of illustrating the similarity or differences of the two methods, I performed the comparison in both ischaemic injury and reperfusion injury cells at 12-hour time point only.

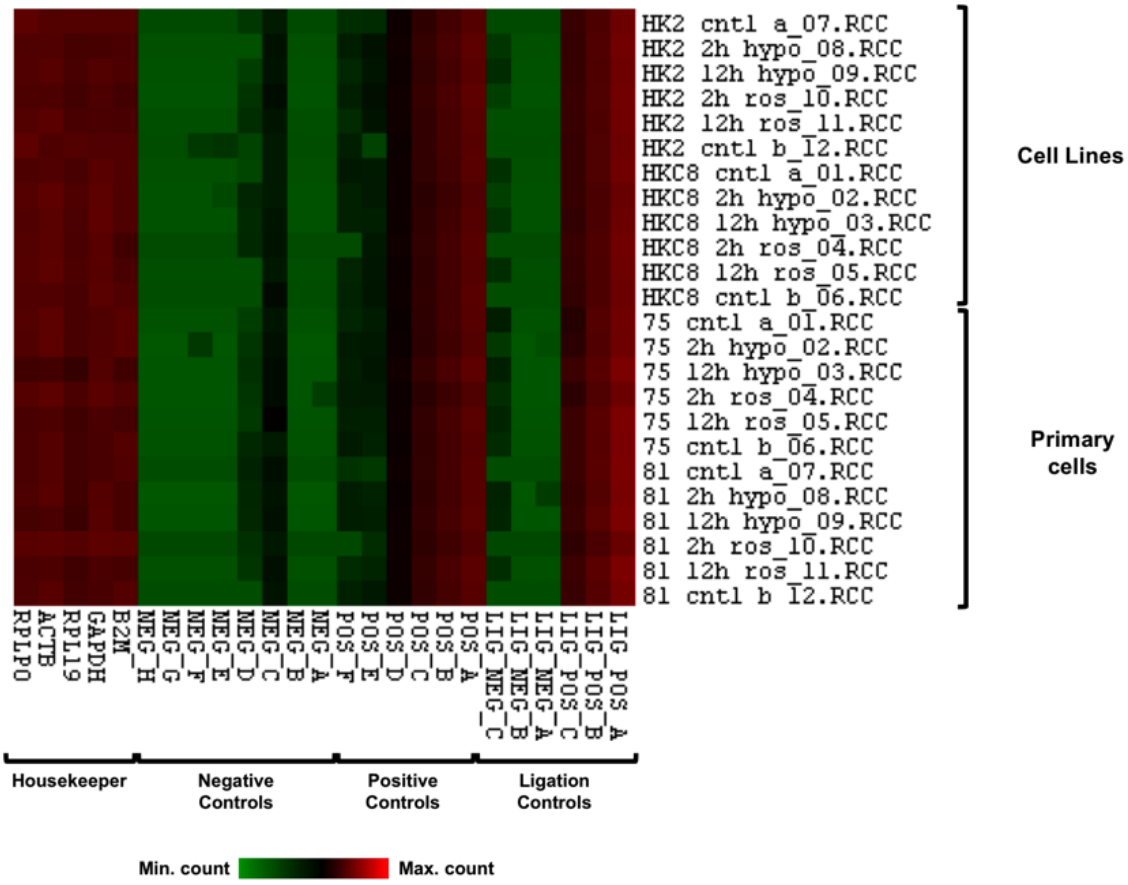

Figure 4-6 Control probes expression

Heatmap illustrating the expression level of ligation controls (3 negative and 3 positive), positive controls (6 probes), negative controls (8 probes) and reference mRNAs (B2M, GAPDH, RPL19, ACTB, RPLP0). Level of expression data was displayed in (log2) of molecule count standardised to the z-score of the probe.

At 12 hour hypoxia, 87 miRNAs that fulfil the selection criteria were identified using reference gene normalisation method, whilst global normalisation method identified 58 miRNAs. Out of these miRNAs, 50 were commonly identified by both methods (Figure 4-7). At 12 hour free radical exposure, reference gene normalisation identified 79 miRNAs that fulfil the selection criteria, whilst only 58 miRNAs were identified by the global normalisation method. 46 miRNAs were commonly identified by the two methods at 12 hour exposure to H_2O_2 (Figure 4-8).

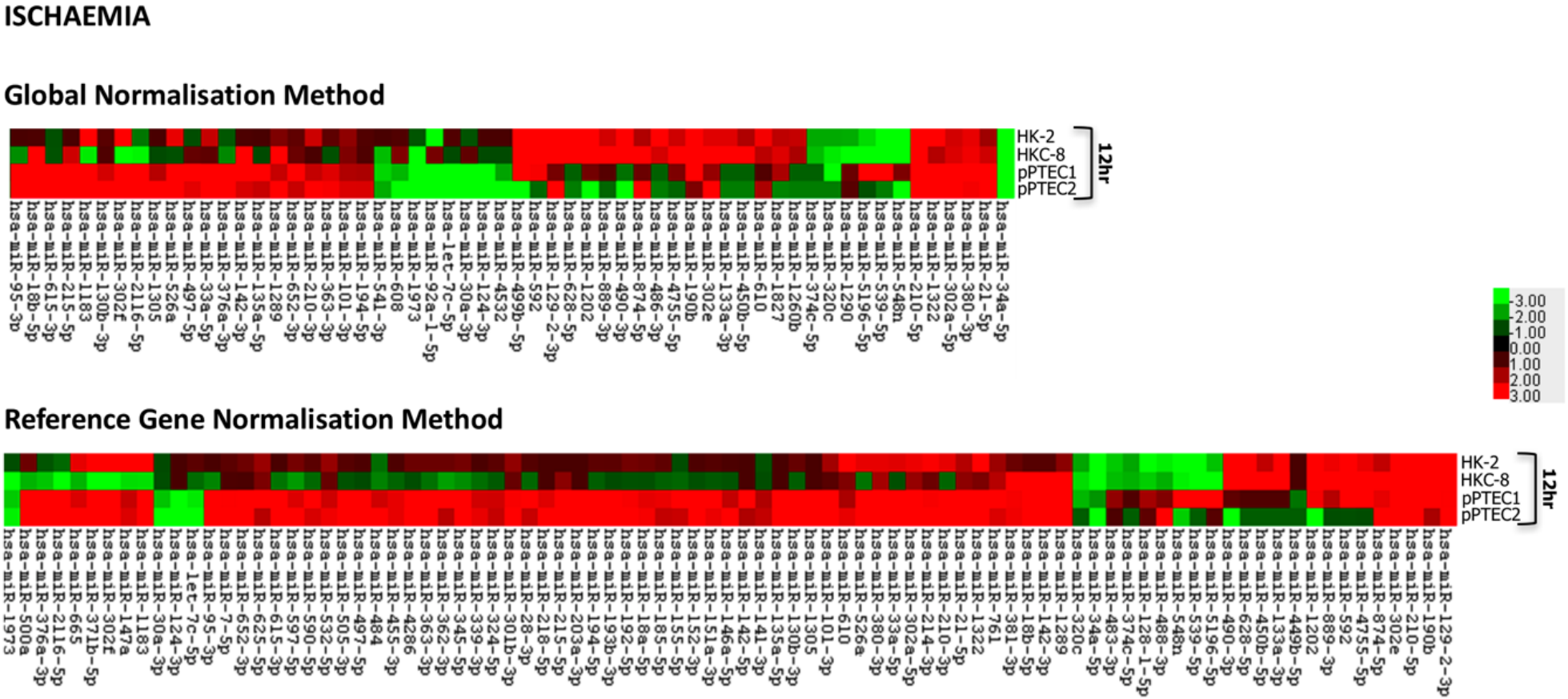

Figure 4-7 Detection of miRNAs using top 100 miRNAs vs reference gene normalisation in hypoxic cells

Heatmap illustrating differential expression of miRNAs in all cell types after 12-hour hypoxia. Detection of miRNA was performed using two different normalisation method; top 100 miRNA normalisation and reference gene normalisation. The latter method detected 50 out of 58 miRNAs detected by top 100 miRNA normalisation method.

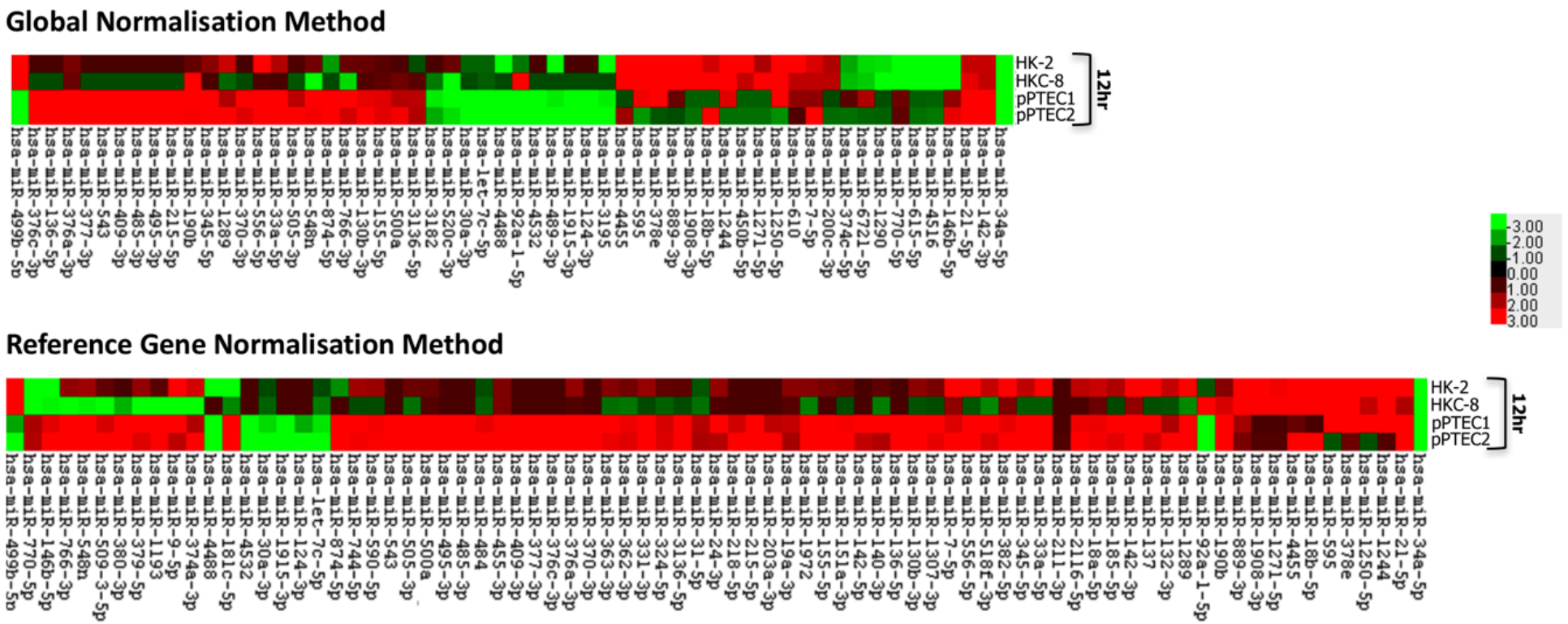

Figure 4-8 Detection of miRNAs using top 100 vs reference gene normalisation in cells exposed to H_2O_2

Heatmap illustrating differential expression of miRNAs in all cell types after 12-hour exposure to free radical. Detection of miRNA was performed using two different normalisation method; top 100 miRNA normalisation and reference gene normalisation. The latter method detected 45 out of 58 miRNAs detected by top 100 miRNA normalisation method.

4.3.3. Assessing Stability of Profile

Alteration in miRNAs profile following IRI in PTECs was detected by calculating the ratio of expression of a miRNA in ischaemia or reperfusion injury to its expression in the non-treated cells. To evaluate the effect of incubation alone (without induction of ischaemia or reperfusion) on the cells, I compared miRNA expression in non-treated cells at 0-hour and 12-hour for every cell type used. The comparison showed that in every cell type, there were a small number of miRNAs which were differentially expressed at the two observation points. However, the expression of the majority of miRNAs in the codeset was not altered by 12-hour incubation alone. The comparison between the two time points was illustrated in Figure 4-9. Detailed analysis of the two primary PTECs showed that the pattern of expression of most miRNAs was similar, which confirms the reproducibility of cell isolation procedure and relatively stable miRNA profile.

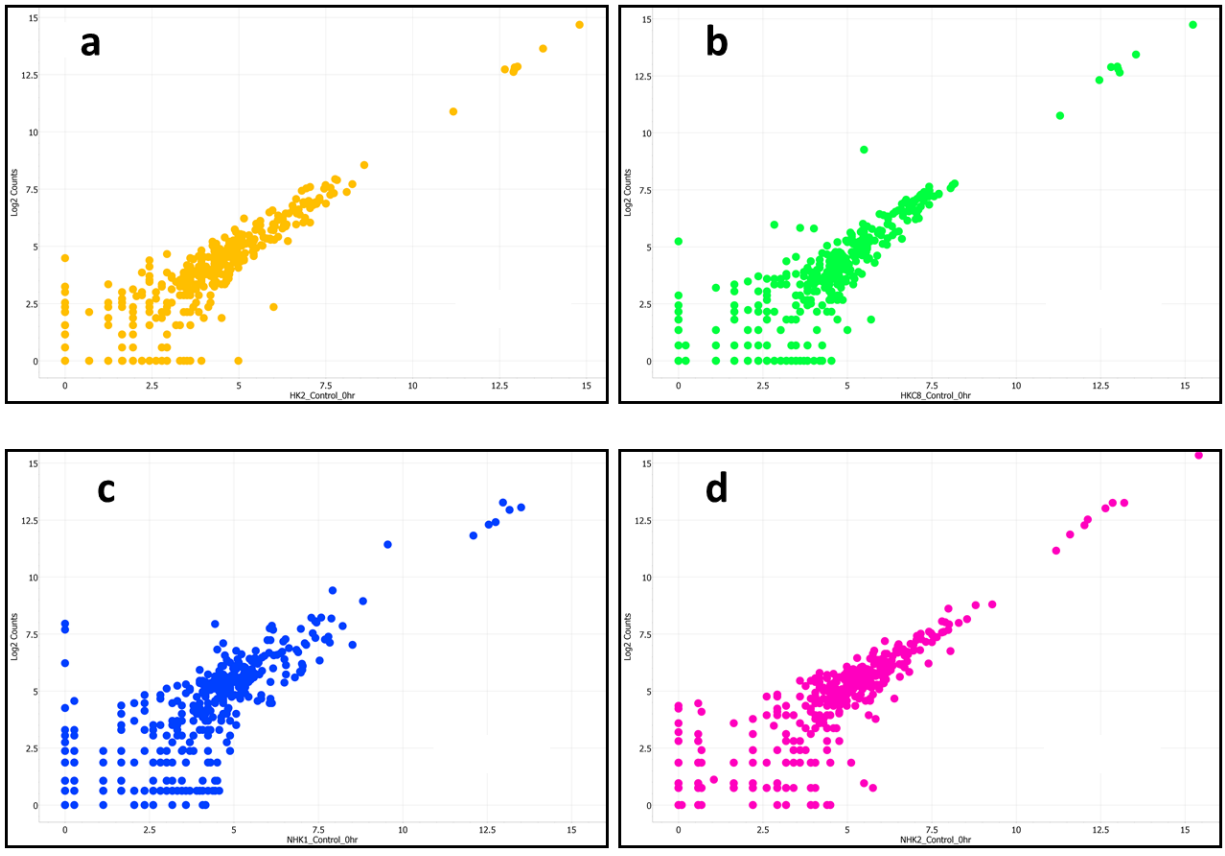

Figure 4-9 MiRNA expression in untreated cells at 0-hour and 12-hour

Scatter plots illustrating miRNA expression in untreated PTECs. Data was displayed as (log2) count of each miRNA. Comparison was made between: (a) HK-2 cells at 12-hour and 0-hour, (b) HKC-8 cells at 12-hour and 0-hour, and (c, d) pPTECs isolated from two different patients at 12-hour and 0-hour.

4.3.4. MicroRNA Profile Following Hypoxia and Induction of Free Radical

For further analysis, we decided to include only the miRNAs which met the selection criteria described in section 2.15.1. These are miRNAs with consistent up or down-regulation of 2-fold change or more, in either both cell lines (HKC-8 and HK-2 cells) or both primary PTECs following a given treatment. The nCounter® platform detected 168 out of 800 miRNAs provided in the codeset fulfilled the selection criteria. The relationship of the number of miRNAs and the treatment condition in which their expression level was found to be significantly altered was illustrated in Figure 4-10.

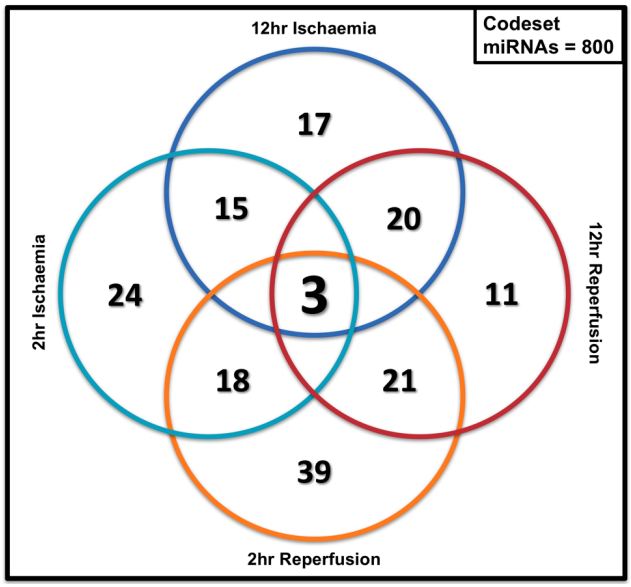

Figure 4-10 Summary of the number of miRNAs significantly altered at a given treatment condition

Codeset miRNAs is the total number of miRNA probes provided in the assay kit. Only miRNAs that met selection criteria were included in this diagram.

To evaluate whether different injury types altered miRNA profile differently, we clustered miRNAs, which fulfilled the selection criteria, based on the direction of their alteration in either ischaemia or reperfusion injury. This is illustrated in Figure 4-11 and Figure 4-12. Analysis of both the 2 and 12-hour time points showed that hypoxia alone or free radical exposure alone produced distinct miRNA signature in PTECs. At 2-hour, only 21 out of 120 miRNAs were identified in both ischaemic injury and reperfusion injury, while 23 out of 87 miRNAs were identified by both injuries at 12-hour. We have identified only three miRNAs that showed significant and consistent up/down-regulation in either all cells, both cell lines, or both primary cells after hypoxia and H_2O_2 treatment; miR-21, miR-376a and miR-190b.

To assess similarities or differences between miRNA profile in cell lines and PTECs, the miRNAs which fulfil the selection criteria were grouped into several categories, based on their pattern of up or down-regulation in either cell lines (HKC-8 and HK-2) or primary PTECs as described in Table 4-1. Expectedly, each cell type produced a unique miRNA signature in response to either ischaemia or reperfusion, highlighting differences in cellular genetic characteristics. These differences are especially apparent between the two primary PTECs and cell lines (HKC-8 and HK-2). This is reflected by the dominance of category 2 and 3, which represent consistent up/down-regulation in either cell lines or primary PTECs at all time points (Table 4-1).

Table 4-1 Categorisation of miRNA profile

Category	Number of altered miRNAs at 2 hour		Number of altered miRNAs at 12 hour	
	Hypoxia	ROS	Hypoxia	ROS
1	5	5	6	3
2	39	24	23	20
3	19	58	29	35
4	0	0	0	1

Category 1: consistent up/down-regulation in all cell types
Category 2: consistent up/down-regulation in cell lines (HKC-8 and HK-2)
Category 3: consistent up/down-regulation in both primary PTECs
Category 4: opposite effect between cell lines (HKC-8, HK-2) and primary PTECs

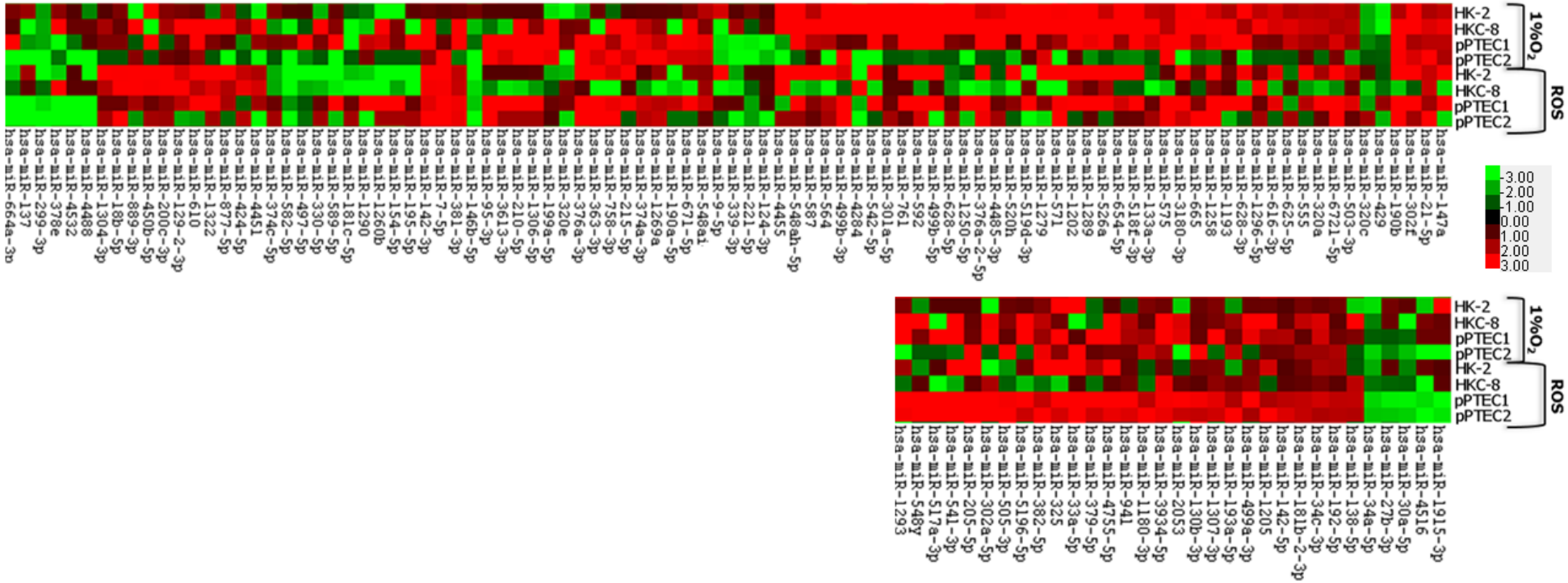

Figure 4-11 MiRNAs profile in all cells at 2-hour time point

Heatmap illustrating differential expression of miRNAs in all cell types after 2-hour hypoxia or free-radical exposure. Data was expressed as fold change of gene expression (ratio of gene expression between treated and non-treated cells at 2-hour). Only miRNAs that fulfil the selection criteria were included. MiRNA clustering was performed solely based on the selection criteria.

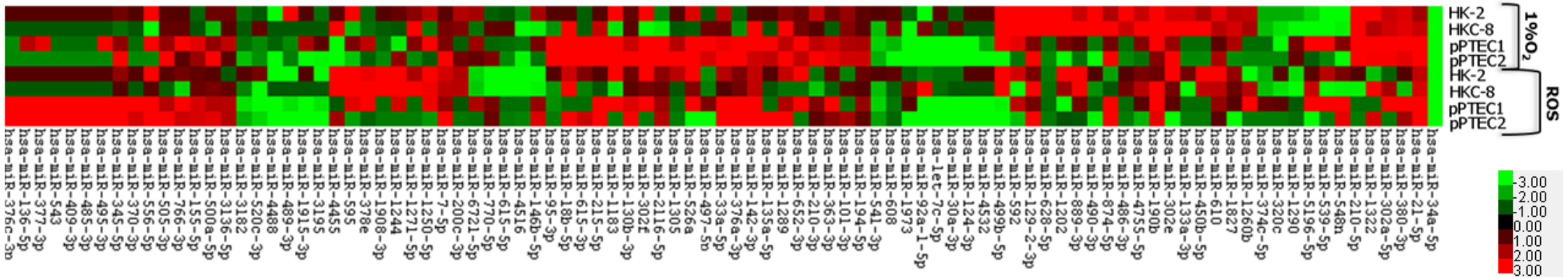

Figure 4-12 MiRNAs profile in all cells at 12-hour time point

Heatmap illustrating differential expression of miRNAs in all cell types after 12-hour hypoxia or free-radical exposure. Data was expressed as fold change of gene expression (ratio of gene expression between treated and non-treated cells at 12-hour). Only miRNAs that fulfil the selection criteria were included. MiRNAs were clustered based on the selection criteria. There was no statistical method applied to rank the miRNAs.

The miRNA expression profile at 2-hour and 12-hour after the same type of injury were also different. Consistent up- or down-regulation of a miRNA at both time points by a given injury may reflect its particular importance in performing a specific cellular function. Therefore, I have listed several miRNAs with the same pattern of expression at both 2-hour and 12-hour in either hypoxia alone or exposure to H_2O_2 alone. This is shown in Figure 4-13.

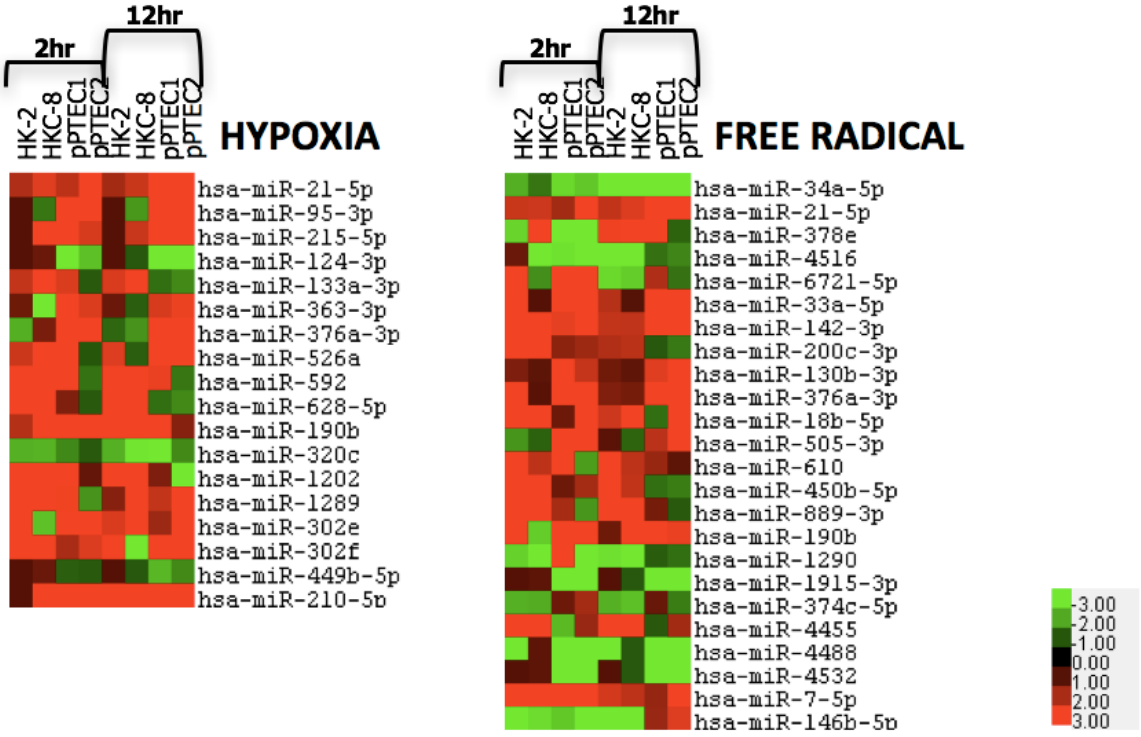

Figure 4-13 Expression pattern of selected miRNAs at 2 and 12-hour hypoxia or free-radical exposure

Heatmap showing expression of miRNAs that were significantly and consistently up- or down-regulated after ischaemia or reperfusion injury. Data was expressed as fold change of gene expression (ratio of gene expression between treated and non-treated cells at 12-hour). MiRNAs were clustered based on the selection criteria without performing a specific statistical analysis.

For the purpose of this study, I focused on 12-hour time point. At this time point, I identified 35 miRNAs with miRNAs level of expression changes unique to ischaemia. Similarly, 12-hour of free-radical injury induced changes in 35 other miRNAs (Figure 4-14). The expression level of 23 miRNAs was significantly altered in both injuries. The magnitude of changes of these miRNAs is shown in Figure 4-15 and Figure 4-16.

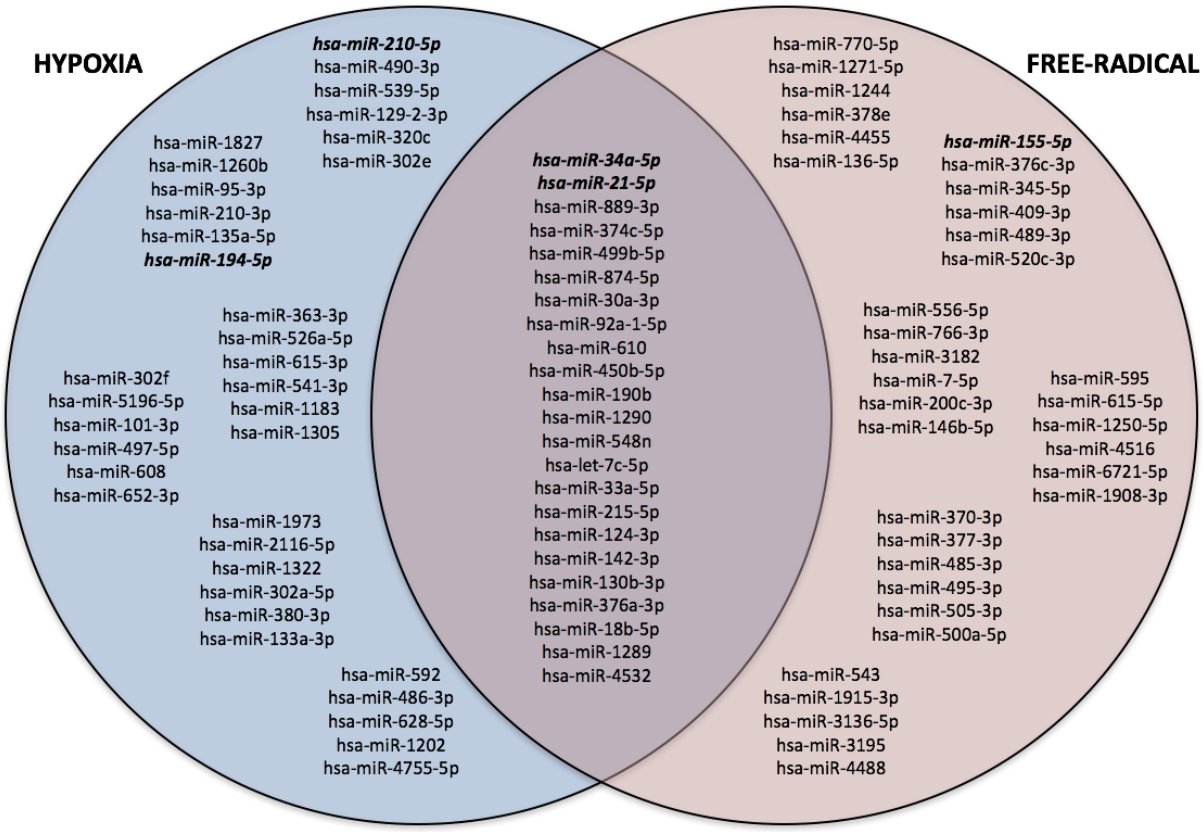

Figure 4-14 Venn diagram showing significantly altered miRNA at 12-hour time point

The diagram enlists selected miRNAs, which were altered after hypoxia only, after exposure to H_2O_2 only, and after both injuries. MiRNAs which have been previously identified in the literature which focused on renal model of IRI (see Table 1.1) were printed in bold italic font

miRNA	HKC-8	HK-2	PTEC1	PTEC2	Category	Magnitude
hsa-miR-95-3p	-1.78	1.00	4.77	29.69	3	17.23
hsa-miR-18b-5p	14.51	1.04	5.07	17.86	3	11.465
hsa-miR-615-3p	-1.13	-1.10	13.22	4.42	3	8.82
hsa-miR-499b-5p	9.30	6.82	4.03	-12.29	2	8.06
hsa-miR-210-5p	7.10	5.41	9.14	9.77	1	7.855
hsa-miR-215-5p	2.35	1.00	10.31	3.38	3	6.845
hsa-miR-1183	-2.69	8.92	5.65	6.66	3	6.155
hsa-miR-592	5.00	6.97	2.75	-1.39	2	5.985
hsa-miR-130b-3p	1.07	1.19	2.42	9.10	3	5.76
hsa-miR-302f	-5.84	8.92	3.50	7.29	3	5.395
hsa-miR-2116-5p	-2.78	-1.54	7.70	3.07	3	5.385
hsa-miR-129-2-3p	6.69	3.50	1.50	3.09	2	5.095
hsa-miR-628-5p	4.83	4.67	-1.30	-1.61	2	4.75
hsa-miR-1202	4.69	4.80	1.47	-8.66	2	4.745
hsa-miR-1305	-1.04	1.00	2.16	7.29	3	4.725
hsa-miR-526a	-1.11	2.60	6.23	3.05	3	4.64
hsa-miR-889-3p	6.44	2.41	1.15	-1.38	2	4.425
hsa-miR-490-3p	4.07	4.71	-1.48	-14.73	2	4.39
hsa-miR-874-5p	6.70	2.08	1.39	5.10	2	4.39
hsa-miR-497-5p	1.30	-1.06	6.10	2.57	3	4.335
hsa-miR-486-3p	2.43	6.11	-1.30	-1.61	2	4.27
hsa-miR-33a-5p	1.24	2.29	2.83	4.82	3	3.825
hsa-miR-4755-5p	5.27	2.37	1.57	-1.35	2	3.82
hsa-miR-1322	2.12	3.03	6.82	2.93	1	3.725
hsa-miR-376a-3p	-1.73	-1.19	4.03	3.29	3	3.66
hsa-miR-190b	3.93	3.28	6.26	1.58	2	3.605
hsa-miR-142-3p	3.89	1.04	4.41	2.46	3	3.435
hsa-miR-302e	4.29	2.53	1.83	3.07	2	3.41
hsa-miR-135a-5p	-1.04	1.00	4.49	2.31	3	3.4
hsa-miR-133a-3p	4.14	2.53	-1.30	-1.61	2	3.335
hsa-miR-302a-5p	2.49	2.40	5.07	2.93	1	3.2225
hsa-miR-21-5p	2.36	2.02	3.38	5.05	1	3.2025
hsa-miR-1289	5.21	1.59	2.30	4.05	3	3.175
hsa-miR-450b-5p	4.17	2.07	-1.30	-1.61	2	3.12
hsa-miR-652-3p	1.38	1.27	3.91	2.31	3	3.11
hsa-miR-380-3p	2.69	2.60	3.24	2.72	1	2.8125
hsa-miR-210-3p	1.00	2.34	2.28	3.07	3	2.675
hsa-miR-363-3p	-1.10	1.25	2.53	2.76	3	2.645
hsa-miR-610	2.19	2.72	1.10	2.04	2	2.455
hsa-miR-1827	2.51	2.21	2.04	-1.68	2	2.36
hsa-miR-101-3p	1.59	1.77	2.08	2.49	3	2.285
hsa-miR-194-5p	1.07	1.11	2.04	2.47	3	2.255
hsa-miR-1260b	2.03	2.29	-1.30	-1.61	2	2.16
hsa-miR-374c-5p	-2.26	-2.08	-1.30	-1.61	2	-2.17
hsa-miR-541-3p	-2.26	1.00	-2.50	-2.10	3	-2.3
hsa-miR-320c	-2.69	-2.08	-3.10	-1.61	2	-2.385
hsa-miR-608	1.61	1.09	-2.20	-4.16	3	-3.18
hsa-miR-1290	-4.38	-2.09	1.37	1.19	2	-3.235
hsa-miR-5196-5p	-4.25	-2.55	3.75	-1.10	2	-3.4
hsa-miR-1973	-3.07	-1.16	-3.36	-3.49	3	-3.425
hsa-miR-539-5p	-3.17	-4.05	4.85	-1.61	2	-3.61
hsa-miR-34a-5p	-4.51	-6.42	-3.46	-5.15	1	-4.885
hsa-miR-92a-1-5p	1.50	-3.99	-3.40	-7.28	3	-5.34
hsa-let-7c-5p	-1.04	1.09	-4.97	-6.76	3	-5.865
hsa-miR-548n	-2.89	-9.30	1.58	-3.10	2	-6.095
hsa-miR-30a-3p	1.27	-1.14	-4.33	-8.95	3	-6.64
hsa-miR-124-3p	-1.04	1.00	-5.69	-11.50	3	-8.595
hsa-miR-4532	-1.04	1.00	-2.02	-20.30	3	-11.16

Figure 4-15 Detailed list of miRNAs that fulfil the selection criteria at 12-hour hypoxia

List of miRNAs which were up/down-regulated by more than 2-fold in either the two cell lines (HKC-8 and HK-2) or in the two primary PTECs after 12 hour hypoxia. MiRNA was categorised based on their patter of expression (category 1: up/down-regulation in all cells, category 2: up/down-regulation in cell lines only, category 3: up/down-regulation in primary cells only, category 4: opposite effect in cell lines vs primary cells). Data was presented as the mean of fold change of expression compared to normoxic cells. Magnitude of expression was calculated by averaging the fold change in the affected cells respective of their miRNA pattern categories). MiRNAs were listed based on the mean of magnitude (from the greatest magnitude of up-regulation at the top of the list to the greatest magnitude of regulation on the bottom of the list).

miRNA	HKC-8	HK-2	PTEC1	PTEC2	Category	Magnitude
hsa-miR-376c-3p	-1.04	1.00	18.13	29.78	3	23.955
hsa-miR-136-5p	-1.04	1.00	27.67	8.66	3	18.165
hsa-miR-376a-3p	1.38	1.50	21.60	14.26	3	17.93
hsa-miR-377-3p	-1.04	1.00	26.95	4.57	3	15.76
hsa-miR-543	-1.04	1.00	17.66	10.02	3	13.84
hsa-miR-409-3p	-1.04	1.00	15.52	9.34	3	12.43
hsa-miR-4455	14.23	8.81	-1.05	1.91	2	11.52
hsa-miR-485-3p	-1.04	1.00	13.37	7.98	3	10.675
hsa-miR-495-3p	-1.04	1.00	9.80	7.98	3	8.89
hsa-miR-595	4.11	10.35	2.68	-1.89	2	7.23
hsa-miR-378e	9.35	2.81	4.29	-1.17	2	6.08
hsa-miR-215-5p	-1.04	1.00	8.37	3.71	3	6.04
hsa-miR-190b	3.12	1.29	8.12	2.73	3	5.425
hsa-miR-345-5p	1.01	1.70	3.57	7.13	3	5.35
hsa-miR-889-3p	6.17	3.81	1.38	-1.06	2	4.99
hsa-miR-1908-3p	4.41	5.46	-1.30	-1.47	2	4.935
hsa-miR-18b-5p	7.25	2.40	-1.30	18.88	2	4.825
hsa-miR-1289	-1.38	2.32	2.08	6.92	3	4.5
hsa-miR-370-3p	-1.04	1.00	6.23	2.53	3	4.38
hsa-miR-556-5p	1.07	6.18	3.97	4.57	3	4.27
hsa-miR-1244	3.92	3.84	2.54	-1.47	2	3.88
hsa-miR-33a-5p	1.01	2.14	3.79	3.51	3	3.65
hsa-miR-450b-5p	2.29	4.89	-1.30	-1.47	2	3.59
hsa-miR-505-3p	-1.17	1.06	2.18	4.80	3	3.49
hsa-miR-1271-5p	4.84	2.06	-1.30	-1.47	2	3.45
hsa-miR-1250-5p	2.85	4.04	2.86	-1.81	2	3.445
hsa-miR-548n	-2.89	1.46	4.08	2.73	3	3.405
hsa-miR-21-5p	2.59	2.27	3.81	4.90	1	3.3925
hsa-miR-874-5p	-1.04	-1.92	3.20	3.50	3	3.35
hsa-miR-610	2.22	3.90	1.78	1.09	2	3.06
hsa-miR-766-3p	-2.52	1.36	3.23	2.42	3	2.825
hsa-miR-130b-3p	1.11	1.33	2.62	2.96	3	2.79
hsa-miR-142-3p	2.25	2.29	3.14	3.18	1	2.715
hsa-miR-155-5p	1.26	1.16	2.53	2.55	3	2.54
hsa-miR-500a-5p	1.42	1.04	2.15	2.71	3	2.43
hsa-miR-7-5p	2.23	2.49	1.75	3.21	2	2.36
hsa-miR-3136-5p	1.20	-1.07	2.18	2.10	3	2.14
hsa-miR-200c-3p	2.19	2.08	-1.03	-1.42	2	2.135
hsa-miR-374c-5p	-2.26	-2.08	1.22	-1.47	2	-2.17
hsa-miR-3182	-1.58	1.02	-2.70	-2.08	3	-2.39
hsa-miR-6721-5p	-2.41	-2.55	2.06	-1.34	2	-2.48
hsa-miR-520c-3p	-9.41	1.38	-3.05	-2.58	3	-2.815
hsa-miR-1290	-4.56	-2.63	-1.09	-1.30	2	-3.595
hsa-miR-770-5p	-4.66	-4.26	1.42	1.28	2	-4.46
hsa-miR-30a-3p	-1.04	-1.33	-3.61	-6.52	3	-5.065
hsa-let-7c-5p	-1.27	-1.34	-3.76	-6.39	3	-5.075
hsa-miR-34a-5p	-3.04	-5.38	-4.33	-8.13	1	-5.22
hsa-miR-615-5p	-6.72	-4.89	-1.30	-1.47	2	-5.805
hsa-miR-4488	-1.04	-52.47	-4.76	-7.42	3	-6.09
hsa-miR-4516	-5.12	-8.76	-1.32	-1.57	2	-6.94
hsa-miR-146b-5p	-2.89	-11.23	1.79	2.60	2	-7.06
hsa-miR-92a-1-5p	6.94	-1.55	-4.67	-14.00	3	-9.335
hsa-miR-4532	-1.04	1.00	-6.92	-12.24	3	-9.58
hsa-miR-489-3p	-1.04	-4.00	-2.70	-17.63	3	-10.165
hsa-miR-1915-3p	-1.04	1.00	-17.86	-7.73	3	-12.795
hsa-miR-124-3p	-1.04	1.00	-3.00	-49.46	3	-26.23
hsa-miR-3195	-1.04	-12.84	-2.71	-57.94	3	-30.325
hsa-miR-499b-5p	11.42	11.16	-2.92	-11.22	4	

Figure 4-16 Detailed list of miRNAs that fulfil the selection criteria at 12-hour after H_2O_2 treatment

List of miRNAs which were up/down-regulated by more than 2-fold in either the two cell lines (HKC-8 and HK-2) or in the two primary PTECs at 12 hour after H_2O_2 treatment. MiRNA was categorised based on their patter of expression (category 1: up/down-regulation in all cells, category 2: up/down-regulation in cell lines only, category 3: up/down-regulation in primary cells only, category 4: opposite effect in cell lines vs primary cells). Data was presented as the mean of fold change of expression compared to non-ischaemic cells. Magnitude of expression was calculated by averaging the fold change in the affected cells respective of their miRNA pattern categories). MiRNAs were listed based on the mean of magnitude (from the greatest magnitude of up-regulation at the top of the list to the greatest magnitude of regulation on the bottom of the list).

To examine possible overlaps between my findings and the results from previous miRNAs profiling studies in kidney IRI, a heatmap illustrating the expression pattern of several miRNAs mentioned in the literatures was generated (Figure 4-17). I found several miRNAs with significant changes in their level of expression, which have also been identified in previous reports. These miRNAs include miR-18a, miR-21, miR-34a, miR-155, miR-194, miR-199a, miR-210, miR-214, miR-494, and miR-877.

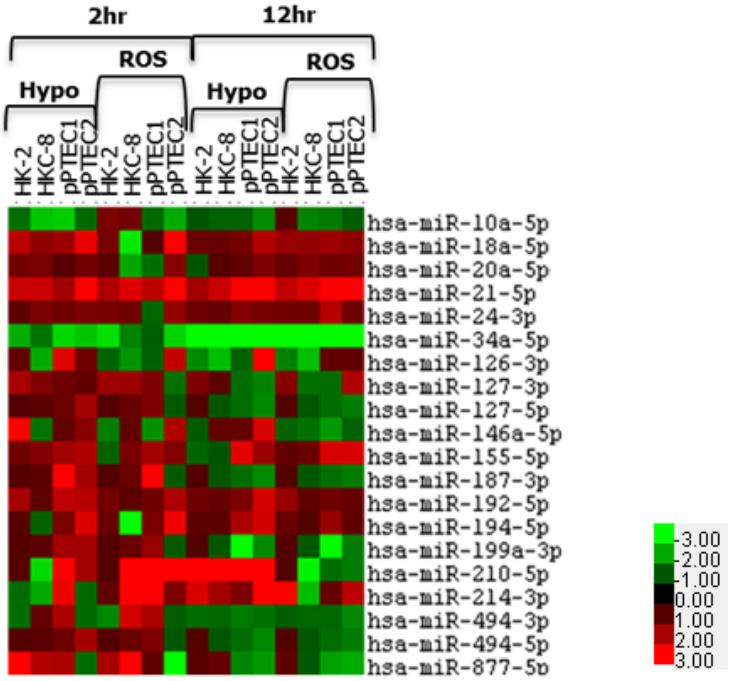

Figure 4-17 Expression of previously identified miRNAs from the literature, in our dataset
Heatmap illustrating the differential expression of previously identified miRNAs from the literature. In our dataset, only a few of these miRNAs showed significant differential level of expression after hypoxia or free-radical exposure. MiRNAs were clustered based on the selection criteria without performing a specific statistical analysis.

4.4. Validation of Profiling Results

Microarray results were validated using real-time quantitative PCR. Several microRNAs were selected from a group of microRNAs that were consistently up/down-regulated in all cells (HKC-8, HK-2 and primary PTECs) following either ischaemia or reperfusion. These include miRNAs which were consistently up/down-regulated following exposure to both injuries, such as miR-21-5p and miR-34a-5p; miRNAs which were consistently altered following ischaemic injury only, such as miR-210-5p and miR-363-3p, and miRNAs which were consistently altered following reperfusion injury only, such as miR-130b-3p and miR-142-3p.

4.4.1. Up-regulation of miR-21 After Hypoxia

Up-regulation of miR-21 was seen consistently in all cells at 12-hour after induction of ischaemia (Figure 4-18). Unlike the result from NanoString® profiling, miR-21 expression was not significant in HKC-8 and HK-2 cells after 2 hours (Figure 4-18; (a) and (b)). In both HKC-8 and HK-2 cells, up-regulation of miR-21 reached its peak at 12-hour following ischaemic injury. In two primary PTECs, miR-21 was significantly up-regulated at both 2 and 12-hour. I later confirmed this up-regulation in two other primary PTECs isolated from different patients (Figure 4-19).

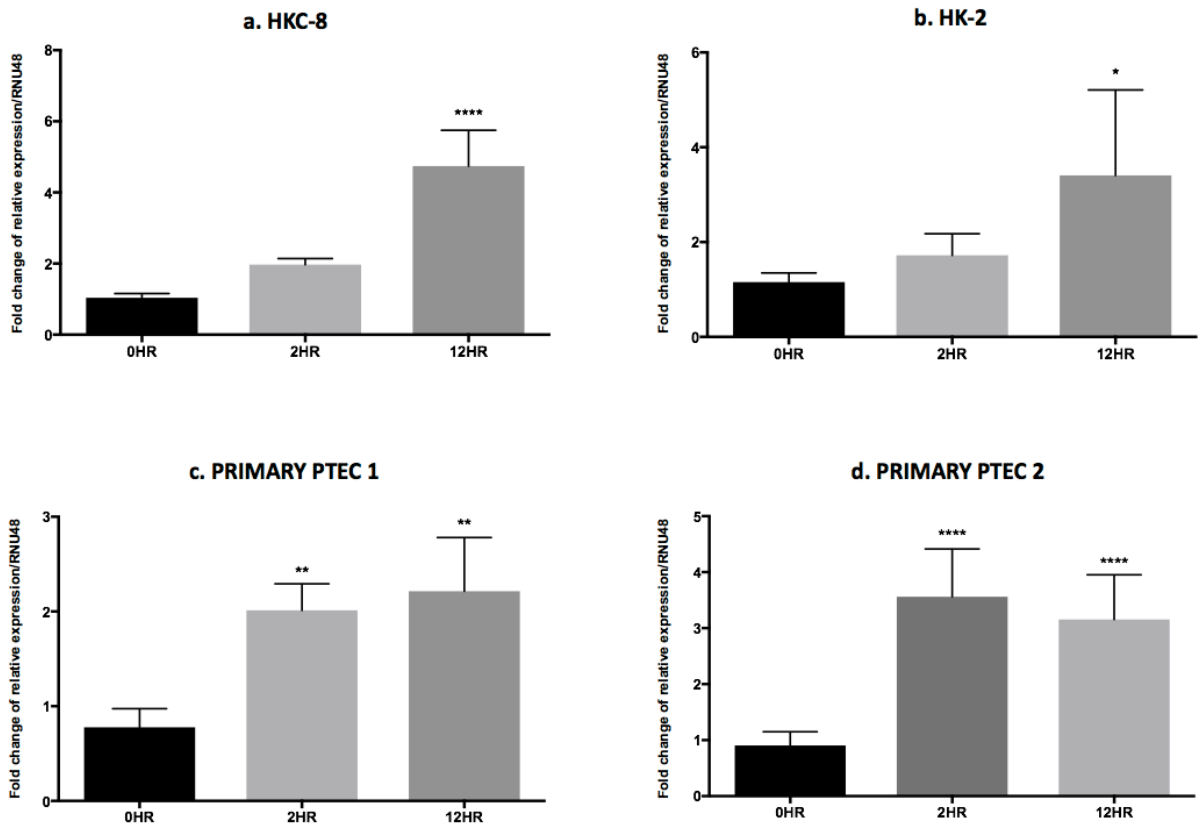

Figure 4-18 MiR-21 expression in PTECs following hypoxia

Expression of miR-21 by real-time qPCR in HKC-8, HK-2 and primary PTECs isolated from two patients, relative to the expression of a housekeeping gene, RNU48. Data was presented as the mean of fold change of relative expression compared to control at 0 hour. Each graph is the result of an experiment performed in three technical replicates. Statistical significance was derived by comparing the mean expression of miR-21 of the treated groups to their respective control at 0-hour using one-way ANOVA with Dunnett's post-hoc analysis. Chart bars represent the mean of fold-change expression + SD (* = $p \leq 0.05$; ** = $p \leq 0.01$; *** = $p \leq 0.001$; **** $p \leq 0.0001$)

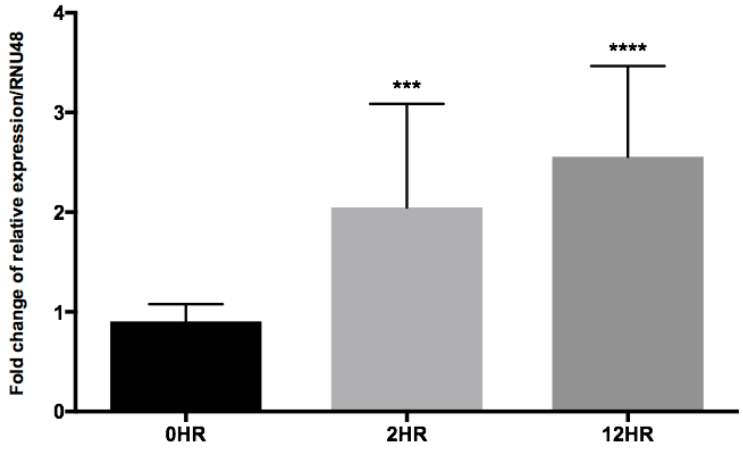

Figure 4-19 Compilation of miR-21 expression in all primary PTECs following hypoxia
Combined analysis of miR-21 expression by real-time qPCR in primary PTECs isolated from four different patients (N=4), relative to the expression of RNU48. Data presented were the results of four independent experiments, each performed in three technical replicates. Results were presented as the mean of fold-change expression + SD compared to normoxic cells at 0 hour. One-way ANOVA with Dunnett's post-hoc analysis was applied to measure existing statistical difference in treated samples compared to untreated samples at 0-hour (*** = $p \leq 0.001$; **** $p \leq 0.0001$)

4.4.2. Up-regulation of miR-21 After Free-Radical Stress

Generally, the level of expression of miR-21 showed a trend of up-regulation in all cells following treatment with H_2O_2 (Figure 4-20). However, the level of increase was not enough to reach statistical significance in HKC-8 cells and one of the primary PTECs (Figure 4-20; (a) and (c)) at the 2-hour observation time-point. Similar to the result from miRNA profiling, 12-hour of H_2O_2 treatment significantly increased miR-21 level of expression in all PTECs. Despite being statistically significant, the fold change increase in miR-21 did not reach two-fold in one of the primary PTECs. Taking into consideration the pre-existing inter-individual differences, the magnitude of changes is also expected to vary across primary cells isolated from different patients. To confirm this finding, the same validation experiment was conducted in additional primary PTECs isolated from two more patients. The combined result revealed a statistically significant increase in miR-21 expression at 12-hour (Figure 4-21). MiR-21 was up-regulated by an average of three folds in all primary PTECs after H_2O_2 treatment, with peak up-regulation occurring at 12-hour after injury.

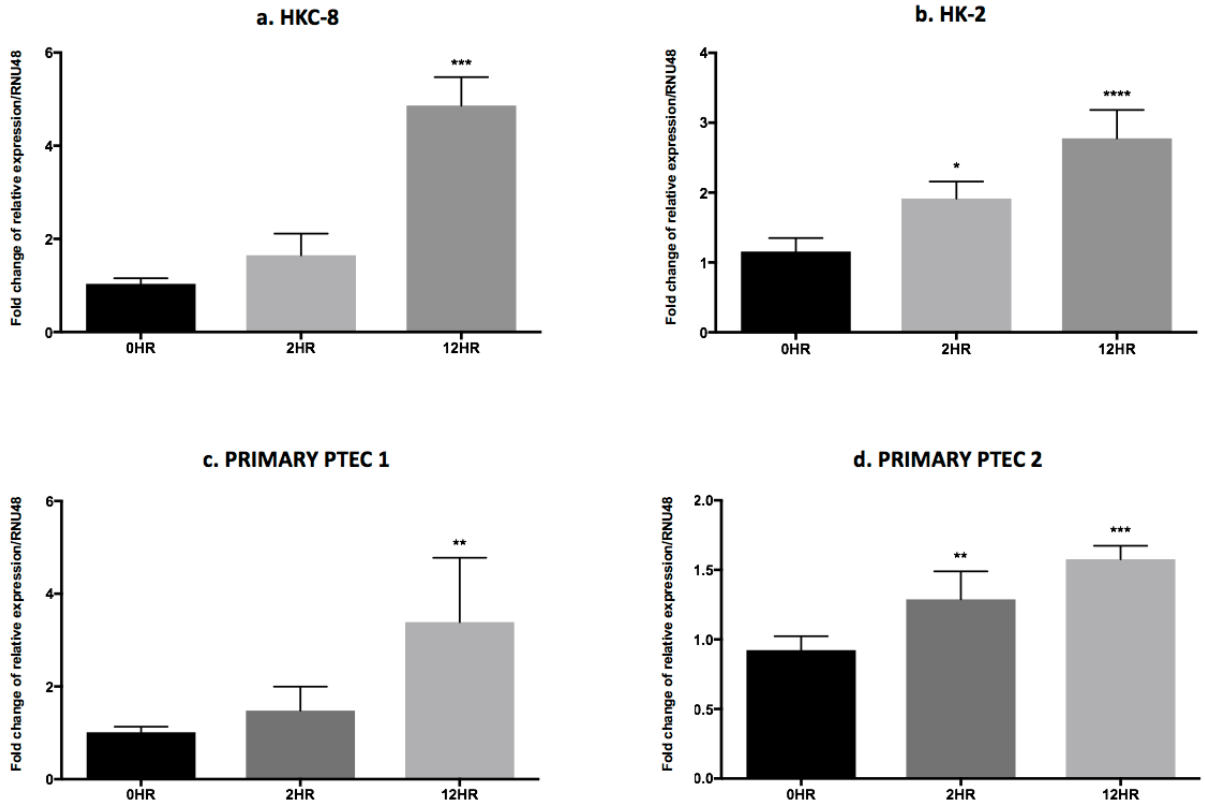

Figure 4-20 MiR-21 expression in PTECs after H_2O_2 treatment

Expression of miR-21by real-time qPCR in HKC-8, HK-2 and two primary PTECs after 2 and 12-hour H_2O_2 treatment. Expression of miR-21 was measured relative to RNU48 expression. Data was presented as the mean + SD of fold-change expression. Each graph presented was the result of a single experiment performed in three technical replicates. One-way ANOVA with Dunnett's post-hoc analysis was applied to detect statistical significance by comparing the mean expression of miR-21 at each time point to untreated cells at 0-hour (* = p ≤0.05; ** = p ≤0.01; *** = p ≤0.001; **** p ≤0.0001)

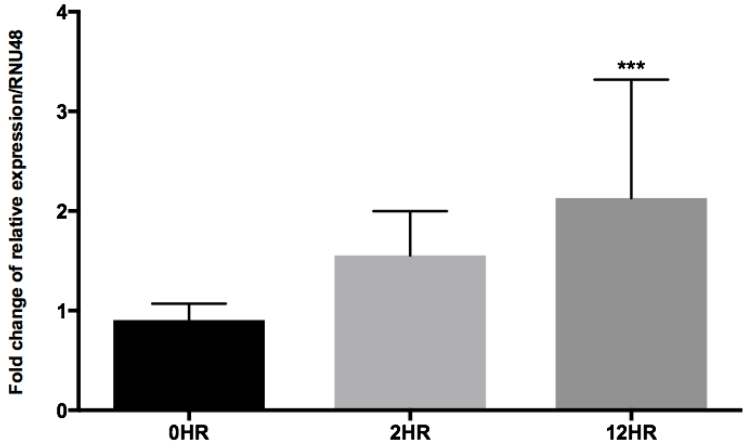

Figure 4-21 MiR-21 expression in all primary PTECs following H_2O_2 treatment

Data showing the mean of fold-change in miR-21 expression at 2 and 12-hour following reperfusion injury, normalised to the expression of RNU48. Expression level of the treated cells at 2 and 12-hour were compared to untreated cells at 0-hour. Data presented were the results of four independent experiments using primary cells isolated from four different patients (N=4). Each experiment was

performed in three technical replicates. Statistical significance was obtained using one-way ANOVA with Dunnett's post-hoc analysis (*** = p ≤0.001)

4.4.3. Expression of miR-34a in hypoxic PTECs

Nanostring profiling showed down-regulation of miR-34a in hypoxic PTECs. Validation with qPCR also detected decrease in miR-34a expression during ischaemia. However, at 2-hour time point, the changes were only found to be statistically significant in primary PTECs (Figure 4-22; (c) and (d)), but not in HKC-8 or HK-2 cells (Figure 4-22; (a) and (b)). The decrease in miR-34a expression persisted, and reached statistical significance in all cells at the 12-hour time point. Generally, 12-hour ischaemia reduced miR-34a expression by approximately 3-4fold in all PTECs. This decrease in miR-34a expression was also verified in two additional primary PTECs isolated from different patients (Figure 4-23).

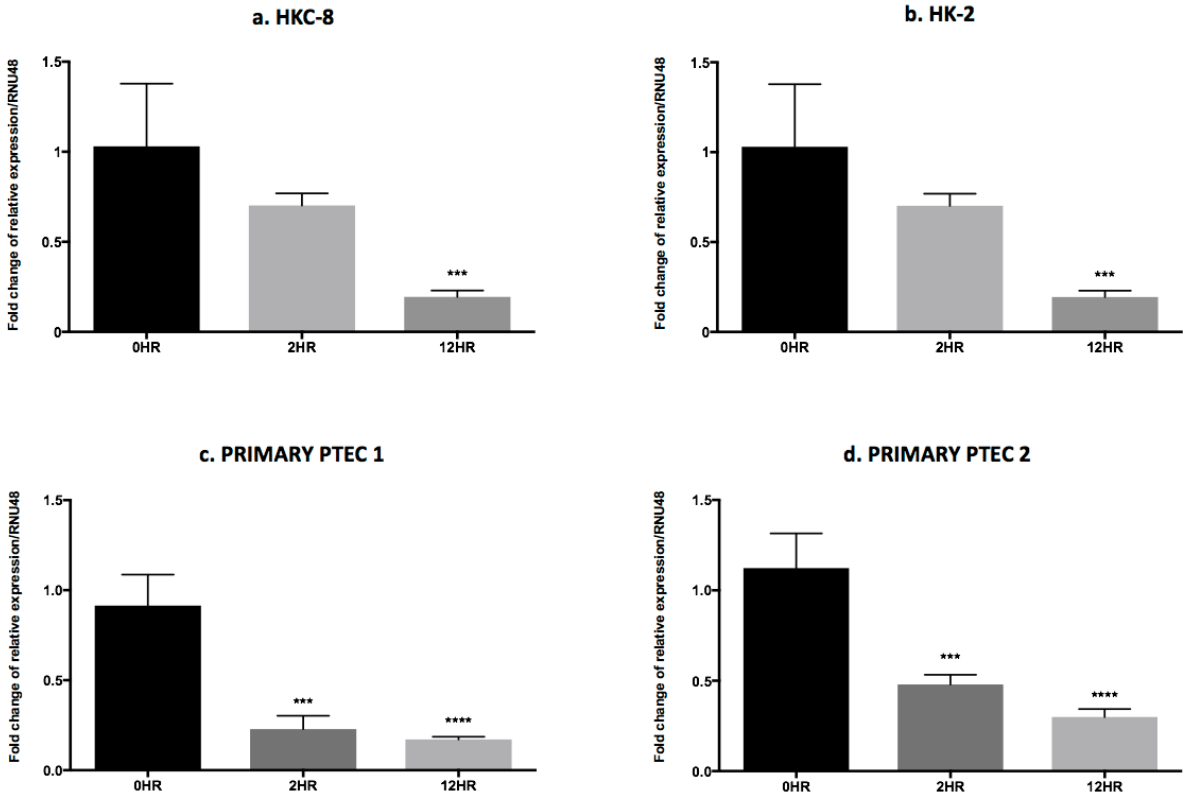

Figure 4-22. MiR-34a expression following hypoxia

qPCR results showing miR-34a expression in HKC-8, HK-2, and two primary PTECs after hypoxia, relative to the expression of a reference gene, RNU48. Each graph was the result of a single experiment performed in three replicates. Data were presented as the mean of fold-change expression + SD. Statistical significance was tested using one-way ANOVA with Dunnett's post-hoc analysis by comparing the mean of fold-change expression in the hypoxic group to the normoxic cells at 0-hour. (** = p ≤0.01; *** = p ≤0.001; **** p ≤0.0001)

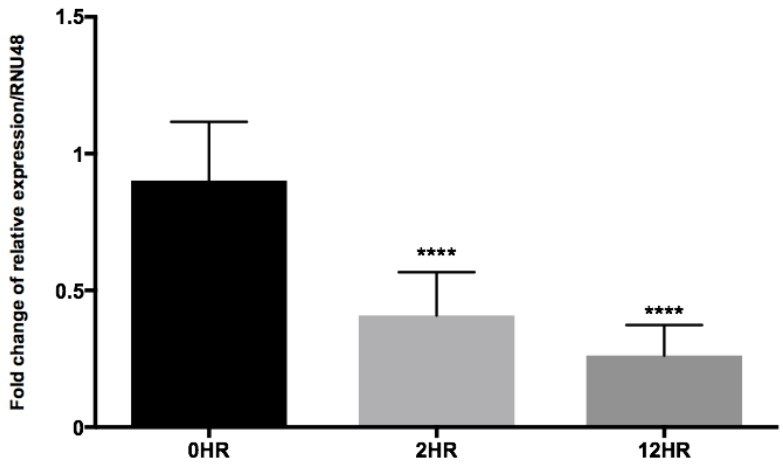

Figure 4-23 MiR-34a expressionin primary PTECs following hypoxia

qPCR results of miR-34a expression in HKC-8, HK-2, and two primary PTECs after hypoxia, relative to the expression of RNU48. Data presented was the result of four independent experiments (N=4), each performed in three technical replicates. Data were presented as fold-change expression compared to the respective control at 0-hour. Statistical significance was tested using one-way ANOVA with Dunnett's post-hoc analysis by comparing the mean miR-34a expression in the treatment group to the control group at 0-hour. (* = $p \leq 0.05$; ** = $p \leq 0.01$; *** = $p \leq 0.001$; **** $p \leq 0.0001$)

4.4.4. Expression of miR-34a After H_2O_2 Treatment

Similar to ischaemia, induction of free radicals in PTECs also decreased miR-34a expression in all PTECs. Again, qPCR did not detect statistically significant changes at the 2-hour time point. The down-regulation of miR-34 was sustained and reached statistical significance at 12-hour after H_2O_2 treatment in all cells (Figure 4-24). Down-regulation was 3-4 fold in HKC-8 and primary PTECs compared to untreated cells (Figure 4-24; (a), (c) and (d)). In HK-2 cells, the expression of miR-34a was only reduced by approximately half of its control level (Figure 4-24; (b)). This finding was further verified by conducting the same experiment in additional primary PTECs isolated from two additional patients. The overall findings concluded that in all primary PTECs, 2 and 12-hour H_2O_2 treatment caused significant down-regulation of miR-34a (Figure 4-25).

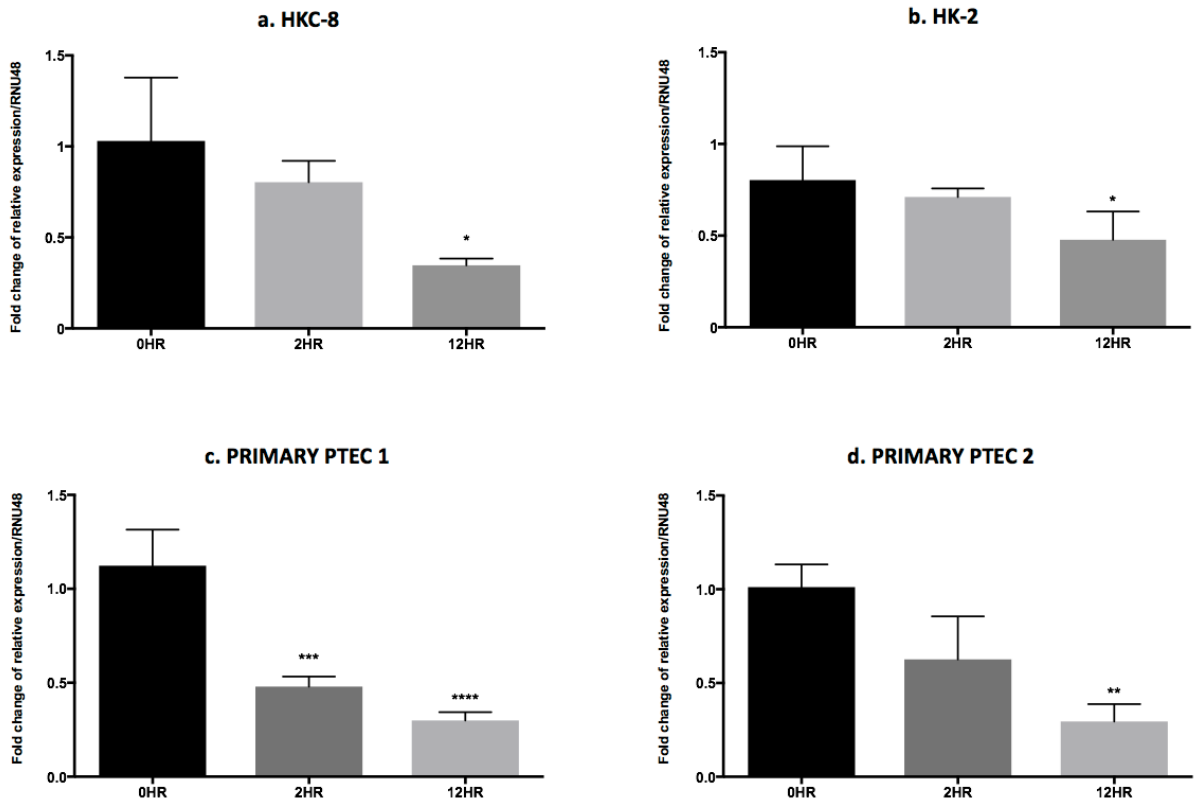

Figure 4-24 Mir-34a expression after H_2O_2 treatment

Mean of fold-change expression of miR-34a by real time qPCR, relative to RNU48 expression, in HKC-8, HK-2, and primary PTECs isolated from two patients. Each graph showed the result of a single experiment performed in three technical replicates. Result was presented as mean + SD. One-way ANOVA test with Dunnett's multiple comparison analysis was applied to compare the mean of each treatment group to control group at 0-hour. (* = p ≤0.05; ** = p ≤0.01; *** = p ≤0.001; **** p ≤0.0001)

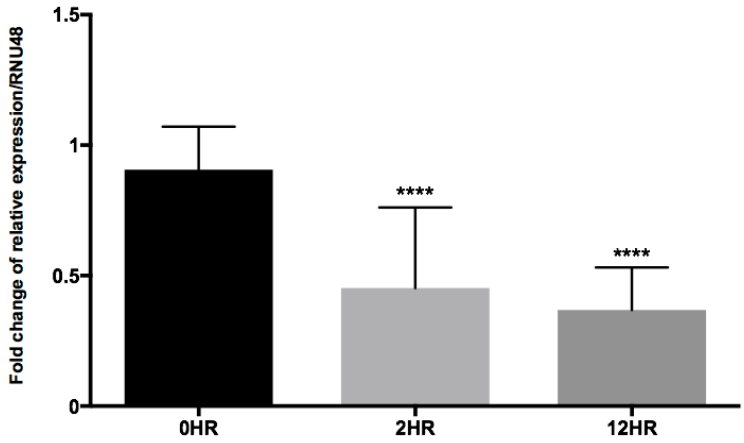

Figure 4-25 MiR-34a expression after H_2O_2 treatment in all primary PTECs

MiR-34a relative expression to RNU48 by real-time qPCR in primary PTECs isolated from different patients. Data presented was the result of four independent experiments (N=4), each performed in three technical replicates Diagram represents the mean of fold-change expression + SD. Statistical significance was tested by comparing the mean of fold-change expression at 2 or 12-hour time points

to untreated cells at 0-hour. Statistical analysis was performed using one-way ANOVA followed by Dunnett's multiple comparison analysis. (**** $p \leq 0.0001$)

4.4.5. Other miRNAs

The expression level of miR-210 and miR-363 were increased in hypoxic primary PTECs, but not after H_2O_2 treatment. Using qPCR, I validated this increase, which showed a significant up-regulation of both miRNAs by 2-fold specifically in response to hypoxic injury (Figure 4-26). In contrast, the expression of miR-130b and miR-142 was increased in response to H_2O_2 treatment (Figure 4-26).

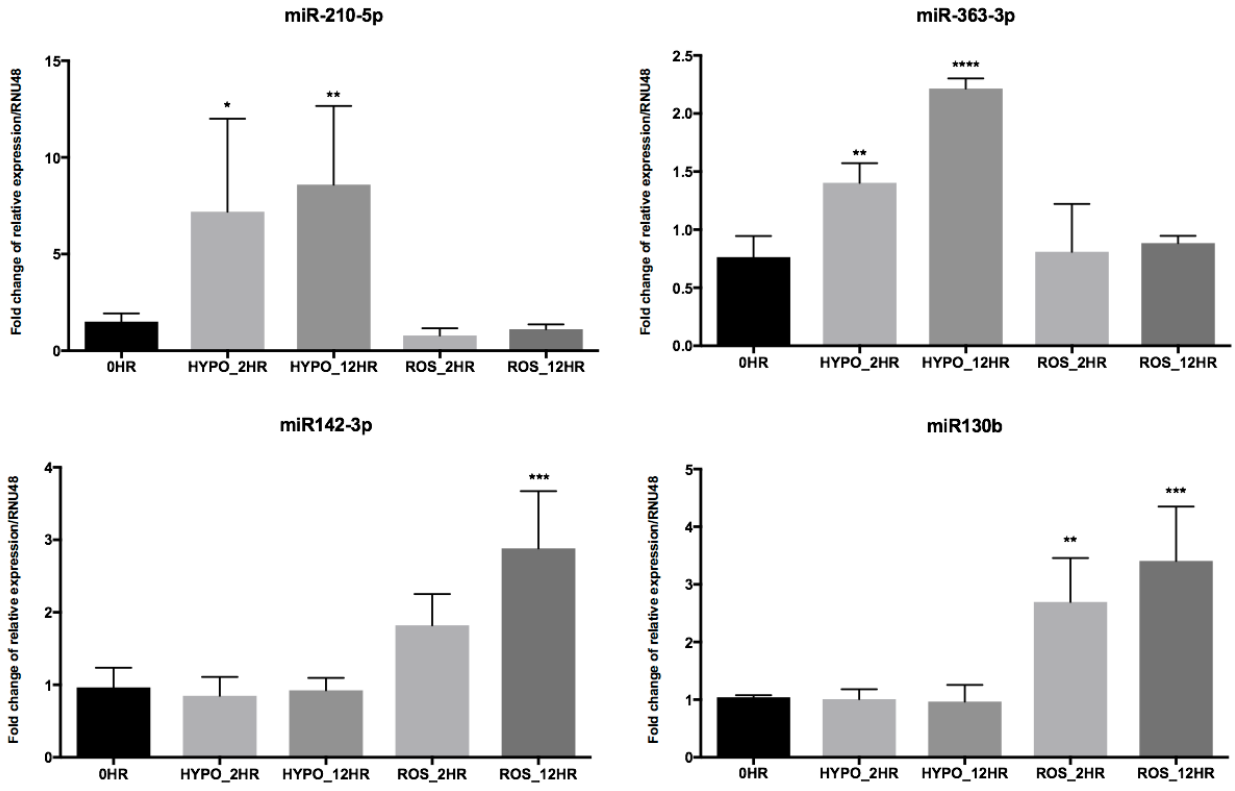

Figure 4-26. Expression level of miR-210, miR-363, miR-130b and miR-142 in hypoxia or after free radical induction

The expression of selected miRNAs in primary PTECs incubated in hypoxia or treated with H_2O_2 by real-time qPCR. Expression of miRNA was normalised to the expression of RNU48 as the reference gene. For each miRNA, experiments were conducted in primary PTECs isolated from three different patients (N=3). Comparison was made between the expression of each miRNA in a treatment time-point to its control at 0-hour. Bar chart represents the mean fold-change expression + SD of the investigated miRNA. One-way ANOVA was applied to detect variance across sample set. Difference in the mean between treatment groups at 2, 12-hour and untreated group at 0-hour were analysed using Dunnett's multiple comparison test. (* = $p \leq 0.05$; ** = $p \leq 0.01$; *** = $p \leq 0.001$; **** $p \leq 0.0001$)

4.5. Functional Analysis and Target Prediction Results

This step of the project was only applied to miRNAs which fulfilled the selection criteria (consistently up/down-regulated in cell lines or both primary PTECs by 2-fold) at 12-hour time point. Firstly, I utilised miRPath to find a potential association between the miRNAs listed in Figure 4-14 to any known biological pathway listed in the KEGG database. MirPath was selected for its practicality, as it allows analysis of a large selection of miRNAs in a single search. Association between a miRNA and a KEGG biological pathway was detected by miRPath through three prediction softwares; Tarbase, microT-CDS and TargetScan. To detect all potential pathways in which a miRNA from our set is targeting, we opted to use genes union selection method. This method calculates the union of targeted genes by the selected miRNAs set, listing all genes targeted by at least one of the miRNAs in the set. MiRPath then identified pathways associated with these genes. With this method, I was able to list all pathways targeted by a single miRNA. The pathways targeted include HIF-1α signalling pathway, regulation of actin cytoskeleton, mTOR signalling pathway and TGF-β signalling pathway. I then selected the pathways which were considered relevant in cellular response to IRI.

From the pathways listed above, I selected the TGF-β signalling pathway which is involved in the cellular response to both ischaemia and reperfusion injury. I identified 45 miRNAs from the dataset, which were predicted to be involved in the regulation of TGF-β signalling pathway. These miRNAs include miR-133a, miR-363, miR-376a, miR-21, miR124, miR34a and miR-142.

4.5.1. Targets of miR-21

Mir-21 is one of the miRNAs which was up-regulated in all cell types. Based on this, I performed target validation and explored the role of miR-21 in the TGF-β signalling pathway in the kidney following IRI. The potential target genes of miR-21 in the TGF-β signalling pathway listed by miRPath can be seen in Figure 4-27.

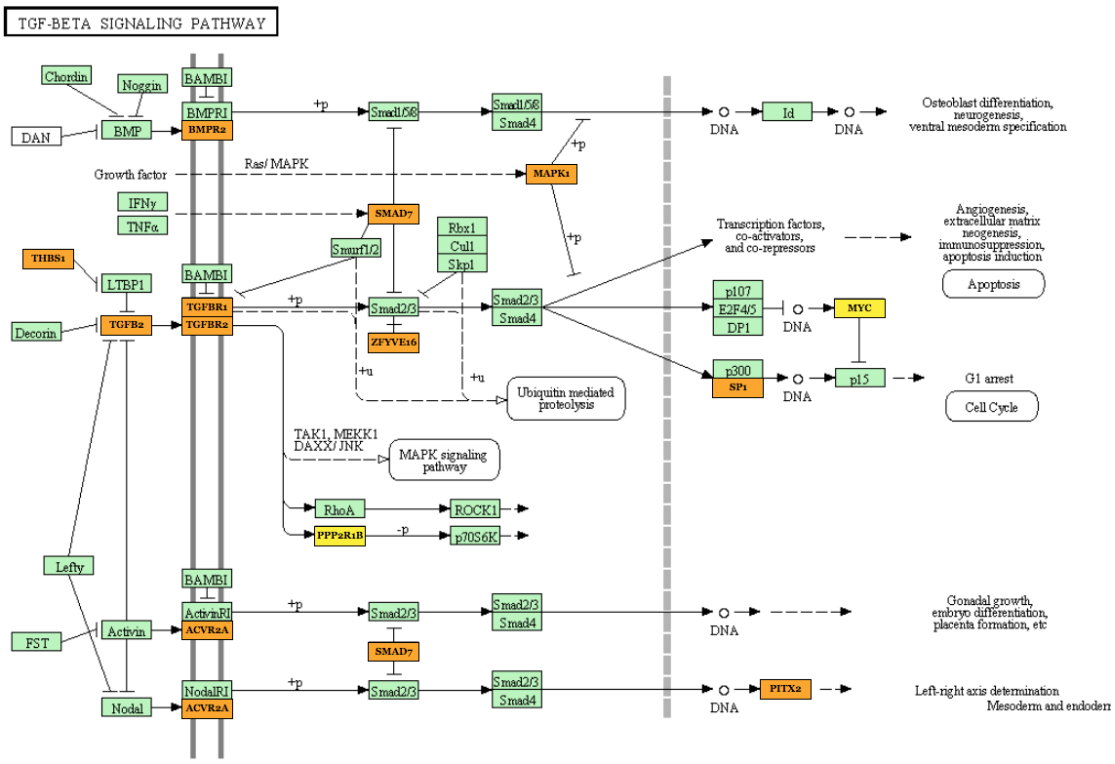

Figure 4-27 Illustration of TGF-β signalling pathway and potential target genes of miR-21

Predicted mRNA targets of miR-21 in the TGF-β signalling pathway. Target genes predicted by two prediction software (both micro-T-CDS and Tarbase) were highlighted in amber, and target genes predicted by only one software (either micro-T-CDS or Tarbase) were highlighted in yellow. Diagram was accessed through miRPath version 2.0 computational tool and KEGG pathway (Kanehisa Laboratories).

As described in the introductory section, all prediction software performed identification of miRNA targets by matching the nucleotide sequence between the seed region of miR-21 (2-8 bases) and 3' untranslated region (UTR) of a potential target mRNA. However, each computational tool utilises a different algorithm, and therefore, it is crucial to use more than one tool to ensure the accuracy of each algorithm. I used miRWalk prediction software as it allows this verification process using three or four available computational tools in parallel. The following mRNA targets from miRPath were also listed by four computational tools in miRWalk: STAT3, IL6R, SMAD7, TGFBR2, BMPR2, TGFB2, CREB5, CDK6 and FASLG (also listed in Table 4-2).

4.5.2. Targets of other potential miRNAs

In addition, I applied the same target prediction steps to other significantly altered miRNAs at 12-hour, which were considered relevant to tubular epithelial cell response to IRI. The result of this analysis is displayed in Table 4-2.

Table 4-2 Predicted mRNA targets of selected miRNAs

miRNA	+/-	Condition	Cells	Pathway	Genes
miR-21-5p	+	Ischaemia and ROS	All	HIF-1 signalling	STAT3, IL6R
				TGF-β signalling	TGFBR2, TGFB2, SMAD7, BMPR2
				PI3K-Akt	PTEN, CREB5, CDK6, FASLG, IL6R
miR-30a-3p	-	Ischaemia	pPTECs	HIF-1 signalling	ANGPT2, AKT3
				TGF-β signalling	CREBBP, PITX2
miR-34a-5p	-	Ischaemia and ROS	All	HIF-1 signalling	ERBB2, PIK3CB, BCL2, PGF, LDHA, PRKCB, MAP2K1, VEGFA, SERPINE1, IL6R
				EMT	NOTCH1, NOTCH2, NOTCH4
				TGF-β signalling	SMAD4, E2F5
miR-363-3p	+	Ischaemia	pPTECs	Extra-cellular matrix receptor	COL2A1, ITGB6, ITGA5, ITGAV, COL1A2, FST, BMPR2
				EMT	SOX4
				TGF-β signalling	FST, BMPR2
				HIF-1 signalling	PIK3R3, PI3CA
miR-376a-3p	+	Ischaemia and ROS	pPTECs	TGF-β signalling	BMPR2
				HIF-1 signalling	PIK3CB
miR-190b	+	Ischaemia and ROS	pPTEC	NFK-B	TAB2, BCL2L1
				TGF-β signalling	ROCK1
miR-200c-3p	+	Ischaemia	HKC-8, HK-2	HIF-1 signalling	EGFR, TCEB1, FLT1, RPS6KB1, EGLN1
				TGF-β signalling	SMAD5, EP300, RPS6KB1
miR-142-3p	+	ROS	All	NFK-B	TAB2, ERC1, IRAK1
				TGF-β signalling	TGFBR1
miR-130b-3p	+	ROS	pPTEC	TGF-β signalling	SMURF2, INHBA, SKP1, SMAD4, TGFB2, TGFBR2, BMPR2
				HIF-1 signalling	EDN1
miR-124-3p	-	Ischaemia	pPTECs	TGF-β signalling	ROCK1, BMPR1B, ROCK2, BMP6, SMAD5, SP1
				HIF-1 signalling	RPS6KB1
miR-302a-5p	+	Ischaemia	All	TGF-β signalling	INHBB, SMAD4
				HIF-1 signalling	BCL2, IGF1R, PIK3R1, PRKCB
miR-7-5p	+	ROS	HKC-8, HK-2	TGF-β signalling	SP1, RPS6KB1
				HIF-1 signalling	FIGF, IGF1R, EGFR, MTOR, RELA, RPS6KB1
miR-155-5p	+	ROS	pPTECs	TGF-β signalling	SMAD2, PPP2CA, GDF6, SP1, ACVR1C, RPS6KB1
miR-18b-5p	+	Ischaemia ROS	pPTECs HKC-8, HK-2	TGF-β signalling	THBS1

Genes listed were selected from miRPath pathways, which overlap with genes obtained from multiple computational analysis performed using miRWalk database. The sign +/- represents direction of changes in the level of expression of a miRNA; (+) = up-regulation and (-) = down-regulation

4.6. Discussion

4.6.1. Assessment of Treatment Effect

4.6.1.1. Assessing the Effect of Hypoxia

The literature suggests various ways of mimicking hypoxia. The most commonly used methods include chemically-induced hypoxia, cell-density mediated hypoxia generation, and by using a hypoxic chamber/incubator. Cell-density mediated hypoxia is generated through over-confluent growth of cells (Marsters *et al.*, 2014). The degree of hypoxia induced by growth over-confluence may not be uniform across all cells within a vessel. Furthermore, over-confluency itself may induce cellular changes, which are difficult to control, in addition to hypoxia. Although relatively inexpensive, chemically mimicking hypoxia (using cobalt chloride or desferoxamine) only targets the HIF-1α downstream response (Triantafyllou *et al.*, 2006). HIF-1α plays an important role in the cellular response to hypoxia, however, it is only one pathway among many other equally important pathways, thus may not reflect the comprehensive picture of the overall cellular response to oxygen deprivation. The use of a hypoxic chamber enables a more physiological resemblance of the effects of hypoxia. A pitfall associated with this method is fluctuating oxygen concentrations due to chamber opening and closing. Although transient loss of the hypoxic environment may not be a major problem, a short period of oxygenation (reperfusion) may interact with the effect of ischaemia. In my experimental setting, the design of the chamber allowed the cells to be inserted and handled under anaerobic conditions, minimising potential exposure to normal oxygen pressure.

Deprivation of oxygen will not immediately lead to cell death, especially in renal PTECs. The unique physiology of renal blood flow enables PTECs to be both accustomed to yet still sensitive to hypoxia. PTECs are able to adapt well to physiological state of hypoxia, due to their constant exposure to a border-line hypoxic environment within the kidney. Assessing the effect of hypoxia by determining cell viability is therefore not an ideal method. To confirm whether hypoxia stimulates changes to PTECs, I stained the cells for HIF-1α.

As described in Chapter 1, HIF is an important transcription factor in determining cellular response to hypoxia. During hypoxia, HIF-1α degradation by PHDs is impaired, leading to the accumulation in HIF-1α. This is followed by dimerization of HIF-α to HIF-β, nuclear localisation and activation of cellular pathways involved in cell survival, apoptosis or fibrogenesis. Immunofluorescence staining of hypoxic HKC-8 cells clearly illustrated HIF-1α in the nucleus (Figure 4-1 panel d-f). Interestingly, intra-nuclear HIF-1α in $CoCl_2$ treated cells

was more prominent compared to the cells treated in a hypoxic chamber for 24 hours. This may be due to the nature of the stabilisation of HIF by $CoCl_2$. Introduction of Co replaces Fe in PHDs, which inhibits their ability to recognise HIF-1α. Therefore, the mechanism of $CoCl_2$ in mimicking the effect of hypoxia is specific and limited to HIF-1α activation, reflected in a strong HIF-1α staining. 24-hour oxygen deprivation does not induce such strong HIF expression. Although HIF is a very important pathway, it is only a part of a more global cellular response to hypoxia associated with numerous pathways and various feedback regulators, which act at multiple levels of HIF regulation; mRNA level, protein level, and transcriptional activity of HIF (Henze and Acker, 2010). These regulators were mainly studied in relation to cancer biology, but may also be potentially important in progression of damage from acute hypoxia.

Furthermore, HIF is a transcription factor that is rapidly degraded, even if the effect of hypoxia persists in the cell. It is possible that evaluation of HIF expression at 24-hour is not the most appropriate time-point to assess hypoxia in a cell. To resolve this, I designed another experiment to confirm that the method of hypoxia induction elicited a biologically significant response in the cell. The effect of hypoxia was quantified using an HRE-luciferase reporter plasmid transfected to HKC-8 cells. Results from this experiment clearly showed that 24-hour incubation in $1\%O_2$ increased HRE driven luciferase expression compared to normoxic cells. Interestingly, the peak luciferase activity was recorded at 12-hour after hypoxia induction and decreased to almost half of its initial increase at 24-hour. This suggests that the cellular response to hypoxia is a very dynamic process involving complex regulatory feedback. A decrease in HRE activity despite continued exposure to low oxygen level suggests a form of cellular adaptation to hypoxia or an attempt to normalise HRE activation. Nonetheless, the increased luciferase activity is evidence that the intervention successfully induced hypoxia in PTECs.

Prior to profiling using NanoString platform, a series of experiments were conducted in HKC-8 and HK-2 cells to detect changes in miR-21 and miR-34 level at 2 hour interval for up to 24-hour, following hypoxic injury. The results of these experiments showed that miR-21 was up-regulated following hypoxia starting at 2-hour, which was followed by a marked increase at 12-hour. Based on this, both 2 and 12-hour time points were selected as the time points for the experiments using NanoString platform.

4.6.1.2. Assessing the Effect of H_2O_2 Treatment

Cells should be stressed enough to induce gene expression changes without significant reduction in cell viability. In this experiment, the cells were treated in H_2O_2 for a maximum of

4 hours, as prolonged exposure to H_2O_2 will result in cell death. Whilst reduced viability demonstrates the effect of H_2O_2 exposure, it does not provide evidence of ROS generation intracellularly. Fluorescence activity of CM-H_2DCFDA was used as a measure of oxidative activity within the cells. This fluorescence activity increased after treatment with 200μM H_2O_2. The emission increased further as H_2O_2 concentration was increased to 400μM. A further increase in H_2O_2 concentration, however, resulted in markedly reduced fluorescence. This may indicate significant cellular stress or even cellular death because of H_2O_2 exposure. At 800μM, the number of events captured by FACS fell to 50% of the original parent population. This suggests significantly compromised cellular viability, thus highlighting the injurious effect of high concentrations of H_2O_2. The flow cytometry result supports previous viability experiments, confirming the optimal concentration of H_2O_2 to be used in HKC-8 experiment is 400μM. To decide the time points of observation for miRNA profiling using NanoString platform, a qPCR to detect changes in miR-21 and miR-34 were performed in HKC-8 and HK-2 cells treated with the specified concentration of H_2O_2. As was observed in hypoxic cells, the expression level of both miRNAs was found to be significantly altered after 2-hour exposure to H_2O_2. The changes were further significantly detected at 12-hour. Based on these findings, 2 and 12-hour were selected as the observation time points in cells treated with H_2O_2.

4.6.2. Global MicroRNA Profiling

4.6.2.1. Assessment of the Technology and Data Analysis

Profiling of miRNA expression in different cells, tissues, treatment conditions and disease processes is an important step in miRNA research. There are several commercial measurement platforms currently available, mainly based on three main technologies; RNA sequencing, reverse transcription-quantitative PCR (qPCR) and microarray hybridisation. Ideally, the platform which provides the best detection rate, should be selected. Detection rate is influenced by several factors, such as assay sensitivity, assay detection cut-off, and the number of probes available within the platform. Although the latter factor does not apply to sequencing-based technology, it is often the deciding factor in choosing between PCR based and microarray hybridisation methods.

Several studies have used the Nanostring nCounter platform in their miRNA profiling method, and have shown excellent robustness and reproducibility. In addition, the fully automated process has allowed minimal manual handling time, which not only reduced the likelihood of user error, but also increased efficiency and practicality.

There are several normalisation methods recommended before changes in the level of miRNA expression could be analysed; (1) using a set of reference/housekeeping genes, (2) using total counts of expression within a sample, and (3) global normalisation method using the top 100 most highly expressed miRNAs. Typically, the first method relies on the selection of at least three reference genes, which are consistent in their expression across different cell types with different treatments. The choice of reference genes is therefore crucial, and the accuracy of the normalisation is highly determined by the number of genes included. With a codeset of approximately 800 miRNAs from different cell types, normalisation of raw data using only three or four genes may not be the best option. In addition, we also showed that the expression level of some of the provided reference mRNAs was significantly altered in the treated group (RPL0, RPL19 and GAPDH were significantly up-regulated in primary TECs following exposure of H_2O_2). Nevertheless, we have shown that the selection of normalisation method did not greatly affect the detection of changes in miRNA expression.

Alternatively, the sum of all counts in each sample can be used to approximately determine the total nucleic acid expression within a sample. This total sum of a sample relative to the mean sum of all counts of each sample can be used to generate a scaling factor. However, this method is not suitable in comparing different cell types with different overall expression profiles, as it may skew the data inappropriately and not produce representative results. More appropriately, I opted to normalise the dataset using the global normalisation method. In a large codeset containing more than 300 probes, it is assumed that the level of expression of only a small portion of the targets assayed may fluctuate in any given sample, and that the level of expression of most will be the same. This method utilises much larger numbers of reporters, thus providing more accuracy. Nevertheless, it is crucial to determine that the fraction of probes used as reporters do not exhibit differential expression from sample to sample. My preliminary analysis showed no significant inter-sample variations exist across the top 100 mostly expressed miRNAs. In parallel, I also analysed the data using reference gene normalisation, to confirm whether the choice of normalisation method altered the findings significantly. The result of this parallel analysis showed reasonably similar findings to the result from global normalisation, especially in regards to the consistently up/down-regulated miRNAs across all cell types.

Assessment of background technical noise in the platform is important to determine background threshold and ascertain that all read-outs were indeed true signal. As mentioned previously, the assay employs negative control probes, in which no target transcripts were supplied. Positive signals coming from these probes can therefore be assumed as technical noise or background. The average expression of these negative controls in a specific sample

can therefore be used as background threshold for that lane. To avoid false discovery, I decided to use the average plus two standard deviation (mean + 2SD) of all negative control probe counts as the background threshold for all samples. This adds a level of stringency to ascertain that any reading above the threshold was a real signal.

4.6.2.2. Ischaemia versus Reperfusion; Distinct but Linked

Clinically, ischaemia and reperfusion injury is one continuous process. The severity of reperfusion injury is closely linked to the initial ischaemic insult, which will determine the total injury suffered by an organ/tissue. However, ischaemia or reperfusion injury involved different mechanistic pathways, and induce distinct effector cellular response. Kalogeris et al. stated that the onset of ischaemia triggers two separate pathologic processes (Kalogeris *et al.*, 2012). Firstly, there are processes which result from ischaemia per se, and secondly are biomolecular changes during ischaemia that contribute to the surge in generation of reactive oxygen species and subsequent activation of the immune system. The data analysis from this experiment showed distinct genetic regulation involved in the two processes, which indicates potential differences in effector pathways involved. However, there are also miRNAs which were commonly up/down-regulated during ischaemia as well as after free radical induction. The *in vitro* ischaemia model used in this experiment only allowed a very short normoxic recovery phase, and the reperfusion model was not preceded by any ischaemic injury. Thus, the altered miRNAs identified in both injuries were very likely to be induced separately by either ischaemia or the presence of free-radicals.

4.6.2.3. Cell lines vs Primary Cells

The miRNA profiling analysis results showed that the expression of a miRNA in primary PTECs is not always similar to its expression in either HKC-8 or HK-2 cells. This is especially of importance in interpreting miRNA studies which base their findings on profiling miRNAs in cell lines only. In addition to differences in platform and technologies used, in my opinion, the genetic discrepancies between immortalised cell lines and primary cells is also a strong contributor to the lack of overlap in the results of currently available miRNA studies.

To accommodate these differences in genetic characteristics, I modified the initial selection criteria for a miRNA of interest. Initially, I intended to include only those miRNAs with level of expression changes in all cells after a given treatment and at all observation points. However, this approach will exclude the majority of miRNAs from the codeset, and may overlook the potential biological importance of a miRNA. Hence, I decided to group the cells used into cell lines (HKC-8 and HK-2) and primary cells (pPTEC 1 and pPTEC 2).

Application of the modified selection criteria allowed more miRNAs to be included. These miRNAs showed similar pattern of up- or down-regulation in either the cell lines or primary PTECs. These are the best microRNA candidates to be analysed further for their involvement in the tubular epithelial cell response to IRI. The distinctly different response between cell lines and primary cells highlights the significance of including human primary cells in this study or any microRNA profiling study.

4.6.3. MiR-21

Due to its abundance in various organs and tissues, miR-21 has been the subject of many miRNA studies. Mir-21 has been linked with an array of biological functions and disease processes, including cancer, inflammation, cardiovascular diseases, various fibrotic processes and epithelial-to-mesenchymal transition. In kidney transplantation, up-regulation of miR-21 has been associated with poorer allograft function, delayed graft function, and development of interstitial fibrosis (Ben-Dov *et al.*, 2012; Scian *et al.*, 2013b; Khalid *et al.*, 2016). Furthermore, miR-21 has also been shown to be involved in various kidney pathologies, including renal cell carcinoma, development of renal fibrosis, and progression to chronic kidney disease (Zhong *et al.*, 2011; Li *et al.*, 2013; Wang *et al.*, 2014b; Zhou and Jiang, 2014; McClelland *et al.*, 2015; Hennino *et al.*, 2016). The precise role of miR-21 in the renal response to IRI, however, is less clear. Some studies suggested up-regulation of miR-21 after IRI may have beneficial and pro-survival effect. In contrast, there is substantial evidence available to link miR-21 to activation of apoptosis, fibrosis and deleterious clinical outcome.

In this study, miR-21 is the only miRNA, which was significantly altered in all PTEC types at all time points after both ischaemia and reperfusion injury. This result reiterates what has been reported by other authors. MiRNA profiling studies conducted in murine and human renal tubular cells also showed rapid up-regulation of miR-21 in hypoxic PTECs compared to normoxic controls (Goodwin *et al.*, 2010; Shapiro *et al.*, 2011). The same findings were also reported in studies using a mouse IRI model (Saikumar *et al.*, 2012; Jia *et al.*, 2013). The expression of miR-21 following free radical injury alone, however, has not been reported. Although all these findings suggest an important role that miR-21 after IRI, it is previously not known whether miR-21 up-regulation is involved in the molecular events following ischaemia *per se*, the events related to the surge in reactive oxygen species following reperfusion, or both. The design of this study allowed me to investigate these potential links individually. Our findings clearly showed that miR-21 was involved in the response to both ischaemia and free radical injuries.

In a study utilising mice IRI model, up-regulation of miR-21 was consistently detected at 24-, 72- and 120-hour (Saikumar *et al.*, 2012). Interestingly, I found that the up-regulation of miR-21 was detectable at as early as 2-hour after injury by approximately 2-fold change, which continued to rise to approximately 3-4 fold change at 12-hour after injury. This finding suggests a role of miR-21 at a very early phase of injury. To my knowledge, there is currently no available data documenting the pattern of miR-21 expression at these early time points.

Using multiple computational analysis software, I identified miR-21 targets, which were considered relevant to renal IRI. Data suggests that mir-21 interacts with the HIF pathway by targeting the gene phosphatase and tensin homology deleted on chromosome 10 (PTEN), which indirectly activates the Akt pathway, leading to HIF stabilisation (Liu *et al.*, 2011). Expression of miR-21 is also activated by the pro-inflammatory cytokine, IL-6 through STAT3-dependent mechanism (Xu *et al.*, 2014). Both IL-6 and STAT3 were also detected in my computational analysis result.

I also identified several potential target genes of miR-21 in the TGF-β pathway, such as SMAD7 and TGFBR2. The interaction between miR-21 and TGF-β pathway is especially important to evaluate the mechanistic link between IRI, early up-regulation of miR-21 and the development of fibrosis as the main mechanism for deterioration in allograft function. This is the main objective and will be discussed in detail in the following chapter.

4.6.4. Other Potential MiRNAs

Akker et al. (van den Akker *et al.*, 2015) highighted on the lack of overlapping results in currently available studies on miRNA in kidney transplantation. In order to find other potential miRNAs, I compared the expression pattern of selected miRNAs in my dataset to their expression reported in the literature. To maintain uniformity in study design and model, I only listed studies that use the ischaemia and reperfusion injury model. The comparison is summarised in Table 4-3.

I observed a similar pattern of change in some of these miRNAs, such as miR-34a, miR-155, miR-194, miR-199 and miR-210. However, a significant proportion of these miRNAs were not significantly altered or were only altered in one type of cell, so were not included in the selection. These differences in findings may be attributed to several factors. Differences in detection platform technology utilised for miRNA profiling, sample types (cellular RNA vs tissue RNA vs body fluids; human vs murine; FFPE vs fresh frozen preparation) have been proposed as a main contributor to the lack of overlap miRNA studies. This could also be the main reason for the differences seen in our profiling result. As seen in Table 4-3, the majority of studies listed performed miRNA profiling in murine tissue.

Table 4-3 Summary of the expression pattern of previously identified miRNAs in the literature compared to their expression pattern in the current dataset

miRNA	Current Dataset			Literature				References
	Expression	Cell Type	Condition	Expression	Model	Specimen	Platform	
miR-10a	No significant changes detected			Up-regulated within 1hr	Rat IRI (45 min. bilateral pedicle clamping; 12hr reperfusion)	Tissue	Microarray qPCR	(Wang *et al.*, 2014a)
miR-18a	No significant changes detected			Tissue: Up-regulated Blood: Down-regulated Urine: Undetectable	Rat IRI (30 min. bilateral pedicle clamping, 24, 72 and 120 hr reperfusion)	Tissue, blood, urine	Microarray	(Saikumar *et al.*, 2012)
miR-20a	No significant changes detected			Up-regulated at day 1	Mice (30 min; unilateral pedicle clamping, 1, 3, 5, 7, 14, 21, 30-day reperfusion)	Tissue	Microarray qPCR	(Goodwin *et al.*, 2010)
miR-21	Up-regulated	All	Ischaemia and ROS	Up-regulated at day 1	Mice (30 min; unilateral pedicle clamping, 1, 3, 5, 7, 14, 21, 30-day reperfusion)	Tissue	Microarray qPCR	(Goodwin *et al.*, 2010)
				Up-regulated	Mice (30 min. unilateral pedicle clamping)	Tissue	Microarray	(Chau *et al.*, 2012)
				Tissue: Up-regulated at 24, 72, 120-hr Blood: Down-regulated Urine: Down-regulated initially, modestly elevated within 72h	Rat IRI (30 min. bilateral pedicle clamping, 24, 72 and 120 hr reperfusion)	Tissue, blood, urine	Microarray	(Saikumar *et al.*, 2012)
miR-24	No significant changes detected			Up-regulated	Mice IRI (30 min. unilateral pedicle clamping)	Tissue	qPCR	(Lorenzen *et al.*, 2014)
					Chemical anoxia for 1hr + ATP repletion for 30min.	HK-2 cells	qPCR	
miR-34a	Down-regulated	All	Ischaemia and ROS	Down-regulated	1% oxygen for 2,4, 6, 12, 24, 48, 72 hr	HK-2 cells	Microarray qPCR	(Du *et al.*, 2012)
miR-127	No significant changes detected			Up-regulated	Rat IRI (45 min. bilateral pedicle clamping, 0, 1, 3, 5, 7-day reperfusion)	Tissue	Microarray qPCR	(Aguado-Fraile *et al.*, 2012)
					1% oxygen for 6 hours, re-oxygenation for 1, 3, 6, 24 hr.	HK-2 cells	qPCR	
miR-146a	No significant changes detected			Up-regulated after day 3	Mice (30 min; unilateral pedicle clamping, 1, 3, 5, 7, 14, 21, 30-day reperfusion)	Tissue	Microarray qPCR	(Goodwin *et al.*, 2010)

miR-155	Up-regulated	pPTEC	ROS	Up-regulated in tissue Down-regulated in blood Unchanged (slight non-significant decrease) in urine	Rat IRI (30 min. bilateral pedicle clamping, 24, 72 and 120 hr reperfusion)	Tissue, blood, urine	Microarray	(Saikumar *et al.*, 2012)
miR-187	No significant changes detected			Rapidly down-regulated, continue to decrease	Mice (30 min; unilateral pedicle clamping; 1, 3, 5, 7, 14, 21, 30-day reperfusion)	Tissue	Microarray qPCR	(Goodwin *et al.*, 2010)
miR-192	No significant changes detected			Rapidly down-regulated, continue to decrease	Mice (30 min; unilateral pedicle clamping; 1, 3, 5, 7, 14, 21, 30-day reperfusion)	Tissue	Microarray qPCR	(Goodwin *et al.*, 2010)
				Up-regulated after 6hr	Rat IRI (45 min. bilateral pedicle clamping, 12hr reperfusion)	Tissue	Microarray qPCR	(Wang *et al.*, 2014a)
miR-194	Up-regulated	pPTEC	Ischaemia	Down-regulated, remain at level ≈ control	Mice (30 min; unilateral pedicle clamping, 1, 3, 5, 7, 14, 21, 30-day reperfusion)	Tissue	Microarray qPCR	(Goodwin *et al.*, 2010)
				Up-regulated after 6hr	Rat IRI (45 min. bilateral pedicle clamping, 12hr reperfusion)	Tissue	Microarray qPCR	(Wang *et al.*, 2014a)
miR-199a-3p	Up-regulated	pPTEC	Ischaemia	Up-regulated after day 3	Mice (30 min; unilateral pedicle clamping; 1, 3, 5, 7, 14, 21, 30-day reperfusion)	Tissue	Microarray qPCR	(Goodwin *et al.*, 2010)
miR-210	Up-regulated	All	Ischaemia	Up-regulated	AKI patients vs healthy control	Plasma	qPCR	(Lorenzen *et al.*, 2011a)
				Up-regulated, most prominent at 4hr and 24hr after reperfusion	Mice IRI (30min. bilateral pedicle clamping)	Tissue	Microarray	(Liu *et al.*, 2012)
miR-214	No significant changes detected			Up-regulated after day 3, wane by day 21	Mice (30 min; unilateral pedicle clamping; 1, 3, 5, 7, 14, 21, 30-day reperfusion)	Tissue (fresh)	Microarray qPCR	(Goodwin *et al.*, 2010)
miR-494	No significant changes detected			Up-regulated rapidly (within 1 hr)	Mice IRI (45 min. bilateral pedicle clamping; 1, 3, 6, 12, 24 48 hr reperfusion)	Tissue	qPCR	(Lan *et al.*, 2012b)
miR-877*	No significant changes detected			Up-regulated at 3, 6 and 24hr.	Mice IRI (27 min. bilateral renal pedicle clamping)	Tissue Plasma	qPCR	(Bellinger *et al.*, 2014)

Previous studies have associated changes in expression of several miRNAs to a number of clinical events in kidney transplantation, including delayed graft function, interstitial fibrosis or tubular atrophy. The expression of these miRNAs, which fulfil the selection criteria in our dataset are summarised in Table 4-4.

Table 4-4 MiRNAs associated with post-transplant clinical events relevant to IRI

Clinical focus	miRNAs	Literatures			Current Dataset		
		+/-	Specimen	Reference	+/-	Cell Type	Condition
DGF	miR-21	+	Tissue	(Wilflingseder *et al.*, 2013)	+	All	Ischaemia and ROS
	miR-21	+	Tissue, urine	(Ben-Dov *et al.*, 2012)			
IF/TA	miR-92a	+	Urine	(Maluf *et al.*, 2014)	-	pPTECs	Ischaemia and ROS
	miR-345	+	Urine	(Maluf *et al.*, 2014)	-	pPTECs	ROS
	miR-142-3p	+	Tissue, urine	(Scian *et al.*, 2011; Ben-Dov *et al.*, 2012)	+	pPTECs	Ischaemia and ROS

The sign +/- represents direction of changes in the level of expression of a miRNA; (+) = up-regulation and (-) = down-regulation. DGF = delayed graft function; IF = interstitial fibrosis; TA = tubular atrophy

4.6.4.1. MiR-34a

The research on miR-34 has been gaining substantial interest since the discovery of its important role as a master regulator in tumour suppression. A long list of cancer types, which include lung, liver, prostate, colon, brain, skin and several haematological malignancies have been shown to down-regulate expression of miR-34 (Bader, 2012). Mir-34 is a miRNA family consisting of three family members; miR-34a, miR34b and miR34c. Mir-34a is identified as the most prevalent across all organs in physiological condition, whilst miR-34b and miR-34c are more specific to lung, ovary, testes and trachea (Bader, 2012). The miR-34 family has a very close homology (80-95%), enabling them to regulate similar target genes involved in tumour-related biological pathways, including cell cycle arrest, inhibition of proliferation, apoptosis, cellular differentiation, inhibition of WNT signalling and p53 activity (Chen and Hu, 2012; Agostini and Knight, 2014).

The role of miR-34 in kidney pathologies has not been extensively studied. Several authors have reported the effect of miR-34 in renal cellular senescence and apoptosis. MiRNA profiling at ageing renal mesangial cells showed up-regulation of miR-34a, which was associated to the suppression of the anti-oxidant activity of thioredoxin reductase 2 *(Txrnd2)*,

which in turn promotes renal senescence (Bai *et al.*, 2011). In relation to ischaemic renal injury, Du et al. showed down-regulation of miR-34a after 24-hour of hypoxia in HK-2 cells (Du *et al.*, 2012). Interestingly, I also observed this down-regulation in other human PTECs, including human primary PTECs after 12-hour of either ischaemia or free radical injury. The same author related post-ischaemic down-regulation of miR-34a to an increase in *Notch1* and *Notch2* expression, which promote EMT (Du *et al.*, 2012). In contrast, induction of IRI in mice resulted in increased expression of miR-34a, which inhibited autophagic activity of renal TECs by direct binding to *Atg4B* mRNA (Liu *et al.*, 2015). The gene *Atg4B* was also identified in our computational tool analysis result.

4.6.4.2. MiR-363

The role of miR-363 was found to be important in the progression of several malignancies. An association between high expression of miR-363 and increased proliferation, poorer prognosis and promotion of chemo-resistance in gastric cancer has been reported (Zhang *et al.*, 2016). However, miR-363 was identified to have a tumour suppressive role in lower gastrointestinal tract malignancy. Down-regulation of miR-363 was linked with increased invasion and cell migration of colorectal cancer, primarily by allowing *Sox4* gene to be over-expressed (Hu *et al.*, 2016), a gene that contributes to cancer cell survival and metastasis.

The link between miR-363 and IRI has not been well studied. To date, mir-363 has only been linked with the HIF-1α pathway in the regulation of haematopoiesis in human leukemic cell lines (Xie *et al.*, 2016). In the kidney, miR-363 was identified as an inducer of EMT in human renal tubular epithelial cell lines by interacting with the TWIST pathway, thereby promoting EMT (Morizane *et al.*, 2016). This data suggests that miR-363 exerts its effect through interaction with the inhibitors of the TWIST pathway. However, further validation to demonstrate that an increase in miR-363 reduces the levels of TWIST inhibitors has not been successful. Interestingly, a previous study in colorectal cancer cells showed that it is inhibition of miR-363 that promotes EMT, proven by reduction in E-cadherin expression (Hu *et al.*, 2016).

Computational analysis or the current dataset detected several target mRNAs of miR-363. Some of which should be explored further. A possible interaction between miR-363 with genes encoding proteins involved in extra-cellular matrix formation, such as Collagen and Integrin-β6 is especially compelling, to relate IRI to subsequent fibrogenic processes within the kidney.

4.6.4.3. MiR-210

MiR-210 has been identified as one of many miRNAs induced by hypoxia, and involved in the regulation of key pathophysiological aspects following hypoxia (also known as a hypoxamir). Its role has been investigated in relation to the progression of various malignant processes. The role of miR-210 in the progression of malignant cells is closely linked with HIF-1α stabilisation (McCormick *et al.*, 2013). MiR-210 facilitates tumour progression through multiple synergistic pathways, such as by increasing the rate of cell cycle progression, interfering with normal DNA repair process, altering normal mitochondrial function and cellular metabolism, aiding malignant cells to evade apoptosis, and promoting angiogenesis and metastatic potential (Qin *et al.*, 2014; Dang and Myers, 2015). MiR-210 is highly expressed in renal cancer cells compared to healthy normal kidney. It is also correlated with poorer prognosis in renal clear cell carcinoma patients (Samaan *et al.*, 2015). In relation to IRI to the kidney, a higher plasma level of miR-210 is associated with activation of vascular endothelial growth factor (VEGF) and increased renal angiogenesis (Liu *et al.*, 2012). In critically ill patients with acute kidney injury, higher plasma levels of miR-210 has been shown to be a predictor of mortality (Lorenzen *et al.*, 2011a). In a kidney transplant cohort, lower urinary level of miR-210 was associated with acute T-cell mediated rejection and more rapid decline in GFR 1-year after transplantation (Lorenzen *et al.*, 2011b).

As a hypoxamir, I expected miR-210 to be upregulated following ischaemia. At a very early time point, this up-regulation could only be seen in primary PTECs. At the 12-hour time point, however, miR-210 was significantly up-regulated across all cell types. This change was seen only in ischaemic PTECs, but not in H_2O_2 treated cells, indicating its close association with HIF-1α signalling. Interestingly, one report showed that even though miR-210 was up-regulated in hypoxia, the majority of its target genes are not classical hypoxia inducible genes. The target genes of miR-210 are involved in regulating cellular metabolic processes and gene expression (Huang *et al.*, 2009). It is hypothesised that miR-210 may act as a mediator of HIF-1α to indirectly switch-off unnecessary cellular function during hypoxia (Huang *et al.*, 2009). In accordance, the computational analysis of miR-210 targets that I performed also did not reveal any miR-210 target genes directly relevant to the renal response to IRI.

Chapter 5. The Role of miR-21 in Kidney Response to IRI

5.1. Introduction and Objectives

There are a number of reports describing the involvement of miR-21 in disease processes. MiR-21 has been identified as one of the miRNAs involved the regulation of cancer cells, thus recognised as an oncomir. High level of expression of miR-21 has been associated with various malignancies, including glioblastomas, cholangiocarcinoma, lung cancer, renal cancer, prostate cancer, and gastrointestinal cancer (Selcuklu *et al.*, 2009; Jazbutyte and Thum, 2010). The involvement of miR-21 in this range of organ malignancies could be explained by the fact that miR-21 was ubiquitously expressed in different human organs, which is an uncommon feature for a miRNA. Furthermore, miR-21 has also been shown to play roles in several biological processes, including inflammation, cellular proliferation, cellular migration and apoptosis (Kumarswamy *et al.*, 2011).

The link between miR-21 and the renal response to IRI was established, largely based upon profiling urinary, plasma, or tissue miR-21 in relation to acute kidney injury (AKI). Although most studies agreed that miR-21 was up-regulated following IRI, data on the implications of this up-regulation for kidney function is still conflicting. Several authors documented the role of miR-21 in decreasing apoptosis and necrosis of tubular cells following IRI, which may have a protective capacity, and that knocking-down miR-21 resulted in cell death (Li *et al.*, 2013; Hu *et al.*, 2014; Xu *et al.*, 2014). On the other hand, others have shown that high expression of miR-21 did not prevent cellular death after an ischaemic insult (Goodwin *et al.*, 2010). These findings suggest that fine-tuning miR-21 levels in response to an injury is essential for cell survival. More importantly, the molecular mechanism on how an increase of miR-21 level after IRI influences cellular function still requires investigation.

In this part of the project, I am interested in investigating the association of higher expression of miR-21 following IRI with changes in PTEC phenotype, and how this may affect kidney function in the longer term. To control biological variation across different PTEC types, only HKC-8 cells were used in the experiments described in this chapter. The main objective of this chapter is to verify known miR-21 mRNA targets, and to assess the relationship of miR-21 to the pathways involved in kidney response to IRI; the TGF-β signalling pathway and HIF-1α signalling pathway. To provide a more complete overview of the role of miR-21 in renal response to IRI, the distribution and quantification of miR-21 in ischaemic and non-ischaemic renal tissue were also assessed.

5.2. Results

5.2.1. Qualitative Assessment of MicroRNA Mimic Transfection

The experiments included in this chapter involved transfection of either miRNA mimic or inhibitor to simulate conditions of a high-level or an absence of miR-21. A method to evaluate successful transfection protocol was therefore needed. Fluorescent-labelled miRNA mimic was utilised to visualise the miRNA transfected into the cells. Incubation of 24-hour with miRNA mimic and transfection reagent was adequate to introduce miRNA mimic molecule into HKC-8 cells. At 24-hour, the delivery of miRNA mimic was visible in almost all cells as shown in Figure 5-1.

To assess the result of the transfection process, miR-21 expression following miR-21 mimic transfection was quantified, and compared to its expression in non-transfected HKC-8 cells and in HKC-8 cells transfected with miRNA mimic with scrambled sequence. MiRNA probe for mature miR-21 sequence as described in Chapter 2 was used in this experiment. The result showed that 24-hour incubation of HKC-8 cells in the transfection complex containing miR-21 mimic molecule increased mature miR-21 expression to more than 80-fold compared to transfection with scrambled miRNA mimic sequence (Figure 5-2). As expected, HKC-8 cells incubated in media only, or addition of transfection reagent to the media did not increase the expression of miR-21.

In summary, the result of transfection procedure applied to HKC-8 cells was qualitatively visible from tracking the incorporation of immunofluorescent-labelled miRNA as well as semi-quantitatively evident in the increase of miR-21 expression following transfection. Taking these factors into consideration, mimic transfection procedure was decided to be performed by incubating HKC-8 cells in the transfection complex containing miRNA mimic or inhibitor for 24-hour.

The objective of over-expressing miR-21 in PTEC in the experiments described in this chapter is to elucidate the molecular mechanism of miR-21 in renal response to IRI. For this purpose, all experiments were performed using HKC-8 cell line, as this cell could be transfected easily and relatively tolerant to the use of transfection reagent. However, the transfection of miR-21 mimic to primary PTECs may be of importance to assess how alteration in miR-21 may affect the viability of primary cells. This could be evaluated by calculating the transfection efficiency of miR-21 mimic in primary cells, which will determine the number of viable cells that uptake miR-21 mimic molecule in relation to varying concentration of the miRNA mimic molecule and the transfection reagent.

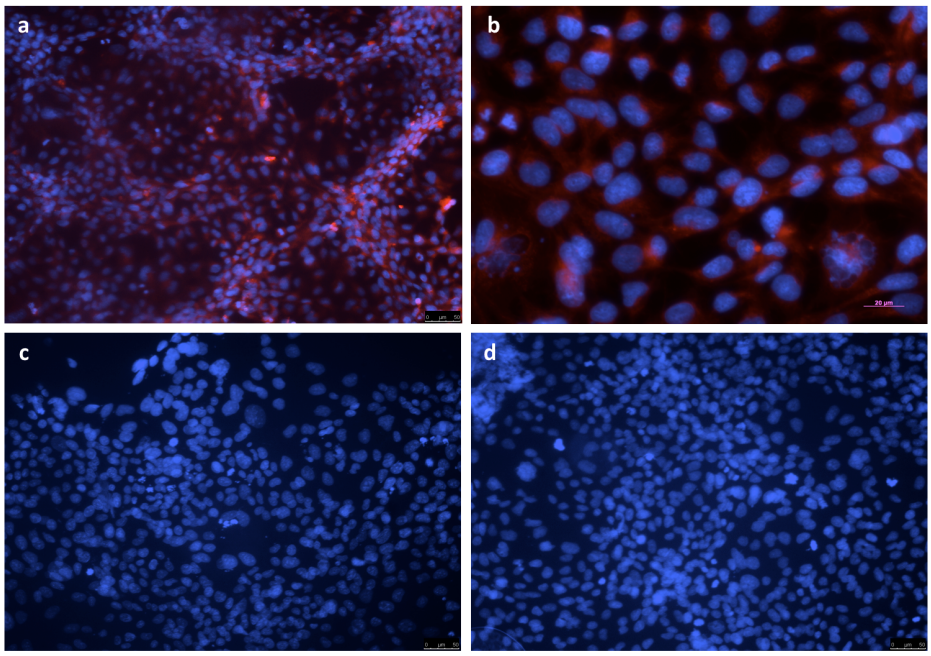

Figure 5-1 Fluorescent-labelled miRNA mimic in HKC-8 cells

Incorporation of fluorescent-labelled miRNA mimic into HKC-8 cells following incubation in transfection complex containing the miRNA mimic and transfection reagent for 24-hour. DAPI was applied for nuclear counter-staining. Slides were visualised at 557/570nm in (a) 100x magnification and (b) in 200x magnification. Non-transfected HKC-8 cells and HKC-8 cells incubated in transfection reagent only for 24-hour were used as comparison (image c and d).

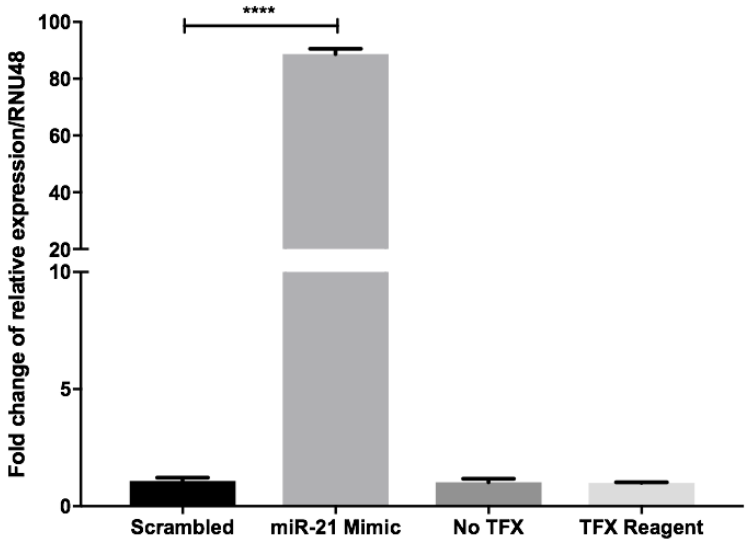

Figure 5-2 MiR-21 Expression after miR-21 mimic transfection

Expression of miR-21 in HKC-8 cells, relative to the expression of RNU48. MiR-21 expression was measured following miR-21 mimic transfection using qPCR. miRNA probe used was specific for mature miR-21 sequence. Samples were incubated for 24-hour in; media only (No TFX), media with transfection reagent only (TFX Reagent), or media with transfection complex containing either scrambled miRNA mimic or miR-21 mimic. Each bar represents the mean of three replicates + SD. Statistical significance was indicated by **** $p \leq 0.0001$, and was calculated using one-way ANOVA test followed by Bonferroni multiple comparison analysis.

5.2.2. SMAD7 is a target of miR-21

The result of computational analysis showed that SMAD7 is a potential target of miR-21. Over-expression of miR-21, therefore, was expected to supress the expression level of SMAD7 level in HKC-8 cells. An experiment comparing the expression of SMAD7 in miR-21 mimic treated cells to non-transfected cells was conducted to verify this assumption. As shown in Figure 5-3, the intensity of SMAD7 was significantly reduced in miR-21 mimic transfected cells, which indicate suppression of SMAD7 by miR-21 over-expression.

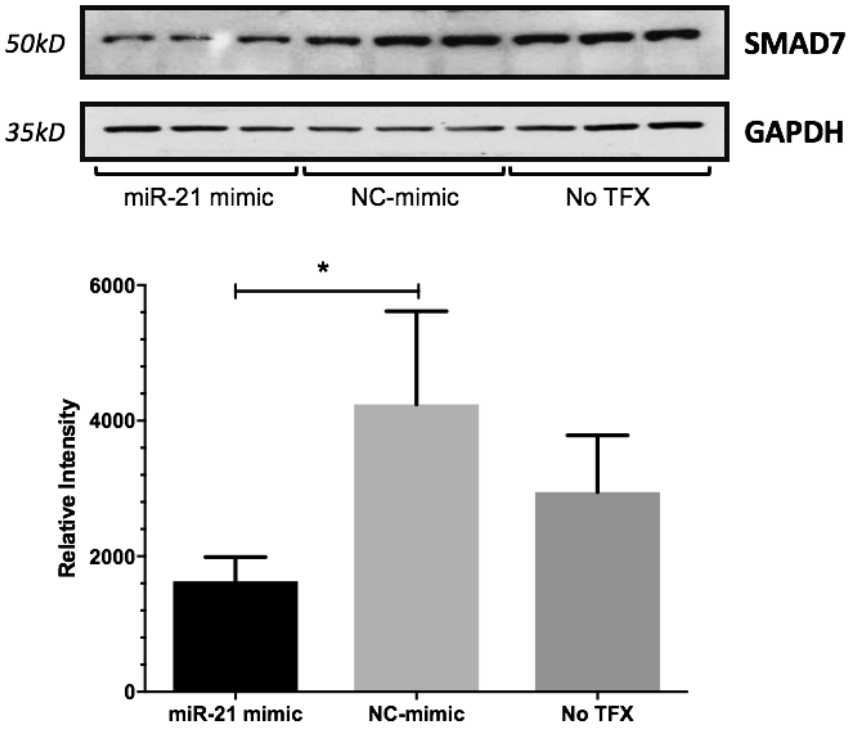

Figure 5-3 SMAD7 expression following miR-21 over-expression

Expression of SMAD7 in miR-21 mimic transfected HKC-8 cells, compared to non-transfected HKC-8 cells (No TFX), and HKC-8 cells transfected with scrambled miRNA mimic control. Each group represents three independent experiments (N=3). SMAD7 expression was quantified by measuring its band intensity in each sample, relative to the band intensity of loading control protein (GAPDH). Data was presented as the mean + SD of band intensity, as measured using ImageJ imaging analysis software. Statistical significance was indicated by * = $p \leq 0.05$, and was calculated using one-way ANOVA test followed by Bonferroni multiple comparison analysis.

5.2.3. MiR-21 over-expression facilitates nuclear translocation of SMAD complexes

SMAD7 is an inhibitory SMAD that functions to block SMAD2/3 activation. Hence, inhibition of SMAD7 by miR-21 would favour SMAD2/3 activation, leading to translocation of SMAD complex into the nucleus. To assess this, antibody against SMAD3 was used to

detect SMAD3 localisation following transfection with miR-21 mimic, in the absence of exogenous TGF-β.

Figure 5-4 showed that transfection of miR-21 induced translocation of SMAD complexes into the nucleus. This is indicated by detection of SMAD3 inside the nuclei in a punctate pattern. This appearance was not observed in non-transfected cells and in cells transfected with scrambled sequence miRNA mimic.

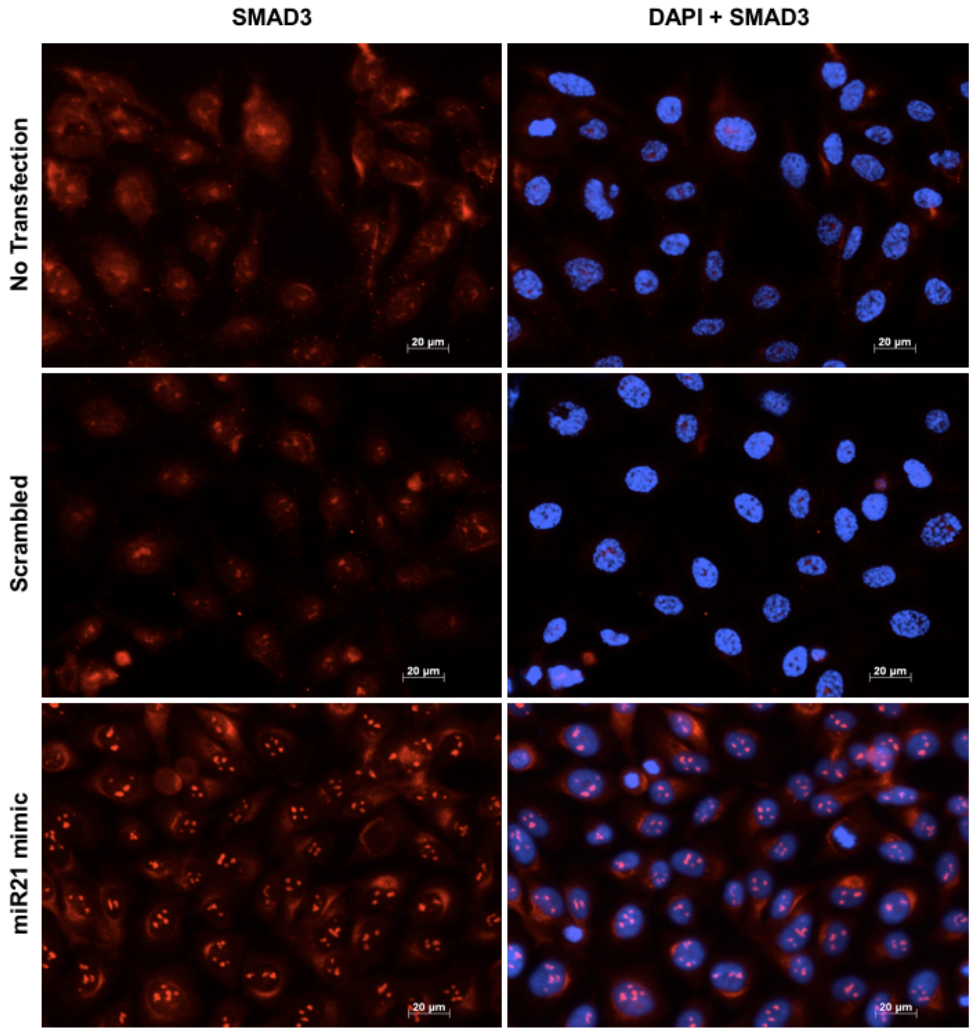

Figure 5-4 Intra-nuclear localisation of SMAD3 in HKC-8 cells over-expressing miR-21

Nuclear translocation of SMAD complexes were detected by applying primary antibody against SMAD3 in HKC-8 cells transfected with miR-21 mimic. Alexa Fluor 546 secondary antibody was used to visualise SMAD3. HKC-8 cells which were not transfected, and cells transfected with scrambled sequence miRNA mimic control were used as comparison. Nuclei were counter-stained using DAPI. Images were captured using fluorescent microscope under 400x magnification. Images displayed were representative of three independent experiments (N=3).

5.2.4. In the absence of TGF-β1, miR-21 did not cause significant increase in SMAD3 activity

To assess whether the observed SMAD3 translocation had any effect on SMAD3 activity, HKC-8 cells containing SMAD3-luciferase reporter plasmid was used. These cells were transfected with miR-21 mimic and were incubated for 24 hour. In the absence of TGF-β1, transfection of miR-21 mimic to HKC-8 cells did not significantly increase SMAD3 activity. Mir-21 mimic transfected cells showed more luciferase activity compared to control groups (Figure 5-5). However, the increase was not enough to reach statistical significance.

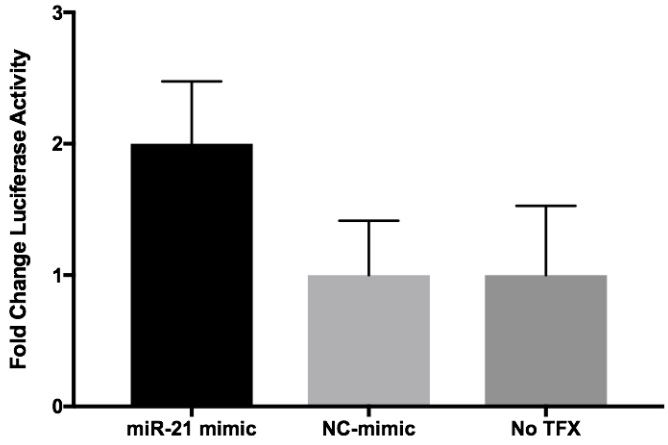

Figure 5-5 The effect of miR-21 over-expression in SMAD3-luciferase activity without TGF-β1
HKC8-cells containing SMAD3-luciferase reporter plasmid were transfected with miR-21 mimic before the measurement of luciferase activity. Data was presented as the mean + SD of fold change in luciferase activity compared to non-coding miRNA mimic-transfected (NC-mimic) cells. Non-transfected group was denoted as No TFX. Statistical analysis was performed with three replicates using One-way ANOVA test, which revealed no statistically significant different between the groups.

5.2.5. MiR-21 sensitised the HKC-8 cell response to TGF-β1

Addition of TGF-β1 after miR-21 transfection resulted in a marked elevation in fold-change increase of SMAD3 activity (Figure 5-6). TGF-β1 at a concentration of 0.1ng/mL was sufficient to induce SMAD3 activity significantly from its activity in the scrambled miRNA mimic transfected cells or in non-transfected cells. A further increase in TGF-β1 concentration increased SMAD3-luciferase activity, creating an even bigger difference between miR-21 transfected cells and the control groups. Differences of luciferase activity between these groups were found to be statistically significant for every concentration of TGF-β1 used.

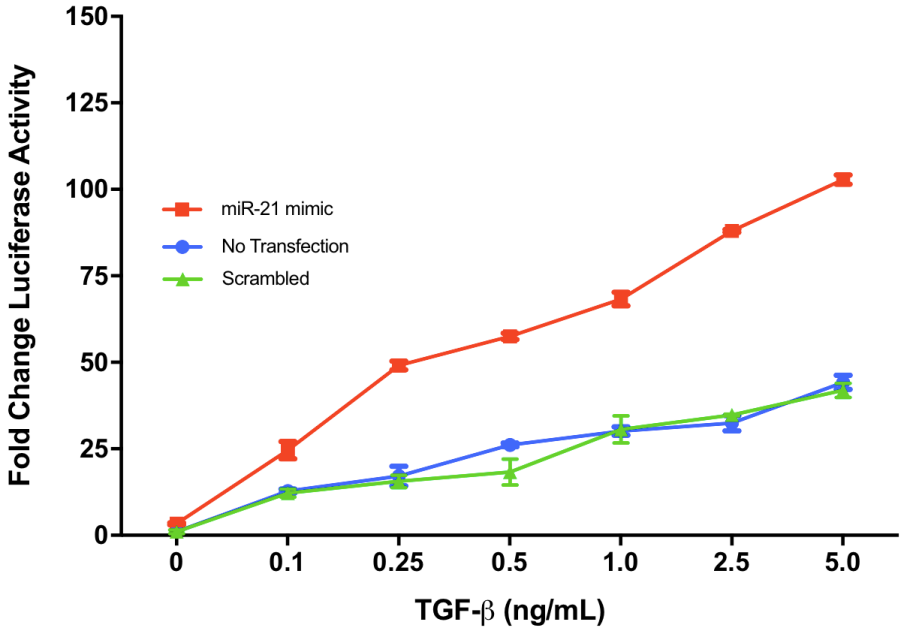

TGF-β1	Groups	pValue	TGF-β1	Groups	pValue
0	miR-21 vs Scrambled	ns	1.0	miR-21 vs Scrambled	≤0.0001
	miR-21 vs No TFX	ns		miR-21 vs No TFX	≤0.0001
	Scrambled vs No TFX	ns		Scrambled vs No TFX	ns
0.1	miR-21 vs Scrambled	≤0.0001	2.5	miR-21 vs Scrambled	≤0.0001
	miR-21 vs No TFX	≤0.0001		miR-21 vs No TFX	≤0.0001
	Scrambled vs No TFX	ns		Scrambled vs No TFX	ns
0.25	miR-21 vs Scrambled	≤0.0001	5.0	miR-21 vs Scrambled	≤0.0001
	miR-21 vs No TFX	≤0.0001		miR-21 vs No TFX	≤0.0001
	Scrambled vs No TFX	ns		Scrambled vs No TFX	ns
0.5	miR-21 vs Scrambled	≤0.0001			
	miR-21 vs No TFX	≤0.0001			
	Scrambled vs No TFX	ns			

Figure 5-6 The effect of miR-21 over-expression and TGF-β1 in SMAD3-luciferase activity

TGF-β1 was added in a range of concentrations (0.1-5ng/mL) to miR-21 mimic-transfected HKC-8 cells. The same treatment was also given to non-transfected HKC-8 cells (No TFX), and cells transfected with scrambled miRNA mimic. Luciferase activity was measured and normalised to the total protein from each sample. Fold-change of luciferase activity was calculated from the ratio of luciferase activity of a sample in each TGF-β1 concentration to its luciferase activity without TGF-β1 (e.g. miR-21 mimic transfected cells at 0.1ng/mL / miR-21 mimic transfected cells at 0 ng/mL). Data was presented as the mean of fold-change + SD. Each value was generated from three experiments (N=3). Data was analysed using Two-way ANOVA followed by comparison of the mean within each concentration (simple effects within the rows) using Tukey's multiple comparison test. (ns = not significant)

5.2.6. Determining TGF-β1 Concentration that Induces a Change in Cellular Morphology

I hypothesised that miR-21 may require the presence of TGF-β1, in order for it to have an effect on PTEC morphology. However, the addition of exogenous TGF-β1 alone has been documented to cause PTEC phenotypic changes. Therefore, it was crucial to identify a

concentration of TGF-β1 that does not elicit a marked change in PTEC. To do this, HKC-8 cells were treated with serial concentration of TGF-β1. The upper limit of TGF-β1 concentration was set at 10ng/mL, as this is the most widely used concentration to induce changes in PTEC morphology documented in the literature.

As expected, normal HKC-8 cells (with no TGF-β1 treatment) expressed E-cadherin, without any evidence of α-SMA expression. Down-regulation of E-cadherin was detectable when TGF-β1 concentration was increased to 0.5ng/mL. Expression of α-SMA started to be detected when HKC-8 cells were treated with 1ng/ml of TGF-β1, which was also accompanied by further decrease in E-cadherin expression. This pattern of an increase in α-SMA expression and decrease in E-cadherin down-regulation became clearer as the TGF-β1 concentration was increased to 5 and 10ng/mL (Figure 5-7). The area of fluorescence of E-cadherin and α-SMA were quantified and plotted against serial concentration of TGF-β1 to obtain pattern of E-cadherin and α-SMA expression changes following TGF-β1 treatment (Figure 5-8). Based on this, 1ng/mL was chosen as the concentration of TGF-β1 to be used in future experiments. This concentration was considered adequate to induce a modification in cellular phenotype without changing the morphological characteristic of PTECs completely.

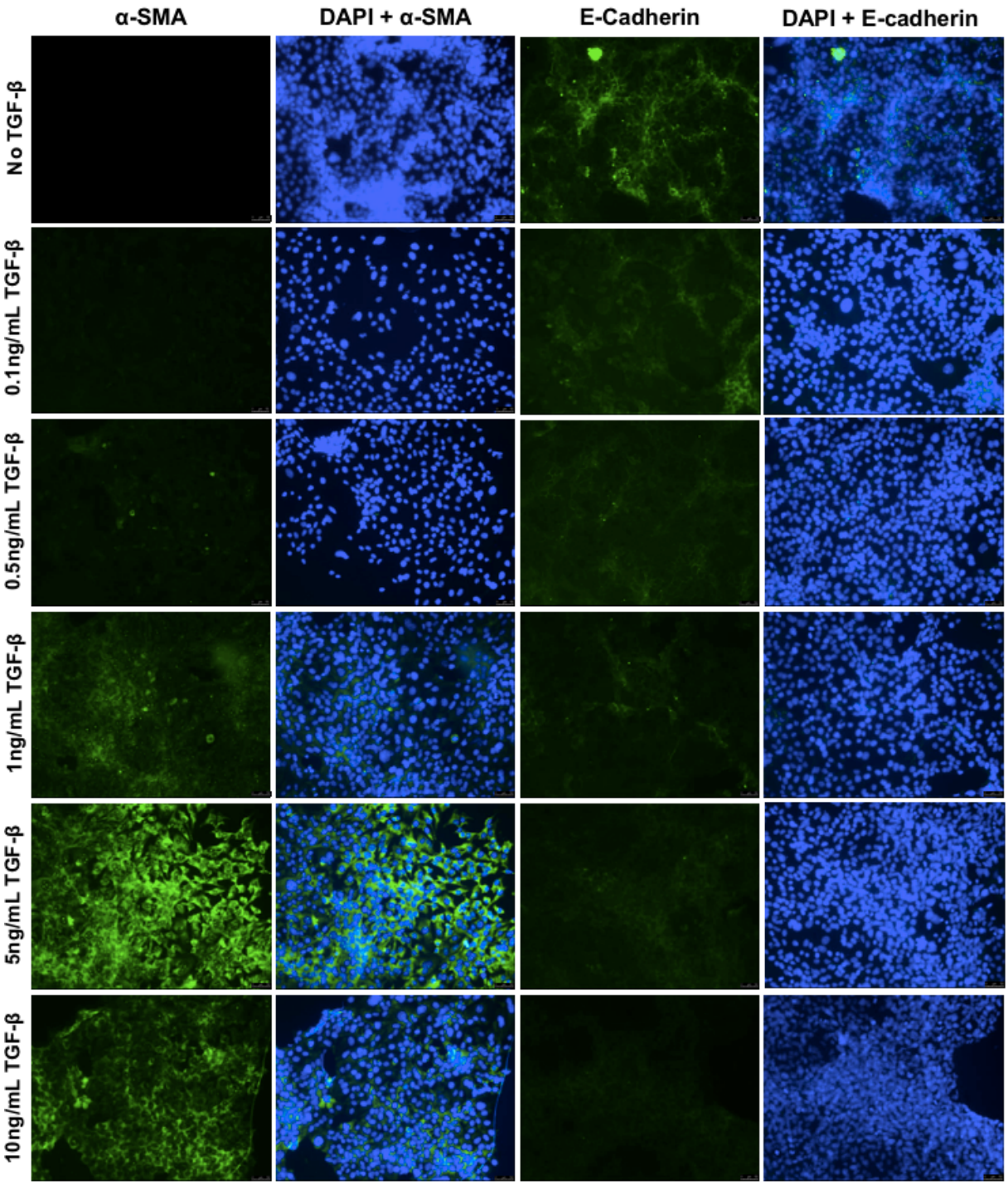

Figure 5-7 The effect of TGF-β1 on the expression of E-cadherin and α-SMA in HKC-8 cells

Expression of E-cadherin and α-SMA following addition of TGF-β1 at the concentrations shown. Proteins of interest were probed using Alexa fluor 488 secondary antibody following incubation with primary antibodies against E-cadherin and α-SMA. DAPI was applied for nuclear staining. Images were captured at 100x magnification. Images displayed were representative of three technical replicates.

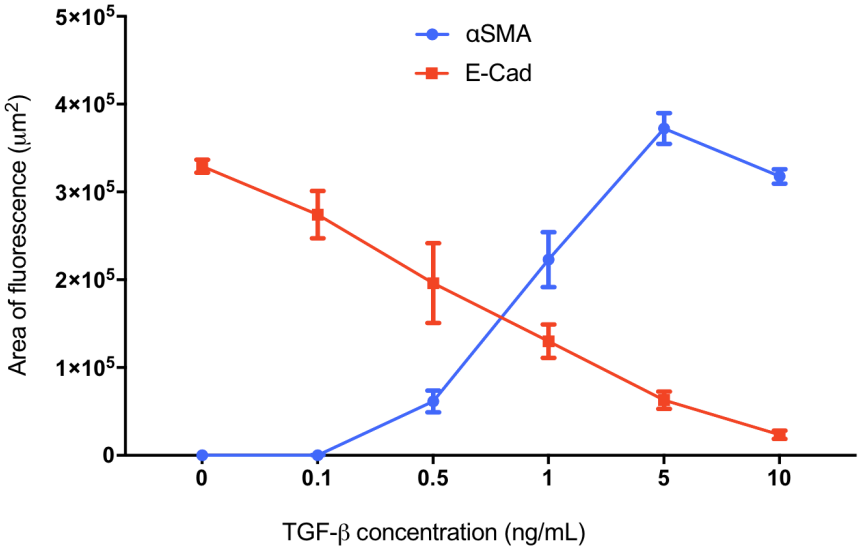

Figure 5-8 Quantification of fluorescence area of E-cadherin and α-SMA in TGF-β1-treated HKC-8 cells

Area of fluorescence of E-cadherin and α-SMA in relation to TGF-β1 treatment at increasing concentrations. Data was presented as the mean of total area of fluorescence in μm^2 per field of view + SD. Analysed images were captured from three different area of a slide. Three slides were analysed for each concentration.

5.2.7. The effect of miR-21 over-expression and TGF-β1 on PTEC morphology

The following experiments were designed to evaluate the effect of the modification of TGF-β1 signalling pathway by miR-21 over-expression in PTEC. Immunofluorescent and Western blot techniques were used to assess changes in PTEC and to quantify protein changes in miR-21 mimic-transfected HKC-8 cells, which were treated with 1ng/mL of TGF-β1. The investigation was focused on the alteration of E-cadherin, as a marker of epithelial cells, and Collagen type 1 and α-SMA as markers of fibrosis.

Figure 5-9 and Figure 5-10 showed down-regulation of E-cadherin expression in HKC-8 cells transfected with miR-21 mimic, and treated with 1ng/mL of TGF-β1. This pattern of down-regulation was detected by two techniques, both of which showed a statistically significant effect. HKC-8 cells transfected with scrambled miRNA mimic and non-transfected cells, and then treated with TGF-β1 were used as controls.

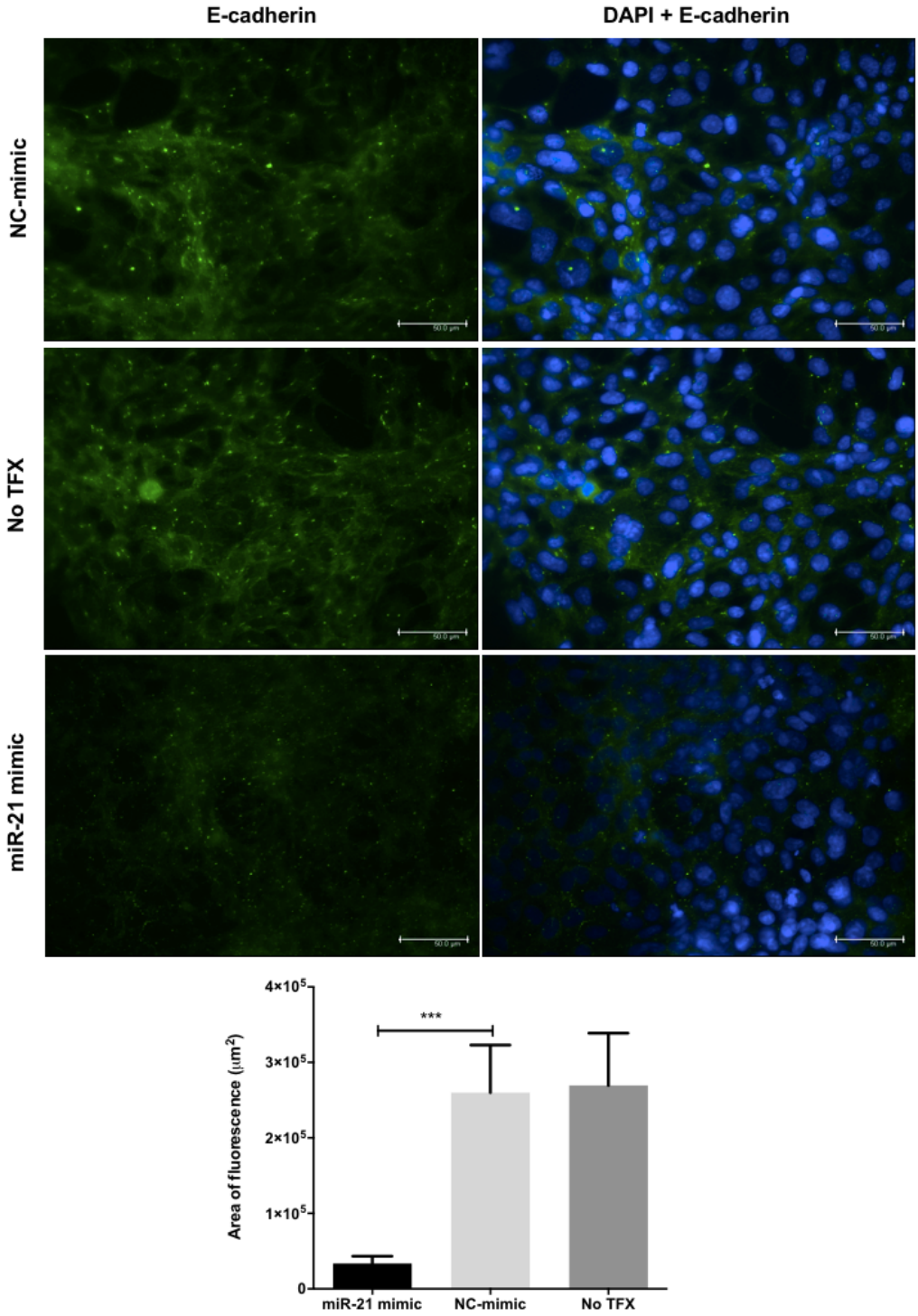

Figure 5-9 Visualisation of E-cadherin expression following miR-21 over-expression and TGF-β1 treatment

E-cadherin expression was assessed in miR-21 mimic transfected HKC-8 cells, non-transfected cells, and HKC-8 cells transfected with scrambled miRNA mimic. Cells were treated with 1ng/mL TGF-β1 for 24 hour prior to analysis. Cells were probed with primary antibody against E-cadherin, followed by AlexaFluor 488 secondary antibody. Total area of fluorescence per field of view was measured from three independent experiments (N=3). Data was presented as the mean of total area of fluorescence in log2 format + SD from three fields of view. Images were captured at 400x magnification, and image analysis were performed using ImageJ software. One-way ANOVA was used to detect statistically significant changes between the groups, followed by Bonferroni post-hoc analysis. (*** = $p \leq 0.001$)

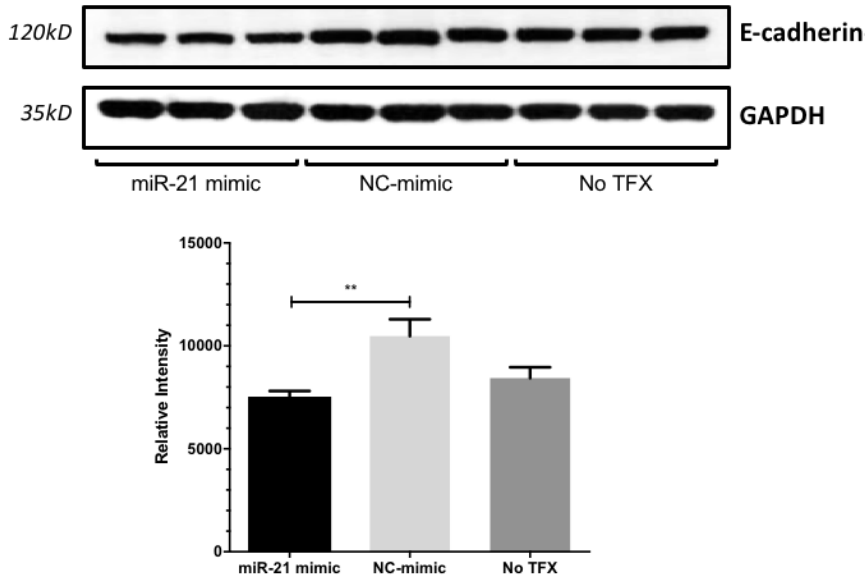

Figure 5-10 Western blot analysis of E-cadherin in HKC-8 cells over-expressing miR-21 treated with TGF-β1

Western blotting was used to detect E-cadherin expression in miR-21 mimic-transfected cells, scrambled miRNA mimic-transfected cells, and non-transfected cells. Band intensity was analysed and measured using ImageJ analysis software. Band intensity of a sample reflects E-cadherin quantity in that sample, relative to the amount of total protein loaded, which was shown by GAPDH expression. Each band represents an independent experiment. Data was presented as the mean of relative intensity + SD of the three bands displayed. Statistical analysis was performed using One-way ANOVA with Bonferroni post-hoc analysis. (** = $p \leq 0.01$)

The expression of α-SMA was markedly increased in cells transfected with miR-21 mimic. Immunofluorescent staining of miR-21 mimic-transfected cells showed prominent development of actin stress-fibres in HKC-8 cells. Without miR-21 mimic, treatment of 1ng/mL of TGF-β1 resulted in less expression of α-SMA in HKC-8 cells. The up-regulation of α-SMA due to miR-21 over-expression in these cells was found to be statistically significant. Western blotting also showed that α-SMA expression in HKC-8 cell lysates after miR-21 mimic transfection was significantly increased.

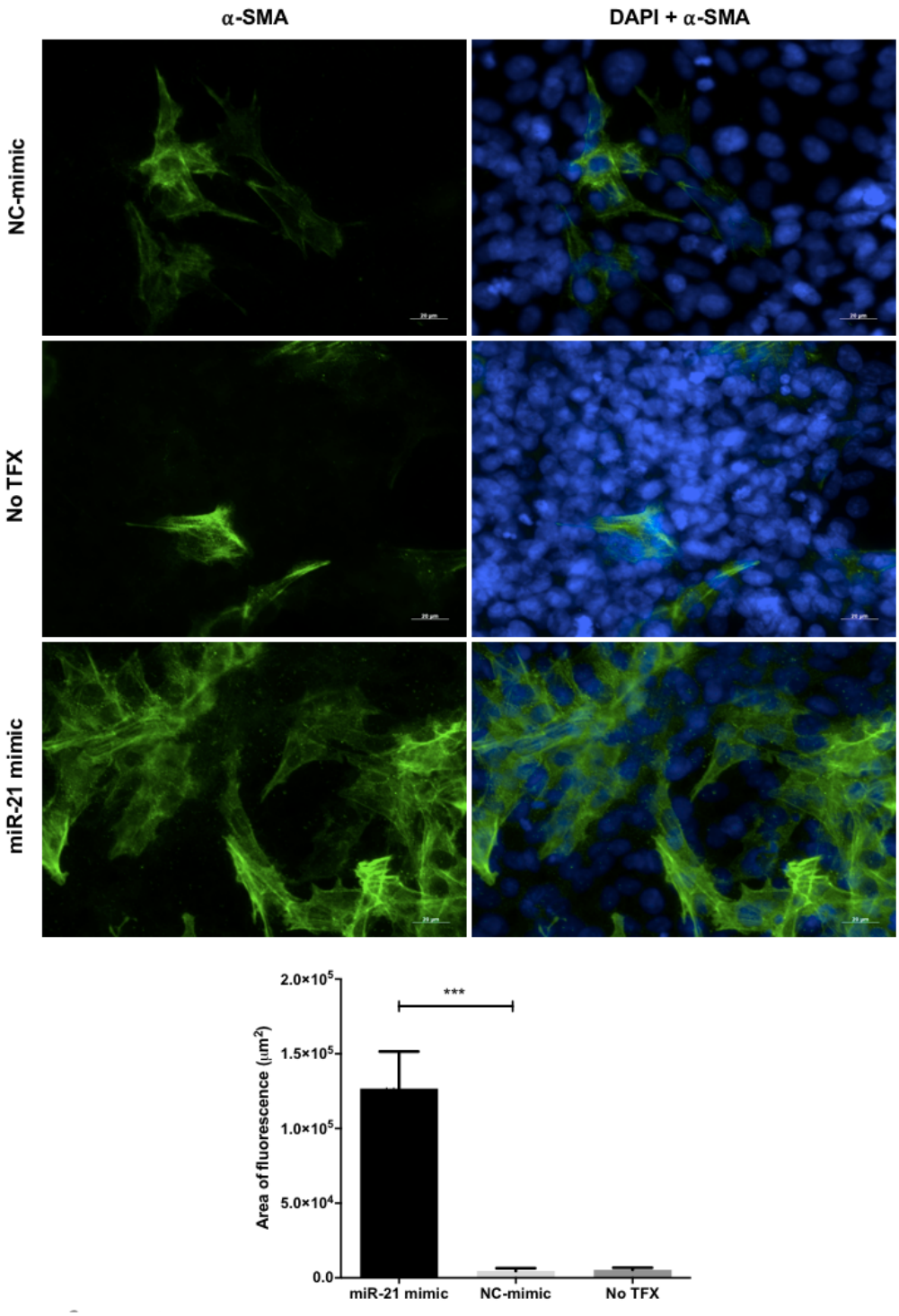

Figure 5-11 The effect of miR-21 over-expression on α-SMA expression in TGF-β1-treated HKC-8 cells

After transfection of miR-21 mimic, HKC-8 cells were treated with 1ng/mL TGF-β1. A primary antibody against α-SMA was used. AlexaFluor 488 was used as secondary antibody, followed by DAPI nuclear counter-staining. Images were viewed at 400x magnification to capture total area of fluorescence per visual field. Experiments were conducted in three independent times (N=3). Data was presented as the mean of total area of fluorescence in log2 format + SD. Image analysis was performed using ImageJ software. One-way ANOVA was used to detect statistically significant changes between the groups, followed by Bonferroni post-hoc analysis. (*** = $p \leq 0.001$)

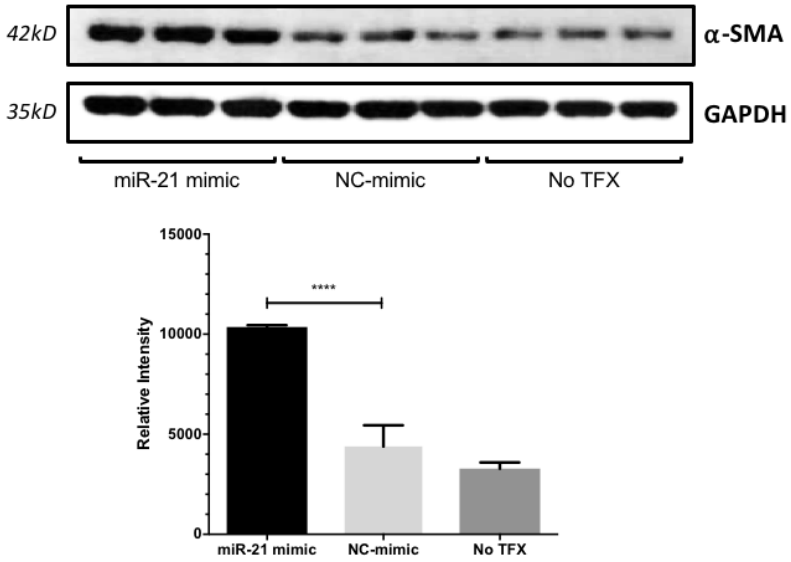

Figure 5-12 α-SMA expression by Western blotting in HKC-8 cells following transfection with miR-21 mimic and TGF-β1 treatment

Evaluation of α-SMA expression by Western blotting. Scrambled miRNA mimic-transfected cells, and non-transfected cells were used as controls. ImageJ analysis software was used to quantify and analyse the α-SMA band intensity relative to GAPDH. Each band represents an independent experiment. Data was presented as the mean of relative intensity + SD of the three bands displayed. Statistical analysis was performed using One-way ANOVA with Bonferroni multiple comparison test. (**** = $p \leq 0.0001$)

Unlike α-SMA, the expression of Collagen type 1 did not show any notable increase by immunofluorescent staining. There was only a very faint increase in Collagen type 1 expression seen in HKC-8 cells transfected with miR-21 mimic compared to the control groups. Quantification of Collagen type 1 using Western blot technique, however, showed that over-expression of miR-21 induced Collagen type 1 protein synthesis.

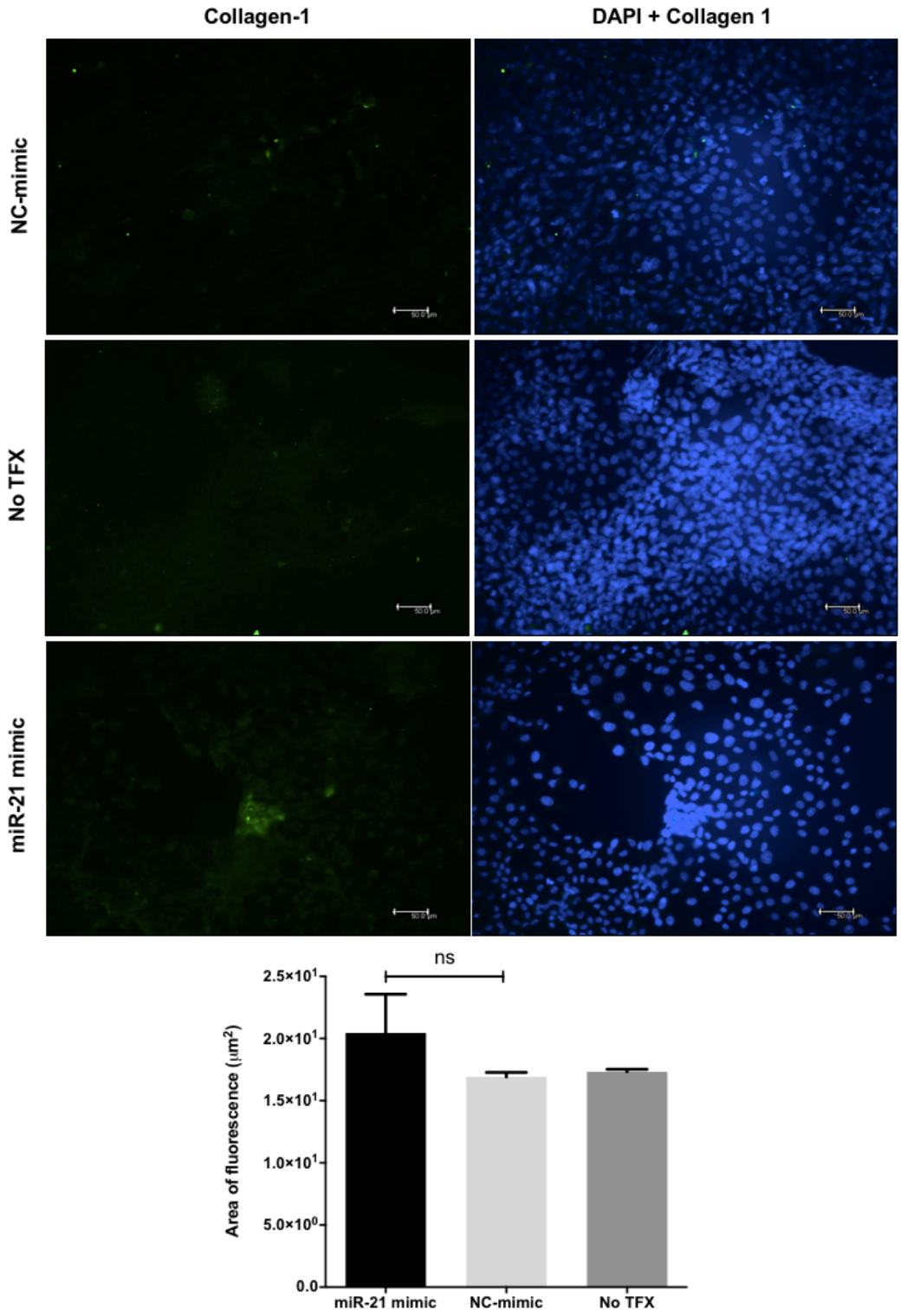

Figure 5-13 Immunofluorescent staining for Collagen-1 following miR-21 over-expression and TGF-β1 treatment

Collagen-1 staining in miR-21 mimic transfected HKC-8 cells, non-transfected cells, and HKC-8 cells treated with scrambled miRNA mimic following treatment with 1ng/mL TGF-β1. AlexaFluor 488 was used as secondary antibody. Images were representative of three independent experiments (N=3). The mean of total area of fluorescence per field of view + SD was analysed. Images were captured under 400x magnification, and image analysis were performed using ImageJ software. One-way ANOVA was applied to detect statistically significant changes between the groups, followed by Bonferroni post-hoc analysis.

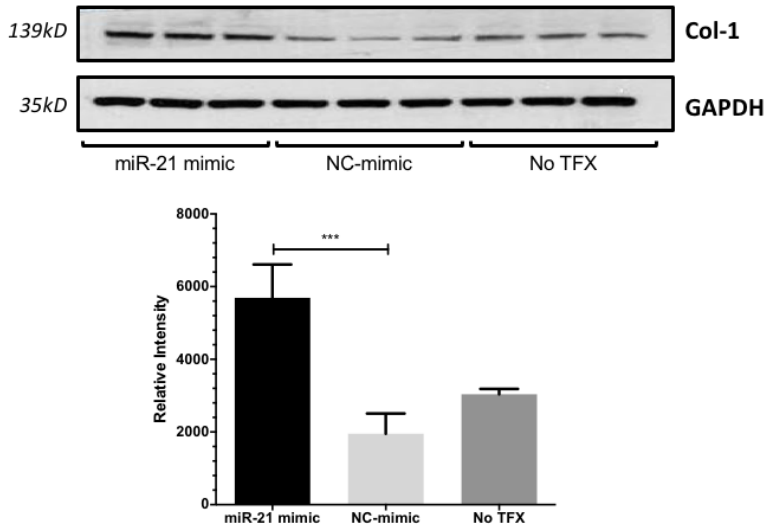

Figure 5-14 Collagen-1 expression by Western blotting in miR-21 mimic transfected-HKC-8 cells

Western blotting for Collagen-1 using lysates from HKC-8 cells transfected with miR-21 mimic, scrambled miRNA mimic, and non-transfected cells. Band intensity was measured by ImageJ software. The mean of band intensity relative to the band intensity of loading control protein, GAPDH was compared between the groups. Comparison of the means between the groups was performed with One-way ANOVA with Bonferroni multiple comparison test. Each band represents an independent experiment. Data was presented as the mean of relative intensity + SD of the three bands displayed. (*** = $p \leq 0.001$)

5.2.8. Hypoxia leads to increase in miR-21 and SMAD7 suppression

Previous experiments have established the relationship between miR-21 up-regulation and SMAD7 inhibition, which was followed by activation of TGF-β1 signalling. To assess whether ischaemia alone can lead to these series of event, the level of expression of miR-21, SMAD7 and SMAD3 activity were measured in hypoxic cells. For this purpose, hypoxia was simulated in HKC-8 cells using several validated methods; by transfection with HIF-1α plasmid, thus increasing HIF-1α expression, by stabilisation of intra-cellular HIF-1α using $CoCl_2$, and incubation in 1%O_2 for 24 hours. To confirm if these methods of inducing or mimicking hypoxia resulted in equal miR-21 up-regulation, qPCR was utilised to detect changes in miR-21 following a given treatment.

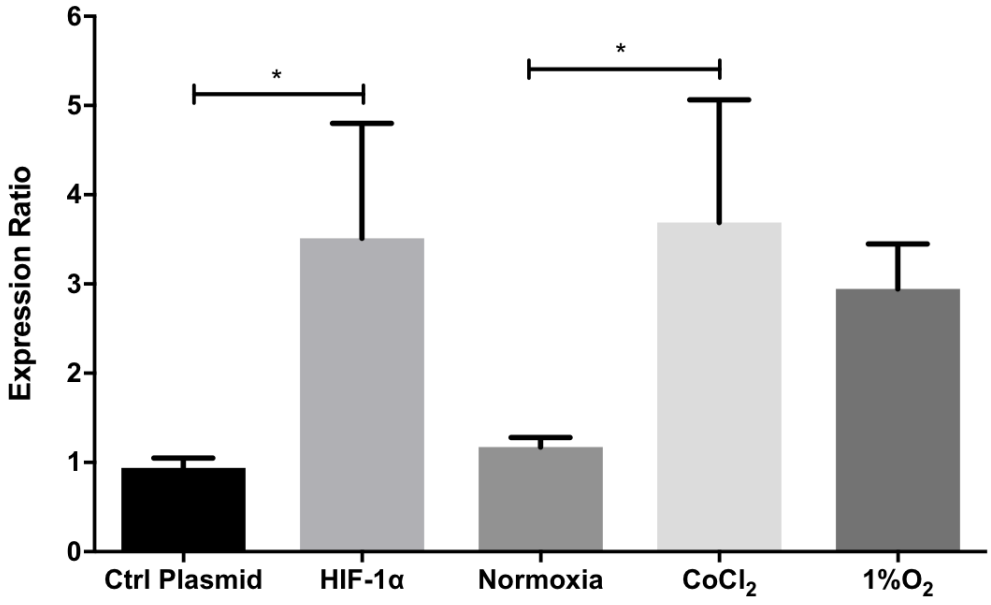

Figure 5-15 MiR-21 level following different methods of inducing hypoxia

Changes in miR-21 level of expression after induction of hypoxia by HIF-1α plasmid transfection, $CoCl_2$ treatment, and incubation in $1\%O_2$, as quantified by real-time PCR. Mir-21 expression was normalised to the reference gene RNU48. Each bar represents the mean of fold-change of expression + SD from three replicates in a single experiment. To detect significant variation, comparison of the means was performed with One-way ANOVA. Multiple comparison test using Bonferroni method was then applied to test the difference of the means between specified groups for statistical significance. (* = $p \leq 0.05$)

Based on my observations using miR-21 mimic, I hypothesise that the increase in miR-21 induced by hypoxia will reduce SMAD7 levels. To test this, Western blotting was used to visualise SMAD7 expression from cell lysates of hypoxic, $CoCl_2$ treated and HIF-1α transfected HKC-8 cells. Figure 5-16 showed that SMAD7 levels were reduced in conditions mimicking hypoxia. Although incubating the cells in $1\%O_2$ for 24-hour led to a reduction in SMAD7 levels, stabilisation of HIF-1α through transfection of HIF-1α plasmid or $CoCl_2$ treatment showed a greater reduction in SMAD7.

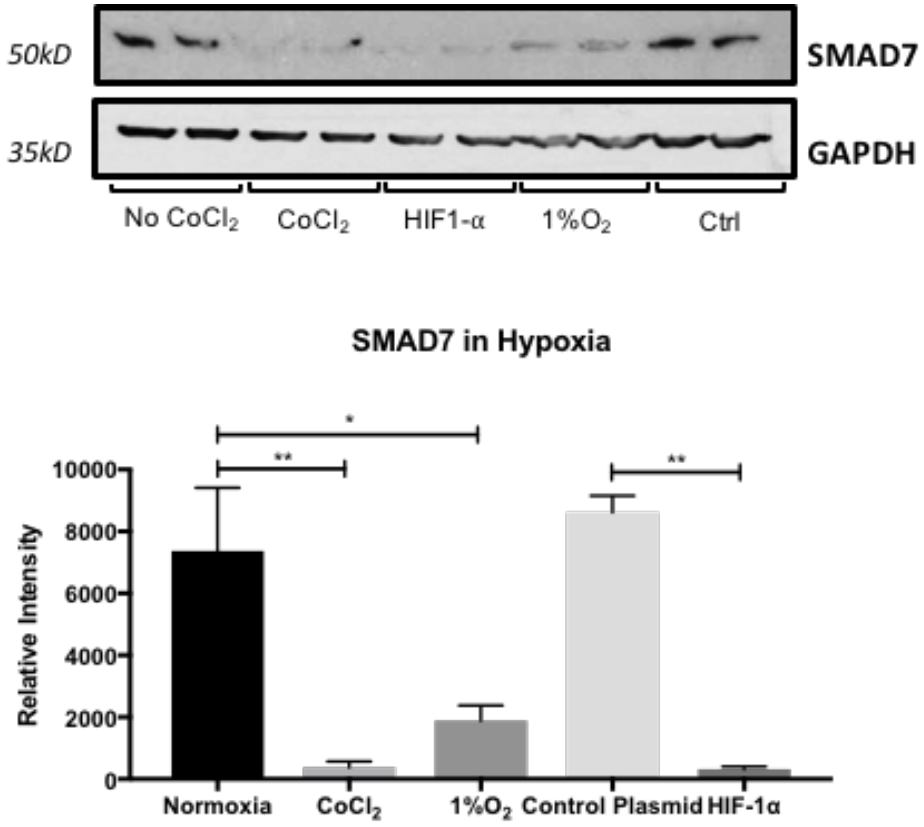

Figure 5-16 SMAD7 expression in hypoxic HKC-8 cells

Western blot results of SMAD7 expression. Hypoxic-like conditions were induced by transfection of HIF-1α plasmid, $CoCl_2$ treatment, and 24-hour incubation in 1%O_2. SMAD7 expression in these cells were compared to normoxic non-transfected HKC-8 cells, and normoxic HKC-8 cells transfected with pCDNA control plasmid. Band intensity was quantified with ImageJ software. Data was presented as the mean of band intensity relative to the intensity of the loading control protein, GAPDH. Each bar represents the mean of 2 samples (N=2) in each group. One-way ANOVA test was used to compare the means. To test for statistical significance between the groups, Bonferroni post-hoc analysis was used. (* = $p \leq 0.05$; ** = $p \leq 0.01$).

The effect of hypoxia to SMAD3 activation was also investigated. To do this, I used a clone of HKC-8 cells stably transfected with SMAD3-luciferase reporter plasmid, which was cultured in conditions to mimic hypoxia as described previously. Compared to HKC-8 cell grown in a normoxic environment, hypoxia induced by 1% O_2 incubation increased SMAD3 reporter activity by approximately 30-fold (Figure 5-17). This increase in SMAD3 reporter activity was even greater when there was an increase in intra-cellular HIF-1α expression, or when HIF-1α was stabilised. The activity of SMAD3 reporter induced by HIF-1α plasmid transfection or CoCl2 were statistically different from the increase of SMAD3 reporter activity induced by 1%O_2. The same clone of HKC-8 cells incubated in the transfection reagent in normoxia was used as controls for HIF-1α plasmid transfection. SMAD3 reporter

activity in this group was no different form the other control groups, ensuring that the transfection process did not affect the observed findings.

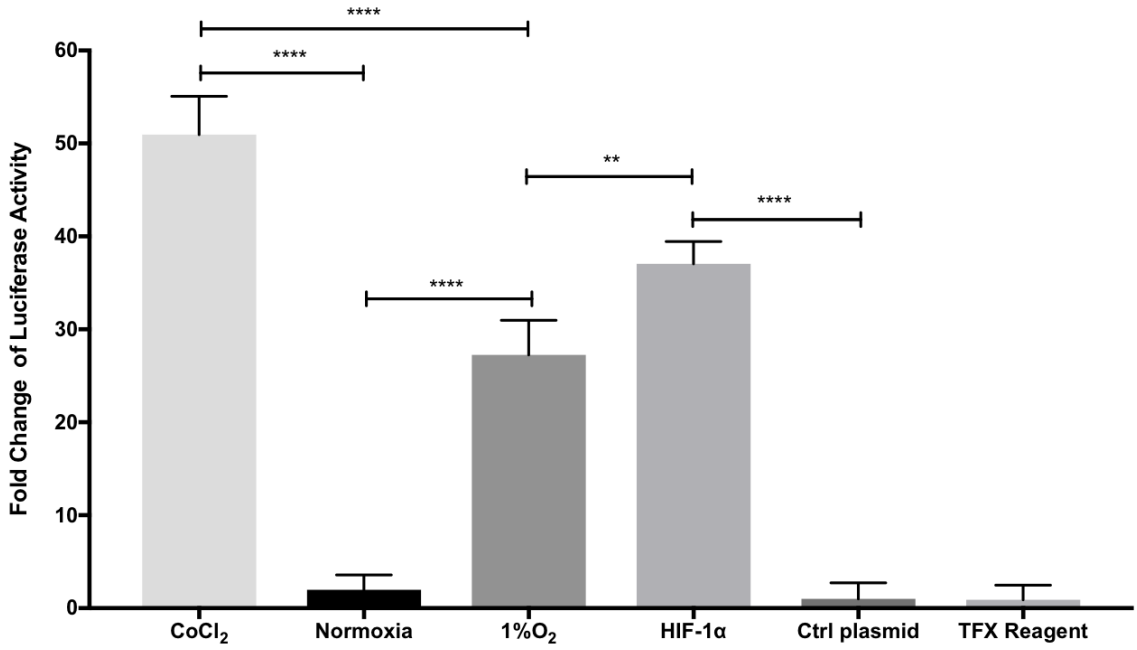

Figure 5-17 SMAD3-luciferase activity in hypoxia or conditions mimicking hypoxia
Measurement of luciferase activity in a SMAD3-luciferase transfected HKC-8 cells. To simulate the effect of hypoxia, cells were cultured for 24-hour in 1% O_2, transiently transfected with HIF-1α plasmid, or treated with $CoCl_2$. The same clone of HKC-8 cells incubated in a normoxic environment were used as control for 1%O_2 and $CoCl_2$ treated groups, whilst cells transfected with pCDNA control plasmid was used as a comparison for HIF-1α-transfected cells. HKC-8 cells incubated with transfection reagent only (denoted as TFX Reagent) were also assessed. Luciferase activity was normalised to the total protein for each sample. Each bar represents the mean + SD of fold change in luciferase activity in three replicates from a single experiment. One-way ANOVA test was used to test for existing statistical significant difference between the means. Multiple comparison test between groups was performed using Bonferroni post-hoc analysis. (** = $p \leq 0.01$; *** = $p \leq 0.001$; **** $p \leq 0.0001$).

As hypoxia led to an increase in miR-21 expression and a subsequent reduction in SMAD7, I hypothesised that hypoxia would make cells more responsive to TGF-β1. To test this hypothesis, I evaluated whether hypoxia increased SMAD3-luciferase reporter gene activity in HKC-8 cells treated with exogenous TGF-β1. To achieve this, the same experimental design was applied with the additional treatment of cells with increasing concentrations of TGF-β1. The results showed that hypoxia or augmentation of HIF-1α concentration significantly increased SMAD3 reporter gene activity in HKC-8 cells (Figure 5-18). HIF-1α stabilisation by $CoCl_2$ caused the greatest change in SMAD3 activity compared to the other hypoxic groups.

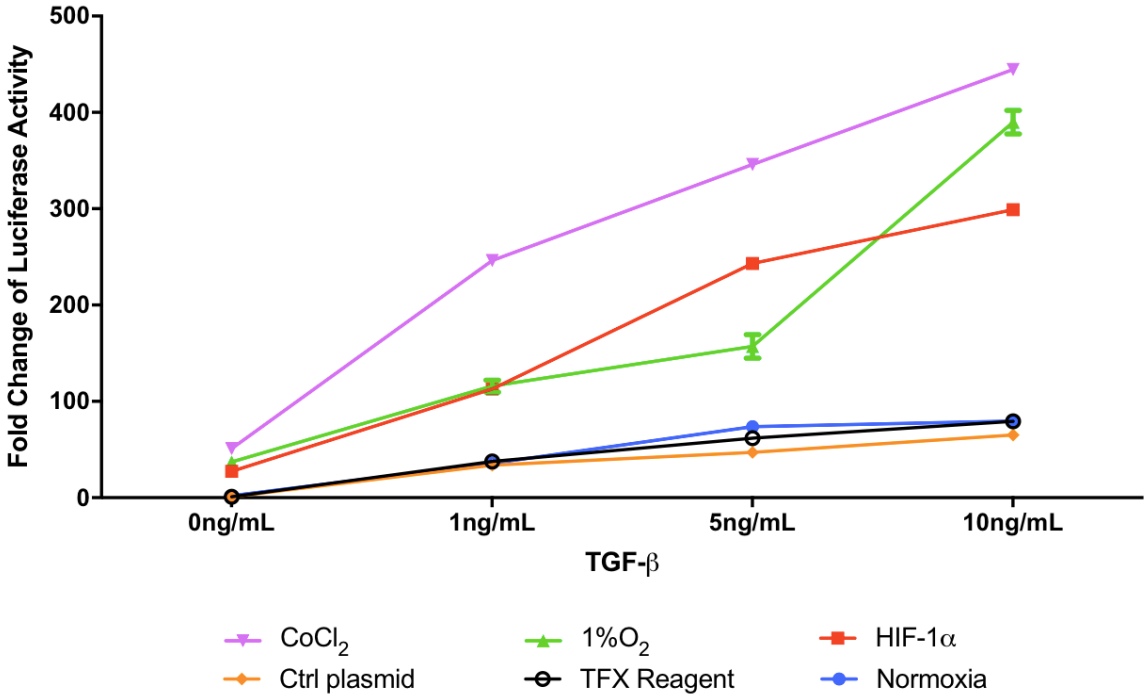

TGF-β1	Groups	pValue
0	Normoxia vs 1%O_2	ns
	Normoxia vs $CoCl_2$	ns
	Control plasmid vs HIF-1α	ns
1	Normoxia vs 1%O_2	p ≤0.01
	Normoxia vs $CoCl_2$	p ≤0.001
	Control plasmid vs HIF-1α	p ≤0.01
5	Normoxia vs 1%O_2	p ≤0.01
	Normoxia vs $CoCl_2$	p ≤0.0001
	Control plasmid vs HIF-1α	p ≤0.0001
10	Normoxia vs 1%O_2	p ≤0.0001
	Normoxia vs $CoCl_2$	p ≤0.0001
	Control plasmid vs HIF-1α	p ≤0.0001

Figure 5-18 SMAD3-luciferase activity in conditions that simulate hypoxia in the presence of exogenous TGF-β1

Experiment was conducted in a clone of HKC-8 cells containing SMAD3-luciferase reporter plasmid. SMAD3-luciferase activity in HKC-8 cells transfected with HIF-1α plasmid, HKC-8 cells treated with CoCl2, and HKC-8 cells incubated in 1% O_2 for 24-hour is shown. Non-transfected normoxic HKC-8 cells, HKC-8 cells containing the control plasmid pCDNA and HKC-8 cells incubated in transfection reagent only were used as controls. All cells were also treated with 0, 1, 5 and 10ng/mL of TGF-β1. Luciferase activity was normalised to the total protein for the respective samples. Each measurement point represents the mean of fold change + SD of luciferase activity compared to non-transfected, normoxic HKC-8 cells without TGF-β1 treatment. Two-way ANOVA was used to detect difference in the means across all groups. Further multiple comparison was performed using Bonferroni post-hoc analysis to test for statistical significant difference between groups.

5.2.9. Inhibition of miR-21 prevents SMAD7 suppression

I have provided evidence establishing a link between ischaemia, miR-21 up-regulation, SMAD7 down-regulation, and subsequent sensitivity of TGF-β1 signalling pathways. Firstly, the effect of miR-21 inhibition on SMAD7 was investigated by transfecting HKC-8 cells with anti-miR-21, and compare the result of transfecting the cell with miR-21 mimic. As shown previously, over-expression of miR-21 lead to suppression of SMAD7. Expectedly, this was not seen in cells treated with anti-miR-21. Inhibition of miR-21 did not result in an increase of SMAD7 expression (see Figure 5-19).

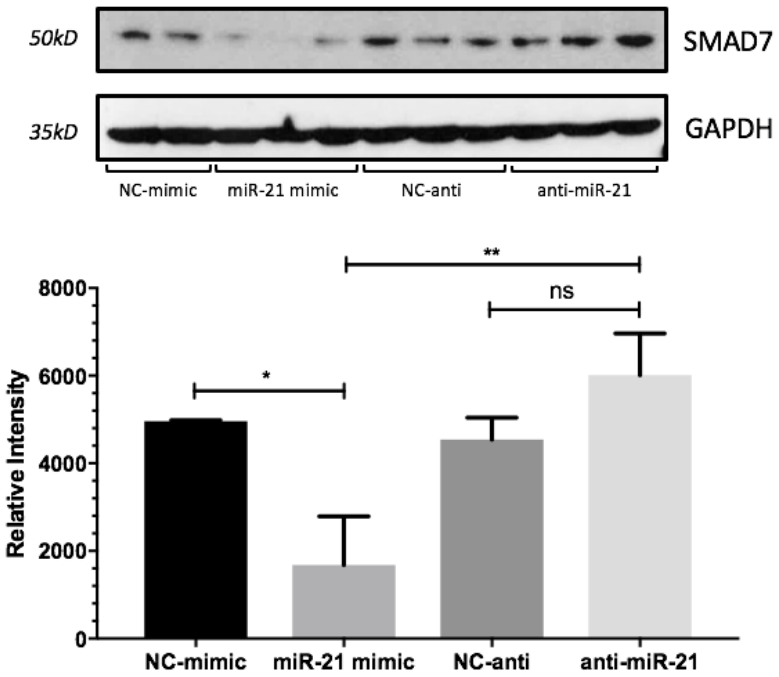

Figure 5-19 The effect of miR-21 inhibition on SMAD7 expression in normoxic HKC-8 cells
Western blot for SMAD7 in normoxic HKC-8 cells. Cells were transfected with miR-21 inhibitor (anti-miR-21) and compared to SMAD7 expression in cells transfected with miR-21 mimic. MiRNA inhibitor with non-coding nucleotide sequence (NC-anti) and scrambled sequence miRNA mimic (NC-mimic) were used as controls. The band intensity was quantified using ImageJ software. Experiment were performed using lysates from three different cells (N=3), except for NC-mimic cells (N=2). Each bar illustrates the quantified intensity of SMAD7 band relative to the intensity of GAPDH. Data was displayed as the mean of relative intensity + SD. Comparison of the means between treatment groups was performed using one-way ANOVA followed by Bonferroni post-hoc analysis (* = $p \leq 0.05$; ** = $p \leq 0.01$; ns = no significant difference detected)

To assess whether inhibition of miR-21 would prevent post-ischaemic SMAD7 down-regulation, HKC-8 cells transfected with miR-21 inhibitor (anti-miR-21) followed by incubation in 1% O_2 for 24-hour to simulate hypoxia. Without anti-miR-21, hypoxia supressed SMAD7 expression. This down-regulation of SMAD7 was not observed in the cells transfected with anti-miR-21 (Figure 5-20).

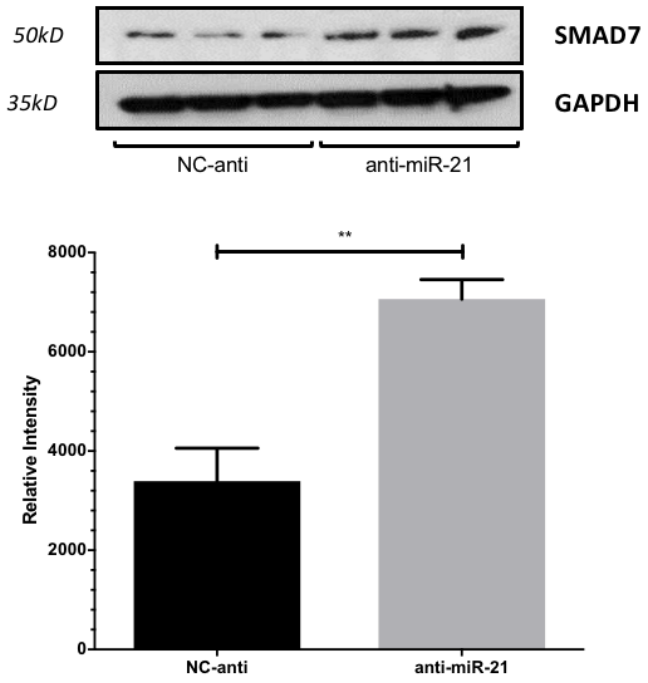

Figure 5-20 The effect of miR-21 inhibition on SMAD7 expression in hypoxic HKC-8 cells
Western blot for SMAD7 in hypoxic HKC-8 cells. Cells were transfected with either miR-21 inhibitor or miRNA inhibitor with non-coding nucleotide sequence (denoted as NC-anti). Band intensity was quantified using ImageJ software. SMAD7 expression in cells with miR-21 inhibitor of each treatment group was compared to SMAD7 expression of its respective non-coding antimiR control. Experiment were performed using lysates from three different cells (N=3). Each bar illustrates the quantified intensity of SMAD7 band relative to the intensity of GAPDH. One-tailed t-test was used to compare the means in each treatment group (** = $p \leq 0.01$)

The same experiment was repeated with the addition of lysates of HKC8 cells transfected with non-coding miRNA inhibitor incubated in normoxic condition to compare the expression of SMAD7 after anti-miR-21 treatment following hypoxia to the basal level of SMAD7 at normoxic condition. The results showed that treating hypoxic TECs with anti-miR-21 brought the level of SMAD7 expression back to its basal level at normoxia (see Figure 5-21).

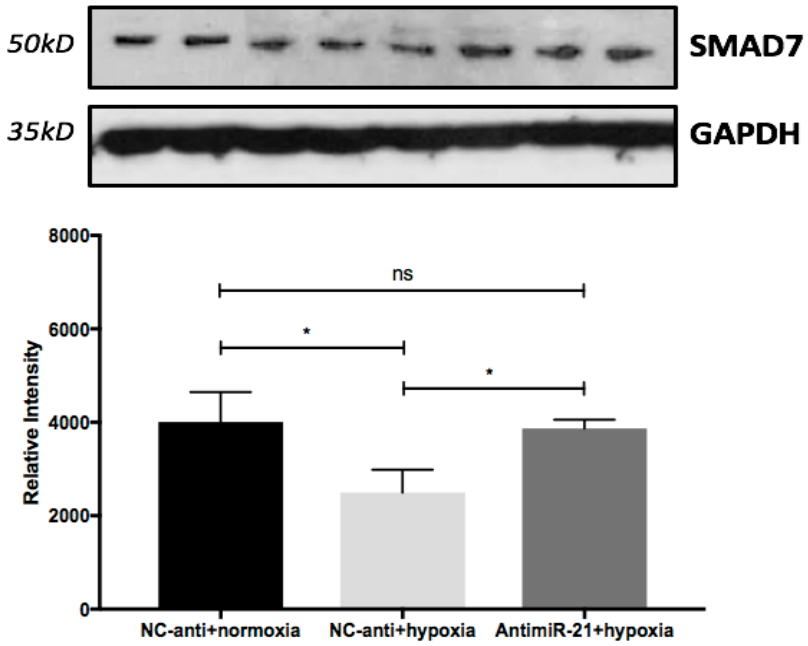

Figure 5-21 SMAD7 expression in hypoxic cells treated with anti-miR-21 and in normoxic cells
Western blot for SMAD7 in hypoxic HKC-8 cells treated with anti-miR-21 (denoted as antimiR-21+hypoxia). Expression level was compared to hypoxic HKC-8 cells transfected with non-coding miRNA inhibitor (denoted as NC-anti+hypoxia). Hypoxia was simulated by incubating the cells in 1%O_2 for 24-hour. Basal SMAD7 level during normoxia was represented by HKC-8 cell transfected with non-coding miRNA inhibitor (denoted as NC-anti+normoxia). Each band represents protein lysate prepared in an independent experiment (N=2 for NC-anti+normoxia and N=3 for other treatment groups). Band intensity was measured using ImageJ software, relative to the expression of GAPDH. Data was presented as the mean of relative intensity + SD. One-way ANOVA test with Bonferroni multiple comparison test was used to detect statistical significance (* = $p \leq 0.05$; ns = no significant difference detected)

5.2.10. Inhibition of miR-21 prevents post-ischaemic SMAD3 activation

The effect of miR-21 inhibition in preventing hypoxia-induced down-regulation of SMAD7 has been shown in the previous section. The next objective was to test whether miR-21 inhibition also resulted in decreased activation of SMAD3. For this purpose, I used HKC-8 cells stably transfected with SMAD3-luciferase reporter plasmid. These cells were co-transfected with anti-miR-21, miR-21 mimic, non-coding antimiR, and miRNA mimic with scrambled nucleotide sequence. The transfected cells were incubated in 1% O_2 to simulate hypoxia, or co-transfected with HIF-1α plasmid to resemble post-ischaemic increase in HIF-1α.

Previous experiments showed that hypoxia alone increased SMAD3-luciferase activity in HKC-8 cells, and the addition of miR-21 mimic was shown to further increase SMAD3 activation. Introduction of anti-miR-21 to hypoxic cells showed the opposite effect, lowering SMAD3-luciferase activity by approximately 2-fold (Figure 5-22). The effect of modifying

miR-21 activity was also assessed using HKC-8 cells containing SMAD3-luciferase reporter gene, which were co-transfected with HIF-1α plasmid. Cells over-expressing miR-21 led to higher SMAD3-luciferase activity compared to scrambled mimic miRNA-transfected cells. Similarly, inhibiting miR-21 reduced SMAD3 activity compared to transfecting the cells with non-coding miRNA inhibitor (Figure 5-23).

The effect of miR-21 mimic or inhibitor transfection was insignificant in the absence of hypoxic injury or HIF-1α over-expression. This is the finding from experiments using the same clone of HKC-8 cells incubated in normoxia for 24-hour, and by transfecting the cells with control plasmid, pCDNA. Although miR-21 mimic increased SMAD3-luciferase activity, and its inhibition reduced SMAD3 activity in normoxic cells, the magnitude of their changes was not statistically significant (Figure 5-24).

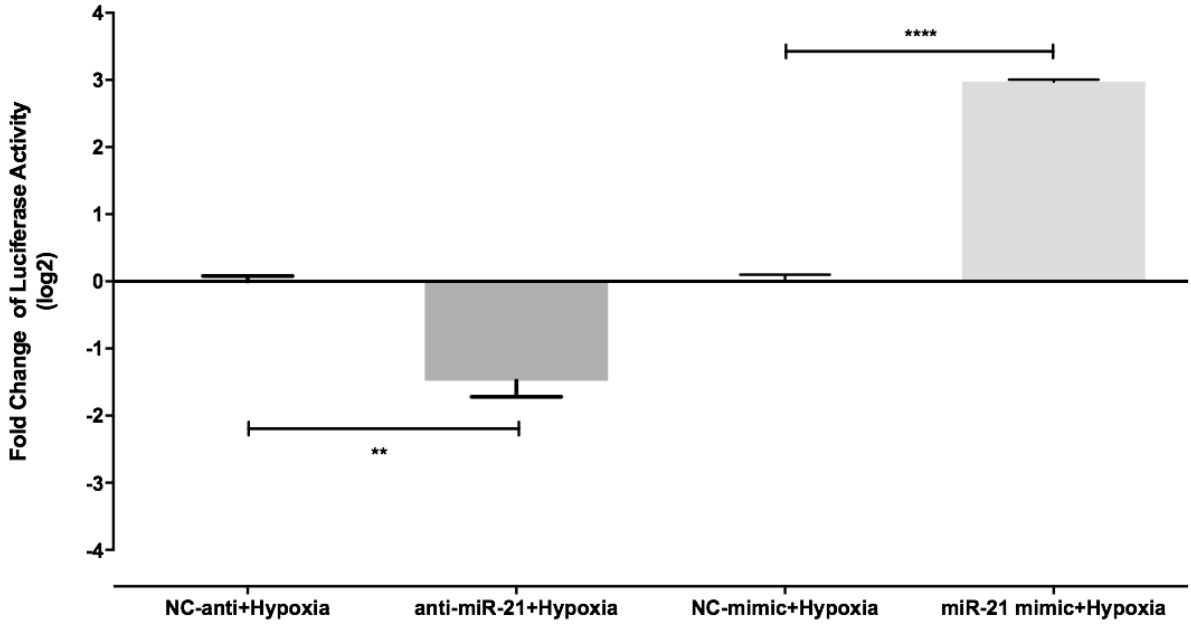

Figure 5-22 The effect of modifying miR-21 function on SMAD3 activity in hypoxic HKC-8 cells
SMAD-3 luciferase activity in HKC-8 cells incubated in 1% O_2 for 24-hour. Cells were transiently transfected with either miR-21 mimic or anti-miR-21 prior to induction of hypoxia. Cells transfected with non-coding sequence antimiR (denoted as NC-anti) and non-coding miRNA mimic (denoted as NC-mimic) were used as controls respectively. Luciferase activity for each group was normalised to protein concentration. Data was presented as the mean fold change of luciferase activity + SD from three replicates. Result presented is from a single experiment representatives of N=3. To test for statistically significant difference between the means, One-way ANOVA test was used, followed by Bonferroni post-hoc analysis. (** = $p \leq 0.01$; **** $p \leq 0.0001$)

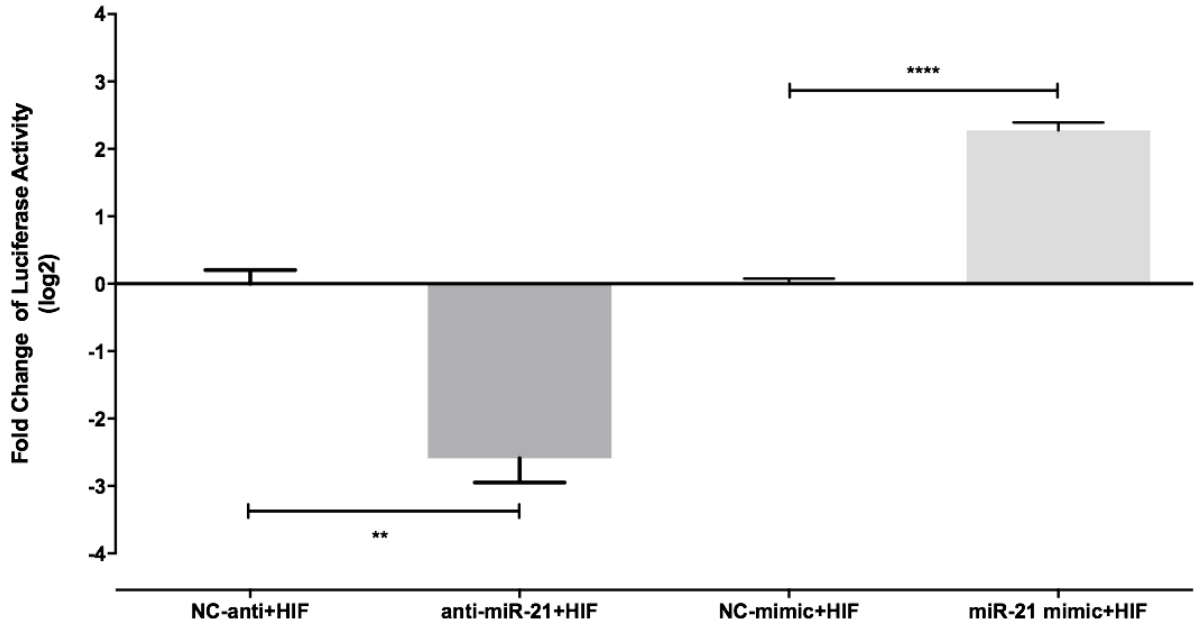

Figure 5-23 The effect of miR-21 inhibition on SMAD3 activity in HIF-1α-transfected HKC-8 cells

SMAD-3 luciferase activity was measured in HKC-8 cells over-expressing HIF-1α following transfection of these cells with miR-21 inhibitor and miR-21 mimic. Luciferase activity was compared to the luciferase activity of cells containing HIF-1α plasmid, which were transfected with non-coding sequence antimiR (denoted as NC-antimiR+HIF) and non-coding miRNA mimic (denoted as NC-mimic+HIF). Luciferase reading for each group was normalised to the total protein concentration quantified in the sample. Data was presented as the mean fold change of luciferase activity + SD from three replicates. Result presented is from a single experiment representatives of N=3. One-way ANOVA and subsequent Bonferroni multiple comparison tests were used to test for statistically significant difference between the means (** = $p \leq 0.01$; **** $p \leq 0.0001$).

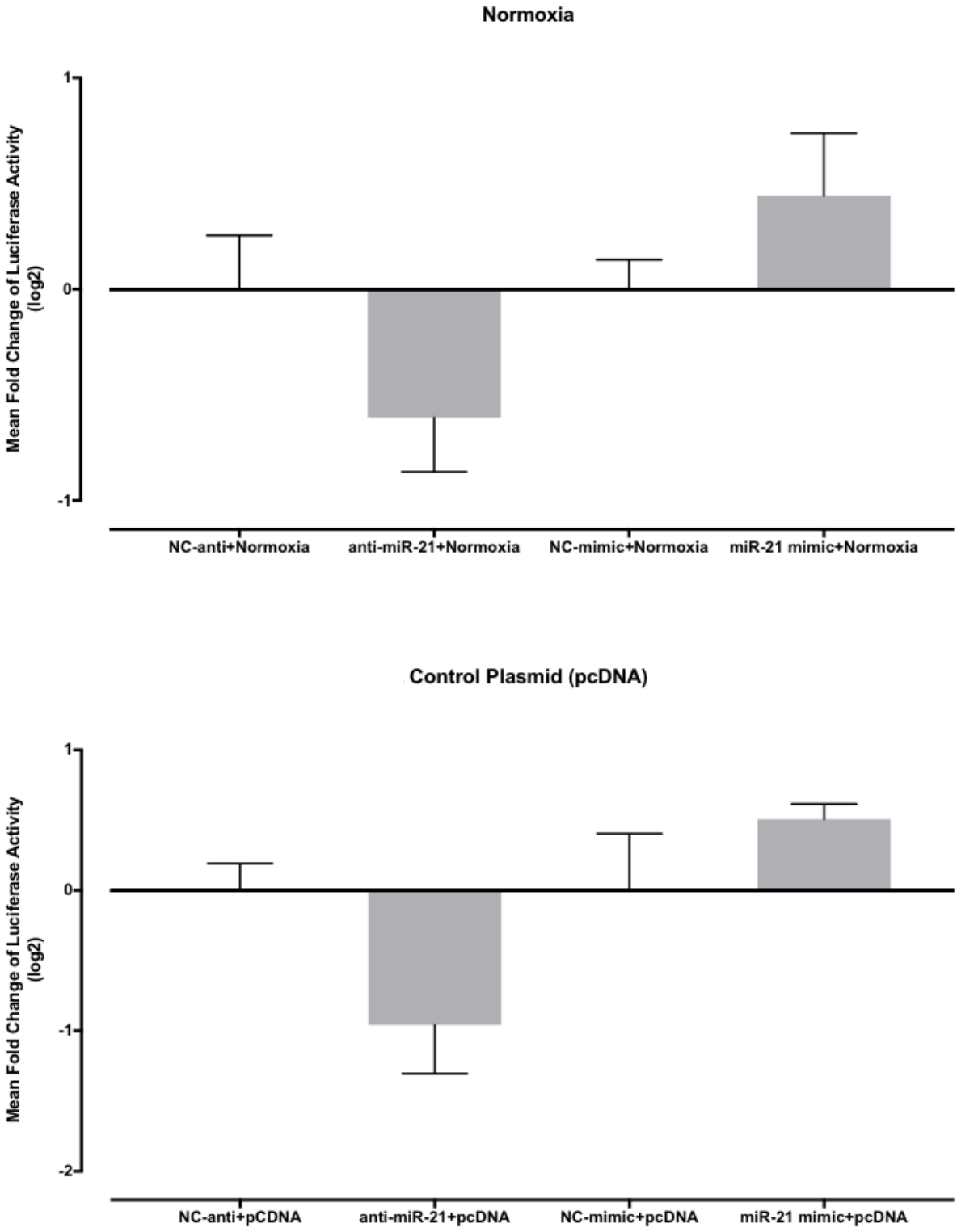

Figure 5-24 The effect of miR-21 inhibition on SMAD3 activity in normoxic HKC-8 cells

The mean fold change of luciferase activity + SD from SMAD-3 luciferase HKC-8 cells grown in normoxic conditions (top), and SMAD-3 luciferase HKC-8 cells transfected with pCDNA as control plasmid (bottom). Data was the result of three replicates. Result presented is from a single experiment representatives of N=3. Cells were transiently transfected with either miR-21 mimic, anti-miR-21, non-coding mimic (denoted as NC-mimic) or non-coding anti-miR (NC-antimiR). One-way ANOVA test was applied, followed by Bonferroni post-hoc analysis, which showed no statistical significant difference between the groups

5.2.11. Tissue Expression and Distribution of miR-21

Evaluation of miR-21 distribution and level of expression in ischaemic renal tissue is essential to verify the in vitro findings. To achieve this objective, I compared miR-21 expression using real-time qPCR using RNA isolated from ischaemic and non-ischaemic renal tissue. The range of miR-21 expression was considerably wide in both groups, especially in the ischaemic group. Nevertheless, it was obvious that miR-21 expression level was significantly higher in ischaemic tissue compared to miR-21 expression in non-ischaemic renal tissue (Figure 5-25).

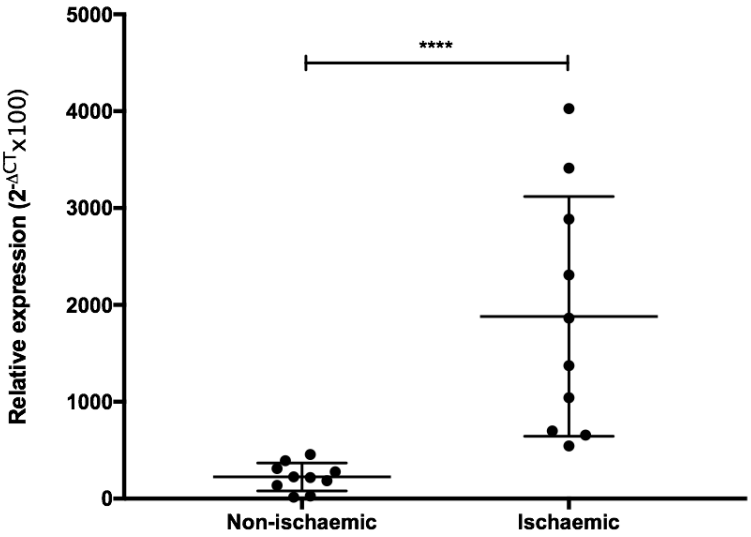

Figure 5-25 Mir-21 expression in ischaemic and non-ischaemic renal tissue

Expression level of miR-21 as measured using real-time qPCR. The unaffected part of kidneys removed for oncological indication was used for non-ischaemic tissues, whilst ischaemic tissues were derived from kidneys deemed unsuitable for transplantation with cold ischaemia time of more than 24-hour. Data was presented as the mean relative expression of miR-21 ($2^{-\Delta CT}$) to the reference gene RNU48. There were 10 kidneys included in non-ischaemia group (N=10), and ten kidneys included in ischaemia group (N=10). To test for statistical significance, comparison of the means was performed using one-tailed t-test. (**** = $p \leq 0.0001$)

Qualitative assessment of miR-21 distribution in renal tissue was performed using *in situ* hybridisation (ISH). Three specimens were randomly selected from each ischaemic and non-ischaemic kidney group. The tissues were incubated in hybridisation mixture containing DIG-labelled miRNA probe for miR-21or DIG-labelled probe with random sequence. I presented the results as individual comparison of three paired specimens (Figure 5-26, Figure 5-27, Figure 5-28). The pairing between a sample from ischaemic kidney group and a sample from non-ischaemic kidney group was performed randomly. Thus, any sample from the ischaemic kidney was eligible to be paired with any of the non-ischaemic kidney samples.

Figure 5-26 and Figure 5-27 show that the expression of miR-21 was stronger in ischaemic renal tissue. It was also shown that miR-21 was predominantly detected in tubular cells. In both figures, miR-21 was undetectable in the non-ischaemic renal tissues. As expected, there was no staining using for scrambled miRNA sequence, indicating no non-specific binding of the probes. Figure 5-28 also showed marked miR-21 expression in the ischaemic tissue. However, this figure showed that miR-21 staining was also observed in the non-ischaemic tissue. MiR-21 expression in Figure 5-28 was also shown to be limited to tubular cells.

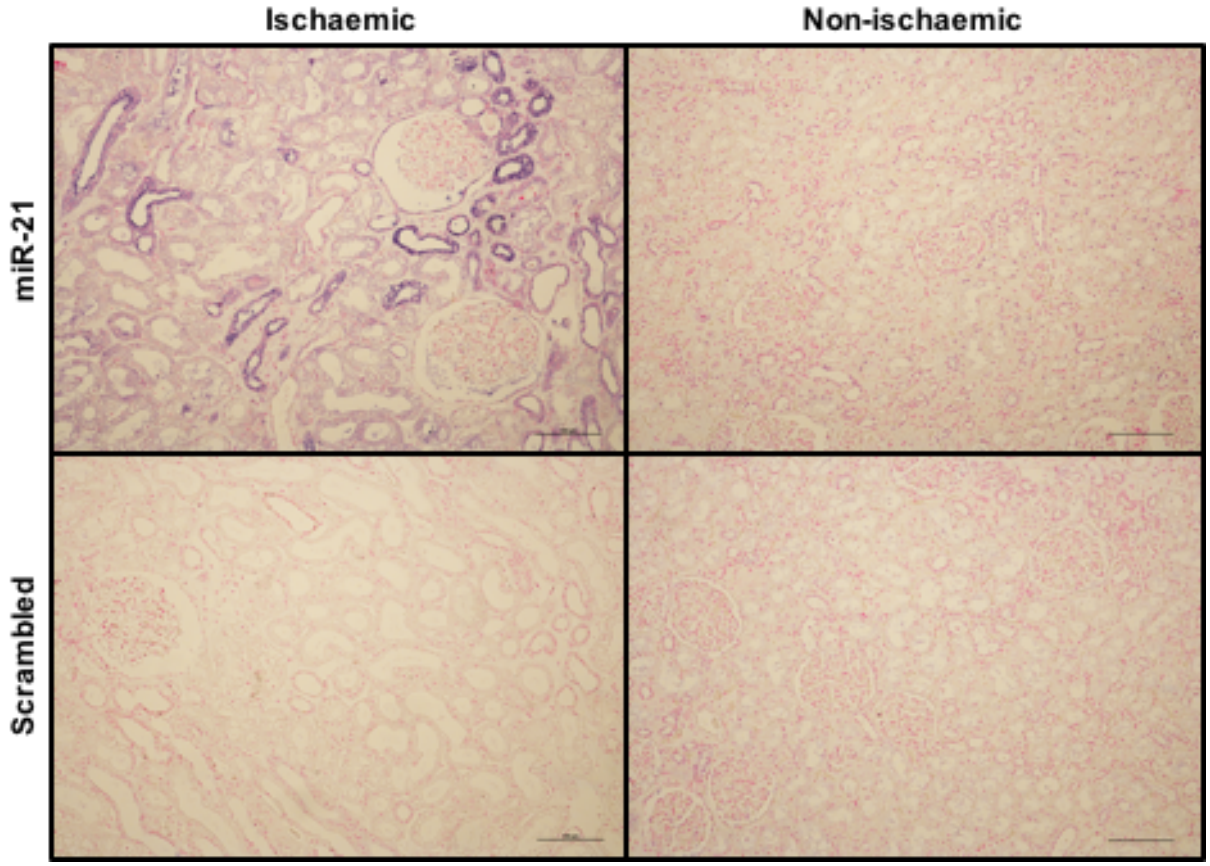

Figure 5-26 Distribution of miR-21 in ischaemic and non-ischaemic renal tissue – comparison 1
MiR-21 distribution in human renal tissue by in situ hybridisation. Ischaemic and non-ischaemic renal tissues were incubated in hybridisation mixture containing 80nM of DIG-labelled ISH probe for miR-21 sequence, or 80nm of DIG-labelled probe with scrambled nucleotide sequence. Anti-DIG antibody conjugated with Alkaline Phosphatase (AP) was subsequently applied, followed by the addition of NBT-BCIP substrate to allow visualisation of miRNAs. Nuclei were stained using nuclear fast red staining. Images were captured at 200x magnification.

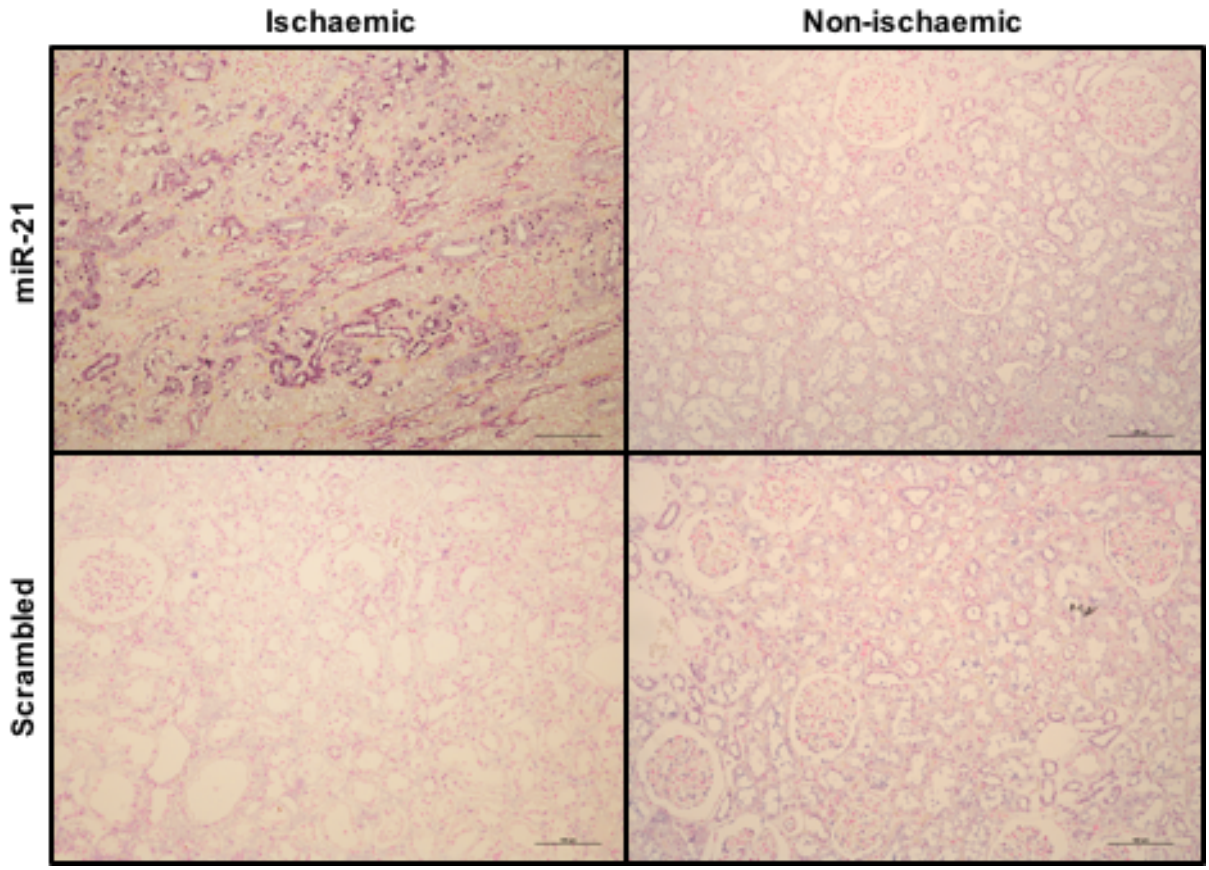

Figure 5-27 Distribution of miR-21 in ischaemic and non-ischaemic renal tissue – comparison 2

In situ hybridisation for miR-21 in ischaemic and non-ischaemic renal tissue. Hybridisation mixture containing DIG-labelled miRNA probe for miR-21 and DIG-labelled scrambled sequence miRNA probe were applied to both tissues. Anti-DIG antibody coupled with AP was applied following probe incubation. To visualise miRNA, NBT-BCIP substrates was added. Nuclei were counter-stained using fast red nuclear staining. Images were captured at 200x magnification.

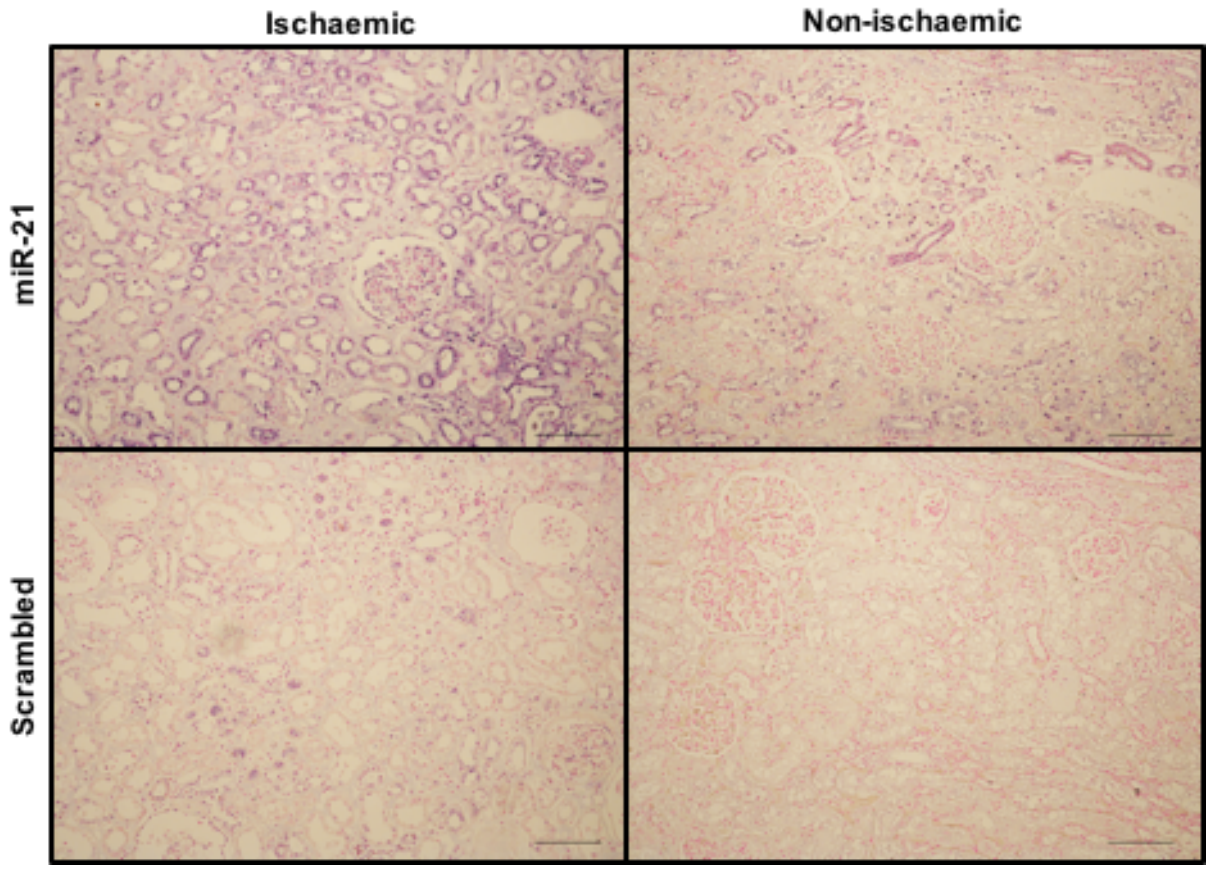

Figure 5-28 Distribution of miR-21 in ischaemic and non-ischaemic renal tissue – comparison 3
In situ hybridisation to detect the presence of miR-21. DIG-labelled probe for scrambled miRNA sequence was used as comparison. Probe bound to miRNA of interest were visualised by adding anti-DIG antibody conjugated to AP followed by the addition of NBT-BCIP substrate. Fast red nuclear staining was used. Slides were visualised at 200x magnification.

5.3. Discussion

5.3.1. Establishing the miR-21 – SMAD7 – SMAD3 axis in the renal response to ischaemia

The involvement of miR-21 in the renal response to IRI has been suggested from the miRNA profiling results. Computational prediction of miRNA targets has also identified various pathways and genes, which may be regulated by miR-21. Ideally, it will be possible to investigate miR-21 involvement in all the pathways relevant to the renal response to IRI, such as PI3K-Akt, HIF-1α signalling and TGF-β signalling pathways. Previous studies performed in our laboratory have shown that hypoxia is associated with changes in cell phenotype, potentially contributing to the progression of injury, and deterioration in renal function. These post-ischaemic morphological changes were closely associated with activation of the TGF-β signalling pathway. Several publications have reported that SMAD3 may regulate the expression of miR-21 (Zhong *et al.*, 2011). In addition, studies on diabetic nephropathy have

described how miR-21 can target SMAD7, and that this is correlated with worse renal structure and function (Wang *et al.*, 2014b; McClelland *et al.*, 2015). However, there is no data on the effect of miR-21 changes following ischaemia on the activity of TGF-β signalling, and how this may affect cellular phenotype. This was the main reason for focusing this part of the study on elucidating the link between miR-21 up-regulation after IRI to alteration in TGF-β signalling activity, and potentially subsequent tubular cell morphological changes.

The TargetScan database predicted a near-perfect complementary interaction between miR-21 and its predicted target site in the 3' UTR of SMAD7 mRNA, suggesting a potentially strong inhibitory effect on SMAD7 function by miR-21. This inhibition of SMAD7 by miR-21 in renal tubular epithelial cells was previously documented by Lin et. al. (Lin *et al.*, 2014). Using rat tubular epithelial cell line, Lin et. al showed inhibition of SMAD7 protein following transfection with lentivirus over-expressing miR-21. I verified this finding in a human tubular epithelial cell line, HKC-8, using a different transfection method. The expression of SMAD7 was lower in human tubular epithelial cells over-expressing miR-21. The implication of lower SMAD7 levels in renal tubular cell, however, has not been well described. Rat tubular cells with miR-21 over-expression and low SMAD7 protein levels showed inhibited proliferation compared to normal cells (Lin *et al.*, 2014). In a high glucose environment rodent tubular epithelial cells, inhibition of SMAD7 by miR-21 enhanced TGF-β1 activity (McClelland *et al.*, 2015). I tested whether this link between miR-21, SMAD7 and activation of TGF-β pathways was also present in an *in vitro* model of IRI using human tubular epithelial cell lines. Using immunofluorescence, I showed that intra-nuclear localisation of SMAD3 occurred in cells over-expressing miR-21. This complements the findings observed by McClelland et. al., which showed increased phosphorylation of SMAD3 in miR-21 mimic transfected rat tubular epithelial cells.

Further, I also explored whether SMAD3 translocation into the nucleus resulted in an increase in the SMAD3/TGF-β activity. In the absence of exogenous TGF-β, miR-21 transfected cells did not show significantly more SMAD3-luciferase activity compared to the control groups. Addition of even very low concentration of TGF-β, however, caused a significant increase in SMAD3-luciferase activity in miR-21 mimic-transfected cells, but not in cells transfected with scrambled miRNA mimic or non-transfected cells. Interestingly, TGF-β has also been shown to play role in the regulation of miR-21. In a breast carcinoma cell line, mutation in the kinase domain of the TGF-β receptor type 1, which inhibits TGF-β signalling, has been shown to reduce pre-miR-21 expression, but not pri-miR-21. This suggests the contribution of TGF-β in maintaining high miR-21 levels in tumour cells in an

autocrine fashion (Davis *et al.*, 2008). SMAD proteins have also been shown to interact with RNA helicase p68, which is a critical sub-unit of the DROSHA microprocessor complex. In addition, SMAD3 knock-out mice also showed reduced miR-21 expression, again suggesting the involvement of SMAD3 in the up-regulation of miR-21.

In a normoxic environment, inhibition of SMAD7 by miR-21 alone was not enough to cause significant alteration to TGF-β activity. The presence of an injury, such as ischaemia, plays a major role in determining if miR-21 up-regulation resulting in an increase in TGF-β activity. The results showed that simulation of hypoxia by 24-hour incubation in hypoxic chamber, or conditions mimicking hypoxia by $CoCl_2$ treatment, or transfection of HIF-1α plasmid, also led to inhibition of SMAD7 and sensitisation of HKC-8 cells to TGF-β. This finding establishes that post-ischaemic miR-21 up-regulation inhibits SMAD7, which has the potential to relieve the inhibition of TGF-β activity. However, the interaction between ischaemia, miR-21 and TGF-β/SMADs activation is more complex, and may involve numerous feedback auto-regulatory mechanisms (Figure 5-29). Several reports have suggested inter-dependence between HIF-1α and SMAD3. Some authors have documented that HIF-1α induced by hypoxia activates the TGF-β/SMAD3 pathway, which may up-regulate genes related to fibrosis (Kimura *et al.*, 2008; Kushida *et al.*, 2016). In contrast, other reports have not found that hypoxia alone activates SMAD3, but instead showed that SMAD3 plays a role in stabilising HIF-1α (Basu *et al.*, 2011). In addition, HIF-1α has also been suggested to occupy direct binding sites on the miR-21 promoter (Liu *et al.*, 2014), which in part also lead to an increase in HIF-1α. MiR-21 has been also shown to regulate PTEN, a suppressor of Akt pathway (Liu *et al.*, 2014; McClelland *et al.*, 2015). Inhibition of PTEN will increase Akt pathway activity, leading to an increase in its down-stream products, such as HIF-1α. Available evidence, therefore suggests that there is an established link between ischaemia, miR-21 and SMADs signalling. In ischaemia, SMAD7 is down-regulated leading to an increase in SMAD3 activity. In addition, the increase in SMAD3 activity will directly up-regulate miR-21, completing a positive feedback system which makes the injured cell more sensitive to TGF-β.

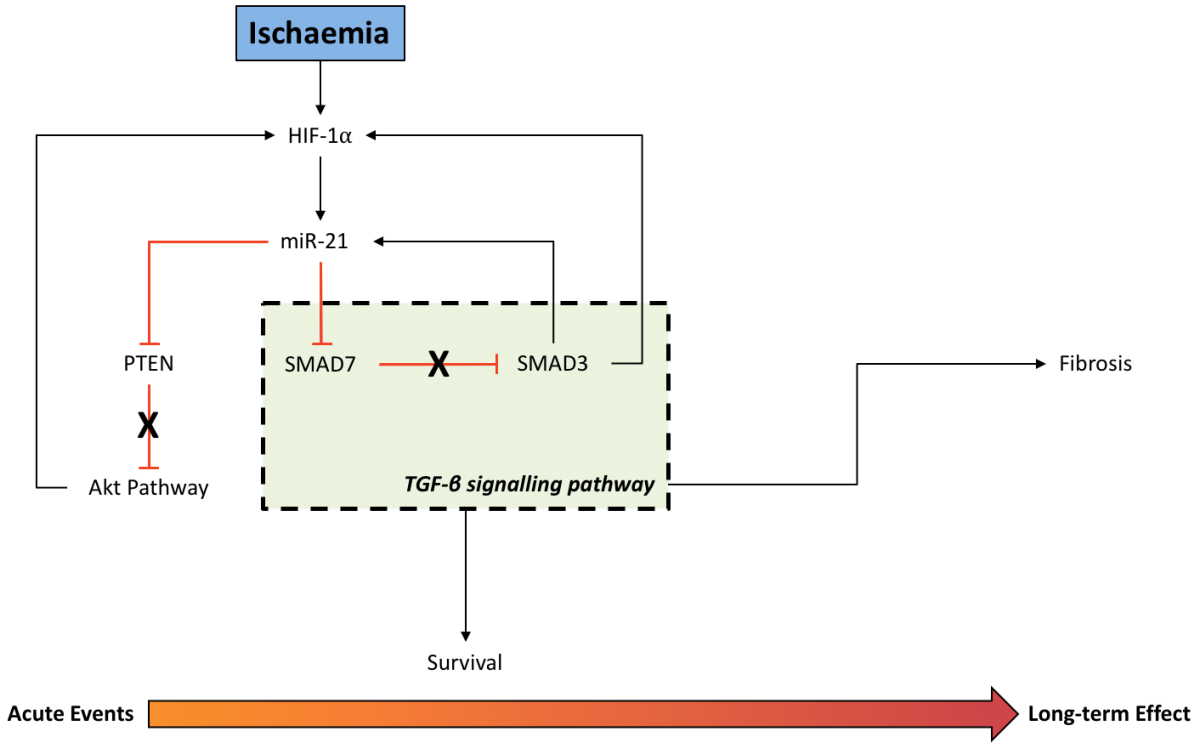

Figure 5-29 The proposed link between ischaemia, miR-21 and TGF-β

The role miR-21 in TGF-β pathway and hypoxia was further confirmed in the experiments using miR-21 inhibitor. Inhibiting miR-21 was shown to prevent the down-regulation of SMAD7 following exposure to either TGF-β or hypoxia. In hypoxia, stabilisation of HIF-1α may lead to increased SMAD3 activity, due to the interdependence of HIF-1α and TGF-β pathways (Basu *et al.*, 2011). The addition of miR-21 inhibitor in these cells significantly reduced SMAD3 activity. In normoxic cells, this significant reduction in SMAD3 activity was not seen, primarily due to the absence of an injury to elevate the baseline SMAD3 activity level. In the mouse model of diabetic nephropathy, the introduction of miR-21 inhibitor has been shown to increase E-cadherin expression and lower α-SMA level (Wang *et al.*, 2014b).

5.3.2. Modification of MiR-21 Expression in Normal vs Disease

The results from experiments using miR-21 mimic or inhibitor during normoxia and hypoxia showed that the effect of modifying miR-21 expression is especially greater when the cells were under stress. This has also been documented in an *in vivo* mouse model. Microarray analysis of healthy kidneys from miR-21 knocked-out mice showed similar genetic expression of predicted miR-21 targets to wild-type mouse. However, differences were only seen after obstruction of the ureter or after induction of IRI (Chau *et al.*, 2012). This is further

supported by Androsavich et al., which showed that miR-21 strongly degraded its mRNA targets in cancer cells, but not in healthy mouse liver (Androsavich *et al.*, 2012). Although there has been no satisfactory explanation for this, it has been proposed that the difference in miR-21 activity in normal and disease condition may be closely related to its low thermodynamic stability and low abundance of its target genes (Androsavich *et al.*, 2012).

Specifically, for the experiments in this study, the differences in miR-21 effect in hypoxic and normoxic conditions may also be related to the level of pre-existing endogenous TGF-β1 induced during hypoxia. The results suggest that miR-21 was not the initiator of injury progression, but rather, act as a mediator which sensitised cells to TGF-β1. The higher level of pre-existing TGF-β1 is, therefore, associated with greater changes facilitated by miR-21.

5.3.3. MiR-21 and changes in TEC morphology

Changes in epithelial cells morphology has been identified as a contributing factor in the progression and deterioration of function in various kidney pathologies. Tissue analysis from diabetic nephropathy rat models showed increased in miR-21 expression, which was associated with increased in Collagen type 1, fibronectin, α-SMA, and decreased in E-cadherin expression in renal epithelial cells (Zhong *et al.*, 2011; McClelland *et al.*, 2015). Similarly, this was also observed in tissue and cells isolated after unilateral ureteric obstruction (UUO). Increased miR-21 expression was detected in the ligated mouse kidney, which was also shown to have higher expression of α-SMA, fibronectin, and collagen type I and IV (Zhong *et al.*, 2011). Furthermore, introducing miR-21 inhibitor agent to the obstructed kidney was shown to reduce the level of TGF-β1, as well as the expression of fibrotic markers, such as α-SMA, fibronectin, and collagen type I (Zarjou *et al.*, 2011).

In the absence of any pathology, such as high glucose level, or artificially-induced interstitial fibrosis, the effect of miR-21 expression on tubular cell morphology has not been described previously. My initial experiment using miR-21 mimic-transfected cells without the addition of exogenous TGF-β revealed no changes in the expression of E-cadherin and α-SMA. Thus, as suggested by the result of SMAD3-luciferase experiment, it appeared that addition of TGF-β was required to induce potentially detectable changes. For this purpose, a low concentration of TGF-β was used, which was sufficient to initiate some phenotypic changes, but not completely alter the normal cellular morphology. In the presence of exogenous TGF-β, the expression of fibrotic markers represented by α-SMA and Collagen type 1 were significantly increased by over-expressing miR-21. This was accompanied by

down-regulation of the epithelial marker E-cadherin. These findings strengthen the argument that miR-21 may have a deleterious effect in renal tubular cells, particularly in combination with an increased level of TGF-β or in the presence of an injury, such as hypoxia.

5.3.4. Post-ischaemic miR-21 expression and distribution in cellular sub-population of the kidney

So far, *in vitro* results have shown that miR-21 level of expression was higher in ischaemic PTECs than in normal PTECs. To validate whether this also occurred *in vivo*, comparison was made between severely hypoxic renal tissue and non-ischaemic tissue. The severely ischaemic tissues were obtained from kidneys which were deemed unsuitable for transplantation for various reasons, and had been in cold ischaemia for more than 12 hours. Despite being grouped under 'non-ischaemic tissues', the kidney tissues used as comparison were obtained from macroscopically normal section of kidneys removed for oncological indications, thus will to have experienced a brief period of ischaemia. This could explain the result in comparison 3 (Figure 5-28), which detected miR-21 in the non-ischaemic kidney. In addition, miR-21 has also been linked with malignancy in the kidney, such as renal cell carcinoma. This could also explain the detection of miR-21, even in the non-ischaemic kidney. Nevertheless, real-time qPCR results still showed significant difference in miR-21 expression between the two-groups, which clearly suggests that ischaemic injury increases miR-21 expression.

Most miRNA profiling studies in the kidney focused their investigation primarily on tubular epithelial cells of the kidney, and indeed documented high level of miR-21 expression in this sub-population of cells. The results of miR-21 *in situ* hybridisation presented in this chapter also showed that miR-21 was detected mainly in tubular cells, and not in the glomerulus. Moreover, the result of several studies focusing on the role of miRNAs in glomerular injury did not detect significantly levels of miR-21 in the glomerulus (Kato *et al.*, 2012; Trionfini and Benigni, 2017). This does not imply that miR-21 has no regulatory function in other cell populations within the kidney. In fact, miR-21 has been shown to repress pro-apoptotic activity, resulting in inhibition of podocyte loss following TGF-β stimulation or in hyperglycaemic glomerular injury. This in part suggests that the effect of miR-21 in the glomerulus is the opposite of its effect in tubulo-interstitial cells (Lai *et al.*, 2015).

In conclusion, I have shown that post-ischaemic miR-21 lead to PTEC sensitisation to TGF-β through a complex regulatory feedback involving SMAD7, SMAD3 and HIF1-α. In a relatively physiological state, or when an injury was transient and tolerable, this is expected to facilitate cellular recovery and survival. When the injury was repetitive or severe, the interaction between miR-21, SMADs signalling and HIF may contribute to the worsening of the effect of the initial injury, resulting in the changes of cellular morphology and fibrogenesis. In kidney transplant settings, the outcome of this interaction becomes more complex and harder to predict, as the organ is more susceptible to injury due to various contributing factors, such as pre-existing morbidities, the use of nephrotoxic medications and the degree of ischaemic and reperfusion injury.

Chapter 6. Thesis Summary

6.1. Summary of Aims and Outcomes

6.1.1. Profiling and Identifying Key MiRNAs Involved in the Renal Response to IRI

In this study, I have identified that ischaemia (induced by treating the cells in 1% O_2 incubator for 12-hour) or ROS treatment (given in the form of H_2O_2 treatment) induced changes in miRNA expression on PTECs. The changes in miRNA expression were detected using a microarray platform, NanoString, and was validated using real-time PCR.

Using different tubular epithelial cell types, I have shown that these changes were unique to different cell types, and especially distinct between cell lines and human primary cells. This is evident from the analysis of the pattern of changes, which showed that most detectable changes in miRNA occurred only in cell line, but not in primary cells, or only in primary cells, but not in cell lines. The findings have also shown that different type of injury left distinct pattern of miRNA changes in cells. Despite the difference in miRNAs pattern in different cells or different injury, a number of miRNAs were found to be consistently up- or down-regulated in all cells at a given time point, suggesting their common involvement in renal response to IRI. These identified miRNAs include miR-21, miR-34a, miR-363, miR-210, miR-142 and miR-130b. These miRNAs were considered as key miRNA candidates to be explored and validated further.

Multiple computational miRNA target prediction databases were used to predict the target of these miRNAs, which highlighted their involvement in pathways related to the renal response to IRI, such as HIF-signalling pathway and TGF-β signalling pathway. The potential role of miR-21 and miR-34a are especially of interest, as the change of expression in both miRNAs were shared consistently by all cell types used in this study. Interestingly, other authors have also reported the involvement of miR-21 and miR-34a in various disease processes in the kidney, unrelated to IRI or kidney transplant setting. This indicates that both miR-21 and miR-34a play essential roles in various cell regulatory mechanisms and function in the kidney.

6.1.2. Functional Analysis of miR-21

MiR-21 was selected to be the focus of this project due to its expression profile pattern in all PTEC types used in this study. Furthermore, despite being frequently investigated for its role in various kidney pathologies, lack of overlap and conflicting research findings has

limited the potential utilisation of miR-21. I was particularly interested in the consequence of miR-21 up-regulation following ischaemia or ROS treatment. The literature has reported that an association between high miR-21 expression with biopsy proven interstitial fibrosis/tubular atrophy (Ben-Dov *et al.*, 2012; Wilflingseder *et al.*, 2013). Others have also associated miR-21 increase to kidney pathologies resulting from a relatively long-term exposure to injury, such as chronic hypoxia or diabetic nephropathy (McClelland *et al.*, 2015).

The change in miR-21 level of expression in this study was detected after exposure to a short-term and transient injury, indicating its role, even in early renal response to injury. The effect of miR-21 up-regulation was then investigated *in vitro* using miR-21 mimic transfection to over-express mature miR-21, or by transfection of anti-miR-21 to inhibit miR-21 production. The link between ischaemia, miR-21 and TGF-β signalling pathway was especially interesting, as previous work by our group has shown that ischaemia may lead to modification in PTEC phenotype through TGF-β pathway activity. SMAD7 was predicted and validated as the target for miR-21. In this study, I observed that up-regulation in miR-21 after ischaemia has led to suppression of SMAD7 and an increase in SMAD3 activity in a renal PTEC cell line. However, the effect of miR-21 up-regulation did not have a significantly detectable consequence in a physiological setting, or in the absence of additional injury, such as ischaemia. In hypoxic cells, over-expression of miR-21 in PTEC showed significantly higher SMAD3-luciferase activity compared to cells with no miR-21 over-expression. Over-expression of miR-21 in PTEC appeared to have sensitised the cells to exogenous TGF-β1, indicated by significantly higher SMAD3-luciferase activity in these cells compared to the cells transfected with non-coding miRNA mimic or the non-transfected cells.

Furthermore, this study has also shown that changes in PTEC phenotype was also exaggerated when miR-21 was over-expressed in PTEC. Treatment with 1ng/mL of TGF-β1 resulted in a reduced E-cadherin expression and an increase in α-SMA and Collagen type 1 expression in PTEC. When this was combined with miR-21 over-expression, the reduction of E-cadherin and the increase in α-SMA and Collagen type 1 were shown to be more obvious.

The link between ischaemia, miR-21 and SMADs activity was further established by the results from experiments using hypoxic PTEC or by simulating the effect of hypoxia using HIF-1α transfection or $CoCl_2$ treatment. These cells showed higher miR-21 level, lower SMAD7 expression and a significant increase in SMAD3-luciferase activity compared to their normoxic controls. These consequences of hypoxia or mimicking hypoxia effect were prevented by transfecting the cells with anti-miR-21.

6.1.3. In vivo Validation

Post-ischaemic increase in miR-21 was validated in this study using real-time PCR and ISH in non-hypoxic and severely hypoxic renal tissues. The expression of miR-21 was significantly higher in hypoxic renal tissues. ISH results further confirmed that miR-21 was selectively distributed in the tubular cells of the kidney. Overall, the objectives and results of the study is summarised in Figure 6-1 .

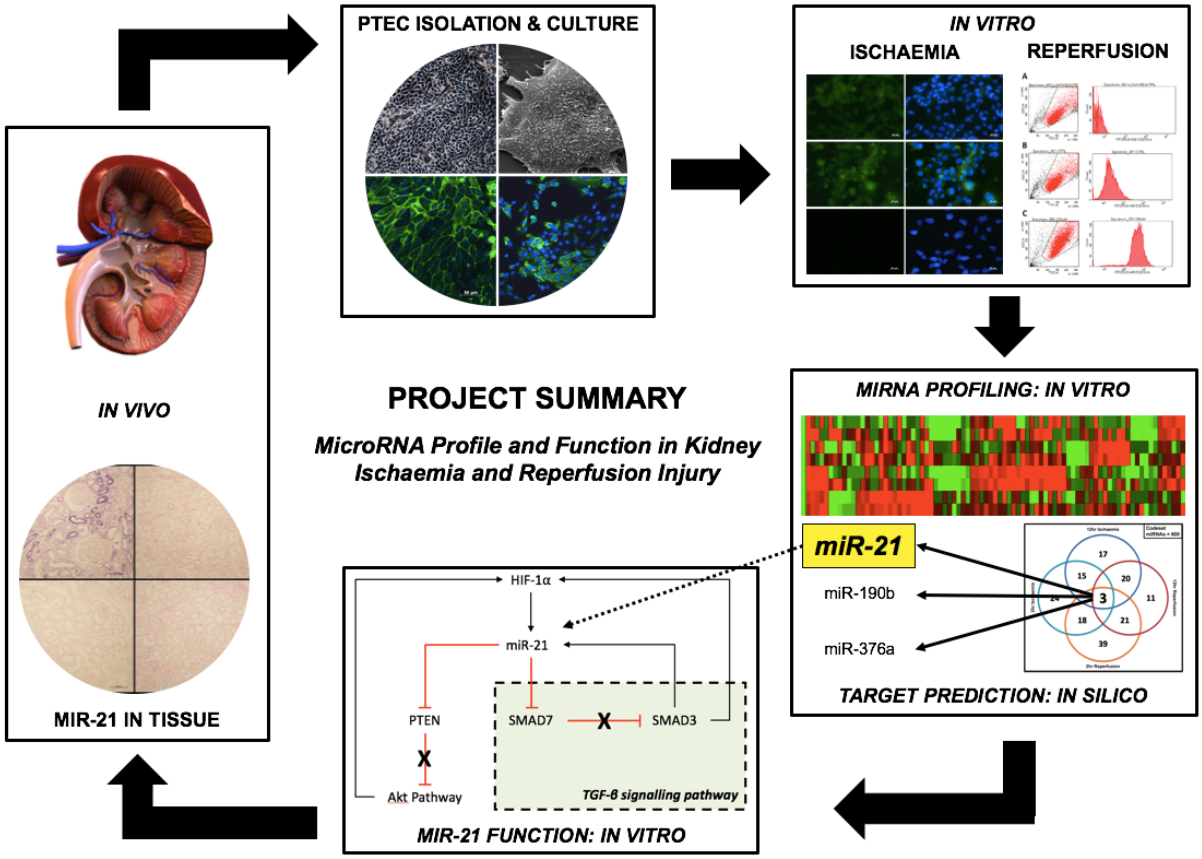

Figure 6-1 Project summary
Schematic illustration of the objectives, steps, and results obtained in this study.

6.2. Overall Discussion

6.2.1. Study Implications

This study has highlighted that short-term and transient ischaemic injury or induction of free-radicals has a clear effect in altering miRNA profile in different types of PTECs. To my knowledge, this is the only study available, which compared the expression of miRNAs in different PTEC cell types following IRI. Significant differences in miRNA profiles following IRI in cell line and PTECs implies that relying on cell lines alone may not be an ideal method

to perform a miRNA profiling study. Thus, careful measures should be taken when extrapolating miRNA profile in immortalised cell lines to human primary cells. The use of four different types of cells has enabled a selective inclusion of candidate miRNAs for further validation and functional analysis. Consistent detection of changes in a miRNA in four different cell type, as was seen for miR-21 in this study, is a strong supporting evidence to highlight the role of that particular miRNA in renal response to IRI.

Biologically, changes in miRNA level indicate activation of pathways, which serves as an effector component of renal response to IRI. In this case, this study has established the association between post-ischaemic miR-21 up-regulation to suppression in the activity of an inhibitory SMAD7, and subsequent increase in SMAD3 activity. This may serve as a crucial response by which PTECs make themselves more sensitive to the presence of growth factor (i.e. TGF-β1). This may be aimed to promote repair and facilitate cell survival. However, when the injury is repetitive, or when the degree of injury is severe, this may lead to continuous activation of a positive feedback mechanism, causing an exaggerated response and uncontrolled repair process, which may be detrimental to long-term organ renal function. Furthermore, this study adds to the knowledge that the link between miR-21 and TGF-β pathway is not only limited to the direct miR-21 regulation by SMAD3. Indeed, this study has shown that miR-21 has an important role in regulating TGF-β signalling through SMAD7. Moreover, this study has also shown that the interaction between miR-21 and TGF-β in the kidney was not only limited to chronic injury or diabetic nephropathy, but also in an IRI model.

6.2.2. Study Limitations

Although the use of four different cell types has added a different perspective to the miRNA profiling results, it must be carefully approached and interpreted. Limitation in time and resources have only allowed the use of 24 samples in the initial profiling using NanoString. This means that only the primary PTECs could only be run in duplicates. Profiling of miRNAs in cell lines (i.e. HK-2 and HKC-8) had to rely only on a single experiment. Regardless, validation of the expression of selected key miRNAs using real-time PCR has shown consistent results in cell lines, which demonstrated the reproducibility of the profiling technique.

The use of H_2O_2 in mimicking reperfusion injury has been reported in many studies. However, induction of free-radical using H_2O_2 only simulated a component of reperfusion injury. Comprehensively, reperfusion injury consists of other equally important components,

such as activation of the immune system. The interaction between tubular cells and the immune system is an important determinant of successful renal recovery or progression of injury, resulting in deterioration in function. This element of reperfusion has not been addressed by the model of reperfusion injury used in this study. This was accepted as the consequence of achieving the aim of profiling miRNA profile in PTECs as two separate injuries, in order to discover the potentially unique miRNA signature changes.

In vivo validation of miR-21 expression in this study was performed on tissues originated from severely ischaemic kidney rejected for transplant, which were compared to the non-ischaemic tissues taken from the normal poles of kidney removed for oncological reasons. Although the expression of miR-21 was significantly different between these tissues, it would be more ideal to use a relatively healthy renal tissue for control, such as tissues from living donor. As has been reported, miR-21 may also be up-regulated in renal cell carcinoma, which could be a potential confounding factor.

6.2.3. Challenges in microRNA Research

The discovery of miRNAs has opened a rapidly growing research field. Initial technical challenges have been overcome by novel methodologies or modifications of existing technologies. Despite these efforts, miRNA research still faces significant obstacles. Increasing number of miRNA research has identified the complexity of miRNA biology, their regulatory roles and the intricate nature of miRNA-mRNA interaction. This complexity will influence the way we interpret, translate and apply available research findings.

Despite the abundance of miRNA profiling studies and mechanistic experiments linking miRNAs to certain disease processes, little progress has been made in understanding the biology of miRNAs themselves. MiRNAs have been shown to be modified and interact with other epigenetic events, which will affect their capability to bind with mRNA (Kim *et al.*, 2010; Yu and Chen, 2010; Singh and Campbell, 2013). Moreover, it is becoming more widely accepted that the regulation of miRNA biogenesis does not take place by a single universal mechanism. Instead, different classes of miRNAs may undergo different processing, regulation and turnover (Davis and Hata, 2009). The details of these mechanisms and their biological consequences remain largely unknown.

A published work on oncogenes by Poliseno et al. described functional role of pseudogenes, which were previously thought to be redundant (Poliseno *et al.*, 2010). Pseudogenes are the transcripts of protein-coding genes, which are highly homologous to their cognate genes, except for several base pairs mismatches. Given this homology, pseudogenes compete with their respective mRNA for miRNA binding, acting as a ‘miRNA

decoy', thus may be involved in disease pathogenesis (Poliseno *et al.*, 2010; Bernardo *et al.*, 2012). This miRNA-pseudogene interaction complicates our attempt to translate the profile of a miRNA of interest to its actual biological role.

Furthermore, different miRNAs may undergo maturation through different pathways. In contrast to the general miRNA maturation process, some miRNAs undergo maturation independent of Drosha or Dicer (Suzuki and Miyazono, 2011; Ha and Kim, 2014). As discussed previously, several authors have also documented interaction between miRNA maturation pathways and intracellular signalling molecules, nuclear genetic machinery and RNA binding proteins (Suzuki and Miyazono, 2011). These complicated interactions should be taken into consideration in the interpretation of profiling results or in drawing conclusion from an experimental model.

It has been proven very difficult to assess the influence of a single miRNA to a particular cellular process or disease pathway. A cellular biological response or a disease process is a result of an orchestrated interaction of many genes requiring fine-tuning by many miRNAs. Theoretically, the different miRNAs may be up- or down-regulated to produce a synchronised biological effect. In reality, however, detection of such up- or down-regulation is not always simple, as the expression of some miRNAs may be altered below a detectable threshold, and yet still contributes to a biologically significant effect. Even if the alteration is detectable, experimental validation of only a single miRNA will only provide a partial picture of an overall biological response. It is almost impossible to design an experimental study that can evaluate a net result of numerous miRNAs interacting together to generate a fine-tuned cellular response.

Another level of complexity in miRNA research is added by the discovery made by Vasudevan *et al.* on how miRNA may directly up-regulate gene expression during cell quiescence. Quiescence is stimulated by several factors, such as contact inhibition, loss of adhesion or serum starvation (Vasudevan *et al.*, 2007). Initially, Vasudevan *et al.* identified two proteins required for translational up-regulation during serum starvation; argonaute 2 (Ago 2) and fragile-X-mental retardation related protein (FXR1). These two key components need to bind to A+U-rich elements (AREs) in the 3' UTR of TNF-α mRNA to increase its translation. The hypothesis that miRNAs may mediate this binding was tested using a computational prediction approach, which identified several miRNAs having seed regions complementary to TNF-α AREs. Hsa-miR-369-3 was found to be necessary for translational up-regulation of the ARE reporter, and that miR-369-3 was reduced in non-quiescent HEK293 cells. Whether this is specific to miRNAs targeting only TNF-α mRNA, or in fact also takes place in other miRNA-mRNA interaction still requires investigation. However,

further observation by the same author on other miRNAs; let7-a and miRcxcr4, showed translational down-regulation of their respective target mRNAs only in proliferating cells, but not in serum starved milieu (Vasudevan *et al.*, 2007; Rusk, 2008). This finding notably adds a different dimension in the design and analysis of miRNA research, but more importantly to how miRNAs can be exploited in a specific cellular condition.

To complicate the matter even further, technological variation in existing profiling platforms, differences in bioinformatics criteria and diversity in experimental design used also affect the result of different studies addressing the same research question. This is evident in the lack of overlapping results shown by many studies performed to investigate the role of miRNAs in kidney transplantation and kidney IRI.

6.2.4. Future Directions

The miRNA profiling results from this study have nominated several miRNAs with the potential to be validated further. The role of a hypoxamiR, miR-210, which can be indirectly involved in HIF-1α activity following ischaemia has not been well documented in kidney transplant setting, especially in its relation to IRI. Other potential candidates are miR-34a and miR-363. The link between miR-34a and the initiation of EMT process after ischaemia can be explored further. The role of miR-363 is especially interesting, due to its interaction with TWIST pathway and subsequent down-regulation in E-cadherin expression. Interestingly, miR-363 has also been linked with genes encoding Collagen and Integrin-β6. Therefore, over-expression of miR-363 is expected to inhibit the expression of both Collagen and Integrin-β6. The resulting effect of this interaction also has the potential to be elucidated further.

MiR-21 is an important player in renal response to IRI and other renal pathologies. This has been documented *in vitro* as well as *in vivo*. There are several literatures, which have already established an association between the higher expression of miR-21 in tissue or plasma to post-transplant graft function. Although these studies are valuable, in my perspective, the level of miR-21 in urine appeared to be especially attractive to be used as potential biomarker and predictor of graft function. Currently available literatures have highlighted the potential use of urinary miR-21 as a biomarker. They detected that miR-21 is up-regulated in mouse hypertensive kidney injury model (Chen *et al.*, 2017), mouse kidney fibrosis model (Chen *et al.*, 2017), human renal interstitial fibrosis/tubular atrophy (IF/TA) (Wang *et al.*, 2012; Maluf *et al.*, 2014; Zununi Vahed *et al.*, 2017), and in acute kidney injury (Saikumar *et al.*, 2012; Du *et al.*, 2013). However, not many studies have documented the use of miR-21 as a predictor of graft function in the context of kidney transplant. A report by

Maluf et al. (Maluf *et al.*, 2014) did not detect miR-21 to be differentially expressed in urine of patients with IF/TA and in patients with normally functioning graft. The other closest available data is reported by Khalid et al. (Khalid *et al.*, 2016), which showed significant correlation between miR-21 level in hypothermic machine perfusate to graft function at 6 and 12 months after transplant. Future studies correlating miR-21 level in the urine or plasma immediately after transplant to graft function will be important if miR-21 is to be adapted as a potential biomarker or predictor.

6.3. Study Conclusion

Ischaemia and reperfusion injury induced changes in miRNA profile in renal proximal tubular epithelial cells, which is involved in the renal response to IRI. One of the miRNAs detected is miR-21, which is involved in the regulation of SMAD signalling following ischaemia. Through its interaction with SMAD7 and SMAD3, miR-21 was shown to make PTEC more sensitive to TGF-β1, which may be essential in cellular repair process and cellular survival. Mir-21 is highly expressed in tubular cells of ischaemic kidneys, further emphasising its role in the renal response to IRI.

List of Publications and Presentations

Manuscript in preparation for publication

1. Situmorang G, Sheerin N (2018). Ischaemia and Reperfusion Injury; Implications for Long-term Transplant Outcome. (submitted for a review article in Pediatric Nephrology journal)
2. Situmorang G, Taher A, Ali S, Kirby J, Sheerin N (2018). MicroRNA Profile and Function in Renal Response to Ischaemia and Reperfusion Injury; A Closer Look at The Role of miR-21. (manuscript in preparation)

Oral and poster presentations at conferences

1. Situmorang G, Taher A, Ali S, Kirby J, Sheerin N (2015). MicroRNA Profile and Function in Kidney Ischaemia and Reperfusion Injury. Oral presentation at MicroRNA Day meeting, Newcastle University, Newcastle upon Tyne, United Kingdom.
2. Situmorang G, Taher A, Ali S, Kirby J, Sheerin N (2017). MicroRNA Profile and Function in Kidney Ischaemia and Reperfusion Injury. Poster presentation at the Blood and Transplant Research Unit in Organ Donation and Transplantation Research Meeting, Cambridge University, United Kingdom.
3. Situmorang G, Taher A, Ali S, Kirby J, Sheerin N (2017). MicroRNA Profile and Function in Kidney Ischaemia and Reperfusion Injury. Oral presentation at the 54th European Renal Association – European Dialysis and Transplant Association (ERA-EDTA) Congress, Madrid, Spain.

Appendix – NanoString Sample Preparation Protocol

The following sections describe materials and methods used in the preparation of samples to be profiled with NanoString platform, as adapted from the NanoString nCounter miRNA Expression Assay Manual.

Materials Required

1. nCounter miRNA Expression Assay Kit (NanoString Technologies, USA)
2. DEPC-treated (or RNASse-free) water
3. 100ng total RNA per sampe, normalised to 33 ng/µl
4. Spectrophotometer (NanoDrop Technologies, USA)
5. Micropipettes (0.5-10µl; 2.0-20µl; 20-200µl)
6. Picofuge with strip-tube adaptor (Applied Biosystem, USA)
7. Thermocycler (Applied Biosystem, USA)
8. nCounter Prep Station (NanoString Technologies, USA)
9. nCounter Digital Analyser (NanoString Technologies, USA)

Thermocycler Protocols

1. Annealing Protocol

   Temperature : 94°C – 1 minute
   65°C – 2 minute
   45°C – 10 minute
   48°C – hold

   Total time : 13 minute

2. Ligation Protocol

   Temperature : 48°C – 3 minute
   47°C – 3 minute
   46°C – 3 minute
   45°C – 5 minute
   65°C – 10 minute
   4°C – hold

   Total time : 24 minute

3. Purification Protocol

Temperature	:	37°C – 2 hours
		70°C – 10 minute
		4°C – hold
Total time	:	2 hours 10 minute

Sample Preparation Protocol

1. RNA sample was normalised to 33 ng/µl using RNAse-free water.
2. 499 µl RNAse-free water was added to 1 µl of the miRNA Assay Controls provided in the kit, in a sterile microcentrifuge tube. Solutions were mixed by vortexing and centrifugation at 1,000G for 30 second. The tube was stored on ice.
3. Annealing master mix was prepared by combining 13 µl of Annealing Buffer, 26 µl of nCounter miRNA Tag Reagent and 6.5 µl of the diluted Assay Controls prepared in Step 2. Solutions were mixed well by pipetting up and down.
4. 3.5 µl of the annealing master mix prepared in Step 3 was aliquoted into each tube of a 12 x 0.2 ml strip tube.
5. 3 µl (100ng) of RNA sample was added to each tube. The tubes were capped and gently flicked to ensure that the solutions were thoroughly mixed. Tubes were centrifuged at 1,000G for 30 second.
6. The tubes strip was placed in a thermocycler and Annealing Protocol (as described in Thermocycler Protocol point 1) was initiated.
7. Ligation master mix was prepared by combining 19.5 µl PEG and 13 µl Ligation Buffer. It was important to pipette PEG slowly to ensure accurate transfer of volume into the mix, as PEG is viscous. The solutions were mixed well by pipetting up and down.
8. Following completion of the Annealing protocol, when the thermocycler has reached 48°C, 2.5 µl of the ligation master mix was added to each tube. Thorough mixing of the solutions was ensured by flicking the tubes gently, which was followed by centrifugation at 1,000G for 30 second. Thermocycler was maintained at 48°C during this process.
9. Tubes were returned to 48°C thermocycler, and were incubated for 5 minute.

10. With the tubes still in place in the heating block, 1 µl of Ligase was added directly to each tube. Incubation temperature was maintained at 48°C. No mixing required at this stage.
11. Immediately after addition of Ligase to the final tube, tubes were recapped and Ligation Protocol (as described in Thermocycler protocol section point 2) was initiated.
12. After Ligation protocol is completed, the tubes were removed from the heat block, and 1 µl Ligation Clean-Up Enzyme was added into each reaction. To mix, tubes were gently flicked followed by centrifugation at 1,000G for 30 second.
13. Tubes were returned into the thermocycler and Purification Protocol (as described in Thermocycler Protocol section point 3) was initiated.
14. After completion of Purification Protocol, 40 µl of RNAse-free water was added to each sample. Ensure samples were thoroughly mixed by pipetting up and down followed by centrifugation at 1,000G for 30 second.
15. Samples were immediately used for miRNA CodeSet hybridisation.

Sample Preparation Protocol

The final hybridisation reaction contained the following component: 10 µl Reporter CodeSet, 10 µl hybridisation buffer, a 5 µl aliquot from the miRNA Sample Preparation protocol, and 5 µl capture ProbeSet. The hybridisation reaction was prepared as follows:

1. Aliquots of both Reporter CodeSet and Capture ProbeSet reagent were thawed on ice. To ensure aliquots were mixed well, the tubes were inverted several times, followed by centrifugation at 1,000G for 15 second.
2. 130 µl of hybridisation buffer was added to the tube containing the Reporter CodeSet to create a master mix containing 130 µl of the Reporter CodeSet and 130 µl of hybridisation buffer. Tuber were inverted several times to mix, followed by centrifugation at 1,000G for 15 second.
3. A 12-tube strip provided in the kit was labelled and cut in half to fit in a picofuge.
4. 20 µl of master mix prepared in Step 2 was added into each of the 12 tubes.
5. Samples from the miRNA Sample Preparation Protocol were denatured by incubation at 85°C for 5 minutes and were quickly stored on ice. 5 µl aliquot from the miRNA Sample Preparation protocol was added to each tube.

6. Thermocycler was pre-heated to 65°C and programmed for 30 µl volume and heated lid option. Time setting was programmed to infinite to ensure that the thermocycler temperature did not change to 4°C at the end of the run.
7. 5 µl of Capture ProbeSet was added to each tube immediately prior to placing the tube at 65°C. To mix, strip tubes were inverted several times and gently flicked, followed by centrifugation at 1,000G for 15 second. It was important that this step was performed as quickly as possible, as minimising the time between the addition of the Capture ProbeSet and the placement of the reaction at 65°C will increase the sensitivity of the assay.
8. Hybridisation assays were incubated for 16 hours, and left at 65°C until ready for further processing in nCounter Prep Station.

Bibliography

A.Vesey, D., Qi, W., Chen, X., Pollock, C.A. and Johnson, D.W. (2009) 'Isolation and Primary Culture of Human Proximal Tubule Cells', in Hewitson, T.D. and Becker, G.J. (eds.) *Kidney Research Experimental Protocols*. Totowa, New Jersey: Humana Press, pp. 19-24.

Abe, K., Li, K., Sacks, S.H. and Sheerin, N.S. (2004) 'The membrane attack complex, C5b-9, up regulates collagen gene expression in renal tubular epithelial cells', *Clin Exp Immunol*, 136(1), pp. 60-6.

Agarwal, V., Bell, G.W., Nam, J.-W. and Bartel, D.P. (2015) 'Predicting effective microRNA target sites in mammalian mRNAs', *eLife*, 4, p. e05005.

Agostini, M. and Knight, R.A. (2014) 'miR-34: from bench to bedside', *Oncotarget*, 5(4), pp. 872-881.

Aguado-Fraile, E., Ramos, E., Sanz-Morales, D., COnde, E., Blanco-Sanchez, I., Stamatakis, K., Peso, L.D., Cuppen, E., Brune, B., Laura, M. and Bermejo, G. (2012) 'miR-127 Protects Proximal Tubule Cells against Ischemia/ Reperfusion: Identification of Kinesin Family Member 3B as miR-127 Target', *PLoS One*, 7(9), pp. 1-14.

Amrouche, L., Rabant, M. and Anglicheau, D. (2014) 'MicroRNA as Biomarkers of Graft Outcome', *Transplant Rev*, 28, pp. 111-118.

Androsavich, J.R., Chau, B.N., Bhat, B., Linsley, P.S. and Walter, N.G. (2012) 'Disease-linked microRNA-21 exhibits drastically reduced mRNA binding and silencing activity in healthy mouse liver', *RNA*, 18(8), pp. 1510-26.

Anglicheau, D., Shama, V.K., Ding, R., Hummel, A., Snopkowski, C., Dadhania, D., Seshan, S.V. and Suthanthiran, M. (2009) 'MicroRNA Expression Profiles Predictive of Human Renal Allograft Status', *PNAS*, 106(13), pp. 5330-5335.

Arany, Z., Huang, L.E., Eckner, R., Bhattacharya, S., Jiang, C., Goldberg, M.A., Bunn, H.F. and Livingston, D.M. (1996) 'An essential role for p300/CBP in the cellular response to hypoxia', *Proc Natl Acad Sci U S A*, 93(23), pp. 12969-12973.

Ardekani, A.M. and Naeini, M.M. (2010) 'The Role of MicroRNAs in Human Diseases', *Avicenna Journal of Medical Biotechnology*, 2(4), pp. 161-179.

Bader, A.G. (2012) 'miR-34 – a microRNA replacement therapy is headed to the clinic', *Front Genet*, 3, p. 120.

Baer, P.C., Bereiter-Hahn, J.r., Schubert, R. and Geigera, H. (2006) 'Differentiation Status of Human Renal Proximal and Distal Tubular Epithelial Cells in vitro: Differential Expression of Characteristic Markers', *Cells Tissues Organs`*, 184, pp. 16-22.

Baer, P.C., Nockher, W.A., Haase, W. and Scherberich, J.E. (1997) 'Isolation of proximal and distal tubule cells from human kidney by immunomagnetic separation: Technical Note', *Kidney Int*, 52(5), pp. 1321-1331.

Bai, X.-Y., Ma, Y., Ding, R., Fu, B., Shi, S. and Chen, X.-M. (2011) 'miR-335 and miR-34a Promote Renal Senescence by Suppressing Mitochondrial Antioxidative Enzymes', *J Am Soc Nephrol*, 22(7), pp. 1252-1261.

Basile, D.P., Anderson, M.D. and Sutton, T.A. (2012) 'Pathophysiology of Acute Kidney Injury', *Comprehensive Physiology*, 2(2), pp. 1303-1353.

Basile, D.P., Donohoe, D., Roethe, K. and Osborn, J.L. (2001) 'Renal ischemic injury results in permanent damage to peritubular capillaries and influences long-term function', *Am J Physiol Renal Physiol*, 281(5), p. F887.

Basile, D.P., Friedrich, J.L., Spahic, J., Knipe, N., Mang, H., Leonard, E.C., Changizi-Ashtiyani, S., Bacallao, R.L., Molitoris, B.A. and Sutton, T.A. (2011) 'Impaired endothelial proliferation and mesenchymal transition contribute to vascular rarefaction following acute kidney injury', *Am J Physiol Renal Physiol*, 300(3), pp. F721-33.

Basile, D.P. and Yoder, M.C. (2014) 'Renal endothelial dysfunction in acute kidney ischemia reperfusion injury', *Cardiovascular & hematological disorders drug targets*, 14(1), pp. 3-14.

Basu, R.K., Hubchak, S., Hayashida, T., Runyan, C.E., Schumacker, P.T. and Schnaper, H.W. (2011) 'Interdependence of HIF-1alpha and TGF-beta/Smad3 signaling in normoxic and hypoxic renal epithelial cell collagen expression', *Am J Physiol Renal Physiol*, 300(4), pp. F898-905.

Bellinger, M.A., Bean, J.S., Rader, M.A., Heinz-Taheny, K.M., Nunes, J.S., Haas, J.V., Michael, L.F. and Rekhter, M.D. (2014) 'Concordant Changes of Plasma and Kidney MicroRNA in the Early Stages of Acute Kidney Injury: Time Course in a Mouse Model of Bilateral Renal Ischemia-Reperfusion', *PLoS One*, 9(4).

Ben-Dov, I.Z., Muthukumar, T., Morozov, P., Mueller, F.B., Tuschi, T. and Suthanthiran, M. (2012) 'MicroRNA Sequence Profiles of Human Kidney Allografts With or Without Tubulointerstitial Fibrosis', *Transplantation*, 94(11).

Bernardo, B.C., Charchar, F.J., Lin, R.C. and McMullen, J.R. (2012) 'A microRNA guide for clinicians and basic scientists: background and experimental techniques', *Heart Lung Circ*, 21(3), pp. 131-42.

Betel, D., Wilson, M., Gabow, A., Marks, D.S. and Sander, C. (2008) 'The microRNA.org resource: targets and expression', *Nucleic Acids Res*, 36(suppl_1), pp. D149-D153.

Bhatt, K., Mi, Q.-S. and Dong, Z. (2011) 'MicroRNA in Kidneys: Biogenesis, Regulation and Pathophysiological Roles', *Am J Physiol Renal Physiol*, 300, pp. F602-F610.

Bijkerk, R., Solingen, C.v., Boer, H.C.d., Pol, P.v.d., Khairoun, M., Bruin, R.G.d. and Oeveren-Rietdijk, A.M.v. (2014) 'Hematopoietic MicroRNA-126 Protects against Renal Ischemia/Reperfusion Injury by Promoting Vascular Integrity', *J. Am. Soc. Nephrol*, 25, pp. 1710-1722.

Biosystems, A. (2007) 'Endogenous Controls for Real-Time Quantitation of miRNA Using TaqMan® MicroRNA Assays' Biosystems, A. Applied Biosystems.

Biosystems, A. (2014) *Real-time PCR Handbook*. Life Technologies(Accessed: 11 November 2014).

Bonventre, J.V. (2010) 'Pathophysiology of AKI: injury and normal and abnormal repair', *Contrib Nephrol*, 165, pp. 9-17.

Bonventre, J.V. and Yang, L. (2011) 'Cellular Pathophysiology of Ischaemic Acute Kidney Injury', *J. Clin Invest*, 121(11), pp. 4210-4221.

Bosch, J.P. (1995) 'Renal reserve: a functional view of glomerular filtration rate', *Semin Nephrol*, 15(5), pp. 381-5.

Bozzola, J.J. (2007) 'Conventional Specimen Preparation Techniques for Scanning Electron Microscopy of Biological Specimens', in Kuo, J. (ed.) *Electron Microscopy Methods and Protocols*. 2nd edn. Totowa, New Jersey: Humana Press, pp. 449-466.

Brar, J.E. and Quigg, R.J. (2014) 'Complement activation in the tubulointerstitium: AKI, CKD, and in between', *Kidney Int*, 86(4), pp. 663-6.

Bronzatto, E.J.M., da Silva Quadros, K.R., Santos, R.L.S., Alves-Filho, G. and Mazzali, M. (2009) 'Delayed Graft Function in Renal Transplant Recipients: Risk Factors and Impact on 1-Year Graft Function: A Single Center Analysis', *Transplant Proc*, 41(3), pp. 849-851.

Brown, C.D.A., Sayer, R., Windass, A.S., Haslam, I.S., Broe, M.E.D., D'Haese, P.C. and Verhulst, A. (2008) 'Characterisation of human tubular cell monolayers as a model of proximal tubular xenobiotic handling', *Toxicology and Applied Pharmacology*, 233, pp. 428-438.

Brown, K.M., Kondeatis, E., Vaughan, R.W., Kon, S.P., Farmer, C.K., Taylor, J.D., He, X., Johnston, A., Horsfield, C., Janssen, B.J., Gros, P., Zhou, W., Sacks, S.H. and Sheerin, N.S. (2006) 'Influence of donor C3 allotype on late renal-transplantation outcome', *N Engl J Med*, 354(19), pp. 2014-23.

Burne, M.J., Daniels, F., El Ghandour, A., Mauiyyedi, S., Colvin, R.B., O'Donnell, M.P. and Rabb, H. (2001) 'Identification of the CD4(+) T cell as a major pathogenic factor in ischemic acute renal failure', *J Clin Invest*, 108(9), pp. 1283-90.

Burne-Taney, M.J., Ascon, D.B., Daniels, F., Racusen, L., Baldwin, W. and Rabb, H. (2003) 'B cell deficiency confers protection from renal ischemia reperfusion injury', *J Immunol*, 171(6), pp. 3210-5.

Burslem, G.M., Kyle, H.F., Nelson, A., Edwards, T.A. and Wilson, A.J. (2017) 'Hypoxia inducible factor (HIF) as a model for studying inhibition of protein-protein interactions', *Chemical Science*, 8(6), pp. 4188-4202.

Canaud, G. and Bonventre, J.V. (2015) 'Cell cycle arrest and the evolution of chronic kidney disease from acute kidney injury', *Nephrol Dial Transplant*, 30(4), pp. 575-83.

Carthew, R.W. and Sontheimer, E.J. (2009) 'Origins and Mechanisms of miRNAs and siRNAs', *Cell*, 136(4), pp. 642-655.

Chaturvedi, S., Yuen, D.A., Bajwa, A., Huang, Y.W., Sokollik, C., Huang, L., Lam, G.Y., Tole, S., Liu, G.Y., Pan, J., Chan, L., Sokolskyy, Y., Puthia, M., Godaly, G., John, R., Wang, C., Lee, W.L., Brumell, J.H., Okusa, M.D. and Robinson, L.A. (2013) 'Slit2 prevents neutrophil recruitment and renal ischemia-reperfusion injury', *J Am Soc Nephrol*, 24(8), pp. 1274-87.

Chau, B.N., Xin, C., Hartner, J., Ren, S., Castano, A.P., Linn, G., Li, J., Tran, P.T., Kaimal, V., Huang, X., Chang, A.N., Li, S., Kaira, A., Grafals, M., Portilla, D., MacKenna, D.A., Orkin, S.H. and Duffield, J.S. (2012) 'MicroRNA 21 Promotes Fibrosis of The Kidney By Silencing Metabolic Pathways', *Sci Transl Med*, 4(121), pp. 1-20.

Chen, C., Lu, C., Qian, Y., Li, H., Tan, Y., Cai, L. and Weng, H. (2017) 'Urinary miR-21 as a potential biomarker of hypertensive kidney injury and fibrosis', *Sci Rep*, 7(1), p. 17737.

Chen, F. and Hu, S.J. (2012) 'Effect of microRNA-34a in cell cycle, differentiation, and apoptosis: a review', *J Biochem Mol Toxicol*, 26(2), pp. 79-86.

Chevalier, R.L. (2016) 'The proximal tubule is the primary target of injury and progression of kidney disease: role of the glomerulotubular junction', *Am J Physiol Renal Physiol*, 311(1), pp. F145-F161.

Chung, A.C., Yu, X. and Lan, H.Y. (2013) 'MicroRNA and Nephropathy: Emerging Concepts', *International Journal of Nephrology and Renovascular DIsease*, 6(169-179).

Conde, E., Alegre, L., Blanco-Sanchez, I., Saenz-Morales, D., Aguado-Fraile, E., Ponte, B., Ramos, E., Saiz, A., Jimenez, C., Ordonez, A., Lopez-Cabrera, M., del Peso, L., de Landazuri, M.O., Liano, F., Selgas, R., Sanchez-Tomero, J.A. and Garcia-Bermejo, M.L. (2012) 'Hypoxia inducible factor 1-alpha (HIF-1 alpha) is induced during reperfusion after renal ischemia and is critical for proximal tubule cell survival', *PLoS One*, 7(3), p. e33258.

Cosio, F.G., Alamir, A., Yim, S., Pesavento, T.E., Falkenhain, M.E., Henry, M.L., Elkhammas, E.A., Davies, E.A., Bumgardner, G.L. and Ferguson, R.M. (1998) 'Patient

survival after renal transplantation: I. The impact of dialysis pre-transplant', *Kidney Int*, 53(3), pp. 767-72.

Dai, Y., Huang, Y.S., Tang, M., Lv, T.Y., Hu, C.X., Tan, Y.H., Xu, Z.M. and Yin, Y.B. (2007) 'Microarray analysis of microRNA expression in peripheral blood cells of systemic lupus erythematosus patients', *Lupus*, 16(12), pp. 939-46.

Dang, K. and Myers, K.A. (2015) 'The role of hypoxia-induced miR-210 in cancer progression', *Int J Mol Sci*, 16(3), pp. 6353-72.

Danobeitia, J.S., Djamali, A. and Fernandez, L.A. (2014) 'The role of complement in the pathogenesis of renal ischemia-reperfusion injury and fibrosis', *Fibrogenesis & Tissue Repair*, 7, pp. 16-16.

Davis, B.N. and Hata, A. (2009) 'Regulation of MicroRNA Biogenesis: A miRiad of mechanisms', *Cell Communication and Signaling*, 7(1), p. 18.

Davis, B.N., Hilyard, A.C., Lagna, G. and Hata, A. (2008) 'SMAD proteins control DROSHA-mediated microRNA maturation', *Nature*, 454(7200), pp. 56-61.

Deng, A., Arndt, M.A., Satriano, J., Singh, P., Rieg, T., Thomson, S., Tang, T. and Blantz, R.C. (2010) 'Renal protection in chronic kidney disease: hypoxia-inducible factor activation vs. angiotensin II blockade', *Am J Physiol Renal Physiol*, 299(6), pp. F1365-73.

Dennler, S., Itoh, S., Vivien, D., ten Dijke, P., Huet, S. and Gauthier, J.-M. (1998) 'Direct binding of Smad3 and Smad4 to critical TGFβ-inducible elements in the promoter of human plasminogen activator inhibitor-type 1 gene', *The EMBO Journal*, 17(11), pp. 3091-3100.

Devarajan, P. (2006) 'Update on Mechanisms of Ischemic Acute Kidney Injury', *J Am Soc Nephrol*, 17, pp. 1503-1520.

Dominguez, J., Gonzalez, A., Crossley, N. and Norambuena, R. (2004) 'Renal transplants with delayed graft function show decreased renal function despite monitoring with postabsorptive levels', *Transplant Proc*, 36(6), pp. 1655-8.

Dragun, D., Hoff, U., Park, J.K., Qun, Y., Schneider, W., Luft, F.C. and Haller, H. (2001) 'Prolonged cold preservation augments vascular injury independent of renal transplant immunogenicity and function', *Kidney Int*, 60(3), pp. 1173-81.

Du, J., Cao, X., Zou, L., Chen, Y., Guo, J., Chen, Z., Hu, S. and Zheng, Z. (2013) 'MicroRNA-21 and Risk of Severe Acute Kidney Injury and Poor Outcomes After Adult Cardiac Surgery', *PLoS One*, 8(5), pp. 1-8.

Du, R., Sun, W., Zhao, A., Yu, Y., Zhao, L., Wang, H., Huang, C. and Sun, S. (2012) 'Hypoxia-Induced Down-Regulation of microRNA-34a Promotes EMT by Targeting the Notch Signaling Pathway in Tubular Epithelial Cells', *PLoS One*, 7(2), pp. 1-12.

Dweep, H. and al., e. (2015) 'miRWalk 2.0: A Comprehensive Atlas of microRNA-target Interactions', *Nat Methods*, 12(8), p. 697.

Eckardt, K.U., Bernhardt, W.M., Weidemann, A., Warnecke, C., Rosenberger, C., Wiesener, M.S. and Willam, C. (2005) 'Role of hypoxia in the pathogenesis of renal disease', *Kidney Int Suppl*, (99), pp. S46-51.

Elshenawy, O.H., Shoieb, S.M., Mohamed, A. and El-Kadi, A.O.S. (2017) 'Clinical Implications of 20-Hydroxyeicosatetraenoic Acid in the Kidney, Liver, Lung and Brain: An Emerging Therapeutic Target', *Pharmaceutics*, 9(1), p. 9.

Emerling, B.M., Weinberg, F., Liu, J.-L., Mak, T.W. and Chandel, N. (2008) 'PTEN regulates p300-dependent hypoxia-inducible factor 1 transcriptional activity through Forkhead transcription factor 3a (FOXO3a)', *Proc Natl Acad Sci U S A*, 105(7), pp. 2622-2627.

Fine, L.G. and Norman, J.T. (2008) 'Chronic hypoxia as a mechanism of progression of chronic kidney diseases: from hypothesis to novel therapeutics', *Kidney Int*, 74(7), pp. 867-72.

Friederich-Persson, M., Thörn, E., Hansell, P., Nangaku, M., Levin, M. and Palm, F. (2013) 'Kidney Hypoxia, Attributable to Increased Oxygen Consumption, Induces Nephropathy Independently of Hyperglycemia and Oxidative ', *Hypertension*, 62(5), p. 914.

Friedewald, J.J. and Rabb, H. (2004) 'Inflammatory cells in ischemic acute renal failure', *Kidney Int*, 66(2), pp. 486-491.

Friedman, R.C., Farh, K.K.-H., Burge, C.B. and Bartel, D.P. (2009) 'Most mammalian mRNAs are conserved targets of microRNAs', *Genome Research*, 19(1), pp. 92-105.

GBD 2013 Mortality and Causes of Death Collaborators (2015) 'Global, regional, and national incidence, prevalence, and years lived with disability for 301 acute and chronic diseases and injuries in 188 countries, 1990–2013: a systematic analysis for the Global Burden of Disease Study 2013', *Lancet*, 386(9995), pp. 743-800.

Goodwin, J.G., Ge, X., Stephan, K., Jurisch, A., Tullius, S.G. and Iacomini, J. (2010) 'Identification of a microRNA Signature of Renal Ischemia Reperfusion Injury', *PNAS*, 107(32), pp. 14339-14344.

Granger, D.N. and Korthuis, R.J. (1995) 'Physiologic Mechanisms of Postischemic Tissue Injury', *Annu Rev Physiol*, 57(1), pp. 311-332.

Granger, D.N. and Kvietys, P.R. (2015) 'Reperfusion injury and reactive oxygen species: The evolution of a concept', *Redox Biol*, 6, pp. 524-551.

Gregory, P.A., Bert, A.G., Paterson, E.L., Barry, S.C., Tsykin, A., Farshid, G., Vadas, M.A., Khew-Goodall, Y. and Goodall, G.J. (2008) 'The miR-200 family and miR-205 regulate epithelial to mesenchymal transition by targeting ZEB1 and SIP1', *Nat Cell Biol*, 10(5), pp. 593-601.

Ha, M. and Kim, V.N. (2014) 'Regulation of microRNA biogenesis', *Nat Rev Mol Cell Biol*, 15(8), pp. 509-524.

Han, W.K., Bailly, V., Abichandani, R., Thadhani, R. and Bonventre, J.V. (2002) 'Kidney Injury Molecule-1 (KIM-1): A novel biomarker for human renal proximal tubule injury', *Kidney Int*, 62(1), pp. 237-244.

Harris, T.A., Yamakuchi, M., Ferlito, M., Mendell, J.T. and Lowenstein, C.J. (2008) 'MicroRNA-126 regulates endothelial expression of vascular cell adhesion molecule 1', *Proc Natl Acad Sci U S A*, 105(5), pp. 1516-21.

Harvey, S.J., Jarad, G., Cunningham, J., Goldberg, S., Schermer, B., Harfe, B.D., McManus, M.T., Benzing, T. and Miner, J.H. (2008) 'Podocyte-specific deletion of dicer alters cytoskeletal dynamics and causes glomerular disease', *J Am Soc Nephrol*, 19(11), pp. 2150-8.

Haug, C.E., Colvin, R.B., Delmonico, F.L., Auchincloss, H., Jr., Tolkoff-Rubin, N., Preffer, F.I., Rothlein, R., Norris, S., Scharschmidt, L. and Cosimi, A.B. (1993) 'A phase I trial of immunosuppression with anti-ICAM-1 (CD54) mAb in renal allograft recipients', *Transplantation*, 55(4), pp. 766-73.

Healthcare Systems Bureau Division of Transplantation and United Network for Organ Sharing (2012) *2012 Annual Report of the U.S. Organ Procurement and Transplantation Network and the Scientific Registry of Transplant Recipients.* Department of Health and Human Services, Health Resources and Services Administration, Healthcare Systems Bureau, Division of Transplantation, Rockville, MD. United Network for Organ Sharing, Richmond, VA; University Renal Research and Education Association, Ann Arbor, MI.

Hennino, M.-F., Buob, D., Van der Hauwaert, C., Gnemmi, V., Jomaa, Z., Pottier, N., Savary, G., Drumez, E., Noël, C., Cauffiez, C. and Glowacki, F. (2016) 'miR-21-5p renal expression is associated with fibrosis and renal survival in patients with IgA nephropathy', *Sci Rep*, 6, p. 27209.

Henze, A.T. and Acker, T. (2010) 'Feedback regulators of hypoxia-inducible factors and their role in cancer biology', *Cell Cycle*, 9(14), pp. 2749-63.

Herrera, J. and Rodriguez-Iturbe, B. (1998) 'Stimulation of tubular secretion of creatinine in health and in conditions associated with reduced nephron mass. Evidence for a tubular functional reserve', *Nephrol Dial Transplant*, 13(3), pp. 623-9.

Heung, M. and Chawla, L.S. (2014) 'Acute Kidney Injury: Gateway to Chronic Kidney Disease', *Nephron Clin Pract*, 127(1-4), pp. 30-34.

Heyman, S.N., Khamaisi, M., Rosen, S. and Rosenberger, C. (2008) 'Renal parenchymal hypoxia, hypoxia response and the progression of chronic kidney disease', *Am J Nephrol*, 28(6), pp. 998-1006.

Heyman, S.N., Rosenberger, C. and Rosen, S. (2010) 'Experimental ischemia–reperfusion: biases and myths—the proximal vs. distal hypoxic tubular injury debate revisited', *Kidney Int*, 77(1), pp. 9-16.

Higgins, D.F., Kimura, K., Bernhardt, W.M., Shrimanker, N., Akai, Y., Hohenstein, B., Saito, Y., Johnson, R.S., Kretzler, M., Cohen, C.D., Eckardt, K.U., Iwano, M. and Haase, V.H. (2007) 'Hypoxia promotes fibrogenesis in vivo via HIF-1 stimulation of epithelial-to-mesenchymal transition', *J Clin Invest*, 117(12), pp. 3810-20.

Higgins, D.F., Kimura, K., Iwano, M. and Haase, V.H. (2008) 'Hypoxia-inducible factor signaling in the development of tissue fibrosis', *Cell Cycle*, 7(9), pp. 1128-32.

Hou, J. and Zhao, D. (2013) 'MicroRNA Regulation in Renal Pathophysiology', *Int J Mol Sci*, 14, pp. 13078-13092.

Hu, C.J., Wang, L.Y., Chodosh, L.A., Keith, B. and Simon, M.C. (2003) 'Differential Roles of Hypoxia-Inducible Factor 1α (HIF-1α) and HIF-2α in Hypoxic Gene Regulation', *Mol Cell Biol*, 23(24), pp. 9361-74.

Hu, F., Min, J., Cao, X., Liu, L., Ge, Z., Hu, J. and Li, X. (2016) 'MiR-363-3p inhibits the epithelial-to-mesenchymal transition and suppresses metastasis in colorectal cancer by targeting Sox4', *Biochem Biophys Res Commun*, 474(1), pp. 35-42.

Hu, H., Jiang, W., Xi, X., Zou, C. and Ye, Z. (2014) 'MicroRNA-21 attenuates renal ischemia reperfusion injury via targeting caspase signaling in mice.', *Am J Nephrol*, 40(3), pp. 215-223.

Huang, X., Ding, L., Bennewith, K., Tong, R., Ang, K.K., Story, M., Le, Q.T. and Giaccia, A.J. (2009) 'Hypoxia inducible mir-210 regulates normoxic gene expression involved in tumor initiation', *Mol Cell*, 35(6), pp. 856-67.

Huen, S.C. and Cantley, L.G. (2015) 'Macrophage-mediated injury and repair after ischemic kidney injury', *Pediatr Nephrol*, 30(2), pp. 199-209.

Huen, S.C. and Cantley, L.G. (2017) 'Macrophages in Renal Injury and Repair', *Annu Rev Physiol*, 79(1), pp. 449-469.

Jakubowski, W. and Bartosz, G. (2000) '2,7-Dichlorofluorescin Oxidation and Reactive Oxygen Species: What Does It Measure?', *Cell Biology International*, 24(10).

Jang, H.R., Gandolfo, M.T., Ko, G.J., Satpute, S.R., Racusen, L. and Rabb, H. (2010) 'B Cells Limit Repair after Ischemic Acute Kidney Injury', *J Am Soc Nephrol*, 21(4), pp. 654-665.

Jang, H.R., Ko, G.J., Wasowska, B.A. and Rabb, H. (2009) 'The interaction between ischemia-reperfusion and immune responses in the kidney', *J. Mol. Med*, 87, pp. 859-864.

Jang, H.R. and Rabb, H. (2009) 'The innate immune response in ischemic acute kidney injury', *Clinical immunology (Orlando, Fla.)*, 130(1), pp. 41-50.

Jazbutyte, V. and Thum, T. (2010) 'MicroRNA-21: from cancer to cardiovascular disease', *Curr Drug Targets*, 11(8), pp. 926-35.

Jeldres, C., Cardinal, H., Duclos, A., Shariat, S.F., Suardi, N., Capitano, U., Hebert, M.-J. and Karakiewicz, P.I. (2009) 'Prediction of Delayed Graft Function After Renal Transplantation', *Canadian Urological Association*, 3(5), pp. 377-382.

Jia, P., Teng, J., Zhou, J., Fang, Y., Zhang, X., Bosnjak, Z.J., Liang, M. and Ding, X. (2013) 'miR-21 Contributes to Xenon-conferres Amelioration of Renal Ischemia-Reperfusion Injury in Mice', *Anesthesiology*, 119(3), pp. 621-630.

John, B., Enright, A.J., Aravin, A., Tuschl, T., Sander, C. and Marks, D.S. (2004) 'Human MicroRNA targets', *PLoS Biol*, 2(11), p. e363.

Johnnidis, J.B., Harris, M.H., Wheeler, R.T., Stehling-Sun, S., Lam, M.H., Kirak, O., Brummelkamp, T.R., Fleming, M.D. and Camargo, F.D. (2008) 'Regulation of progenitor cell proliferation and granulocyte function by microRNA-223', *Nature*, 451(7182), pp. 1125-9.

Jose, M.D., Le Meur, Y., Atkins, R.C. and Chadban, S.J. (2003) 'Blockade of macrophage colony-stimulating factor reduces macrophage proliferation and accumulation in renal allograft rejection', *Am J Transplant*, 3(3), pp. 294-300.

Jung, G.O., Yoon, M.R., Kim, S.J., Sin, M.J., Kim, E.Y., Moon, J.I., Kim, J.M., Choi, G.S., Kwon, C.H., Cho, J.W. and Lee, S.K. (2010) 'The risk factors of delayed graft function and comparison of clinical outcomes after deceased donor kidney transplantation: single-center study', *Transplant Proc*, 42(3), pp. 705-9.

Jung, M., Mollenkopf, H.J., Grimm, C., Wagner, I., Albrecht, M., Waller, T., Pilarsky, C., Johannsen, M., Stephan, C., Lehrach, H., Nietfeld, W., Rudel, T., Jung, K. and Kristiansen, G. (2009) 'MicroRNA profiling of clear cell renal cell cancer identifies a robust signature to define renal malignancy', *J Cell Mol Med*, 13(9b), pp. 3918-28.

Kalogeris, T., Baines, C.P., Krenz, M. and Korthuis, R.J. (2012) 'Cell Biology of Ischaemia/Reperfusion Injury', *In Rev cell mol Biol*, 298, pp. 229-317.

Kamiyama, M., Garner, M.K., Farragut, K.M. and Kobori, H. (2012) 'The Establishment of a Primary Culture System of Proximal Tubule Segments Using Specific Markers from Normal Mouse Kidneys', *Int J Mol Sci*, 13, pp. 5098-5111.

Kanehisa, M. and Goto, S. (2000) 'KEGG: kyoto encyclopedia of genes and genomes', *Nucleic Acids Res*, 28(1), pp. 27-30.

Kapitsinou, P.P., Jaffe, J., Michael, M., Swan, C.E., Duffy, K.J., Erickson-Miller, C.L. and Haase, V.H. (2012) 'Preischemic targeting of HIF prolyl hydroxylation inhibits fibrosis associated with acute kidney injury', *Am J Physiol Renal Physiol*, 302(9), pp. F1172-9.

Kapitsinou, P.P., Sano, H., Michael, M., Kobayashi, H., Davidoff, O., Bian, A., Yao, B., Zhang, M.Z., Harris, R.C., Duffy, K.J., Erickson-Miller, C.L., Sutton, T.A. and Haase, V.H. (2014) 'Endothelial HIF-2 mediates protection and recovery from ischemic kidney injury', *J Clin Invest*, 124(6), pp. 2396-409.

Kapper, S., Beck, G., Riedel, S., Prem, K., Haak, M., van der Woude, F.J. and Yard, B.A. (2002) 'Modulation of chemokine production and expression of adhesion molecules in renal tubular epithelial and endothelial cells by catecholamines', *Transplantation*, 74(2), pp. 253-60.

Kashani, K., Al-Khafaji, A., Ardiles, T., Artigas, A., Bagshaw, S.M., Bell, M., Bihorac, A., Birkhahn, R., Cely, C.M., Chawla, L.S., Davison, D.L., Feldkamp, T., Forni, L.G., Gong, M.N., Gunnerson, K.J., Haase, M., Hackett, J., Honore, P.M., Hoste, E.A., Joannes-Boyau, O., Joannidis, M., Kim, P., Koyner, J.L., Laskowitz, D.T., Lissauer, M.E., Marx, G., McCullough, P.A., Mullaney, S., Ostermann, M., Rimmele, T., Shapiro, N.I., Shaw, A.D., Shi, J., Sprague, A.M., Vincent, J.L., Vinsonneau, C., Wagner, L., Walker, M.G., Wilkerson, R.G., Zacharowski, K. and Kellum, J.A. (2013) 'Discovery and validation of cell cycle arrest biomarkers in human acute kidney injury', *Crit Care*, 17(1), p. R25.

Kato, M., Park, J.T. and Natarajan, R. (2012) 'MicroRNAs and the glomerulus', *Experimental Cell Research*, 318(9), pp. 993-1000.

Kato, M., Putta, S., Wang, M., Yuan, H., Lanting, L., Nair, I., Gunn, A., Nakagawa, Y., Shimano, H., Todorov, I., Rossi, J.J. and Natarajan, R. (2009) 'TGF-beta activates Akt kinase through a microRNA-dependent amplifying circuit targeting PTEN', *Nat Cell Biol*, 11(7), pp. 881-9.

Kato, M., Zhang, J., Wang, M., Lanting, L., Yuan, H., Rossi, J.J. and Natarajan, R. (2007) 'MicroRNA-192 in diabetic kidney glomeruli and its function in TGF-beta-induced collagen expression via inhibition of E-box repressors', *Proc Natl Acad Sci U S A*, 104(9), pp. 3432-7.

Kehrer, J.P. and Klotz, L.-O. (2015) 'Free radicals and related reactive species as mediators of tissue injury and disease: implications for Health', *Critical Reviews in Toxicology*, 45(9), pp. 765-798.

Kelly, K.J., Williams, W.W., Colvin, R.B., Meehan, S.M., Springer, T.A., Gutierrez-Ramos, J.C. and Bonventre, J.V. (1996) 'Intercellular adhesion molecule-1-deficient mice are protected against ischemic renal injury', *Journal of Clinical Investigation*, 97(4), pp. 1056-1063.

Kelly, K.J., Williams, W.W., Jr., Colvin, R.B. and Bonventre, J.V. (1994) 'Antibody to intercellular adhesion molecule 1 protects the kidney against ischemic injury', *Proc Natl Acad Sci U S A*, 91(2), pp. 812-6.

Khalid, U., Ablorsu, E., Szabo, L., Jenkins, R.H., Bowen, T., Chavez, R. and Fraser, D.J. (2016) 'MicroRNA-21 (miR-21) expression in hypothermic machine perfusate may be predictive of early outcomes in kidney transplantation', *Clin Transplant*, 30(2), pp. 99-104.

Kim, Y.K., Heo, I. and Kim, V.N. (2010) 'Modifications of small RNAs and their associated proteins', *Cell*, 143(5), pp. 703-9.

Kimura, K., Iwano, M., Higgins, D.F., Yamaguchi, Y., Nakatani, K., Harada, K., Kubo, A., Akai, Y., Rankin, E.B., Neilson, E.G., Haase, V.H. and Saito, Y. (2008) 'Stable expression of HIF-1alpha in tubular epithelial cells promotes interstitial fibrosis', *Am J Physiol Renal Physiol*, 295(4), pp. F1023-9.

Kinsey, G.R., Li, L. and Okusa, M.D. (2008) 'Inflammation in Acute Kidney Injury', *Nephron. Experimental nephrology*, 109(4), pp. e102-e107.

Kinsey, G.R. and Okusa, M.D. (2014) 'Expanding role of T cells in acute kidney injury', *Curr Opin Nephrol Hypertens*, 23(1), pp. 9-16.

Kinsey, G.R., Sharma, R., Huang, L., Li, L., Vergis, A.L., Ye, H., Ju, S.T. and Okusa, M.D. (2009) 'Regulatory T cells suppress innate immunity in kidney ischemia-reperfusion injury', *J Am Soc Nephrol*, 20(8), pp. 1744-53.

Kinsey, G.R., Sharma, R. and Okusa, M.D. (2013) 'Regulatory T cells in AKI', *J Am Soc Nephrol*, 24(11), pp. 1720-6.

Kobayashi, H., Gilbert, V., Liu, Q., Kapitsinou, P.P., Unger, T.L., Rha, J., Rivella, S., Schlondorff, D. and Haase, V.H. (2012) 'Myeloid cell-derived hypoxia-inducible factor attenuates inflammation in unilateral ureteral obstruction-induced kidney injury', *J Immunol*, 188(10), pp. 5106-15.

Kolaczkowska, E. and Kubes, P. (2013) 'Neutrophil recruitment and function in health and inflammation', *Nat Rev Immunol*, 13(3), pp. 159-75.

Kondo, K., Klco, J., Nakamura, E., Lechpammer, M. and Kaelin, W.G., Jr. (2002) 'Inhibition of HIF is necessary for tumor suppression by the von Hippel-Lindau protein', *Cancer Cell*, 1(3), pp. 237-46.

Koo, D.D.H., Welsh, K.I., Roake, J.A., Morris, P.J. and Fuggle, S.V. (1998) 'Ischemia/Reperfusion Injury in Human Kidney Transplantation', *Am J Pathol*, 153(2), pp. 557-566.

Koshiol, J., Wang, E., Zhao, Y., Marincola, F. and Landi, M.T. (2010) 'Strengths and limitations of laboratory procedures for microRNA detection', *Cancer Epidemiol Biomarkers Prev*, 19(4), pp. 907-11.

Kosieradzki, M. and Rowinski, W. (2008) 'Ischemia/Reperfusion Injury in Kidney Transplantation: Mechanism and Prevention', *Transplant Proc*, 40, pp. 3279-3288.

Krupa, A., Jenkins, R., Luo, D.D., Lewis, A., Phillips, A. and Fraser, D. (2010) 'Loss of MicroRNA-192 promotes fibrogenesis in diabetic nephropathy', *J Am Soc Nephrol*, 21(3), pp. 438-47.

Kumar, P., Shen, Q., Pivetti, C.D., Lee, E.S., Wu, M.H. and Yuan, S.Y. (2009) 'Molecular mechanisms of endothelial hyperpermeability: implications in inflammation', *Expert Rev Mol Med*, 11, pp. e19-e19.

Kumarswamy, R., Volkmann, I. and Thum, T. (2011) 'Regulation and function of miRNA-21 in health and disease', *RNA Biol*, 8(5), pp. 706-13.

Kushida, N., Nomura, S., Mimura, I., Fujita, T., Yamamoto, S., Nangaku, M. and Aburatani, H. (2016) 'Hypoxia-Inducible Factor-1alpha Activates the Transforming Growth Factor-beta/SMAD3 Pathway in Kidney Tubular Epithelial Cells', *Am J Nephrol*, 44(4), pp. 276-285.

Kvietys, P.R. and Granger, D.N. (2012) 'Role of reactive oxygen and nitrogen species in the vascular responses to inflammation', *Free Radical Biology and Medicine*, 52(3), pp. 556-592.

Lai, J.Y., Luo, J., O'Connor, C., Jing, X., Nair, V., Ju, W., Randolph, A., Ben-Dov, I.Z., Matar, R.N., Briskin, D., Zavadil, J., Nelson, R.G., Tuschl, T., Brosius, F.C., Kretzler, M. and Bitzer, M. (2015) 'MicroRNA-21 in Glomerular Injury', *J Am Soc Nephrol*, 26(4), pp. 805-816.

Lan, R., Geng, H., Polichnowski, A.J., Singha, P.K., Saikumar, P., McEwen, D.G., Griffin, K.A., Koesters, R., Weinberg, J.M., Bidani, A.K., Kriz, W. and Venkatachalam, M.A. (2012a) 'PTEN loss defines a TGF-beta-induced tubule phenotype of failed differentiation and JNK signaling during renal fibrosis', *Am J Physiol Renal Physiol*, 302(9), pp. F1210-23.

Lan, Y.-F., Chen, H.-H., Lai, P.-F., Cheng, C.-F., Huang, Y.-T., Lee, Y.-C., Chen, T.-W. and Lin, H. (2012b) 'MicroRNA-494 Reduces ATF3 Expression and Promotes AKI', *Journal American Society of Nephrology*, 23, pp. 2012-2023.

Lebranchu, Y., Halimi, J.M., Bock, A., Chapman, J., Dussol, B., Fritsche, L., Kliem, V., Oppenheimer, F., Pohanka, E., Salvadori, M., Soergel, M. and Tufveson, G. (2005) 'Delayed graft function: risk factors, consequences and parameters affecting outcome-results from MOST, A Multinational Observational Study', *Transplant Proc*, 37(1), pp. 345-7.

Lee, R.C., Feinbaum, R.L. and Ambros, V. (1993) 'The C. elegans heterochronic gene lin-4 encodes small RNAs with antisense complementarity to lin-14', *Cell*, 75(5), pp. 843-854.

Lee, S.O., Masyuk, T., Splinter, P., Banales, J.M., Masyuk, A., Stroope, A. and Larusso, N. (2008) 'MicroRNA15a modulates expression of the cell-cycle regulator Cdc25A and affects hepatic cystogenesis in a rat model of polycystic kidney disease', *J Clin Invest*, 118(11), pp. 3714-24.

Leemans, J.C., Stokman, G., Claessen, N., Rouschop, K.M., Teske, G.J.D., Kirschning, C.J., Akira, S., van der Poll, T., Weening, J.J. and Florquin, S. (2005) 'Renal-associated TLR2 mediates ischemia/reperfusion injury in the kidney', *The Journal of Clinical Investigation*, 115(10), pp. 2894-2903.

Legouis, D., Bataille, A., Hertig, A., Vandermeersch, S., Simon, N., Rondeau, E. and Galichon, P. (2015) 'Ex vivo analysis of renal proximal tubular cells', *BMC Cell Biology*, 16(1), p. 12.

Li, L., Xu, J., Yang, D., Tan, X. and Wang, H. (2010) 'Computational approaches for microRNA studies: a review', *Mamm Genome*, 21(1-2), pp. 1-12.

Li, Y. and Kowdley, K.V. (2012) 'MicroRNAs in common human diseases', *Genomics Proteomics Bioinformatics*, 10(5), pp. 246-53.

Li, Y.-F., Jing, Y., Hao, J., Frankfort, N.C., Zhou, X., Shen, B., Liu, X., Wang, L. and Li, R. (2013) 'MicroRNA-21 in the pathogenesis of acute kidney injury', *Protein Cell*, 4(11), pp. 813-819.

Lin, L., Gan, H., Zhang, H., Tang, W., Sun, Y., Tang, X., Kong, D., Zhou, J., Wang, Y. and Zhu, Y. (2014) 'MicroRNA21 inhibits SMAD7 expression through a target sequence in the 3' untranslated region and inhibits proliferation of renal tubular epithelial cells', *Mol Med Rep*, 10(2), pp. 707-12.

Linfert, D., Chowdhry, T. and Rabb, H. (2009) 'Lymphocytes and ischemia-reperfusion injury', *Transplant Rev*, 23(1), pp. 1-10.

Liu, F., Lou, Y.-L., Ruan, Q.-F., Xie, A., Guo, F., Cui, S.-P., Deng, Z.-F. and Wang, Y. (2012) 'Upregulation of MicroRNA-210 Regulates Renal Angiogenesis Mediated by Activation of VEGF Signaling Pathway under Ischemia/Perfusion Injury in vivo and in vitro', *Kidney Blood Pressure Research*, 35, pp. 182-191.

Liu, J., Wei, Q., Guo, C., Dong, G., Liu, Y., Tang, C. and Dong, Z. (2017) 'Hypoxia, HIF, and Associated Signaling Networks in Chronic Kidney Disease', *Int J Mol Sci*, 18(5), pp. 1-17.

Liu, L.Z., Li, C., Chen, Q., Jing, Y., Carpenter, R., Jiang, Y., Kung, H.F., Lai, L. and Jiang, B.H. (2011) 'MiR-21 induced angiogenesis through AKT and ERK activation and HIF-1alpha expression', *PLoS One*, 6(4), p. e19139.

Liu, X.J., Hong, Q., Wang, Z., Yu, Y.Y., Zou, X. and Xu, L.H. (2015) 'MicroRNA-34a Suppresses Autophagy in Tubular Epithelial Cells in Acute Kidney Injury', *Am J Nephrol*, 42(2), pp. 168-75.

Liu, Y., Nie, H., Zhang, K., Ma, D., Yang, G., Zheng, Z., Liu, K., Yu, B., Zhai, C. and Yang, S. (2014) 'A feedback regulatory loop between HIF-1α and miR-21 in response to hypoxia in cardiomyocytes', *FEBS Letters*, 588(17), pp. 3137-3146.

Loboda, A., Jozkowicz, A. and Dulak, J. (2012) 'HIF-1 versus HIF-2--is one more important than the other?', *Vascul Pharmacol*, 56(5-6), pp. 245-51.

Lorenzen, J.M., Kaucsar, T., Schauerte, C., SChmitt, R., Rong, S., Hubner, A., Scherf, K., Fiedler, J., Martino, F., Kumarswamy, R., Kolling, M., Sorensen, I., Hinz, H., Heineke, J., Rooij, E.v., Haller, H. and Thum, T. (2014) 'MicroRNA-24 Antagonism Prevents Renal Ischemia Reperfusion Injury', *J Am Soc Nephrol*, 25, pp. 2717-2729.

Lorenzen, J.M., Kielstein, J.T., Hafer, C., Gupta, S.K., Kumpers, P., Fauhaber-Walter, R., Haller, H., Fliser, D. and Thum, T. (2011a) 'Circulating miR-210 Predicts Survival in Critically Ill Patients with Acute Kidney Injury', *Clin J Am Soc Nephrol*, 6, pp. 1540-1546.

Lorenzen, J.M., Volkmann, I., Fiedler, J., Schmidt, M., Scheffner, I., Haller, H., Gwinner, W. and Thum, T. (2011b) 'Urinary miR-210 as a Mediator of Acute T-Cell Mediated Rejection in Renal Allograft Recpients', *Am J Transplant*, 11, pp. 2221-2227.

Maarouf, O.H., Aravamudhan, A., Rangarajan, D., Kusaba, T., Zhang, V., Welborn, J., Gauvin, D., Hou, X., Kramann, R. and Humphreys, B.D. (2016) 'Paracrine Wnt1 Drives Interstitial Fibrosis without Inflammation by Tubulointerstitial Cross-Talk', *J Am Soc Nephrol*, 27(3), pp. 781-90.

Maluf, D.G., Dumur, C.I., SUh, J.L., Scian, M.J., King, A.L., Cathro, H., Lee, J.K., gehrau, R.C., Brayman, K.L., Gallon, L. and Mas, V.R. (2014) 'The Urine microRNA Profile may Help Monitor Post-Transplant Renal Graft Function', *Kidney Int*, 85, pp. 439-449.

Malyszko, J., Lukaszyk, E., Glowinska, I. and Durlik, M. (2015) 'Biomarkers of delayed graft function as a form of acute kidney injury in kidney transplantation', 5, p. 11684.

Mammen, C., Al Abbas, A., Skippen, P., Nadel, H., Levine, D., Collet, J.P. and Matsell, D.G. (2012) 'Long-term risk of CKD in children surviving episodes of acute kidney injury in the intensive care unit: a prospective cohort study', *Am J Kidney Dis*, 59(4), pp. 523-30.

Marsters, P., Alhamdan, R. and Campbell, B.K. (2014) 'Cell density-mediated pericellular hypoxia and the local dynamic regulation of VEGF-a splice variants in ovine ovarian granulosa cells', *Biol Reprod*, 91(2), p. 35.

McClelland, A.D., Herman-Edelstein, M., Komers, R., Jha, J.C., Winbanks, C.E., Hagiwara, S., Gregorevic, P., Kantharidis, P. and Cooper, M.E. (2015) 'miR-21 promotes renal fibrosis in diabetic nephropathy by targeting PTEN and SMAD7', *Clin Sci (Lond)*, 129(12), pp. 1237-49.

McCormick, R.I., Blick, C., Ragoussis, J., Schoedel, J., Mole, D.R., Young, A.C., Selby, P.J., Banks, R.E. and Harris, A.L. (2013) 'miR-210 is a target of hypoxia-inducible factors 1 and 2 in renal cancer, regulates ISCU and correlates with good prognosis', *Br J Cancer*, 108(5), pp. 1133-42.

Melnikov, V.Y., Faubel, S., Siegmund, B., Lucia, M.S., Ljubanovic, D. and Edelstein, C.L. (2002) 'Neutrophil-independent mechanisms of caspase-1– and IL-18–mediated ischemic acute tubular necrosis in mice', *The Journal of Clinical Investigation*, 110(8), pp. 1083-1091.

Miao, J., Lesher, A.M., Miwa, T., Sato, S., Gullipalli, D. and Song, W.C. (2014) 'Tissue-specific deletion of Crry from mouse proximal tubular epithelial cells increases susceptibility to renal ischemia-reperfusion injury', *Kidney Int*, 86(4), pp. 726-37.

Miglinas, M., Supranaviciene, L., Mateikaite, K., Skebas, K. and Kubiliene, A. (2013) 'Delayed graft function: risk factors and the effects of early function and graft survival', *Transplant Proc*, 45(4), pp. 1363-7.

Minamino, T., Komuro, I. and Kitakaze, M. (2010) 'Endoplasmic Reticulum Stress As a Therapeutic Target in Cardiovascular Disease', *Circ Res.*, 107, pp. 1071-1082.

Mole, D.R., Blancher, C., Copley, R.R., Pollard, P.J., Gleadle, J.M., Ragoussis, J. and Ratcliffe, P.J. (2009) 'Genome-wide association of hypoxia-inducible factor (HIF)-1alpha and HIF-2alpha DNA binding with expression profiling of hypoxia-inducible transcripts', *J Biol Chem*, 284(25), pp. 16767-75.

Moll, S., Ebeling, M., Weibel, F., Farina, A., Rosario, A.A.D., Hoflack, J.C., Pomposiello, S. and Prunotto, M. (2013) 'Epithelial Cells as Active Player In Fibrosis: Findings from an In Vitro Model', *PLoS One*, 8(2), p. e56575.

Monteiro, R.M., Camara, N.O., Rodrigues, M.M., Tzelepis, F., Damiao, M.J., Cenedeze, M.A., Teixeira Vde, P., dos Reis, M.A. and Pacheco-Silva, A. (2009) 'A role for regulatory T cells in renal acute kidney injury', *Transpl Immunol*, 21(1), pp. 50-5.

Morizane, R., Fujii, S., Monkawa, T., Hiratsuka, K., Yamaguchi, S., Homma, K. and Itoh, H. (2016) 'miR-363 induces transdifferentiation of human kidney tubular cells to mesenchymal phenotype', *Clin Exp Nephrol*, 20(3), pp. 394-401.

Naesens, M., Li, L., Ying, L., Sansanwal, P., Sigdel, T.K., Hsieh, S.C., Kambham, N., Lerut, E., Salvatierra, O., Butte, A.J. and Sarwal, M.M. (2009) 'Expression of complement components differs between kidney allografts from living and deceased donors', *J Am Soc Nephrol*, 20(8), pp. 1839-51.

Nangaku, M. (2006) 'Chronic hypoxia and tubulointerstitial injury: a final common pathway to end-stage renal failure', *J Am Soc Nephrol*, 17(1), pp. 17-25.

Nangaku, M., Rosenberger, C., Heyman, S.N. and Eckardt, K.U. (2013) 'Regulation of hypoxia-inducible factor in kidney disease', *Clin Exp Pharmacol Physiol*, 40(2), pp. 148-57.

NanoString Technologies Inc (2014) 'nCounter Analysis System, Digital Genomics for Pathway-based Translational Research Brochure' 4 NanoString Technologies, I. NanoString Technologies, Inc.

NanoString Technologies Inc. (2010) *nCounter miRNA Expression Assay Manual*. NanoString Technologies, Inc.

National Kidney Foundation (2002) 'K/DOQI clinical practice guidelines for chronic kidney disease: evaluation, classification, and stratification', *Am J Kidney Dis*, 39(2 Suppl 1), pp. S1-266.

National Kidney Foundation-Kidney Disease Improving Global Outcomes (2012) 'Summary of Recommendation Statements', *Kidney Int Suppl*, 3(1), pp. 5-14.

Neto, J.S., Nakao, A., Kimizuka, K., Romanosky, A.J., Stolz, D.B., Uchiyama, T., Nalesnik, M.A., Otterbein, L.E. and Murase, N. (2004) 'Protection of transplant-induced renal ischemia-reperfusion injury with carbon monoxide', *Am J Physiol Renal Physiol*, 287(5), p. F979.

Ngo, J.P., Kar, S., Kett, M.M., Gardiner, B.S., Pearson, J.T., Smith, D.W., Ludbrook, J., Bertram, J.F. and Evans, R.G. (2014) 'Vascular geometry and oxygen diffusion in the vicinity of artery-vein pairs in the kidney', *Am J Physiol Renal Physiol*, 307(10), p. F1111.

NHSBT (2017) *Organ Donation and Trasnplantation Activity Report 2016/2017*. National health Service, Blood and Transplant.

Nuovo, G.J. (2010) 'In situ detection of microRNAs in paraffin embedded, formalin fixed tissues and the co-localization of their putative targets', *Methods*, 52, pp. 307-315.

O'Connell, R.M., Taganov, K.D., Boldin, M.P., Cheng, G. and Baltimore, D. (2007) 'MicroRNA-155 is induced during the macrophage inflammatory response', *Proc Natl Acad Sci U S A*, 104(5), pp. 1604-9.

Ojo, A.O., Wolfe, R.A., Held, P.J., Port, F.K. and Schmouder, R.L. (1997) 'Delayed graft function: risk factors and implications for renal allograft survival', *Transplantation*, 63(7), pp. 968-74.

Ounissi, M., Cherif, M., Abdallah, T.B., Bacha, M., Hedri, H., Abderrahim, E., Goucha, R., Kheder, A., Slama, R.B., Derouiche, A., Chebil, M., Bardi, R., Sfar, I. and Gorgi, Y. (2013) 'Risk factors and consequences of delayed graft function', *Saudi J Kidney Dis Transpl*, 24(2), pp. 243-6.

Paller, M.S., Hoidal, J.R. and Ferris, T.F. (1984) 'Oxygen free radicals in ischemic acute renal failure in the rat', *J Clin Invest*, 74(4), pp. 1156-64.

Pastorelli, L.M., Wells, S., Fray, M., Smith, A., Hough, T., Harfe, B.D., McManus, M.T., Smith, L., Woolf, A.S., Cheeseman, M. and Greenfield, A. (2009) 'Genetic analyses reveal a requirement for Dicer1 in the mouse urogenital tract', *Mamm Genome*, 20(3), pp. 140-51.

Paul, R., Ewing, C.M., Robinson, J.C., Marshall, F.F., Johnson, K.R., Wheelock, M.J. and Isaacs, W.B. (1997) 'Cadherin-6, a Cell Adhesion Molecule Specifically Expressed in the Proximal Renal Tubule and Renal Cell Carcinoma', *Cancer Research*, 57, pp. 2741-2748.

Peng, Q., Li, K., Smyth, L.A., Xing, G., Wang, N., Meader, L., Lu, B., Sacks, S.H. and Zhou, W. (2012) 'C3a and C5a promote renal ischemia-reperfusion injury', *J Am Soc Nephrol*, 23(9), pp. 1474-85.

Perico, N., Cattaneo, D., Sayegh, M.H. and Remuzzi, G. (2004) 'Delayed Graft Function in Kidney Transplantation', *Lancet*, 364, pp. 1814-1827.

Pesavento, T.E. (2009) 'Kidney transplantation in the context of renal replacement therapy', *Clin J Am Soc Nephrol*, 4(12), pp. 2035-9.

Poliseno, L., Salmena, L., Zhang, J., Carver, B., Haveman, W.J. and Pandolfi, P.P. (2010) 'A coding-independent function of gene and pseudogene mRNAs regulates tumour biology', *Nature*, 465(7301), pp. 1033-1038.

Pulskens, W.P., Teske, G.J., Butter, L.M., Roelofs, J.J., van der Poll, T., Florquin, S. and Leemans, J.C. (2008) 'Toll-like receptor-4 coordinates the innate immune response of the kidney to renal ischemia/reperfusion injury', *PLoS One*, 3(10), p. e3596.

Qi, W., Johnson, D.W., Vesey, D.A., Pollock, C.A. and Chen, X. (2007) 'Isolation, propagation and characterization of primary tubule cell culture from human kidney', *Nephrology*, 12, pp. 155-159.

Qin, Q., Furong, W. and Baosheng, L. (2014) 'Multiple functions of hypoxia-regulated miR-210 in cancer', *Journal of Experimental & Clinical Cancer Research*, 33(1), p. 50.

Rabb, H., Daniels, F., O'Donnell, M., Haq, M., Saba, S.R., Keane, W. and Tang, W.W. (2000) 'Pathophysiological role of T lymphocytes in renal ischemia-reperfusion injury in mice', *Am J Physiol Renal Physiol*, 279(3), pp. F525-31.

Rabinowitz, M.H. (2013) 'Inhibition of hypoxia-inducible factor prolyl hydroxylase domain oxygen sensors: tricking the body into mounting orchestrated survival and repair responses', *J Med Chem*, 56(23), pp. 9369-402.

Racusen, L.C., Monteil, C., Sgrignoli, A., Lucksay, M., Marouillat, S., Rhi, J.G.S. and Morin, J.-P. (1996) 'Cell lines with extended in vitro growth potential from human renal proximal tubule: Characterization, response to inducers, and comparison with established cell lines', *Journal of Laboratory and Clinical Medicine*, 129(3), pp. 318-329.

Raedschelders, K., Ansley, D.M. and Chen, D.D.Y. (2012) 'The cellular and molecular origin of reactive oxygen species generation during myocardial ischemia and reperfusion', *Pharmacology & Therapeutics*, 133(2), pp. 230-255.

Ratcliffe, P.J. (2007) 'HIF-1 and HIF-2: working alone or together in hypoxia?', *J Clin Invest*, 117(4), pp. 862-5.

Ratliff, B.B., Abdulmahdi, W., Pawar, R. and Wolin, M.S. (2016) 'Oxidant Mechanisms in Renal Injury and Disease', *Antioxid Redox Signal*, 25(3), pp. 119-46.

Redfield, R.R., Scalea, J.R., Zens, T.J., Muth, B., Kaufman, D.B., Djamali, A., Astor, B.C. and Mohamed, M. (2016) 'Predictors and outcomes of delayed graft function after living-donor kidney transplantation', *Transpl Int*, 29(1), pp. 81-7.

Renner, B., Strassheim, D., Amura, C.R., Kulik, L., Ljubanovic, D., Glogowska, M.J., Takahashi, K., Carroll, M.C., Holers, V.M. and Thurman, J.M. (2010) 'B Cell Subsets Contribute to Both Renal Injury and Renal Protection after Ischemia/Reperfusion', *Journal of immunology (Baltimore, Md. : 1950)*, 185(7), pp. 4393-4400.

Rifkin, D.E., Coca, S.G. and Kalantar-Zadeh, K. (2012) 'Does AKI truly lead to CKD?', *J Am Soc Nephrol*, 23(6), pp. 979-84.

Rooij, E.v. (2011) 'The Art of MicroRNA Research', *Circulation Research*, 108, pp. 219-234.

Rosa, A., Ballarino, M., Sorrentino, A., Sthandier, O., De Angelis, F.G., Marchioni, M., Masella, B., Guarini, A., Fatica, A., Peschle, C. and Bozzoni, I. (2007) 'The interplay between the master transcription factor PU.1 and miR-424 regulates human monocyte/macrophage differentiation', *Proc Natl Acad Sci U S A*, 104(50), pp. 19849-54.

Rosenberger, C., Mandriota, S., Jürgensen, J.S., Wiesener, M.S., Hörstrup, J.H., Frei, U., Ratcliffe, P.J., Maxwell, P.H., Bachmann, S. and Eckardt, K.-U. (2002) 'Expression of Hypoxia-Inducible Factor-1α and -2α in Hypoxic and Ischemic Rat Kidneys', *J Am Soc Nephrol*, 13(7), pp. 1721-1732.

Rosenberger, C., Pratschke, J., Rudolph, B., Heyman, S.N., Schindler, R., Babel, N., Eckardt, K.U., Frei, U., Rosen, S. and Reinke, P. (2007) 'Immunohistochemical detection of hypoxia-inducible factor-1alpha in human renal allograft biopsies', *J Am Soc Nephrol*, 18(1), pp. 343-51.

Rusk, N. (2008) 'When microRNAs activate translation', *Nat Meth*, 5(2), pp. 122-123.

Ryan, M.J., Johnson, G., Kirk, j., Fuerstenberg, S.M., Zager, R.A. and Torok-Storb, B. (1994) 'HK-2: An Immortalized Proximal Tubule Epithelial Cell Line From Normal Adult Human Kidney', *Kidney Int*, 45, pp. 48-57.

Safran, M., Kim, W.Y., O'Connell, F., Flippin, L., Günzler, V., Horner, J.W., DePinho, R.A. and Kaelin, W.G. (2006) 'Mouse model for noninvasive imaging of HIF prolyl hydroxylase activity: Assessment of an oral agent that stimulates erythropoietin production', *Proc Natl Acad Sci U S A*, 103(1), pp. 105-110.

Saikumar, J., Hoffmann, D., Kim, T.-M., Gonzalez, V.R., Zhang, Q., Goering, P.L., Brown, R.P., Bijol, V., Park, P.J., Waikar, S.S. and Vaidya, V.S. (2012) 'Expression, Circulation and Excretion Profile of MicroRNA-21, -155, and -18a Following Acute Kidney Injury', *Toxocoligal Sciences*, 129(2), pp. 256-267.

Salamzadeh, J., Sahraee, Z., Nafar, M. and Parvin, M. (2012) 'Delayed graft function (DGF) after living donor kidney transplantation: a study of possible explanatory factors', *Ann Transplant*, 17(3), pp. 69-76.

Salmela, K., Wramner, L., Ekberg, H., Hauser, I., Bentdal, O., Lins, L.E., Isoniemi, H., Backman, L., Persson, N., Neumayer, H.H., Jorgensen, P.F., Spieker, C., Hendry, B., Nicholls, A., Kirste, G. and Hasche, G. (1999) 'A randomized multicenter trial of the anti-ICAM-1 monoclonal antibody (enlimomab) for the prevention of acute rejection and delayed onset of graft function in cadaveric renal transplantation: a report of the European Anti-ICAM-1 Renal Transplant Study Group', *Transplantation*, 67(5), pp. 729-36.

Samaan, S., Khella, H.W., Girgis, A., Scorilas, A., Lianidou, E., Gabril, M., Krylov, S.N., Jewett, M., Bjarnason, G.A., El-said, H. and Yousef, G.M. (2015) 'miR-210 is a prognostic marker in clear cell renal cell carcinoma', *J Mol Diagn*, 17(2), pp. 136-44.

Schena, F.P., Serino, G. and Sallustion, F. (2014) 'MicroRNAs in Kidney Disease: New Promising Biomarkers for Diagnosis and Monitoring', *Nephrol Dial Transplant*, 29, pp. 755-763.

Schindelin, J., Rueden, C.T., Hiner, M.C. and Eliceiri, K.W. (2015) 'The ImageJ ecosystem: An open platform for biomedical image analysis', *Molecular Reproduction and Development*, 82(7-8), pp. 518-529.

Schumacher, C.A., Baartscheer, A., Coronel, R. and Fiolet, J.W.T. (1998) 'Energy-dependent Transport of Calcium to the Extracellular Space During Acute Ischemia of the Rat Heart', *J Mol Cell cardiol*, 30, pp. 1631-1642.

Scian, M.J., Maluf, D.G., David, K.G., Archer, K.J., Suth, J.L., Wolen, A.R., Mba, M.U., Massey, H.D., King, A.L., Gehr, T., Cotterell, A., Posner, M. and Mas, V. (2011) 'MicroRNA Profiles in Allograft Tissues and Paired Urines Associate with Chronic Allograft Dysfunction with IF/TA', *Am J Transplant*, 11, pp. 2110-2122.

Scian, M.J., Maluf, D.G. and Mas, V.R. (2013a) 'MiRNAs in Kidney Transplantation', *Expert Rev Mol Diagn*, 13(1), pp. 93-104.

Scian, M.J., Maluf, D.G. and Mas, V.R. (2013b) 'MiRNAs in kidney transplantation: potential role as new biomarkers', *Expert Rev Mol Diagn*, 13(1), pp. 93-104.

Selcuklu, S.D., Donoghue, M.T. and Spillane, C. (2009) 'miR-21 as a key regulator of oncogenic processes', *Biochem Soc Trans*, 37(Pt 4), pp. 918-25.

Senel, F.M., Karakayali, H., Moray, G. and Haberal, M. (1998) 'Delayed graft function: predictive factors and impact on outcome in living-related kidney transplantations', *Ren Fail*, 20(4), pp. 589-95.

Sequeira-Lopez, M.L., Weatherford, E.T., Borges, G.R., Monteagudo, M.C., Pentz, E.S., Harfe, B.D., Carretero, O., Sigmund, C.D. and Gomez, R.A. (2010) 'The microRNA-processing enzyme dicer maintains juxtaglomerular cells', *J Am Soc Nephrol*, 21(3), pp. 460-7.

Sethupathy, P., Borel, C., Gagnebin, M., Grant, G.R., Deutsch, S., Elton, T.S., Hatzigeorgiou, A.G. and Antonarakis, S.E. (2007) 'Human microRNA-155 on chromosome 21 differentially interacts with its polymorphic target in the AGTR1 3' untranslated region: a mechanism for functional single-nucleotide polymorphisms related to phenotypes', *Am J Hum Genet*, 81(2), pp. 405-13.

Sethupathy, P., Corda, B. and Hatzigeorgiou, A.G. (2006) 'TarBase: A comprehensive database of experimentally supported animal microRNA targets', *RNA*, 12(2), pp. 192-197.

Shapiro, M.D., Bagley, J., Latz, J., Godwin, J.G., Ge, X., Tullius, S.G. and Iacomini, J. (2011) 'MicroRNA Expression Data Reveals a Signature of Kidney Damage following Ischemia Reperfusion Injury', *PLoS One*, 6(8).

Sharma, A.K., Tolani, S.L., Rathi, G.L., Sharma, P., Gupta, H. and Gupta, R. (2010) 'Evaluation of factors causing delayed graft function in live related donor renal transplantation', *Saudi J Kidney Dis Transpl*, 21(2), pp. 242-5.

Sharpe, C.C. and Dockrell, M.E.C. (2012) 'Primary Culture of Human Renal Proximal Tubule Epithelial Cells and Interstitial Fibroblasts', in Mitry, R.R. and Hughes, R.D. (eds.) *Human Cell Culture Protocols*. Totowa, NJ: Humana Press, pp. 175-185.

Sheerin, N.S., Risley, P., Abe, K., Tang, Z., Wong, W., Lin, T. and Sacks, S.H. (2008) 'Synthesis of complement protein C3 in the kidney is an important mediator of local tissue injury', *Faseb j*, 22(4), pp. 1065-72.

Shi, S., Yu, L., Chiu, C., Sun, Y., Chen, J., Khitrov, G., Merkenschlager, M., Holzman, L.B., Zhang, W., Mundel, P. and Bottinger, E.P. (2008) 'Podocyte-selective deletion of dicer induces proteinuria and glomerulosclerosis', *J Am Soc Nephrol*, 19(11), pp. 2159-69.

Singh, P.K. and Campbell, M.J. (2013) 'The Interactions of microRNA and Epigenetic Modifications in Prostate Cancer', *Cancers*, 5(3), pp. 998-1019.

Snyder, R.A., Moore, D.R. and Moore, D.E. (2013) 'More donors or more delayed graft function? A cost-effectiveness analysis of DCD kidney transplantation', *Clin Transplant*, 27(2), pp. 289-96.

Spiegel, J.C., Lorenzen, J.M. and Thum, T. (2011) 'Role of microRNAs in Immunity and Organ Transplantation', *Expert Rev Mol Med*, 13, pp. 1-13.

Stanczyk, J., Pedrioli, D.M., Brentano, F., Sanchez-Pernaute, O., Kolling, C., Gay, R.E., Detmar, M., Gay, S. and Kyburz, D. (2008) 'Altered expression of MicroRNA in synovial fibroblasts and synovial tissue in rheumatoid arthritis', *Arthritis Rheum*, 58(4), pp. 1001-9.

Steegh, F.M.E.G., Gelens, M.A.C.J., Nieman, F.H.M., van Hooff, J.P., Cleutjens, J.P.M., van Suylen, R.J., Daemen, M.J.A.P., van Heurn, E.L.W., Christiaans, M.H.L. and Peutz-Kootstra, C.J. (2011) 'Early Loss of Peritubular Capillaries after Kidney Transplantation', *J Am Soc Nephrol*, 22(6), pp. 1024-1029.

Sui, W., Dai, Y., Huang, Y., Lan, H., Yan, Q. and Huang, H. (2008) 'Microarray analysis of MicroRNA expression in acute rejection after renal transplantation', *Transpl Immunol*, 19(1), pp. 81-5.

Sutton, T.A. (2009) 'Alteration of microvascular permeability in acute kidney injury', *Microvasc Res*, 77(1), pp. 4-7.

Sutton, T.A. and Molitoris, B.A. (1998) 'Mechanisms of cellular injury in ischemic acute renal failure', *Semin Nephrol*, 18(5), pp. 490-7.

Suzuki, H.I. and Miyazono, K. (2011) 'Emerging complexity of microRNA generation cascades', *J Biochem*, 149(1), pp. 15-25.

Suzuki, T., Kimura, M., Asano, M., Fujigaki, Y. and Hishida, A. (2001) 'Role of atrophic tubules in development of interstitial fibrosis in microembolism-induced renal failure in rat', *Am J Pathol*, 158(1), pp. 75-85.

Systems, R.D. (2015) *Immunostaining Images: Cadherin-6/KCAD*. Available at: https://www.rndsystems.com/resources/ihc-images/Cadherin-6-KCAD (Accessed: 20 September 2015).

Szeto, C.C. and Li, P.K. (2014) 'MicroRNAs in IgA nephropathy', *Nat Rev Nephrol*, 10(5), pp. 249-56.

Takaori, K., Nakamura, J., Yamamoto, S., Nakata, H., Sato, Y., Takase, M., Nameta, M., Yamamoto, T., Economides, A.N., Kohno, K., Haga, H., Sharma, K. and Yanagita, M. (2016) 'Severity and Frequency of Proximal Tubule Injury Determines Renal Prognosis', *J Am Soc Nephrol*, 27(8), pp. 2393-406.

Takaori, K. and Yanagita, M. (2016) 'Insights into the Mechanisms of the Acute Kidney Injury-to-Chronic Kidney Disease Continuum', *Nephron*, 134(3), pp. 172-176.

Tanaka, S., Tanaka, T. and Nangaku, M. (2014) 'Hypoxia as a key player in the AKI-to-CKD transition', *Am J Physiol Renal Physiol*, 307(11), p. F1187.

Tanaka, T. (2017) 'A mechanistic link between renal ischemia and fibrosis', *Med Mol Morphol*, 50(1), pp. 1-8.

Thornton, M.A., Winn, R., Alpers, C.E. and Zager, R.A. (1989) 'An evaluation of the neutrophil as a mediator of in vivo renal ischemic-reperfusion injury', *Am J Pathol*, 135(3), pp. 509-515.

Thraves, P., Salehi, Z., Dritschilo, A. and Rhim, J.S. (1990) 'Neoplastic transformation of immortalized human epidermal keratinocytes by ionizing radiation', *Proc Natl Acad Sci U S A*, 87, pp. 1174-1177.

Thurman, J.M., Ljubanović, D., Royer, P.A., Kraus, D.M., Molina, H., Barry, N.P., Proctor, G., Levi, M. and Holers, V.M. (2006) 'Altered renal tubular expression of the complement inhibitor Crry permits complement activation after ischemia/reperfusion', *Journal of Clinical Investigation*, 116(2), pp. 357-368.

Tili, E., Michaille, J.J., Costinean, S. and Croce, C.M. (2008) 'MicroRNAs, the immune system and rheumatic disease', *Nat Clin Pract Rheumatol*, 4(10), pp. 534-41.

Triantafyllou, A., Liakos, P., Tsakalof, A., Georgatsou, E., Simos, G. and Bonanou, S. (2006) 'Cobalt induces hypoxia-inducible factor-1alpha (HIF-1alpha) in HeLa cells by an iron-independent, but ROS-, PI-3K- and MAPK-dependent mechanism', *Free Radic Res*, 40(8), pp. 847-56.

Trionfini, P. and Benigni, A. (2017) 'MicroRNAs as Master Regulators of Glomerular Function in Health and Disease', *J Am Soc Nephrol*, 28(6), pp. 1686-1696.

van den Akker, E., Dor, F., IJzermans, J. and de Bruin, R. (2015) 'MicroRNAs in Kidney Transplantation: Living up to Their Expectations?', *Journal of Transplantation*, 2015.

Van der Hauwaert, C., Savary, G., Gnemmi, V., Glowacki, F., Pottier, N., Bouillez, A., Maboudou, P., Zini, L., Leroy, X., Cauffiez, C., Perrais, M. and Aubert, S. (2013) 'Isolation and characterization of a primary proximal tubular epithelial cell model from human kidney by CD10/CD13 double labeling', *PLoS One*, 8(6), p. e66750.

Vasudevan, S., Tong, Y. and Steitz, J.A. (2007) 'Switching from repression to activation: microRNAs can up-regulate translation', *Science*, 318(5858), pp. 1931-4.

Venkatachalam, M.A., Weinberg, J.M., Kriz, W. and Bidani, A.K. (2015) 'Failed Tubule Recovery, AKI-CKD Transition, and Kidney Disease Progression', *J Am Soc Nephrol*, 26(8), pp. 1765-1776.

Ventura, A., Young, A.G., Winslow, M.M., Lintault, L., Meissner, A., Erkeland, S.J., Newman, J., Bronson, R.T., Crowley, D., Stone, J.R., Jaenisch, R., Sharp, P.A. and Jacks, T. (2008) 'Targeted deletion reveals essential and overlapping functions of the miR-17 through 92 family of miRNA clusters', *Cell*, 132(5), pp. 875-86.

Verma, S.K. and Molitoris, B.A. (2015) 'Renal Endothelial Injury and Microvascular Dysfunction in Acute Kidney Injury', *Semin Nephrol*, 35(1), pp. 96-107.

Vester, B. and Wengel, J. (2004) 'LNA (Locked Nucleic Acid): High-Affinity Targeting of Complementary RNA and DNA', *Biochemistry*, 43(42), pp. 13233-13241.

Vlachos, I.S., Zagganas, K., Paraskevopoulou, M.D., Georgakilas, G., Karagkouni, D., Vergoulis, T., Dalamagas, T. and Hatzigeorgiou, A.G. (2015) 'DIANA-miRPath v3.0: deciphering microRNA function with experimental support', *Nucleic Acids Res*, 43(Web Server issue), pp. W460-W466.

Waldman, S.A. and Terzic, A. (2009) 'Applications of microRNA in cancer: Exploring the advantages of miRNA', *Clin Transl Sci*, 2(3), pp. 248-9.

Wang, G., Kwan, B.C., Lai, F.M., Choi, P.C., Chow, K.M., Li, P.K. and Szeto, C.C. (2010) 'Intrarenal expression of microRNAs in patients with IgA nephropathy', *Lab Invest*, 90(1), pp. 98-103.

Wang, G., Kwan, B.C., Lai, F.M., Chow, K.M., Li, P.K. and Szeto, C.C. (2012) 'Urinary miR-21, miR-29, and miR-93: novel biomarkers of fibrosis', *Am J Nephrol*, 36(5), pp. 412-8.

Wang, J.-f., Yi-feng, Z., Li, H.-w., Wang, F., Bian, Q., Lai, X.-l. and Yu, G. (2014a) 'Screening plasma miRNAs as biomarkers for renal ischemia-reperfusion injury in rats', *Medical Science Monitor*, 20, pp. 283-289.

Wang, J.Y., Gao, Y.B., Zhang, N., Zou, D.W., Wang, P., Zhu, Z.Y., Li, J.Y., Zhou, S.N., Wang, S.C., Wang, Y.Y. and Yang, J.K. (2014b) 'miR-21 overexpression enhances TGF-beta1-induced epithelial-to-mesenchymal transition by target smad7 and aggravates renal damage in diabetic nephropathy', *Mol Cell Endocrinol*, 392(1-2), pp. 163-72.

Wang, Z., Zhu, Q., Li, P.L., Dhaduk, R., Zhang, F., Gehr, T.W. and Li, N. (2014c) 'Silencing of hypoxia-inducible factor-1alpha gene attenuates chronic ischemic renal injury in two-kidney, one-clip rats', *Am J Physiol Renal Physiol*, 306(10), pp. F1236-42.

Wei, Q., Bhatt, K., He, H.Z., Mi, Q.S., Haase, V.H. and Dong, Z. (2010) 'Targeted deletion of Dicer from proximal tubules protects against renal ischemia-reperfusion injury', *J Am Soc Nephrol*, 21(5), pp. 756-61.

Weigmann, A., Corbeil, D., Hellwig, A. and Huttner, W.B. (1997) 'Prominin, a novel microvilli-specific polytopic membrane protein of the apical surface of epithelial cells, is targeted to plasmalemmal protrusions of non-epithelial cells', *Proc Natl Acad Sci U S A*, 94(23), pp. 12425-30.

Weinberg, J.M. (1991) 'The cell biology of ischemic renal injury', *Kidney Int*, 39(3), pp. 476-500.

Wilflingseder, J., Regele, H., Perco, P., Kainz, A., Soleiman, A., Muhlbacher, F., Mayer, B. and Oberbauer, R. (2013) 'miRNA profiling discriminates types of rejection and injury in human renal allografts', *Transplantation*, 95(6), pp. 835-41.

Wilflingseder, J., Reindl-Schwaighofer, R., Sunzenauer, J., Kainz, A., Heinzel, A., Mayer, B. and Oberbauer, R. (2014) 'MicroRNAs in Kidney Transplantation', *Nephrol Dial Transplant*, pp. 1-8.

Wilusz, J.E., Sunwoo, H. and Spector, D.L. (2009) 'Long noncoding RNAs: functional surprises from the RNA world', *Genes Dev*, 23(13), pp. 1494-504.

Witkos, T.M., Koscianska, E. and Krzyzosiak, W.J. (2011) 'Practical Aspects of microRNA Target Prediction', *Current Molecular Medicine*, 11(2), pp. 93-109.

Wolfe, R.A., Ashby, V.B., Milford, E.L., Ojo, A.O., Ettenger, R.E., Agodoa, L.Y., Held, P.J. and Port, F.K. (1999) 'Comparison of mortality in all patients on dialysis, patients on dialysis awaiting transplantation, and recipients of a first cadaveric transplant', *N Engl J Med*, 341(23), pp. 1725-30.

Wu, H., Chen, G., Wyburn, K.R., Yin, J., Bertolino, P., Eris, J.M., Alexander, S.I., Sharland, A.F. and Chadban, S.J. (2007) 'TLR4 activation mediates kidney ischemia/reperfusion injury', *J Clin Invest*, 117(10), pp. 2847-59.

Xie, Y., Li, W., Feng, J., Wu, T. and Li, J. (2016) 'MicroRNA-363 and GATA-1 are regulated by HIF-1α in K562 cells under hypoxia', *Molecular Medicine Reports*, 14(3), pp. 2503-2510.

Xu, X., Kriegel, A.J., Jiao, X., Liu, H., Bai, X., Olson, J., Liang, M. and Ding, X. (2014) 'miR-21 in Ischemia/Reperfusion Injury: A Double-Edged Sword?', *Physiol Genomics*, 46, pp. 789-797.

Yago, T., Petrich, B.G., Zhang, N., Liu, Z., Shao, B., Ginsberg, M.H. and McEver, R.P. (2015) 'Blocking neutrophil integrin activation prevents ischemia–reperfusion injury', *The Journal of Experimental Medicine*, 212(8), p. 1267.

Yang, L., Besschetnova, T.Y., Brooks, C.R., Shah, J.V. and Bonventre, J.V. (2010) 'Epithelial cell cycle arrest in G2/M mediates kidney fibrosis after injury', *Nat Med*, 16(5), pp. 535-43, 1p following 143.

Yarlagadda, S.G., Coca, S.G., Garg, A.X., Doshi, M., Poggio, E.D., Marcus, R.J. and Parikh, C.R. (2008) 'Marked Variation in The Definition and Diagnosis of Delayed Graft Function: A Systematic Review', *Nephrol Dial Transplant*, 23, pp. 2995-3003.

Yarlagadda, S.G., Coca, S.G., Jr., R.N.F., Poggio, E.D. and Parikh, C.R. (2009) 'Association between Delayed Graft Function and Allograft and Patient Survival: A Systematic Review and Meta-analysis', *Nephrol Dial Transplant*, 24, pp. 1039-1047.

Yu, B. and Chen, X. (2010) 'Analysis of miRNA Modifications', *Methods Mol Biol*, 592, pp. 137-48.

Zarjou, A., Yang, S., Abraham, E., Agarwal, A. and Liu, G. (2011) 'Identification of a microRNA signature in renal fibrosis: role of miR-21', *Am J Physiol Renal Physiol*, 301(4), pp. F793-801.

Zhang, P.F., Sheng, L.L., Wang, G., Tian, M., Zhu, L.Y., Zhang, R., Zhang, J. and Zhu, J.S. (2016) 'miR-363 promotes proliferation and chemo-resistance of human gastric cancer via targeting of FBW7 ubiquitin ligase expression', *Oncotarget*, 7(23), pp. 35284-92.

Zhang, Z., Peng, H., Chen, J., Chen, X., Han, F., Xu, X., He, X. and Yan, N. (2009) 'MicroRNA-21 protects from mesangial cell proliferation induced by diabetic nephropathy in db/db mice', *FEBS Lett*, 583(12), pp. 2009-14.

Zhong, X., Chung, A.C., Chen, H.Y., Meng, X.M. and Lan, H.Y. (2011) 'Smad3-mediated upregulation of miR-21 promotes renal fibrosis', *J Am Soc Nephrol*, 22(9), pp. 1668-81.

Zhou, B., Wang, S., Mayr, C., Bartel, D.P. and Lodish, H.F. (2007) 'miR-150, a microRNA expressed in mature B and T cells, blocks early B cell development when expressed prematurely', *Proc Natl Acad Sci U S A*, 104(17), pp. 7080-5.

Zhou, T.B. and Jiang, Z.P. (2014) 'Role of miR-21 and its signaling pathways in renal diseases', *J Recept Signal Transduct Res*, 34(5), pp. 335-7.

Zhou, W., Farrar, C.A., Abe, K., Pratt, J.R., Marsh, J.E., Wang, Y., Stahl, G.L. and Sacks, S.H. (2000) 'Predominant role for C5b-9 in renal ischemia/reperfusion injury', *Journal of Clinical Investigation*, 105(10), pp. 1363-1371.

Zununi Vahed, S., Omidi, Y., Ardalan, M. and Samadi, N. (2017) 'Dysregulation of urinary miR-21 and miR-200b associated with interstitial fibrosis and tubular atrophy (IFTA) in renal transplant recipients', *Clin Biochem*, 50(1-2), pp. 32-39.